# GEOCHEMISTRY OF IGNEOUS ROCKS ASSOCIATED WITH THE MMH PORPHYRY COPPER DEPOSIT, CHUQUICAMATA DISTRICT, CHILE

Jessica Wilson

Submitted in Partial Fulfillment of the Requirements
For the Degree of Bachelor of Sciences, Honours
Department of Earth Sciences
Dalhousie University, Halifax, Nova Scotia
April 2011

# Distribution License

DalSpace requires agreement to this non-exclusive distribution license before your item can appear on DalSpace.

NON-EXCLUSIVE DISTRIBUTION LICENSE

You (the author(s) or copyright owner) grant to Dalhousie University the non-exclusive right to reproduce and distribute your submission worldwide in any medium.

You agree that Dalhousie University may, without changing the content, reformat the submission for the purpose of preservation.

You also agree that Dalhousie University may keep more than one copy of this submission for purposes of security, back-up and preservation.

You agree that the submission is your original work, and that you have the right to grant the rights contained in this license. You also agree that your submission does not, to the best of your knowledge, infringe upon anyone's copyright.

If the submission contains material for which you do not hold copyright, you agree that you have obtained the unrestricted permission of the copyright owner to grant Dalhousie University the rights required by this license, and that such third-party owned material is clearly identified and acknowledged within the text or content of the submission.

If the submission is based upon work that has been sponsored or supported by an agency or organization other than Dalhousie University, you assert that you have fulfilled any right of review or other obligations required by such contract or agreement.

Dalhousie University will clearly identify your name(s) as the author(s) or owner(s) of the submission, and will not make any alteration to the content of the files that you have submitted.

If you have questions regarding this license please contact the repository manager at dalspace@dal.ca.

Grant the distribution license by signing and dating below.

_____ _____

Name of signatory Date

DALHOUSIE UNIVERSITY
*Inspiring Minds*

**Department of Earth Sciences**
Halifax, Nova Scotia
Canada B3H 4J1
(902) 494-2358
FAX (902) 494-6889

DATE: April 20, 2011

AUTHOR: Jessica Wilson

TITLE: Geochemistry of Igneous Rocks Associated with the MMH Porphyry Copper Deposit, Chuquicamata District, Chile

Degree: BSc. Convocation: May Year: 2011

## Abstract

The MMH deposit is located 7 km to the south of the Chuquicamata mine within the Chuquicamata District in northern Chile, in the Domeyko Cordillera. The two deposits are located on opposite sides of the West Fault, a section of a regional (Domeyko) orogen-parallel fault system with ca. 35 km of strike-slip displacement. The MMH has a tabular shape, parallel to and adjoining the West Fault. MMH, held and operated by the state-owned company CODELCO, contains resources of more than one billion tonnes of copper ore, and is being prepared for open pit mining.

The focus of this thesis is the igneous geochemistry of the MMH deposit. The ore at MMH is hosted by the MM Granodiorite (Triassic; U-Pb in zircon 237-222 Ma), which is intruded by the MM Porphyry (Eocene; U-Pb in zircon 39 Ma) and the MM Quartz Porphyry (Eocene; U-Pb in zircon 36 Ma). The deposit contains Cu-(Mo) porphyry type mineralization (Re-Os in molybdenite $\leq$37.3 Ma) and potassic alteration at depth, overprinted at higher levels by a younger (32-31 Ma), high sulphidation Cu-(Ag-As) ore characterized by high-grade hydrothermal breccia bodies. The genetic relationship between the Cu-(Mo) and Cu-(Ag-As) mineralization and Tertiary porphyries is still to be proven.

Trace element geochemistry reveals that the Triassic MM Granodiorite and the Eocene MM Porphyry have nearly identical trace-element geochemical signatures. Both are the equivalent of volcanic or sub-volcanic andesite, whereas the Eocene MM Quartz Porphyry is closer to a rhyodacite in composition. All have calc-alkaline - to some extent adakitic - characteristics. Electron microprobe analyses show that whereas the plagioclase in MM Granodiorite has been pervasively albitized, the plagioclase in MM Porphyry is oligoclase-andesine.

The surprising geochemical similarity between Triassic and Eocene host rocks suggests that tectonic conditions and magma generation in the Triassic was not very different to the Tertiary for this region of northern Chile. These results are in conflict with the commonly held thinking that the Triassic was a time of tectonic extension and relaxation. One implication is that the Triassic and Paleozoic basement in the Domeyko Cordillera may be more prospective for porphyry copper type deposits than previously though. Another implication is that the composition of the mantle and lower crust in the Domeyko Cordillera may have more to do with the formation of giant porphyry type copper-molybdenum deposits than previously envisaged.

The MMH igneous host rocks have geochemical similarities with the Fortuna Igneous Complex, which is juxtaposed to the Chuquicamata deposit west of the West Fault, and with the El Abra Porphyry Complex, which is 35 km north, on the east side of the regional fault.

# TABLE OF CONTENTS

# TABLE OF FIGURES

# TABLE OF TABLES

## ACKNOWLEDGMENTS

First and foremost I would like to thank my supervisor Marcos Zentilli for his relentless enthusiasm and support. His endless energy and knowledge has been inspirational at every stage of this work. I would also like to thank Ricardo Boric and Jaime Díaz from CODELCO Norte for allowing the use of proprietary data and for their contributions to the thesis. Furthermore I would like to thank Dan MacDonald, Gordon Brown, Luke Hilchie, Yana Fedortchouk, Rebecca Jamieson and Christian Rafuse for their assistance in the completion of this work. I would like to thank all of my professors from the Dalhousie Earth Science Department for facilitating my knowledge in all aspects of geology In particular I would like to recognize Anne-Marie Ryan for her commitment to education. Her guidance and classes were instrumental in my decision to pursue a BSc. in Earth Science. Finally I would like to thank my mom for being the foundation upon which all of my accomplishments have been built. Muchas Gracias!

# CHAPTER 1: INTRODUCTION

## 1.1 General Statement

The Chuquicamata mining district, site of one of the three largest open pit mines in the world, is located northeast of the port city of Antofagasta in northern Chile (Fig. 1.2). Mined continuously since 1915, the Chuquicamata open pit has a length of 5 km, width of 3 km and depth of >1 km, and has copper resources of over 10 billion metric tonnes of ore (e.g. Ossandón et al. 2001). Besides its extraordinary size, what makes this giant copper deposit all the more interesting is that it is truncated on its west side by the important north-south regional structure denominated Falla Oeste or West Fault (Fig. 1.1) with a strike-slip displacement of ~35 km. This circumstance has led to speculation and an intense search for the "missing half" of Chuquicamata across the fault, identifying several mineralized bodies, but so far none that meets the qualifications. One of these mineralized bodies is the MMH (Mina Ministro Hales; originally known as *Mansa Mina* or MM) which is 7 km to the south of Chuquicamata on the opposite side of the West Fault (see Fig. 1.1). The MMH deposit, the subject of this thesis, has been classified as another supergiant Cu-Mo type porphyry deposit within the Chuquicamata District. The deposit has a tabular shape, parallel to and adjoining the West Fault and involves numerous fault slices (Boric et al. 2009). This thesis attempts to shed some light onto the question of the relationship of the MMH deposit with other copper-molybdenum deposits in the Chuquicamata District.

Open pit mining of MMH is scheduled to begin in 2013 (Boric et al. 2009), to be followed by underground mining in the next decade. As part of the preparation for mining, a full review of the geological model of MMH is underway, and one of the aspects being considered is the better definition and characterization of the host rocks.

This thesis provides the first systematic, internally-consistent geochemical analysis of characteristic rock units as shown in the geological maps and sections.

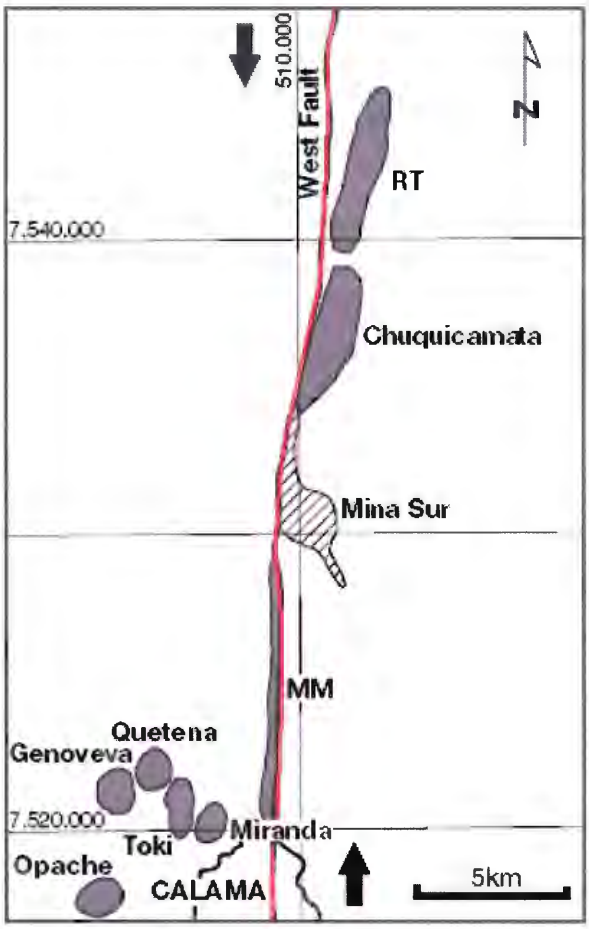


**Figure 1.1** Areal map of the Chuquicamata District, northern Chile. This map shows the spatial relationship between the MM (MMH) ore deposit and Chuquicamata ore deposit. The distance between the two is approx 7 km. This figure also indicates the location of RT or Radomiro Tomic and Mina Sur, both of which are mines with mineralization related to the Chuquicamata Intrusive Complex. The Opache, Genoveva, Toki and Quetena deposits are satellite porphyry deposits that are currently being explored. (modified from Sillitoe 2010).


**Figure 1.2** map showing the arc-parallel distribution of Cu porphyries from central to northern Chile (Sillitoe 2010).

## 1.2 Overview of Cu Porphyry Systems

The conceptual models of copper porphyry systems have evolved over the last forty years and the consensus today is that the majority of the most significant deposits formed at the roots of subduction-related stratovolcanoes (Sillitoe 2010, Guilbert & Park 1986, Sillitoe 1973). They are comprised of hydrothermally and tectonically altered sub-volcanic rock centered around stock systems. These stock "porphyry" systems are emplaced 1.5-4 km beneath the surface from subaerial volcanic eruptions (Sillitoe, 1973). The stock systems are the upper extensions of plutonic intrusive bodies at depth. These plutonic bodies are result of calc-alkaline arc magmatism above active continental subduction zones. On the large scale, this activity results in a high density of linearly disposed arc parallel deposits such as in northern Chile (Fig. 1.2). On the small scale, this magmatism results in multiple porphyry and stock systems originating from a single massive batholith at depth (Sillitoe 2010). Not only are these porphyry systems spatially related, they evolve within a time span of roughly 10-20 million years also known as "metallogenic epochs" (Sillitoe 2010). The tight-knit temporal and spatial relationships of porphyry deposits proves to be advantageous in terms of exploration methods and often results in districts of Cu mines such as the Chuquicamata Mining District.

For an up-to-date description and discussion of porphyry copper type deposits, the reader is referred to a comprehensive review by Sillitoe (2010).

### 1.3 Chuquicamata District

The Chuquicamata Mining District lies 2.8 km above sea level in the Atacama Desert of northern Chile (22° 17.5'5 S, 68 ° 54.5' W). The copper oxide outcrops were first exploited by the Incas in pre-colonial times and subsequently by the Spanish conquistadors (Ossandón et al. 2001, Guilbert & Park 1986). Modern operations began in 1879 with Chilean and British companies. In 1915 the Chuquicamata open-pit mine was established in order to extract disseminated copper oxide ore. The South Mine (Mina Sur) (see Fig. 1.1) which is comprised of *exotic* (oxides laterally displaced from their original source) copper ore related to the Chuquicamata porphyry system was discovered in 1957. The Radomiro Tomic (RT) mine (see Fig. 1.1), which is north of Chuquicamata but part of the same porphyry system, was initiated in the 1960s. The MMH deposit was discovered in 1967; its geology is discussed in more detail below in section 1.4. To date, the region has produced 2.155 billion metric tons of ore averaging 1.52% Cu, equating to 87.02 Million tonnes (Mt) of Cu metal. Projected resources for the district predict another 11.45 billion tonnes at 0.76% Cu still in the ground (Ossandón et al 2001). As result of the phenomenally large concentration of Cu ore, Chuquicamata ranks in the top three current copper producing districts in the world, and was for the majority of the 20$^{th}$ century, the largest copper mine in the world. The Chuquicamata District is owned and operated by the Corporación del Cobre de Chile or CODELCO which is a state-owned mining company.

The Chuquicamata Intrusive Complex contains the vast majority of ore mineralization. It occurs in contact with the eastern side of the West Fault and extends 9 km from its contact with the West Fault into the Radomiro Tomic Mine to the north. The

Chuquicamata Intrusive Complex is composed of three porphyry systems, East Porphyry, West Porphyry and Banco Porphyry, which are temporally and texturally separate but compositionally similar (Ossandón et al. 2001, McInnes et al. 1999). The East porphyry is the earliest intrusion and the largest in volume and ore mineralization (Ossandón et al. 2001, McInnes et al. 1999). McInnes et al. (1999) described all three units as monzogranite porphyries. The Chuquicamata Intrusive Complex ore body terminates against the West Fault, juxtaposing the unit against the economically barren Fortuna Intrusive Complex.

The West Fault is part of the intricate and extensive Domeyko Fault system. It truncates many of the porphyry deposits in the region including Chuquicamata. The truncation of these major Cu porphyry deposits indicates that there may be "missing portions" somewhere along the adjacent side of the West Fault. Although it is generally agreed upon that the movement since the time of emplacement has been between 35 and 37 km sinistral, there have been reversals in movement throughout its existence (e.g. Tomlinson & Blanco 1997). There is also evidence of vertical displacement within the system (e.g. McInnes et al. 1999). The post mineralization displacement along the West Fault is significant in that it has determined where the "missing half" of Chuquicamata has gone and whether or not the potential ore exists and is extractable.

**1.4 Previous Work**

Due to its economic importance, the Chuquicamata district has been extensively studied. The most recent and comprehensive review of the Chuquicamata Mining District was written by Ossandón et al. in 2001. For a more in depth look into the entirety of the district, the reader is encouraged to review that publication.

MMH was discovered by the Chilean Exploration Company, a part of the American Anaconda Company, in 1967, by accident (Sillitoe et al. 1996). The company was planning to use the area as a waste site for Mina Sur and drilling was conducted to ensure the gravel covered area was not underlain by economic mineralization, resulting in the breakthrough. The deposit was originally named MM for "Mansa Mina". That name, which has a double meaning in Chilean Spanish, still persists in the literature and everyday usage, but the name of the mine was recently changed by the company to Mina Ministro Hales after a former Minister of Mines Mr. Alejandro Hales (1923-2001) thus MMH. In 1972 the Corporación Nacional del Cobre de Chile or CODELCO took over the Chuquicamata district and in 1978 conducted a geophysical survey and shallow drilling program. Through this work, a vein of copper mineralization was discovered to the west of the West Fault. From 1990-1992 approximately 35,000m of deep drilling was completed and from 1993 to 1995, a mine shaft and tunnels were also constructed. This investigation of MMH resulted in the recognition that it was a giant porphyry copper deposit (Sillitoe et al. 1996). As of 2009, there had been 170,000 m of core drilled and 7.3 km of underground workings (Boric et al. 2009). The most significant events and studies are listed in Table 1.1.

| Event | Company or Person Responsible | Date |
|---|---|---|
| Discovery of MMH | Chilean Exploration Company | 1967 |
| Investigation into potential of deposit | CODELCO | 1972 |
| First abstract written on MMH | Alvarez & Miranda | 1991 |
| Structural, mineralogical and dating study | Zentilli et al. | 1994 |
| First comprehensive review of MMH and comparison with Chuquicamata | Sillitoe et al. | 1996 |
| Economic model of MMH | Muller & Quiroga | 2003 |
| Mineralogical study of sulphides | Tobey | 2005 |
| Review and update of the geology | Boric et al. | 2009 |

**Table 1.1** Significant studies and benchmarks of MMH.

### 1.5 Methods

The emphasis of this study is on petrology of the sub-volcanic porphyritic rocks. This thesis uses whole-rock geochemical analysis to compare samples from MMH with those of other deposits in the district that could possibly be connected to MMH. This objective is carried out by the evaluation of the major and trace element geochemical signatures of the intrusive and host rock units of MMH and comparing that with work previously done on other copper porphyry deposits of interest such as Chuquicamata, Fortuna and El Abra (see Fig. 1.3). This thesis also uses petrographic analysis done by optical microscopy and an electron-microprobe analysis to identify and characterize the silicate minerals as well as the sulphide minerals.

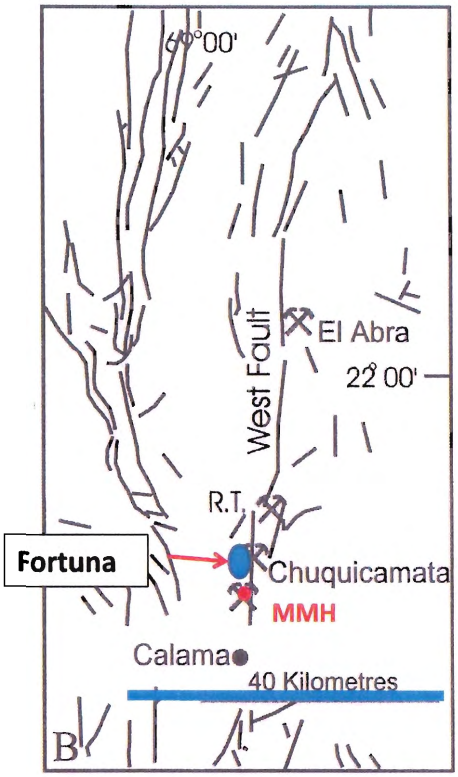


**Figure 1.3** Location of MMH, Chuquicamata, Fortuna igneous complex and El Abra. (modified from Sillitoe 2010)

The data are then discussed in the context of other geochemical, mineralogical and geochronological data available.

# CHAPTER 2: IGNEOUS ROCKS OF PORPHYRY COPPER DEPOSITS

## 2.1 Igneous Petrology

Porphyry copper deposits (PCD) are known to develop preferentially within calc-alkaline subvolcanic systems associated with subduction zones. The reader is directed to a comprehensive review by Richard Sillitoe, recognized authority on the subject and who has worked on MMH (Sillitoe 2010). According to the current models, porphyry systems, which develop at depths of ca. 4 km, are the shallower expressions of large batholiths at paleodepths of 5-15km. These batholiths transfer magma, fluids and heat through pipes and chambers to the overlying porphyry systems causing the host rock to fracture and thus allowing for magmatic-hydrothermal mineralization (see Fig. 2.1). This results in the development of pervasive veining and stock systems above the roof of the batholith, the geometry and placement of which are controlled by structural factors of the host rock.

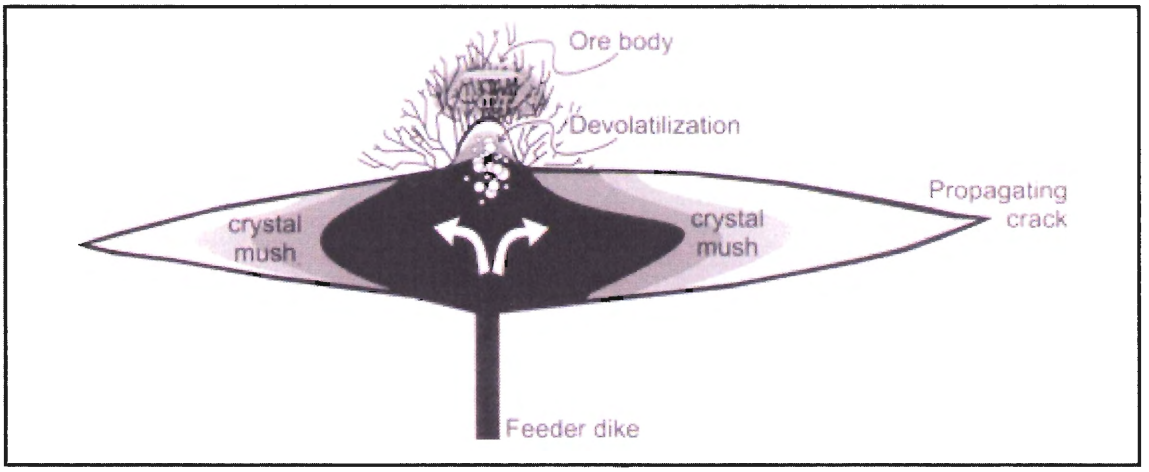


**Figure 2.1** Illustration showing a magma chamber that been saturated with volatiles which has led to devolatilization and fracturing of the host rock. (Candela & Picolli 2005)

During the time of porphyry generation, the batholiths are suspended at neutral buoyancy (Sillitoe 2010). When new magma is injected into the batholith from beneath the more buoyant components of the magma (e.g. volatiles and silicates) rise to the top of

the batholith. This will continue until the top of the magma chamber is saturated in volatiles. The growth of feldspars and quartz, which are volatile free, supersaturate the remaining magma with supercritical fluid. At some point a fluid phase is separated that occupies more space than in solution; fluid pressure exerted by the volatiles becomes greater than the lithostatic pressure exerted by the host rock plus the tensional strength of the rocks, and the host rock will fracture (see Fig. 2.1). In the absence of tectonic stresses, fractures are random and stockworks irregular; where there is an active shear system (e.g. Chuquicamata, MMH, Lindsay 1997) , fractures show preferred orientation and form dyke-like bodies. These fractures will be filled with the buoyant components of the magma as well as the devolatilized magmatic fluid. This process often repeats itself over an extended period of time (up to 5 million years in the case of Andean porphyry deposits (Sillitoe 2010), and creates successive generations of porphyries. The accumulation of these successive porphyries is what constitutes a porphyry system.

### 2.1.1 Magmatic Processes

Porphyry Cu deposits (PCD) are exclusively related to I-type, metaluminous calc-alkaline arc magma. The composition can range from calc-alkaline diorite, quartz diorite, and granodiorite to quartz monzonite (monzogranite).

As the name indicates, an inherent characteristic of PCD is that the ores are associated with porphyritic rocks. Porphyry intrusions generally contain phenocrysts of feldspar, quartz, hornblende and biotite with a fine-grained aplitic groundmass. The phenocrysts result from differential crystallization that occurs within the relatively stagnant magma chamber, prior to devolatilization. At deeper levels, within the magma chamber, the high Fe and Mg concentrations impede nucleation of felsic minerals such as

quartz and feldspars (Candela & Picolli 2005). As result, a relatively small number of phenocrysts form, also known as. Many of the feldspar phenocrysts show zoning which is result of slow growth under variable conditions. The aplitic groundmass forms from pressure quenching and devolatilization during the rapid ascent of the magma. The magma under these conditions becomes more felsic as well as supersaturated with volatiles. The combination of this rapid decrease in pressure and temperature facilitates the nucleation of small crystals which constitutes the groundmass of the porphyry.

Quartz in typical granites is anhedral and interstitial whereas in porphyries it is often phenocrystic. Many shallow porphyries with hydrothermal magmatic ore are called "quartz porphyries" due to their high proportion of "quartz eyes". Quartz eyes are spheroidal quartz phenocrysts that are prevalent in quartz porphyries, even after alteration. Quartz eyes form due to the ease at which quartz nucleates in supercooled granite dykes. Many quartz phenocrysts show resorbtion features, such as reentrants representing dissolution of already formed phenocrysts (e.g. Candela & Picolli 2005). These rocks also typically contain some phenocrystic feldspar.

### 2.1.2 Hydrothermal Alteration Processes

Alteration-mineralization zoning in PCD affects several cubic kilometres of rock. The formation of the hydrothermal alteration zones in PCD is due to a two-phase fluid (which originates from a supercritical gas) that is emitted from the magma chamber. This two phase fluid is composed mainly of a low-density vapour as well as hypersaline liquid or brine. The brine has a salinity between 35-70 wt% (NaCl equivalent) whereas the vapour is composed mainly of volatiles such as $SO_2$, $H_2S$, $CO_2$, HCl, and HF. The Cu atoms reside in the vapour phase whereas the Mo resides in the brine. Sulfur ligands in

the vapour phase act as Cu transporting agents whereas the Mo is transported by Cl ligands in the brine (e.g. Candela & Picolli 2005).

PCD are characteristically developed in a stockwork, which is a complex system of structurally controlled or randomly oriented veins and veinlets. The stockwork system controls the ascent of the metal-rich magma fluid and thus, the Cu and Mo sulphides precipitate in the veins. Gustafson and Hunt (1975) have described and categorized these veins which will be discussed later in this chapter. As the magmatic fluid ascends, the temperature decreases which increases the S fugacity (e.g. Sillitoe 2010). As the S fugacity increases the precipitation of Cu sulphides changes as well as the alteration mineral assemblages. This change in mineral assemblages is what defines the various alteration zones. In stratigraphic (or temporal) order from lowest to highest, the alteration zones that occur are: sodic-calcic, potassic, chloritic-sericite, sericitic and advanced argillic (see Fig. 2.2). A propylitic zone can occur around the outer edges of the porphyry system (see Fig. 2.2). The deeper zones of the porphyry system are the first to be affected by hydrothermal alteration with the shallower hydrothermal zones occurring later. This creates overprinting of older zones by younger (i.e. chlorite-sericite zone overprints potassic zone) (Sillitoe 2010). It should be noted that the terms sericitic and phyllic are synonymous.

### 2.1.3 Alteration Zones

The sodic-calcic zone occurs at the base of the porphyry system and is typically not well defined (hence it is not represented in Fig. 2.2). Key minerals of this zone are albite and/or oligoclase, actinolite, magnetite ± diopside ± epidote ± garnet. Veins that occur in this zone are comprised of magnetite and actinolite. The sodic-calcic zone is typically devoid of sulphides and thus, is of no economic interest (Sillitoe 2010)

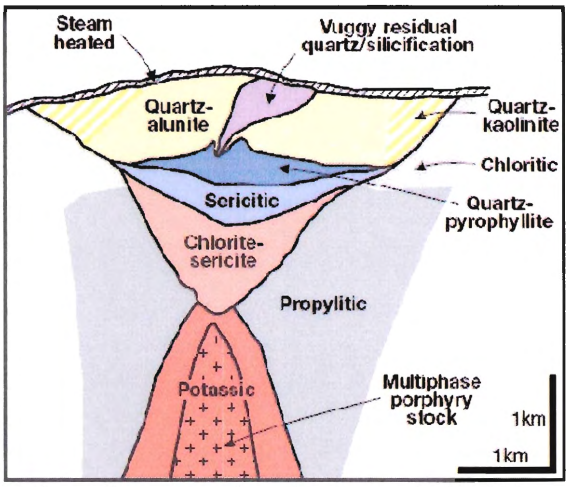


**Figure 2.2** Vertical successions of porphyry alteration zones. It should be noted that the indicated quartz-kaolinite and quartz-alunite regions constitute the advanced argillic zone and the sericite and chlorite-sericite regions comprise the phyllic zone. Another point this figure displays is the vertical gap between the potassic and advanced argillic economic zones. (Sillitoe 2010)

The potassic zone constitutes the majority of the lower part of the Cu porphyry systems, especially in the Cu porphyry deposits of northern Chile (Fig. 2.2). Typical gangue mineral assemblages include: biotite, K-feldspar ± actinolite ± epidote ± sericite ± andalusite ±albite ± carbonate ± tourmaline ±magnetite. Biotite is the predominant alteration mineral in the more mafic porphyry intrusions whereas K-feldspar is more dominant in the more felsic porphyry intrusions with both types containing sodic plagioclase (Sillitoe 2010). Typical sulphide mineral assemblages that occur are: pyrite-

chalcopyrite, chalcopyrite ± bornite, bornite ± digenite ± chalcocite. Bornite signifies a high sulphidation state and occurs in the deeper, more central part of Cu ore deposits. The bornite-rich assemblages grade into chalcopyrite-bornite with decreasing sulphidation. As the potassic zone grades into the propylitic zone, increasing amounts of pyrite will occur as halos around the chalcopyrite, bornite and any other sulphides that may occur.

The chloritic alteration that occurs within the propylitic zone is a succession of potassic alteration and thus is a result of the same process (Fig. 2.2). This alteration is caused by chlorite replacing biotite and remaining amphiboles. The unit is characterized by chlorite-magnetite with occasional sericite and hematite (Lindsay 1997).

The phyllic zone is divided by Sillitoe (2010) into two categories: the chlorite-sericite and the sericitic zones. The chlorite-sericite is distinguishable by its pale green colour. It occurs in the stratigraphically higher portions of the Cu deposit (see Fig. 2.2) and often overprints pre-existing potassic alteration assemblages. A distinguishing feature of this zone is the alteration of biotite to chlorite, plagioclase to sericite and magnetite to hematite (Sillitoe 2010). Key gangue minerals that occur in this zone are: chlorite, sericite/illite and hematite. The main sulphide assemblage that occurs within this zone is chalcopyrite-pyrite (Sillitoe 2010). The sericitic alteration zone can partially or wholly overprint potassic and chlorite-sericite alteration assemblages. Partial overprint occurs as zoned halos around veins of sericitic alteration. There sericitic alteration can produce either a greenish-grey colour (such as in Chuquicamata) and host chalcopyrite-bornite assemblages or produce a white colour and contain only pyrite. Key minerals assemblages include: quartz, sericite ± prophyllite ±carbonate ± tourmaline ± specularite (Sillitoe 2010).

The advanced argillic zone forms a lithocap in the upper regions of the Cu porphyry environment. It is formed by low temperature and high sulphidation conditions as well as interactions with meteoric water. The development of advanced argillic lithocaps is more developed in lithologies with low acid-buffering capacities (such as felsic igneous rocks) than in those with high acid-buffering capacities (such as mafic igneous rocks) (Sillitoe 2010). Sillitoe (2010) divided the advanced argillic zone into two categories: the quartz-pyrophyllite zone and the quartz ± kaolinite ± alunite zone. The quartz-pyrophyllite (pyrophyllite is a hydrated alumina silicate, $Al_2Si_4O_{10}(OH)_2$) is the stratigraphically lower unit of the advanced argillic lithocap and as such, it represents the higher temperature, higher sulphidation, lower pH region of the advanced argillic lithocap. The quartz ± kaolinite ± alunite (kaolinite is a type of clay, $Al_2Si_2O_2(OH)_4$ and alunite is a type of sulphate $KAl_2(SO_4)_2(OH)_6$) is the stratigraphically upper region of the advanced argillic zone. It forms under lower temperature, lower sulphidation and higher pH conditions.

### 2.1.4 Veining

Gustafson and Hunt (1975) identified three generations of vein types in the El Salvador Cu porphyry complex and their classification system is still accepted and used today. These vein categories in order of age are: A-type quartz veins, B-type quartz veins and D-type quartz veins.

A-type quartz veins contain silicate assemblages of: quartz + K-feldspar + anhydrite ± biotite. The sulphide assemblage is comprised of: chalcopyrite + bornite ± molybdenite. These veins range from 50 to 95% quartz. Occasionally, halos of K-

feldspar develop around these veins. As these veins are the first veins to form, they are typically cut by later B-type and D-type veins.

B-type veins contain silicate assemblages of: quartz + anhydrite with no K-feldspar. The sulphide assemblage is comprised of: molybdenite + chalcopyrite ± pyrite ± bornite. These veins typically have coarse grained quartz and lack alteration halos. These veins types typically truncate older A-type veins but are truncated by younger D-type veins.

D-type veins contain silicate assemblages of: anhydrite + quartz ± carbonate. The sulphide assemblage is comprised of: pyrite ± chalcopyrite ± bornite ± enargite ± sphalerite ± galena. These veins typically contain open spaces and truncate the older A- and B-type veins.

Sulphide mineralization associated with veining is not necessarily contained within the vein boundaries. Often time regions that are pervasively affected by veining will contain sulphide assemblages typical of the vein type(s) disseminated throughout the host rock (Corbett 2009)

### 2.1.5 Second Boiling

As mentioned above, second boiling occurs at the top of a magma chamber that is saturated with respect to volatiles (Fig. 2.3). Once the hydrostatic pressure of this silicate-volatile phase exceeds the confining pressure of the wall rock (~1 kb), the volatile phase will undergo an increase in volume. The magnitude of the pressure being exerted by this increase in volume will cause the wall rock to fracture, given this process is occurring in the upper limits of the crust (i.e. < 4km) (Burnham 1979). These fractures will occur in the direction of the less stress which generally is in an upward direction. In zones with no

active faulting or tectonic stress, this creates a concentric system of stocks and veins that originate at the top of the magma chamber and splay upward in a conical fashion (Fig. 2.3). The stocks and veins created by second boiling are filled with the buoyant crystalline magma that are mostly comprised of felsic minerals. This magma coexists with the volatile phase at the top of the magma chamber and with the two-phase magmatic fluid mentioned in the above (section 2.1.2). As hydrostatic pressures and temperatures decrease, the metals will exsolve from the two-phase fluid and precipitate within the veins and stocks.

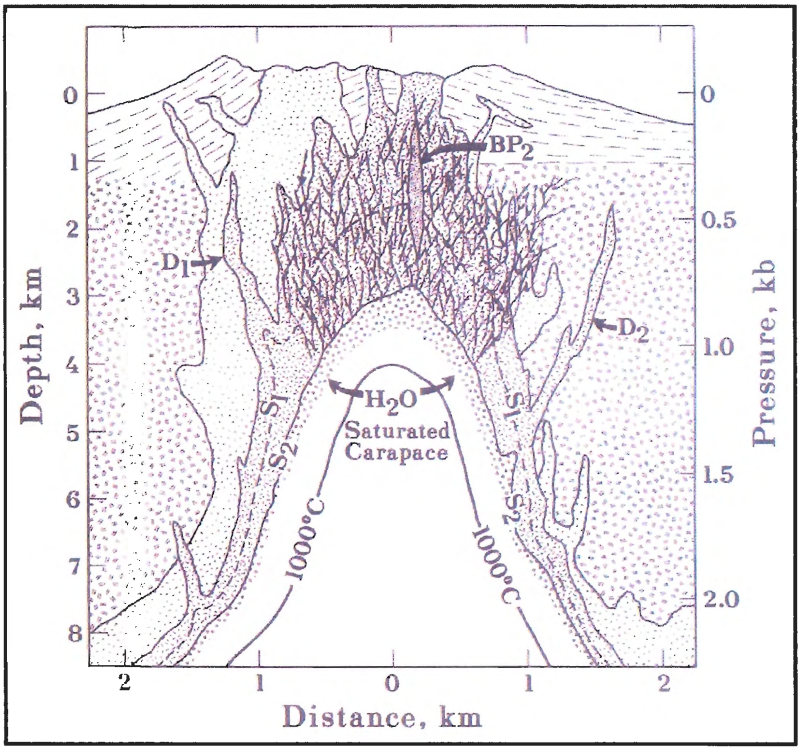


**Figure 2.3** A magma chamber undergoing second boiling. $S_2$ represents the $H_2O$ saturated solvus and $S_1$ represents the devolatilization boundary. $D_1$, $D_2$ represent dykes that occur as result of second boiling and $BP_2$ represents a breccia pipe. The fractures illustrated above the magma chamber represent the veins and dykes that result from the increase in volume of the magmatic fluid. (Burnham 1979)

### 2.1.6 Supergene Enrichment

Supergene (meaning genesis from above) enrichment occurs by descending meteoric waters oxidizing and dissolving hypogene (primary) ore and redistributing it in a more horizontal manner, creating a supergene (secondary) enrichment cap. Sulphuric acid is created by oxidizing pyrite and thus, the more pyrite that is available, the more effective the supergene enrichment will be. This process occurs when the porphyry system is exhumed and is considered to be a form of weathering. Faulting can also facilitate supergene enrichment as it allows the groundwater to penetrate a greater surface area; thus, increasing oxidation capabilities. These oxides are typically not economical; however, from this supergene enrichment cap, metals leach from the oxidized ore and are carried down by groundwater and react with the hypogene sulphides at the supergene-hypogene boundary near the paleo-water-table. This process produces secondary sulphides with higher metal content than primary hypogene sulphides, hence "supergene enrichmnent". This enhances the economic potential of the Cu ore. Porphyry deposits that have not undergone supergene enrichment and depend on their primary or hypogene Cu grade of ca. 0.5% may not be economical unless the metal prices are anomalously high.

When the supergene solutions move laterally down the water table, "exotic" deposits are formed, such as those mined at Mina Sur in Chuquicamata (Fig. 1.1.) and encountered east of the West Fault at MMH.

## 2.2 Tectonic Setting

Porphyry copper deposits are associated with convergent plate boundaries and the transfer of heat from the Earth's interior to the outer crust. Under oceanic-continental convergent conditions, serpentinized mantle along with oceanic crust, ocean-floor sediments and ocean water are subducted beneath the overlying continental lithosphere (Fig. 2.4). At depths which satisfy certain pressure and temperature conditions for various components of the descending slab, the buoyant, hydrous components will rise and metasomatize the overlying mantle. This results in hydrous arc magmas which form volcanic arc systems such as the Andes. Porphyries are a part of the arc systems and can be thought of as subvolcanic rocks.

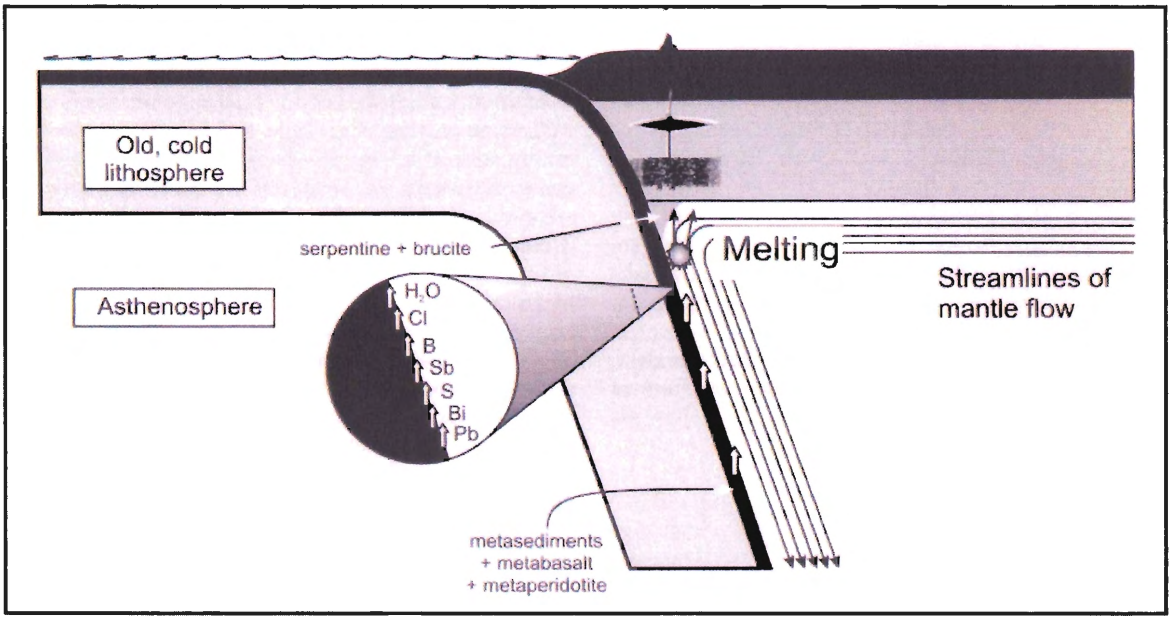


**Figure 2.4** The oceanic-continental convergent environment under which porphyries form. This illustration emphasizes the input from the subducting slab, the mantle and the lower portions of the continental lithosphere. (Candela & Picolli 2005)

### 2.2.1 Origin of Cu

Although porphyries occur along all convergent margins, not all porphyries contain economic amounts of Cu. The reason for this is not known and can only be speculated. The origin of Cu in a porphyry system can come from a combination of places. It is possible for the Cu to come from the subducting slab itself if the ocean floor had additional Cu added to it through oceanic hydrothermal alteration processes. It is also possible to have Cu contributed from mantle sources. These sources include calc-alkaline magmas and basaltic andesites mixing with the ascending magma in an open-system environment beneath the crust (see Fig. 2.4). There is also evidence that lower crustal sources could be a contributor to Cu concentrations such as the Bagdad Cu-Mo porphyry deposit in northern Arizona (Barra et al. 2002). It is likely that many of the economical Cu deposits have contributions from all the sources mentioned above. Porphyries that form in environments that are devoid of such mechanisms will likely not be economical.

### 2.2.2 Structural Control of Porphyry Deposits

Obliquity of crustal deformation has control on the ratio of plutonism to volcanism. Strike-slip environments, such as that of the ancestral West Fault, creates local transpressional or pull-apart settings (e.g. Sibson 2001) which facilitate the ascent of magma in the lower crust and enhance permeability during the hydrothermal mineralization process. In northern Chile, the transtensional pull apart features that were caused by a reversal of dextral sheer along the West Fault in the Eocene resulted in dilation and emplacement of large batholiths (Candela & Picolli 2005). These batholiths acted as the parental sources of magma, magmatic fluid and heat to the porphyries within the Chuquicamata district as well as the many other porphyries in close proximity.

### 2.2.3 Adakites

Term "adakite" was originally used to describe igneous rocks that were generated as result of the subduction of young (≤25 Ma) oceanic crust. Under these conditions, the basaltic portion of the subducting slab partially melts after dehydration (i.e. after it has undergone amphibolite to eclogite intensity metamorphism). As result of this process, adakites have the following geochemical signature: $SiO_2 \geq 56$ wt percent, $Al_2O_3 \geq 15$ wt percent, MgO normally <3 wt percent, Mg number ≈0.5, Sr ≥400 ppm, Y ≤18 ppm, Yb ≤ 1.9 ppm, Ni ≥20 ppm, Cr ≥30 ppm, Sr/Y ≥20, La/Yb ≥20, and $^{87}Sr/^{86}Sr \leq 0.7045$ (e.g. Richards and Kerrich, 2007). The use of the term adakite can be confusing as it implies both geochemical and genetic characteristics. Since the term was first used, rocks with adakitic geochemical characteristics have been discovered to exist in environments other than that previous described (e.g. Castillo 2006). Not only do adakites have implications for the study of crustal recycling, many of the world's major Cu porphyry deposits have adakitic characteristics, namely high Sr/Y and La/Yb ratios (Richards & Kerrich 2007). This brings into question what the relation is between adakites and Cu porphyry deposits. This question is discussed in more detail below (see section 5.3), in the context of the geochemistry of MMH porphyries.

# CHAPTER 3: GEOLOGY OF THE CHUQUICAMATA DISTRICT

## 3.1 Geology of the Chuquicamata Open Pit Mine

### 3.1.1 Chuquicamata Porphyry Complex

The Chuquicamata Porphyry Complex is comprised of three separate porphyries: the Este (East) Porphyry, the Oeste (West) Porphyry and the Banco Porphyry (Fig. 3.1), all of which were emplaced within the strike-slip fault system during the evolution of the Eocene-Oligocene magmatic arc (Arnott 2003). As mentioned in section 1.3, these porphyries are mineralogically similar but variations occur in texture and age. It should be noted that classification of this porphyry system has been variable due to intense alteration and deformation (Arnott 2003), however; it is generally accepted that three distinct porphyries exist in the Chuquicamata open pit.

The Este Porphyry is the oldest and most extensive of the group comprising greater than 80% of the exposed mineralized rock. The unit has a granular to prophyritic texture with phenocrysts phases (which comprise >65% of volume) in contact with one another (Lindsay 1997). The phenocrysts are comprised of the following minerals: euhedral plagioclase >2mm, poikilitic K-feldspar with biotite, plagioclase and quartz inclusions, biotite booklets, elongate quartz eyes and occasionally hornblende. The minerals comprising the medium-grained groundmass are deformed quartz, plagioclase and K-feldspar (Ossandón et al. 2001, Lindsay 1997). This unit has been classified by Lindsay (1997) as a matrix-poor monzogranitic porphyry. Mineralogically and compositionally, the dyke-like Banco and Oeste Porphyries are similar to Este leaving the units to be distinguished mainly by texture. The Banco Porphyry is more porphyritic and is also finer grained than the Este Porphyry (Ossandón et al. 2001). It is distinguished by having a bimodal distribution of plagioclase phenocrysts of different sizes in an

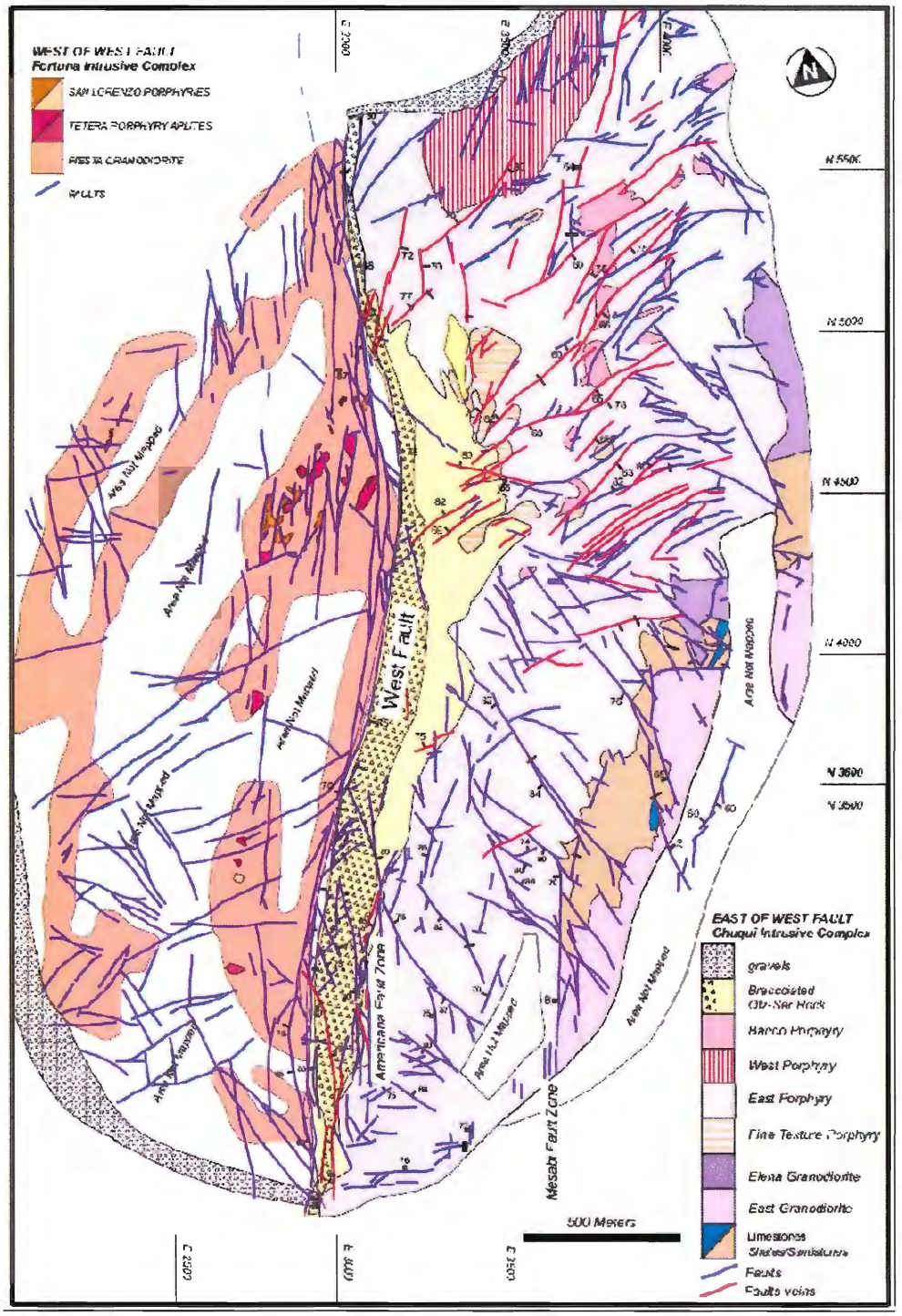


**Figure 3.1** Geological map of the Chuquicamata open pit as of 1998. Local latitude and longitude coordinates along the sides in 500m intervals. Shading defines lithologic units and lines define fault and vein structures (Ossandón et al. 2001).

| Rock Unit | Age range Ma | Method | Reference |
|---|---|---|---|
| Pre-mesozoic basement | 300 - 200 | Ar/Ar in biotite | Maksaev (1990) |
| Fortuna Complex | 39.3 - 37.6 | U-Pb zircon | Dilles et al. (1997); Ballard (2001) |
| Este Porphyry | 34.6 | ELA-ICP-MS | Ballard (2001) |
| Este Porphyry | 33.9 | Ar/Ar in biotite | Reynolds et al. (1998); Arnott (2003) |
| Potassic alteration | 34 .0 - 33.7 | Ar/Ar in biotite | Reynolds et al. (1998); Arnott (2003) |
| Oeste Porphyry | 33.5 | ELA-ICP-MS | Ballard (2001) |
| Banco Porphyry | 33.3 | ELA-ICP-MS | Ballard (2001) |
| Banco Porphyry | 33.1 | Ar/Ar in K-spar | Reynolds et al. (1998); Arnott (2003) |
| Quartz-Sericite alteration | 31.1 | Ar/Ar in sericite | Zentilli et al (1994); Reynolds et al. (1998) |
| Supergene enrichment | 19 - 15 | Ar/Ar in alunite | Sillitoe & McKee (1996) |

**Table 3.1** Ages of the three porphyries (Este, Oeste & Banco) that occur in the Chuquicamata mine along with other relevant units, indicating geochronological methods used.

aphanitic quartz-feldspar-biotite matrix (Lindsay 1997, Ossandón et al. 2001). The contact with the Este Porphyry is sharp. The Banco Porphyry does not contact the Oeste Porphyry (Lindsay 1997). Arnott (2003) concluded that the Banco Porphyry was intruded 0.5 My after the end of potassic alteration mineralization and is thus less mineralized with Cu. Banco was affected by the quartz-molybdenum veining phase at ca. 32 Ma and the later quartz-sericite alteration-mineralization phase (ca. 31 Ma).

The Oeste Porphyry comprises <5% of the rock exposed in the Chuquicamata open pit and occurs mostly in the stratigraphically higher portions. The unit is distinguished from Este as being more matrix dominated. Geochronogical dates indicate that the Banco Porphyry and the Oeste Porphyry intruded shortly after the Este Porphyry (table 3.1). Furthermore, Ossandón et al. (2001) suggest that due to the gradational boundaries between the porphyries, it is possibly that all three porphyries are in fact locally indistinguishable from each other and easy to confuse.

### 3.1.2 Fortuna Complex

The Fortuna Intrusive Complex occurs on the western side of the West Fault in the Chuquicamata open-pit mine (Fig. 3.1). It is 5 km wide and 22 km long (Dilles et al. 1997) and is mostly mined as waste to achieve slope stability (Arnott 2003). The proximity to the Chuquicamata Porphyry Complex is result of post-ore mineralization sinistral movement along the West Fault, which is discussed in section 3.3 (Ossandón et al. 2001). The Fortuna Intrusive Complex is comprised of 3 separate components (Fig. 3.1). The oldest is the Antena Granodiorite which Dilles et al. (1997) dated between 39.0 and 39.6 Ma. This unit contains fine to medium grained hornblende and biotite (Dilles et al. 1997). It is thought that this unit correlates with El Abra Granodiorite which is 35 km to the north on the eastern side of the west fault. The Fiesta Granodiorite is a younger unit (37.6 Ma from Dilles et al. 1997) that intrudes the Antena Granodiorite unit and is of similar composition. It is the largest unit within the Fortuna Intrusive Complex. The Fiesta Granodiorite grades into the San Lorenzo Porphyry System, including the Fortuna Leucocratic Intrusion, for which the ages are synchronous or slightly younger than Fiesta (Dilles et al. 1997).

Because the Fortuna Intrusive Complex is spatially juxtaposed to the Chuquicamata Intrusive Complex, the two were once thought to be of the same porphyry system, with the Fortuna Intrusive Complex representing the deeper roots of the Chuquicamata Intrusive Complex (e.g. Sillitoe 1973). Recent evidence (e.g. Arnott 2003) indicates that this concept is invalid. As mentioned above, Fortuna Intrusive Complex has been related to El Abra Granodiorite based on geochronological and field studies (39-38

Ma, thus 4-5 My older than Chuquicamata Intrusive Complex 34-33 Ma). Thus, Fortuna is not a cogenetic parent to Chuquicamata.

### 3.1.3 Pre-Chuquicamata Granodiorites

Both the Elena and East Granodiorites predate the Chuquicamata porphyries which lie to the west of them (Fig. 3.1). The East Granodiorite is the older of the two with textural evidence indicating no connection to the Chuquicamata Porphyries (Ossandón et al. 2001). The Elena Granodiorite however, is mineralogically and texturally similar to the Este Porphyry of the Chuquicamata Porphyry Complex (Ossandón et al. 2001). Radiometric dating of the Elena Granodiorite indicates a Jurassic to Early Cretaceous age (Ossandón et al. 2001). Both of the lithologies are economically barren (Ossandón et al. 2001), and form the Mesozoic host lithologies for the Chuquicamata Porphyry Complex. These Mesozoic host rocks are analogous in age and composition to the Triassic granodiorite (Granodiorite MMH) that represents the host of porphyries and mineralization at MMH (see Chapter 3.2)

### 3.1.4. Hydrothermal Alteration of the Chuquicamata Porphyry Complex

Chuquicamata rocks have been extensively altered by potassic alteration and high-sulphidation phyllic (quartz-sericite) alteration (Ossandón et al. 2001), but the distribution of alteration zones does not follow the classical concentric "onion" disposition of Lowell & Guilbert (1970) with potassic followed outwards by phyllic followed outwards by argillic and propilytic. Instead, the potassic alteration in Chuquicamata is followed outwards (to the east) by propilytic (chloritic) alteration, and the phyllic zone is central, adjoining the Falla Oeste (Fig. 3.2). Reynolds et al. (1998) demonstrated that the phyllic alteration is considerably younger than the potassic alteration and thus belongs to a

different cycle; the control exerted by the Falla Oeste and the age of this alteration show similarities with what is observed in MMH.

### 3.1.5 Supergene Enrichment

After the alteration-mineralization process was finished around 31 Ma, exhumation and erosion proceeded at around 50 m per million years (Maksaev & Zentilli 1999) with the most intense weathering occurring around 20 Ma when 450m of overlying rock had been removed (Sillitoe & McKee 1996). There is still some low grade supergene enrichment in the North pit area within the quartz-sericite zone (Ossandón et al. 2001). The Mina Sur south of Chuquicamata open pit consists of "exotic" copper oxide minerals (chrysocolla, etc.), which were derived from supergene enrichment, but were displaced a few kilometres from its source (hence exotic) into Tertiary gravels. Supergene enrichment also affected MMH at the same time as Chuquicamata, and its higher levels east of the West Fault contain some exotic ores identical to those of Mina Sur.

## 3.2 Geology of the MMH Deposit

The MMH deposit is located at 22°22'45" S, 68°54'50" W at an elevation of 2400 m above sea level in the Atacama Desert of northern Chile. It is 7 km south of the Chuquicamata open pit mine and 7 km north of the town of Calama (see fig 1.1). It runs parallel to West Fault on its western side and extends 7 km N-S and 200-300 m E-W with a depth of 1200 m below the bedrock surface (Boric et al. 2009) (Fig.. 3.2). It is estimated to have 12.6 Mt (million metric tonnes) of Cu metal, qualifying it as a supergiant porphyry Cu-type deposit (Boric et al. 2009).

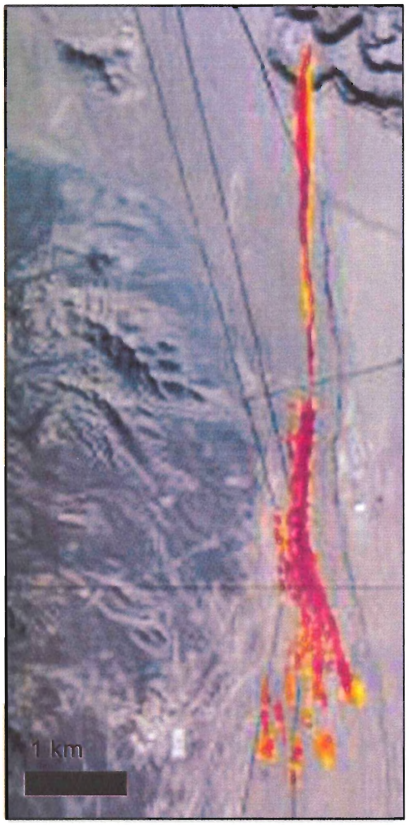


**Figure 3.2** satellite image of the MMH deposit with ore grades superimposed where purple is high Cu grade (from MM mine records).

### 3.2.1 Eastern Portion of MMH Mine

On the eastern side of the West Fault, directly adjacent to the porphyritic complex, the basement rock is comprised of unmineralized Paleozoic metadiorite and amphibolites (Sillitoe et al. 1996). Due to the presence of a narrow fault-bounded basin, alluvial gravels, which overlie the bedrock, are 700-1000 m thick (Sillitoe et al. 1996, Boric et al. 2009). These gravels contain an exotic oxide blanket (Boric et al. 2009).

### 3.2.2 MM Granodiorite

The MMH deposit occurs on the western portion of the West Fault. The MM Granodiorite hosts the majority of the hypogene ore. Sillitoe et al. (1996) describes it to be a medium-grained hypidiomorphic-granular granodiorite and Boric et al. (2009)

describes it as pervasively altered. According to Proffett (2008), the MM Granodiorite has a quartz-rich-mafic poor portion with up to 35% quartz and 4-7% mafics as well as a quartz poor-mafic rich portion with up to 25% quartz and 10-12% mafics. Both Boric et al. (2009) and Proffett (2008) recognize the granodiorite to be Triassic in age. This Granodiorite is cut by two north-striking porphyritic dikes which will be discussed in the following sections.

### 3.2.3 MM Porphyry

The MM Porphyry lies deep in the MMH deposit adjacent to the West Fault (Boric et al. 2009). It contains euhedral phenocrysts of plagioclase, biotite and biotitized hornblende throughout the unit with some locations containing anhedral interstitial quartz and K-feldspar between the phenocrysts, and others with a fine grained aplitic groundmass (Proffett 2008). The unit was dated with U/Pb zircon methods which provided an age of 38.9 ± 0.4 Ma (Boric et al. 2009). The unit has undergone potassic alteration so that secondary K-feldspar appears as rims and veinlets within K-feldspar (Boric et al. 2009). Opaque minerals that occur within the unit are bornite, chalcopyrite, chalcocite and minor digenite.

### 3.2.4 MM Quartz Porphyry

The MM Quartz Porphyry is distinguished by its abundance of quartz eyes (spheroidal quartz crystals that are millimetres in diameter) (Boric et al. 2009). It has been affected by potassic alteration and is noted to have blue-green sericite, K-feldspar as well as anhydrite (Boric et al. 2009). This unit cuts the MM Porphyry and is dated by U/Pb methods to be 35.5 ± 0.6 Ma (Boric et al. 2009).

### 3.2.5 Other Geologic Units

A rock mapped as Hornblende Porphyry was sampled in DHH 3173 at 888.5 m, but there is insufficient data to characterize it; dark patches consist of chlorite; its geochemistry is similar to MM Porphyry.

Dacite dykes cut all of the units mentioned above and are classified by their assemblage of hornblende and plagioclase with minor quartz (Boric et al. 2009). They are cut by the hydrothermal breccias and some are considered Mesozoic in age (Boric et al. 2009).

The hydrothermal breccias are spatially "rooted" in the MM Porphyry (Boric et al. 2009). Areas that contain rotated quartz clasts show the highest Cu grades in the MMH deposit along with As, Ag and Zn (Boric et al. 2009). The hydrothermal breccia unit shows argillic alteration in places and represents a transition between typical Cu-Mo porphyry and epithermal high sulphidation mineralization (Boric et al. 2009).

### 3.2.6 Hypogene Mineralization

The earliest phase of hypogene mineralization was the potassic alteration. The mineral assemblages associated with this phase include K-feldspar and quartz altered from plagioclase as well as chloritized remnants of hydrothermal biotite and hornblende (Sillitoe et al. 1996). This unit contains opaque assemblages such as bornite-chalcopyrite nuclei with chalcopyrite halos (Boric et al. 2009).

The next sequence in hypogene alteration was sericitic alteration whereby previous textures were obliterated and minerals were replaced with quartz and sericite. This phase contains the majority of Cu-bearing minerals (Sillitoe et al. 1996). This mineralization

produced sulphides such as pyrite and enargite and is found in the upper western portions of the deposit (Sillitoe et at. 1996).

The last stage of hypogene mineralization occurred as late stage high sulphidation Cu (Ag + As) with advanced argillic alteration and the formation of hydrothermal breccias discussed in section 3.2.5 (Boric et al. 2009). This zone is comprised of quartz, alunite, pyrophyllite and sericite with minor kaolinite (Sillitoe et al. 1996). This mineralization zone is contained in the easternmost portions of the MMH unit in the top 400m of the deposit (Sillitoe et al. 1996). As indicated above, supergene and exotic copper minerals occur in the near-surface of the MMH deposit.

### 3.2.7 Ages of Hypogene Phases

Boric et al. (2009) report Re/Os ages on molybdenite that suggest the first hypogene mineralization phase occurred at ca. 37.3 Ma. This phase may be associated with the recognized Eocene porphyries, but no intrusions have been identified as the parents of the high sulfidation bodies with hypogene alunite that yields $^{40}Ar/^{39}Ar$ ages of 31.4 to 32.2 Ma (Boric et al. 2009).

### 3.2.8 Supergene Mineralization

Supergene mineralization and weathering has affected the upper 60 to 150 m of sulphide bearing country rock in the MMH deposit (Sillitoe et al. 1996). The supergene leached cap composes the top 50 to 60m which is underlain by partially oxidized sulphides and then chalcocite enrichment underlies this (Sillitoe et al. 1996). The alunite produced from supergene enrichment in the central MMH body was dated using K/Ar methods to produce dates between 20.8 +/- 0.6 Ma and 20.4 +/-0.6 Ma (Sillitoe et al. 1996).

## 3.3 The West Fault

Structural events within the Chuquicamata District have been controlled by the West Fault which is the northern most section of the Domeyko Fault System (Tomlinson & Blanco 1997). The fault is by far the most prominent structural feature in the area as it is a 3m thick gouge and brecciated zone that cuts mineralization of the Chuquicamata porphyries. A dextral precursor to the West Fault is represented in the Chuquicamata deposit by a high-temperature ductile shear zone (Lindsay 1997). Transtensional domains associated with it may have facilitated the emplacement and mineralization of super giant Cu porphyries within the Chuquicamata District; a weak domain in the crust that allowed magma to rise rapidly to the near surface. The brittle equivalent of this ancestral fault, now the West Fault, was responsible for the post mineralization displacement of those same porphyries it helped create (e.g. Tomlinson & Blanco 1997). This section examines both the horizontal and vertical displacement of the West Fault and its evolution over time.

### 3.3.1 Horizontal Displacement of the West Fault

The first tectonic event that occurred in the region was a shortening event which occurred between 44 and 38.5 Ma (Eocene) (Tomlinson & Blanco 1997). This age correlates with the emplacement of the El Abra Mine to the north of Chuquicamata as well as the Fortuna Intrusive Complex and the MMH deposit. With the knowledge that El Abra and Fortuna are of the same origin, this puts a lower constraint on the age of strike-slip movement within the West Fault to 37 Ma which is the age of final cooling of the Fortuna-El Abra complex (Tomlinson & Blanco 1997). The West Fault must have formed by 31 Ma as it cut the sericitic alteration within Chuquicamata which has been dated by

Zentilli (1995) as 31 Ma (Tomlinson & Blanco 1997). If the Chuquicamata Porphyry System was in fact emplaced as result of the formation of the West Fault system, then the dates from those porphyries indicate the fault began to develop around 34-33 Ma (Tomlinson & Blanco 1997). Dextral mylonitic shears within these porphyries indicate that the fault's movement was dextral from its initiation until 31 Ma (Lindsay 1997; Tomlinson & Blanco 1997).

At 31 Ma there was a reversal in movement along the West Fault due to a shift in the tectonic nature of the Arica Bend (refer to Fig. 1.2) to the north (Tomlinson & Blanco 1997). This new sinistral strike-slip motion along the West Fault began post-mineralization with respect to the Chuquicamata Porphyry System. This movement continued until around 19 Ma as the upper age constraint is provided by the Huasco Ignimbrite which overlies the West Fault and shows no signs of sinistral displacement (Tomlinson & Blanco 1997). Field correlations collected by Tomlinson & Blanco (1997) indicate that the amount of net sinistral displacement within the Chuquicamata District is equivalent to 37 km for the Chuquicamata Porphyry System and 35 km for the Fortuna-El Abra Complex.

### 3.3.2 Vertical Displacement of the West Fault System

McInnes et al. (1999) used the apatite (U-Th)/He thermochronometry method to measure the vertical displacement along the West Fault system. This method is effective for dating tectonic events that occur in the uppermost crust as it measures the cooling history between 45°C and 90°C. Through this method, they determined there has been a minimum of 600 m ± 100 m of post mineral vertical displacement along the West Fault with the western block uplifted relative to the eastern block. Since Chuquicamata is at an

elevation of ~3000 m above sea level, these findings would imply that the western half of Chuquicamata must be at an elevation of ~3600m somewhere along the western flank of the West Fault. MMH is located at 2400 m elevation and thus, this data indicates that MMH cannot be the other half of Chuquicamata. The eastern half of MMH should be at an elevation of roughly 1800m somewhere along the east side of the West Fault (McInnes et al. 1999). Part of the interpretation of McInnes et al. (1999) was challenged by Tomlinson et al. (2001) who argue that using their extensive field evidence for 35-37 Km strike-slip displacement, the missing portion of the Chuquicamata deposit may have escaped exhumation, depending on the full displacement path, and may lie immediately below the surface between Calama and Sierra Limón Verde to the south, "waiting to be discovered and exploited".

# CHAPTER 4: PETROGRAPHY OF THE MMH DEPOSIT

Petrography of the MMH samples was determined using both optical microscopy methods and electron microprobe analysis (EMP). Both methods were conducted at Dalhousie University laboratories.

## 4.1. Optical Microscopy

Optical microscopy was applied to 15 core chip samples from MMH that were selected as representative samples by M.Zentilli in 2010 (Table 4.1). From these samples, both thin sections and polished sections were made and analyzed. The thin sections were used to identify silicate minerals and textures using plain polarized light (PPL) and cross polarized light (XPL). Polished sections were observed using reflected light and were used to identify sulphide minerals and textures.

| Samples of MMH analized by Activation Labs Inc | | | | |
|---|---|---|---|---|
| Sample Q series | Diamond Drillhole | From m | To m | Rock Unit in Log |
| ZMMH-04 | 3173 | 888.50 | 888.63 | Hb Porphyry |
| ZMMH-05 | 3173 | 853.75 | 853.86 | MM Grd |
| ZMMH-07 | 4903 | 1012.00 | 1012.25 | PMM |
| ZMMH-09 | 4884 | 158.90 | 159.00 | PMM |
| ZMMH-10 | 5014 | 161.00 | 161.20 | MM Grd |
| ZMMH-11 | 4976 | 897.87 | 898.00 | POQ |
| ZMMH-12 | 4976 | 1128.00 | 1128.12 | POQ |
| ZMMH-13 | 4976 | 1123.78 | 1123.90 | POQ |
| ZMMH-14 | 4976 | 1241.00 | 1241.12 | PMM |
| ZMMH-15 | 4976 | 1286.47 | 1286.60 | PMM |
| ZMMH-17 | 4976 | 855.40 | 855.50 | MM Grd |
| ZMMH-18 | 4976 | 845.85 | 845.95 | MM Grd |
| ZMMH-20 | 4976 | 870.90 | 871.05 | MM Grd |
| ZMMH-21 | 4976 | 883.20 | 883.24 | PMM |
| ZMMH-23 | 4976 | 1064.00 | 1064.15 | MM Grd |
| Cu 1333 | Chuquicamata pit | | | Banco Porphyry |
| Cu 2022 | Chuquicamata pit | | | Este Porphyry |

**Table 4.1** Drillcore samples from MMH used for petrographic and whole-rock geochemical analysis. Included in the whole-rock geochemical analysis were two samples from Chuquicamata, one from the Banco Porphyry unit and one from the Este Porphyry unit.

### 4.1.1. MM Porphyry

*Observations*

The PMM samples contain feldspar phenocrysts, biotite, quartz ± feldspar groundmass, veins and sulphides.

The feldspar phenocrysts range in length from 5 mm to 2 mm and are generally subhedral prismatic (Fig. 4.1). Most of these feldspar phenocrysts are plagioclase with a few K-feldspar. Primary zoning is observed in some of the feldspar phenocrysts as many have alteration rims and penetrative alteration veins (Fig. 4.2). The samples are variably affected by sericitization whereby some of the samples show little or no remnant feldspar, whereas others only contain sericite along cleavage planes within feldspar.

The biotite that is observed occurs within clusters of variable size where the micaceous crystals are aligned sub-parallel to one another and look to be "shredded". The clusters are irregularly shaped and vary in size between 1.5mm and 0.5mm. Within some of the larger biotite crystals, microlath inclusions of rutile are observed. In sample ZMMH-14 (DDH 4976) these rutile inclusions are euhedral and aligned in two directions at angles of 60°-120° (see photo within appendix 2). Within some samples, there are poikilitic biotites that contain inclusions of quartz, anhedral rutile (probably exsolution from biotite or recrystallization from titanite), apatites, zircons and sulphides (eg ZMMH 7). Much of the biotite has undergone chloritization.

The groundmass ranges from medium to fine grained quartz and occasionally contains sericite, presumably from altered feldspars (Fig. 4.2).

The veins are mostly comprised of quartz along with sulphides such as chalcopyrite, pyrite and chalcocite. The veins range in width from >0.5mm to 1.5 mm and contain vugs along with iron oxide.

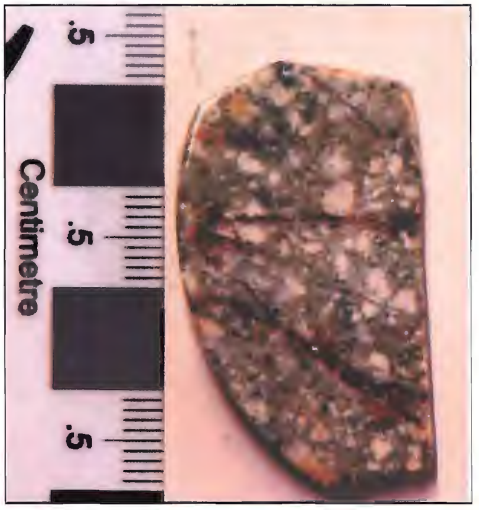


**Figure 4.1** Photograph of a core chip sample of the MM Porphyry

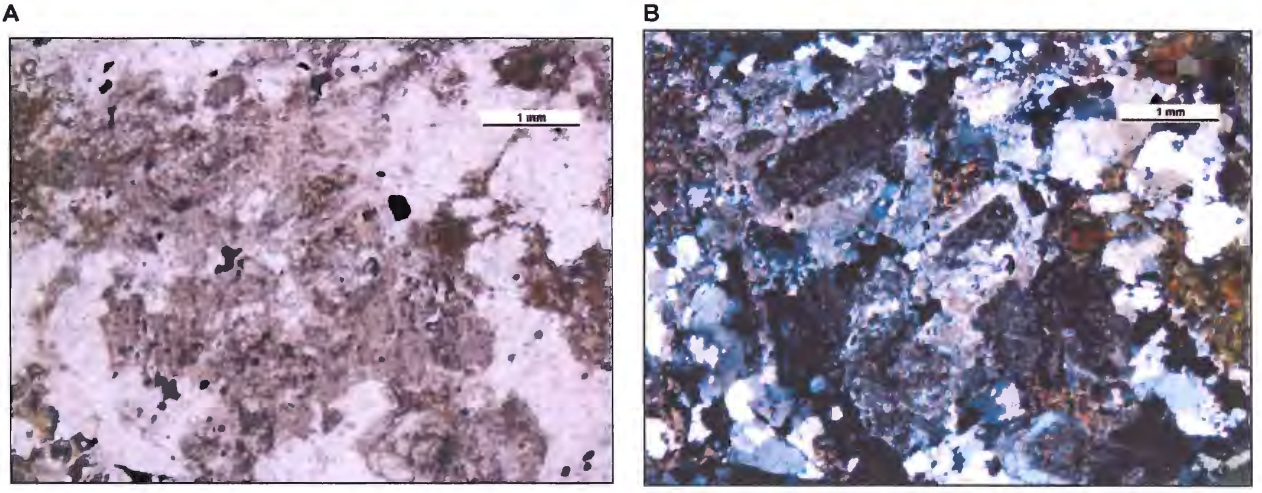


**Figure 4.2** Microphotographs of the MM Porphyry. **A)** was taken in plain polarized light (PPL) and shows how the altered feldspars have accumulated a dingy brownish-grey colour; **B)** was taken in cross polarized light (XPL) and shows zoning of the feldspar phenocrysts.

*Discussion*

The size and zoning of feldspar phenocrysts is typical of porphyry-type rock. The alteration rims and penetrative alteration veins observed in most samples are characteristic of textural overprint by potassic and/or phyllic alteration phases (Fig. 4.2). The variable amount of sericitization that occurs within the feldspar phenocrysts in each sample is indicative of the level of alteration in that sample. Many of the samples contain evidence of initially undergoing potassic alteration, then subsequent phyllic alteration. See appendix 2 for description of secondary alteration of individual samples

The biotite is characteristic of hydrothermal mineralization. The preferred alignment of the elongate crystals indicates that they formed under a stress field such as would occur during hydrothermal alteration. The poikilitic texture observed within the biotite is also indication of the secondary nature of the mineral (see photograph of ZMMH-14 in appendix 2). Furthermore, Tobey (2005) has attributed a "shredded" texture (whereby the edges of the biotite crystals are rough and uneven, see appendix 2) to biotite in MMH that is of secondary nature (see photograph of ZMMH-14). The exsolution of the rutile was likely caused by alteration of the primary (igneous) biotite or titanite. The "immobile" behaviour of titanium in the rocks, where Ti changes mineralogy but remains in the same volume of rock, is significant when the geochemistry of the rocks is discussed in Chapter 5.

Due to the incompatible chemical nature of titanium, the element was exsolved during the alteration process to form rutile. The presence of rutile poikiloblasts within biotite crystals indicates that the biotite overprinted primary mafic minerals (possibly

amphibole). The chloritization of biotite that occurs in many samples is likely a result of chlorite-sericite alteration.

The occurrence of veins within the samples observed is controlled by alteration levels as well as structural controls. There is no characteristic vein type that is associated with a certain lithologic unit. Using Gustafson & Hunt's (1975) vein classification guide as described in section 2.1.4, all three types of veins (A, B, D) were observed to be present within the MM Porphyry samples. The sulphides that are present in the sample are likely a reflection of these vein types as well as secondary alteration. Veining and sulphide assemblages are discussed in more depth with respect to the individual samples in appendix 2.

### 4.1.2 MM Granodiorite

*Observations*

Granodiorite MM is a hypidiomorphic, equigranular assemblage of feldspar, quartz and chloritized biotite (Fig. 4.4). It is not a "porphyry". The feldspar is intergrown, zoned and commonly shows alteration rims with a sericitized center. Many of the samples have been so pervasively sericitized that there is no remnant feldspar. The crystal size ranges from 1.5mm-3mm along the length.

The quartz grains are anhedral and range in size depending on the amount of alteration that the sample has undergone. Samples that have undergone more alteration have larger quartz grains and a higher proportion of quartz in the sample.

The chloritized biotite occurs in irregularly shaped clusters ranging in size from 2 mm to 0.5 mm this remnant biotite is often poikilobastic with inclusions of quartz, rutile, sulphides and apatites.

The sulphides are disseminated and typically occur within close proximity to the biotite remnants or within veins. Veining occurs irregularly throughout the samples observed with thickness of >0.5mm to 2.5mm.

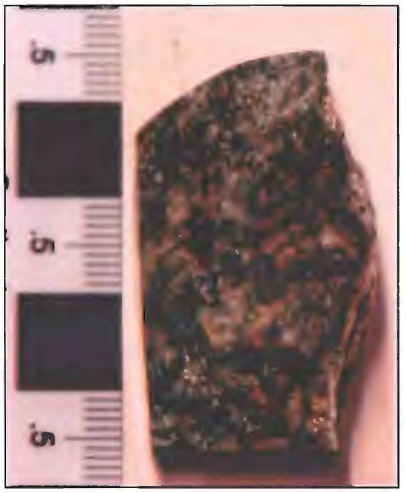

**Figure 4.3** This is an example photo of a core chip sample of the MM Granodiorite

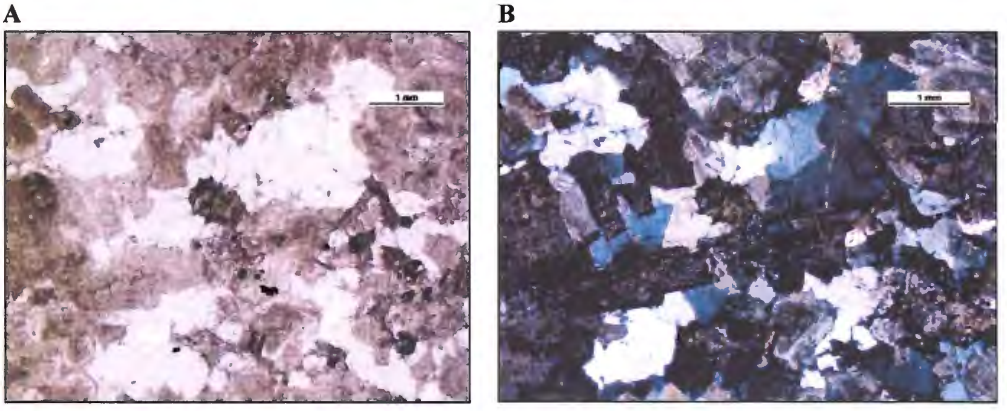


**Figure 4.4** Microphotographs taken of the MM Granodiorite. **A)** was taken in plain polarized light (PPL) whereas **B)** was taken in cross polarized light (XPL). Both of these photos display the hypidomorphic texture observed in the MM Granodiorite. The PPL photo shows the brownish-grey colour that the feldspars accumulated from secondary alteration.

*Discussion*

The hypidomorphic texture observed as well as the silicate mineral assemblage of feldspar + quartz + biotite is typical of a granodiorite.

The hydrothermal alteration of Granodiorite MM greatly affected the texture of the samples. The pervasive alteration of feldspars which has resulted in sericitization as well as alteration rims has altered the original shape and character of the feldspars and has in some cases left them unrecognizable.

The correlation of the proportion of quartz and alteration is likely the result of deterioration of feldspar to sericite + quartz under acidic alteration conditions. This indicates that the quartz within the MM Granodiorite could have originated anywhere between primary igneous conditions to sometime during the subsequent secondary alteration processes.

Further evidence for pervasive alteration of the MM Granodiorite samples comes from the chloritization of biotite in all of the obtained samples. The poikiloblastic texture observed indicates that the biotite was likely secondary before it was chloritized.

The veining that occurs is a function of the alteration that the individual sample has undergone and has more to do with the location of the sample than the primary igneous lithology. The sulphides that are present in the samples were emplaced by secondary alteration rather than primary igneous processes. For a further discussion of the vein types and sulphides that occur in each sample see appendix 2.

### 4.1.3 MM Quartz Porphyry

*Observations*

The MM Quartz Porphyry samples are characterized by large rounded quartz phenocrysts with diameters >6mm (Fig. 4.6). There are also feldspar phenocrysts which have been completely sericitized in two of the three samples. The remnant feldspar that does occur is zoned and is affected by sericitization along its cleavage planes. These

feldspars are between 4.25 mm and 0.5 mm long. The groundmass is aplitic and is comprised of quartz with sericite. The unit contains pervasive veining with some of the veins containing vugs. Sulphides generally occur within or in close proximity to the veins.


**Figure 4.5** This is an example photo of a core chip sample of the MM Quartz Porphyry

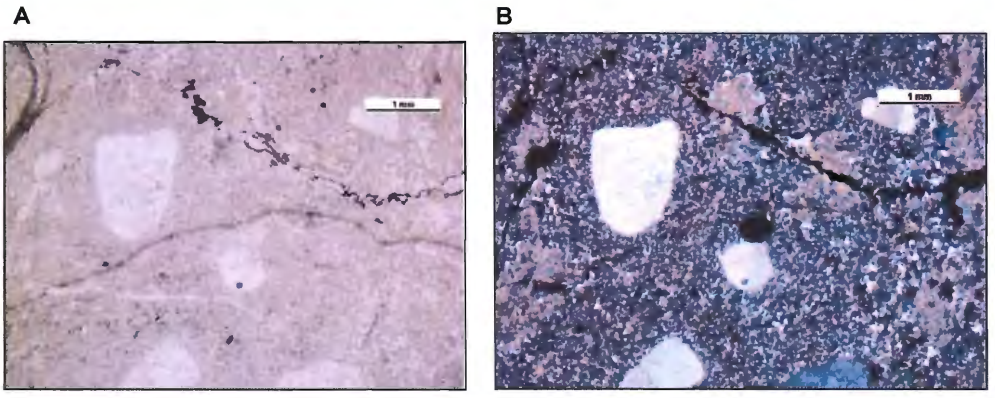


**Figure 4.6** Microphotographs photos taken of the MM Quartz Porphyry. **A)** was taken in plain polarized light (PPL) **B)** was taken in cross polarized light (XPL). Both of these photos show the characteristic quartz phenocrysts known as "quartz eyes"

*Discussion*

The bimodal grain size is what classifies this unit as porphyry. The MM Quartz Porphyry is characterized by the large, spheroidal quartz phenocrysts which are commonly referred to as "quartz eyes" (Fig. 4.6).

The more felsic composition of this unit means that it contains a high proportion of feldspar and thus, it is more susceptible to sericitization when undergoing acidic alteration phases. This is likely why the majority of the samples are so pervasively altered. Another implication of the felsic composition of this unit is that it would have formed after the more mafic MM Porphyry which contains biotite. This is supported by the U/Pb dating cited in Boric et al. (2009).

**4.2 Electron Microprobe Analysis**

The electron microprobe analysis works by bombarding a carbon-coated polished section with an electron beam. This causes x-rays to be emitted from the point where the electron beam was shot. Having calibrated the microprobe with known standards, the emitted x-ray levels can be quantitatively measured and used to identify the proportion of elements present in the spot being analyzed to an accuracy and precision approaching 1% (Goldstein et al. 2003). The elements that were analyzed for in the silicates were: K, Cr, Mn, Na, Al, Ca, Ti, Mg, Si, Fe, P, Cl, Ni, F, S and Ba. 150 points were analyzed.

In this study, three polished sections were analyzed in the electron microprobe, each one representing one of the three lithologies identified at MMH. Sample ZMMH-14 (DDH 4976 1241.00-1241.12m) was used to represent the MM Porphyry, ZMMH-10 (DDH 5014 161.0-161.2m) was used to represent the MM Granodiorite and ZMMH-11

(DDH 4976 897.87 – 898.00 m) was used to represent the MM Quartz Porphyry (see table 4.1). These samples were selected because they appeared to be the least altered samples.

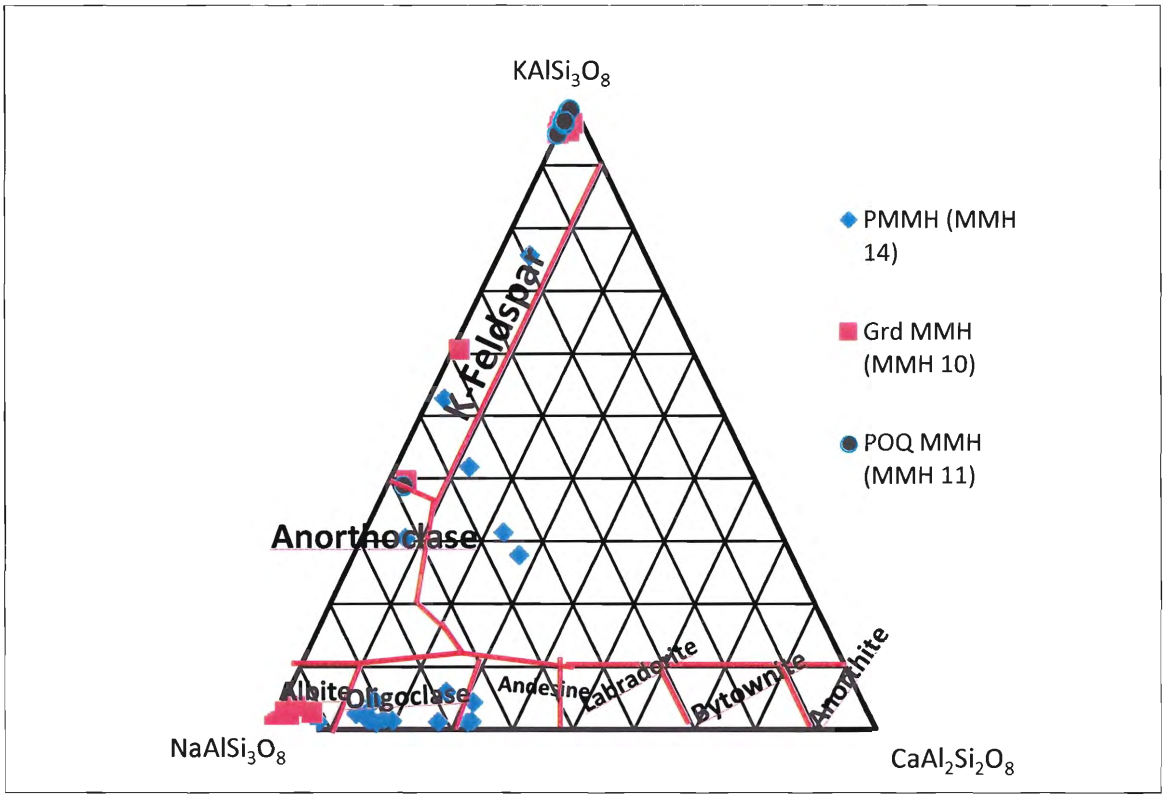


**Figure 4.7** A ternary diagram of the feldspar end member classification. The diagram shows that the majority of the MM Porphyry data points (PMMH) fall into the oligoclase field, indicating that albitization has not been intense in this rock unit. The plagioclase in the Granodiorite MM (Grd MMH) has been completely albitized. Thus a distinction between the two rocks can be made using the feldspar composition. The MM Quartz Porphyry (POQ MM) mostly falls into the K-feldspar field.

### 4.2.1 MM Porphyry

| Feldspar end member | Proportion |
|---|---|
| K-feldspar | 39% |
| Albite | 0% |
| Andesine | 13% |
| Oligoclase | 35% |
| Anorthoclase | 4% |
| Unstable | 9% |

**Table 4.2** The proportion of each feldspar end member with respect to the population of feldspar phenocrysts within the MM Porphyry. Taken from sample ZMMH-14 (DDH 4976 1241.00-1241.12m) with EMP analysis. Total number of feldspar points that were analyzed is 23.

*Discussion*

The data indicates that K-feldspar phenocrysts have a uniform composition whereas the plagioclase phenocrysts that are predominantly oligoclase contain portions that are andesine, anorthoclase, K-feldspar or unstable (see appendix 1). The phenocrysts with a K-feldspar composition could have originated under primary conditions or under potassic alteration conditions. Barium was not tested for in this sample so it is not possible to tell which of the two situations has occurred. It is likely that within the sample there is both primary and secondary K-feldspar. The oligoclase phenocrysts are likely relatively unaltered phenocrysts with compositions that reflect primary igneous conditions. The majority of the data points in plagioclase from the MM Porphyry are categorized as Oligoclase (see Fig. 4.7 and table 4.2). This is an important distinction because plagioclase in the Triassic MM Granodiorite is completely albitized.

The electron microprobe analysis of feldspars is therefore very useful in distinguishing between MM Porphyry and MM Granodiorite.

### 4.2.2 MM Granodiorite

| Feldspar end member | Proportion |
|---|---|
| K-Feldspar | 39% |
| Albite | 52% |
| Andesine | 0% |
| Oligoclase | 0% |
| Anorthoclase | 0% |
| Unstable | 9% |

**Table 4.3** The proportion of each feldspar end member with respect to the population of feldspar phenocrysts within the MM Granodiorite. Taken from sample ZMMH-10 (DDH 5014 161.0-161.2m) with EMP analysis. Total number of feldspar points that were analyzed is 23.

*Discussion*

EMP data shows that K-feldspar and albite often occurred together in the same phenocryst (see appendix 1). This secondary mineral assemblage is typical of potassic alteration as the alkalis are very mobile under acidic conditions. The exclusive presence of albite and K-feldspar (see Fig. 4.7 and table 4.3) indicates that the MM Granodiorite samples have been pervasively altered, which is very different from MM Porphyry.

### 4.2.3 MM Quartz Porphyry

| Feldspar end member | Proportion |
|---|---|
| K-feldspar | 96% |
| Unstable | 1% |

**Table 4.4** The proportion of each feldspar end member with respect to the population of feldspar phenocrysts within the MM Granodiorite. Taken from sample ZMMH-11 (DDH 4976 897.87 – 898.00 m) with EMP analysis. Total number of feldspar points that were analyzed is 26.

| | |
|---|---|
| Analysis that contain Ba | 38% |
| Analysis that do not contain Ba | 62% |

**Table 4.5** The number of feldspar analyses in sample ZMMH-11 that contain barium compared to those that do not.

*Discussion*

The results from the EMP analysis indicate that all analyzed feldspar phenocrysts were K-feldspar (see Fig. 4.7 and table 4.4). This agrees with the mineralogically evolved composition of the MM Quartz Porphyry. Arnott (2003) stated that primary K-feldspars tend to contain barium whereas secondary K-feldspars do not. Therefore, the EMP analysis indicates that the phenocrysts in the MM Quartz Porphyry were likely primary K-feldspar. When the samples underwent potassic alteration, portions of the primary K-feldspar was replaced by secondary K-feldspar (table 4.5).

### 4.2.4 Sulphides

As previously mentioned, sulphide mineralization is more dependent on veining and secondary alteration processes than it is on primary lithology. For this reason, the results are more indicative of alteration processes rather than reflective of primary igneous lithology. Since the samples were taken at various depths from different cores, these EMP

results are likely more reflective of the local sulphide assemblages rather than that of the lithologic units. The elements analyzed using the EMP for the sulphides were: Mo, S, As, Fe, Pb, Ag, Co, Ti, Ca, Cu, Sn, Sb, Mn, Zn and W. 97 points were analyzed.

*Results*

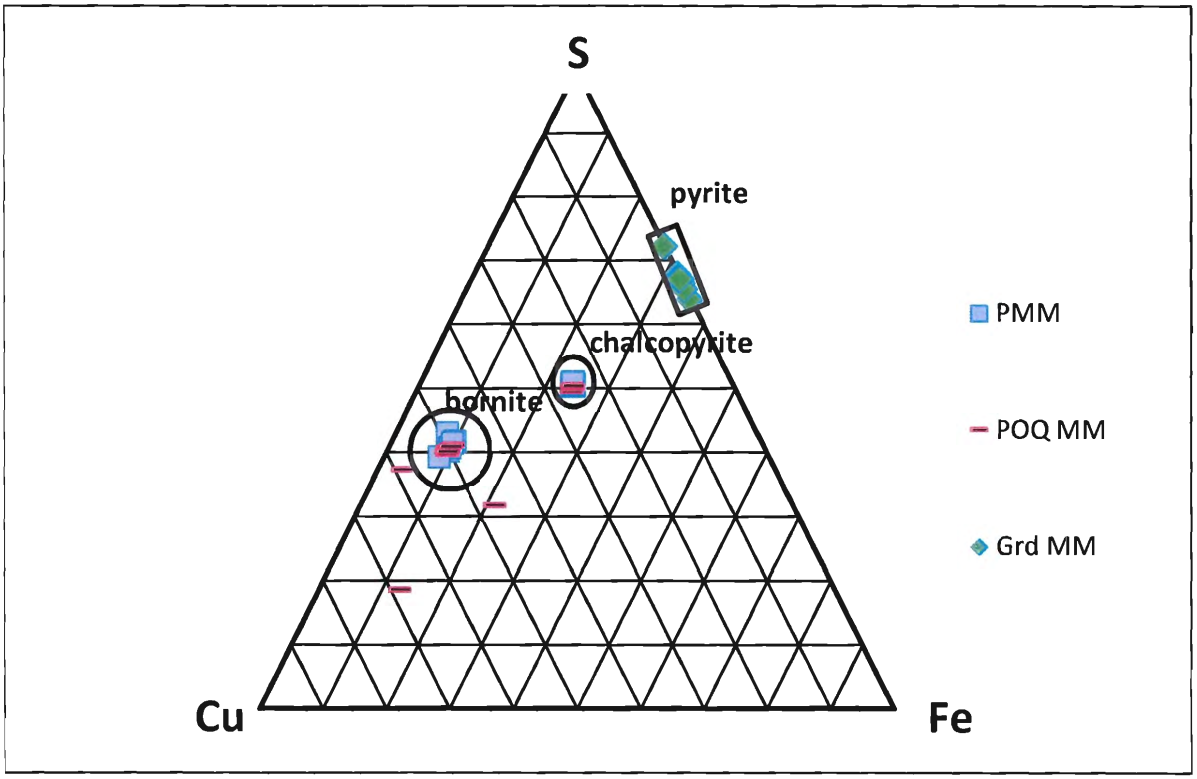


**Figure 4.8** Geochemical fields of three sulphide minerals were superimposed on this ternary diagram in order to classify the result from EMP analysis.

| Sulphide Mineral | Proportion in MM Porphyry | Proportion in MM Granodiorite | Proportion in MM Quartz Porphyry |
|---|---|---|---|
| Chalcopyrite | 71% | 0% | 37% |
| Bornite | 29% | 0% | 63% |
| Pyrite | 0% | 100% | 0% |

**Table 4.6** The proportions of chalcopyrite, bornite and pyrite found in the EMP analysis of the MM Porphyry, the MM Granodiorite and the MM Quartz Porphyry.

*Discussion*

The proportion of chalcopyrite and bornite in the MM Quartz Porphyry and in the MM Porphyry is typical of potassic alteration as well as A-type and B-type veining. It is interesting that the MM Granodiorite contains only pyrite and no chalcopyrite or bornite. Optical microscopic observations confirm this finding. The EMP results of the feldspars in Chapter 4.2.2. indicate that the unit has undergone secondary alteration and thus, the pyrite is likely a result of that alteration. It is probable that the MM Granodiorite has undergone chloritic alteration, distal to mineralization (Propilytic; Sillitoe 2010), and is consistent with a passive role of the MM Granodiorite as host to mineralizing porphyries.

# CHAPTER 5: GEOCHEMISTRY

A whole-rock geochemical analysis was done on the MMH deposit in order to gain insight into the primary geochemical signatures of the lithological units within the deposit as well as the entire MMH deposit itself. The elements and compounds that were analyzed for were: MnO, $Al_2O_3$, $Fe_2O_3$, MgO, CaO, $Na_2O$, $TiO_2$, $P_2O_5$, Au, Ag, As, Ba, Be, Bi, Br, Cd, Co, Cr, Cs,Cu, Ga, Ge, Hf, Hg, In, Ir, Mo, Nb, Ni, Pb, Rb, S, Sb, Sc, Se, Sn, Nb, Sr, Ta, Th, U, Y, Zr, La, Ce, Pr, Nd, Sm, Eu, Gd, Dy, Tb, Dy, Ho, Yb, Er, Tl, Tm and Lu. This geochemical analysis also allows for comparisons between the MMH deposit and the other Eocene-Oligocene porphyry deposits within the Chuquicamata district and northern Chile.

## 5.1 Analytical Methods

Samples from drillcore (Table 4.1) were selected as representative by consultation with MMH personnel, and were collected by M. Zentilli at the core repositories of CODELCO Norte in 2010. All samples were cleaned to avoid oxidation or staining, and trimmed using a diamond saw to eliminate excessive veining or alteration. Saw marks were then removed using inert grinding materials on a glass plate, washed with distilled water, dried, and packed in individual plastic bags.

Samples were sent by courier to Activation Laboratories Ltd. in 1336 Sandhill Drive, Ancaster, Ontario, L9G 4V5 Canada. The rocks were all prepared according to Code RX2: crushed and pulverized with mild steel, considered best for low contamination. Analyses were performed following Codes 4E-XRF and 4E-ICP/MS using research grade analytical procedures, plus S was analyzed by infrared methods.

Analytical results are shown in appendix 4. The elements Ga, Pb, Sn, Nb and Rb were analyzed using pressed pellet XRF (X-ray fluorescence) to achieve best detection limits and accuracy. Some elements, such as Rb, have been analyzed by 2 methods (see Fig.. 5.1, vertical axis PP-XRF (pressed-pellet X-ray fluorescence) horizontal axis FUS-MS (fusion mass spectrometry). In general the results are very similar, except for values at the low and high end of compositions. In the case of Rb, the method preferred is XRF.

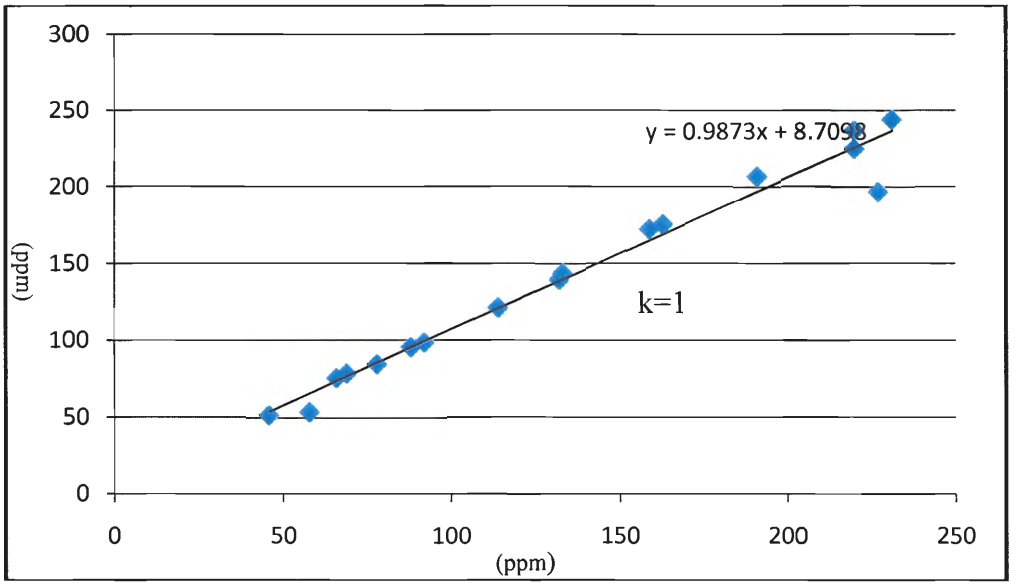


**Fig 5.1** This table shows the results of two different analytical methods preformed on the same samples for one element. The X-axis shows the FUS-MS results and the Y-axis shows the PP-XRF results. The resulting linear correlation indicates that the two methods gave similar results.

The results obtained for international standards analyzed are indicated in appendix 3 and can be used to assess accuracy, and duplicates were run (ZMMH 15Q and 17Q) to give information on precision (reproducibility).

The following information about the preparation of samples for whole-rock geochemical analysis was taken from the ACTLAB website:

http://www.actlabs.com/page.aspx?menu=74&app=244&cat1=595&tp=2&lk=no

$SiO_2$, $Al_2O_3$, $Fe_2O_3$, MgO, MnO, CaO, $TiO_2$, $Na_2O$, $K_2O$, $P_2O_5$, Ba, Be, Bi, Cs, Ga, Ge, Hf, In, Mo, Nb, Rb, Sn, Sr, Ta, Th, U, V, Y, Zr, La, Ce, Pr, Nd, Sm, Eu, Gd, Tb, Dy, Ho, Er, Tl, Tm, Yb and Lu were analyzed by the MS-ICP/FUS-MS method. Samples were prepared in batches and mixed with a flux of lithium metaborate and lithium tetraborate. The batches were then fused in an induction furnace. Afterwards, the melt was poured into a solution of 5% nitric acid and mixed until dissolved. Desired major oxides and trace elements were tested for using a Thermo Jarrell-Ash ENVIRO II ICP (www.actlabs.com).

Cd, Cu, Ni, Pb, S and Zn were tested for using Total Digestion ICP (TD-ICP). A 0.25 g aliquot of the sample was digested with $HClO_4$, $HNO_3$, HCl and HF at 200°C until fuming and was then diluted with aqua regia. This method is used for elements contained in magnetite, choromite, barite, spinels and massive sulphides (www.actlabs.com).

Au, Ag, As, Br, Co, Cr, Hg, Ir, Sb, Sc, Se, W and Zn were tested for using instrumental neutron activation analysis (INAA). Samples were prepared using 1 g aliquots encapsulated in a polyethylene vial. The samples were irradiated with flux wires at a thermal neutron flux and then left for 7 days to allow for the Na-24 to decay. The decay-corrected activities were then compared to a certified international reference calibration (www.actlabs.com).

Ga, Pb, Sn, Nb and Rb were tested for using PP-XRF. Analyses were done on 6 g pressed powder pellets from each sample. The mass absorption coefficient was found by measuring the Compton scatter of the Rh-tube and corrections were made for the background and mass absorption (www.actlabs.com).

## 5.2 Major Elements

The $SiO_2$ values for the MMH deposit lie between 55 and 79 wt%. Generally, the MM Porphyry is less felsic than the MM Quartz Porphyry. Using classification from Rickwood (1989) and Le Maitre et al. (1989) in figure 5.2, rock compositions for the MMH deposit plot in the medium to high K calc alkaline field (Fig. 5.2). Three samples from the MM Porphyry and one sample from each of the MM Quartz Porphyry and MM Granodiorite plot in the shoshonite series field.

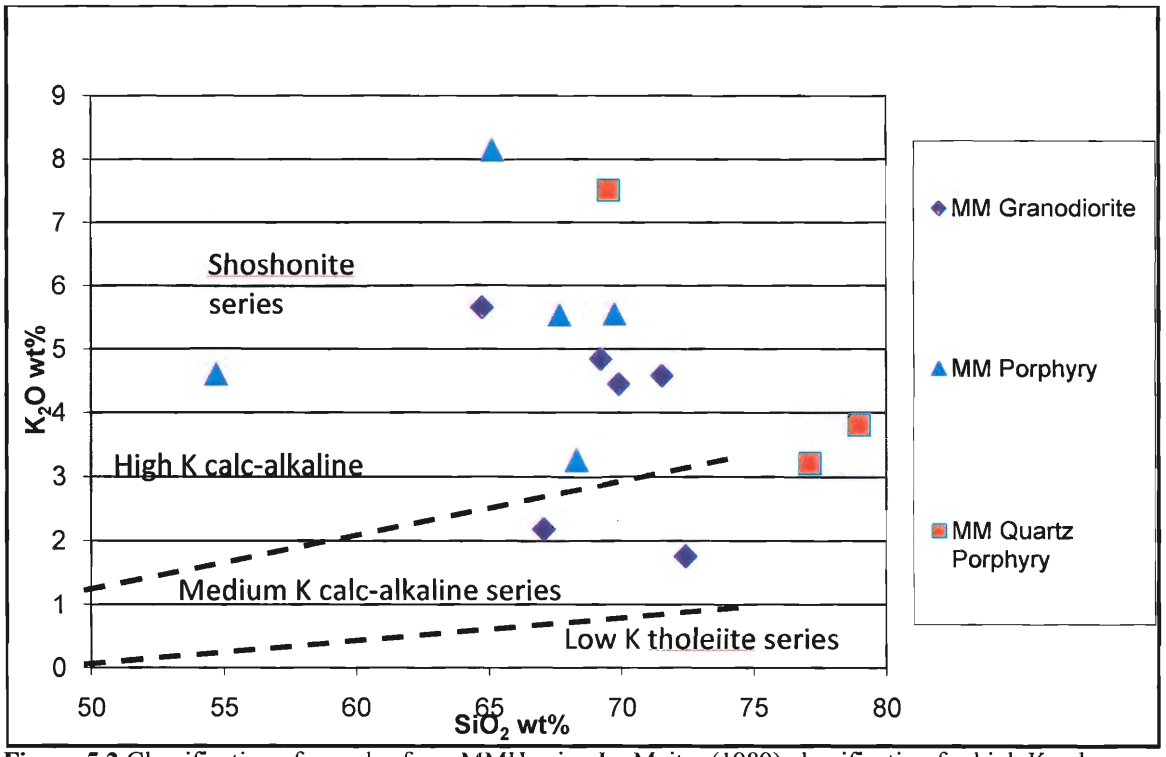


**Figure 5.2** Classification of samples from MMH using Le Maitre (1989) classification for high K calc-alkaline series, medium K calc-alkaline series and low K tholeiite series as well as Rickwood (1989) classification for shoshonite series. The high $K_2O$ values are most likely due to potassic alteration.

$SiO_2$ content vs. major element plots are shown in Fig. 5.3. These diagrams show that $Al_2O_3$, MnO, MgO and $P_2O_5$ have a general trend of decreasing with increasing $SiO_2$. This type of trend is indicative of major element fractionation into solid phases during the crystallization process. Deviations from a straight-line curve are likely due to secondary alteration processes that have affected concentrations of the relatively mobile elements.

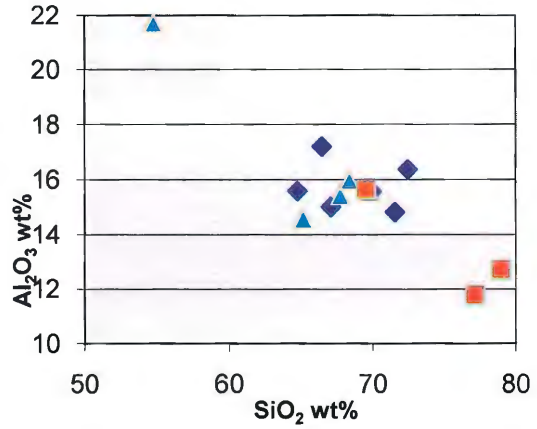
22
20
18
16
14
12
10
$Al_2O_3$ wt%
50
60
70
80
$SiO_2$ wt%

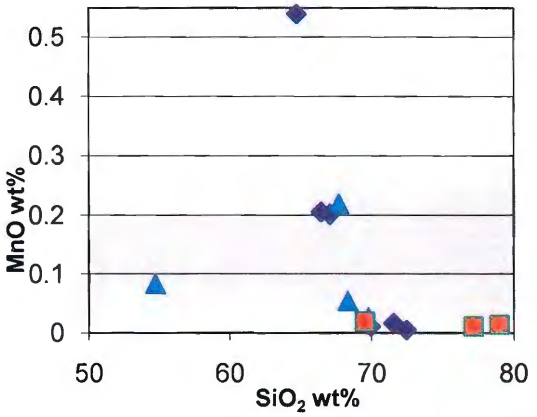
0.5
0.4
0.3
0.2
0.1
0
MnO wt%
50
60
70
80
$SiO_2$ wt%

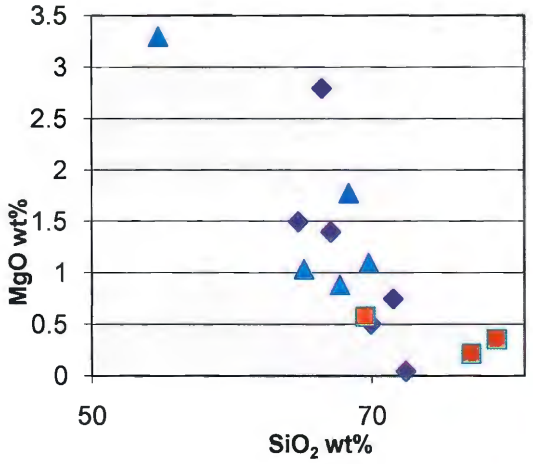
3.5
3
2.5
2
1.5
1
0.5
0
MgO wt%
50
70
$SiO_2$ wt%

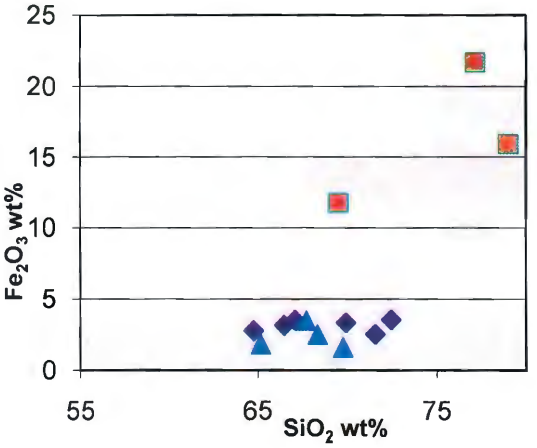
25
20
15
10
5
0
$Fe_2O_3$ wt%
55
65
75
$SiO_2$ wt%

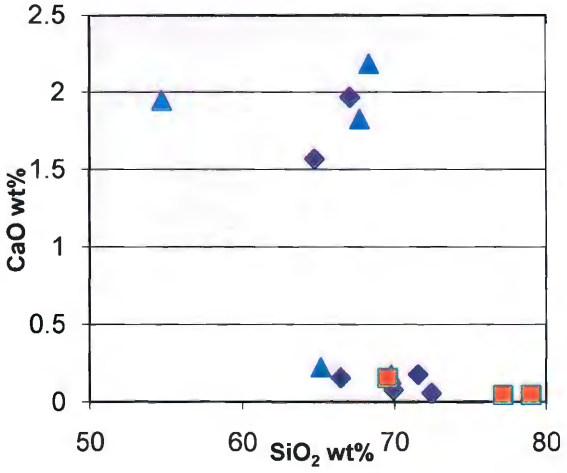
2.5
2
1.5
1
0.5
0
CaO wt%
50
60
70
80
$SiO_2$ wt%

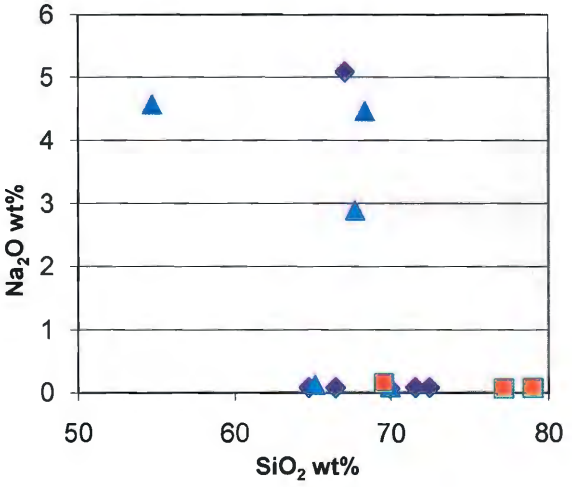
6
5
4
3
2
1
0
$Na_2O$ wt%
50
60
70
80
$SiO_2$ wt%

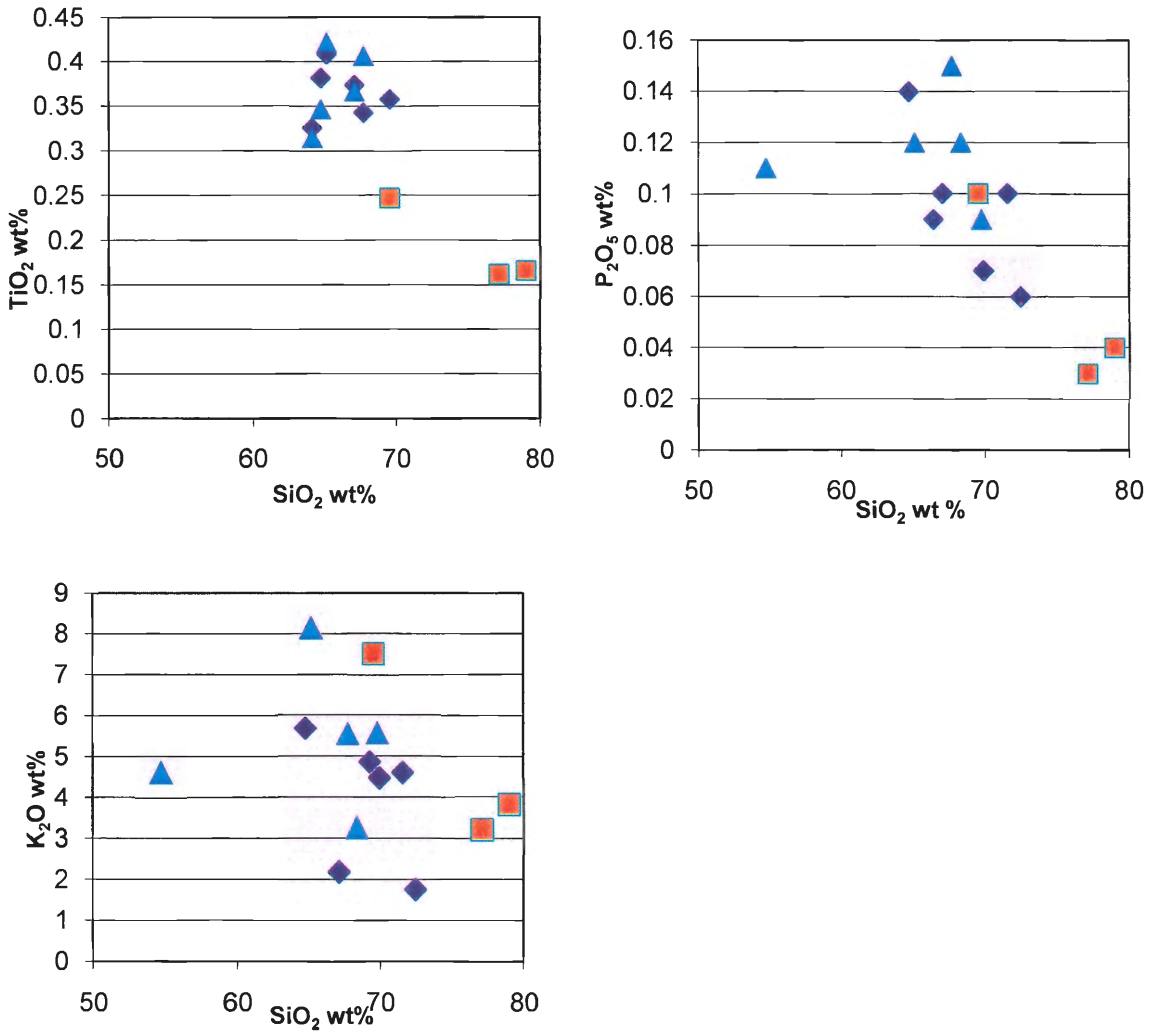


**Fig 5.3** Variation diagrams of major elements plotted for MM Granodiorite, MM Porphyry and MM Quartz Porphyry. Legend same as Fig. 5.2

The alkali-oxide ($Na_2O$ and $K_2O$) vs. $SiO_2$ and CaO vs. $SiO_2$ show irregular trends. This is likely due to redistribution of these elements during the highly acidic hydrothermal alteration processes that affected the MMH deposit such as potassic and phyllic alteration.

Like the $Fe_2O_3$ vs. $SiO_2$ plot, the $TiO_2$ vs. $SiO_2$ plot shows that the MM Granodiorite unit and the MM Porphyry fall into almost identical geochemical fields. Ti is a very immobile element and thus, the nearly identical geochemical field of MM

Granodiorite and MM Porphyry is indicative that the two units formed under similar geochemical conditions.

The $SiO_2$ vs. $Fe_2O_3$ relationship is similar for MM Granodiorite and MM Porphyry samples whereas the MM Quartz Porphyry has a much higher content of Fe.

**5.3 Trace Element Geochemistry**

Trace element geochemistry is more effective in evaluating the primary igneous traits of MMH than major element geochemistry. This is because the trace elements are less likely to be affected by hydrothermal alteration processes. Samples from MM Porphyry and MM Quartz Porphyry were plotted on a Winchester & Floyd (1977) volcanic/sub-volcanic classification diagram (Fig. 5.4) to determine which rock types they are classified as. This classification diagram uses relatively immobile trace elements (Zr, $TiO_2$, Nb and Y) which are useful for classification of rocks which have undergone hydrothermal alteration. From Fig. 5.4 we can see that the MM Porphyry (PMM) and the MM Quartz Porphyry (POQ MM) fall into the andesite and rhyodacite fields. The MM Granodiorite on the Winchester & Floyd (1977) diagram plots in the andesite field. It is not clear why two samples of Grd MM plot in the alkaline field.

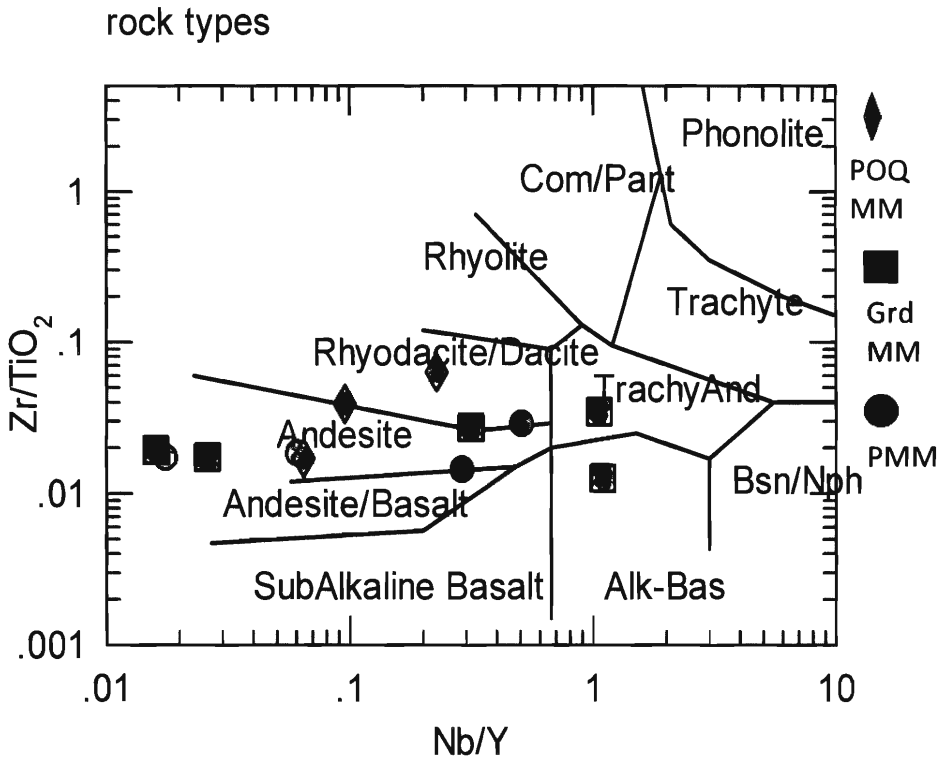


**Fig 5.4** Discrimination diagram for volcanic rocks after Winchester & Floyd (1977) was used to classify the sub-volcanic MM Porphyry (PMM) and MM Quartz Porphyry (POQ MM) units of the MMH deposit. The MM granodiorite was also included in this classification diagram (Grd MM)

The rock/chondrite diagram in Figure 5.5 shows concentrations of trace element relative to the primitive mantle source. Figure 5.5 shows that the MM Porphyry, the MM Granodiorite and the MM Quartz Porphyry have almost identical enrichment patterns. This indicates that the units formed under almost identical geochemical conditions with respect to trace elements. This is indicative that the units have originated from the same parental magma source.

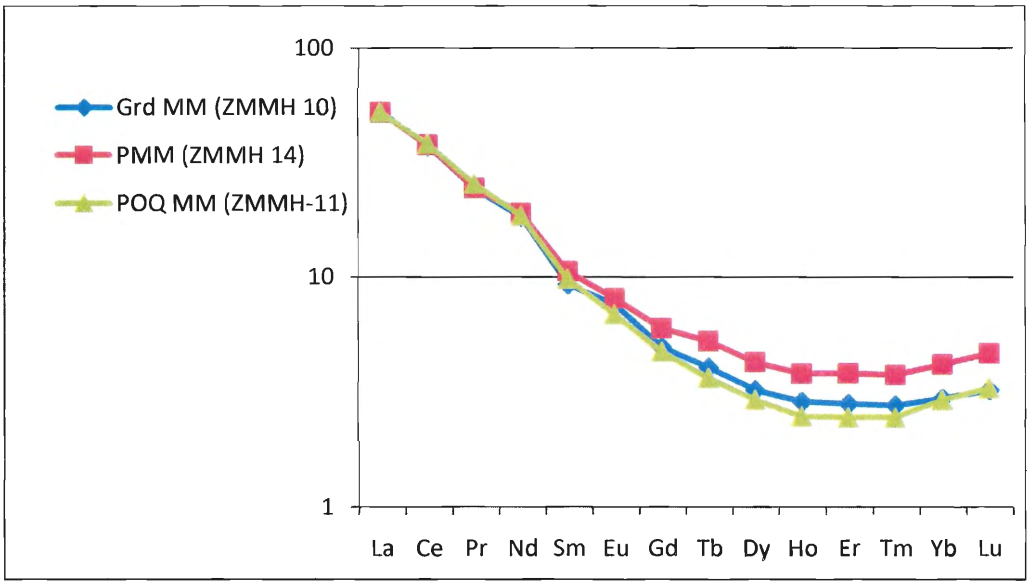


**Figure 5.5** Chondrite-normalized REE plot shows enrichment in incompatible REE. Sample ZMMH-10 was used to represent the MM Granodiorite, ZMMH-14 was used to represent the MM Porphyry and ZMMH-11 was used to represent the MM Quartz Porphyry. The curves suggest the both the Triassic and Eocene magmas experienced hornblende fractionation.

Adakites were discussed in Chapter 2. As was mentioned, adakitic geochemical signatures, especially high Sr/Y and La/Yb ratios ($\geq$ 20) are important in exploration as many of the world's major porphyry Cu deposits have adakitic composition. As shown in table 5.1, many of the Sr/Y and La/Yb ratios from the various lithologies in MMH do not fully meet the adakitic classification levels. Within each lithology, less than half of the samples have both the Sr/Y ratio and La/Yb ratio $\geq$ 20

| Sample | Lithology | Sr/Y | La/Yb |
|---|---|---|---|
| ZMMH 05Q | Grd MM | 15 | 38 |
| ZMMH 23Q | Grd MM | 1 | 17 |
| ZMMH 17Q | Grd MM | 4 | 16 |
| ZMMH 18Q | Grd MM | 31 | 20 |
| ZMMH 20Q | Grd MM | 19 | 21 |
| ZMMH 10Q | Grd MM | 41 | 27 |
| ZMMH 07Q | PMM | 41 | 33 |
| ZMMH 09Q | PMM | 15 | 19 |
| ZMMH 15Q | PMM | 29 | 23 |
| ZMMH 21Q | PMM | 7 | 23 |
| ZMMH 14Q | PMM | 46 | 19 |
| ZMMH 11Q | POQ MM | 26 | 27 |
| ZMMH 12Q | POQ MM | 8 | 19 |
| ZMMH 13Q | POQ MM | 8 | 23 |

**Table 5.1** The values of Sr/Y and La/Yb for each individual sample from MMH. The shaded boxes indicate ratio values that do not fall into the adakitic geochemical signature

Figure 5.6 is a classification diagram by Baldwin & Pearce (1982) for productive vs. non-productive porphyries. Through an empirical study they found that porphyries with low Mn and Y were more likely to be productive than those with higher values. The application of this diagram to data from MMH indicates that the data from the MM Quartz Porphyry falls into the productive field, most of the data from the MM Porphyry falls into the sub-productive field and the data from the MM Granodiorite is split between the productive field and the non-productive field.

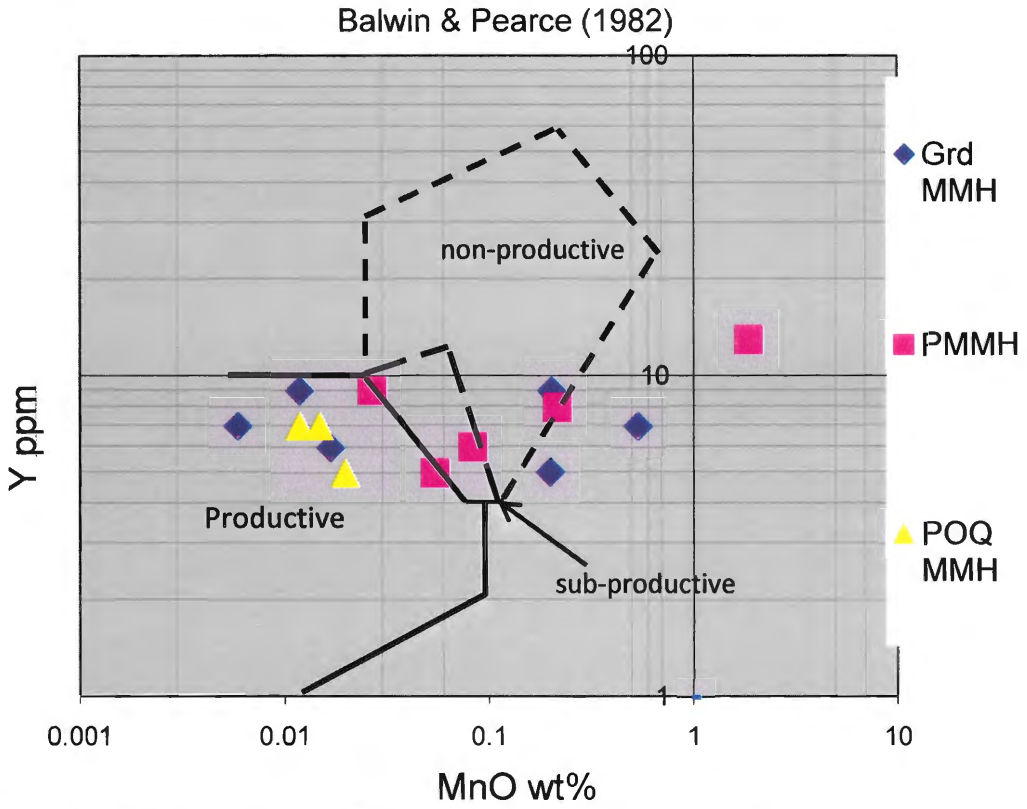


**Figure 5.6** Baldwin and Pearce (1982) classification diagram of productive vs. non-productive copper porphyries.

X-Y plots of trace elements vs. $SiO_2$ were used for comparison of the trace element values within the three lithologic units at MMH (Fig. 5.7). Figure 5.8 is a Zr vs. $TiO_2$ plot for MM Granodiorite, MM Porphyry and MM Quartz Porphyry. Zr and $TiO_2$ were used in this plot as they are both incompatible elements which are highly resistant to the type of highly acidic hydrothermal alteration that these samples have been subjected to. The findings from this comparison show that the values from MM Granodiorite and MM Porphyry fall into the same geochemical fields. In the trace element vs. $SiO_2$ plots, the MM Quartz Porphyry has similar trace element values as the MM Granodiorite and the MM Porphyry however, two of the samples have a higher proportion of $SiO_2$. This is expected as it was observed earlier that the MM Quartz Porphyry is much more felsic than the other two units and thus, has a higher proportion of quartz and lesser values of

most other minerals that would contain trace elements. In the Zr vs. $TiO_2$ plot, the MM Quartz Porphyry plots in a separate field that MM Granodiorite and MM Porphyry (Fig. 5.8). Again, this is likely due to the more felsic nature of the unit.

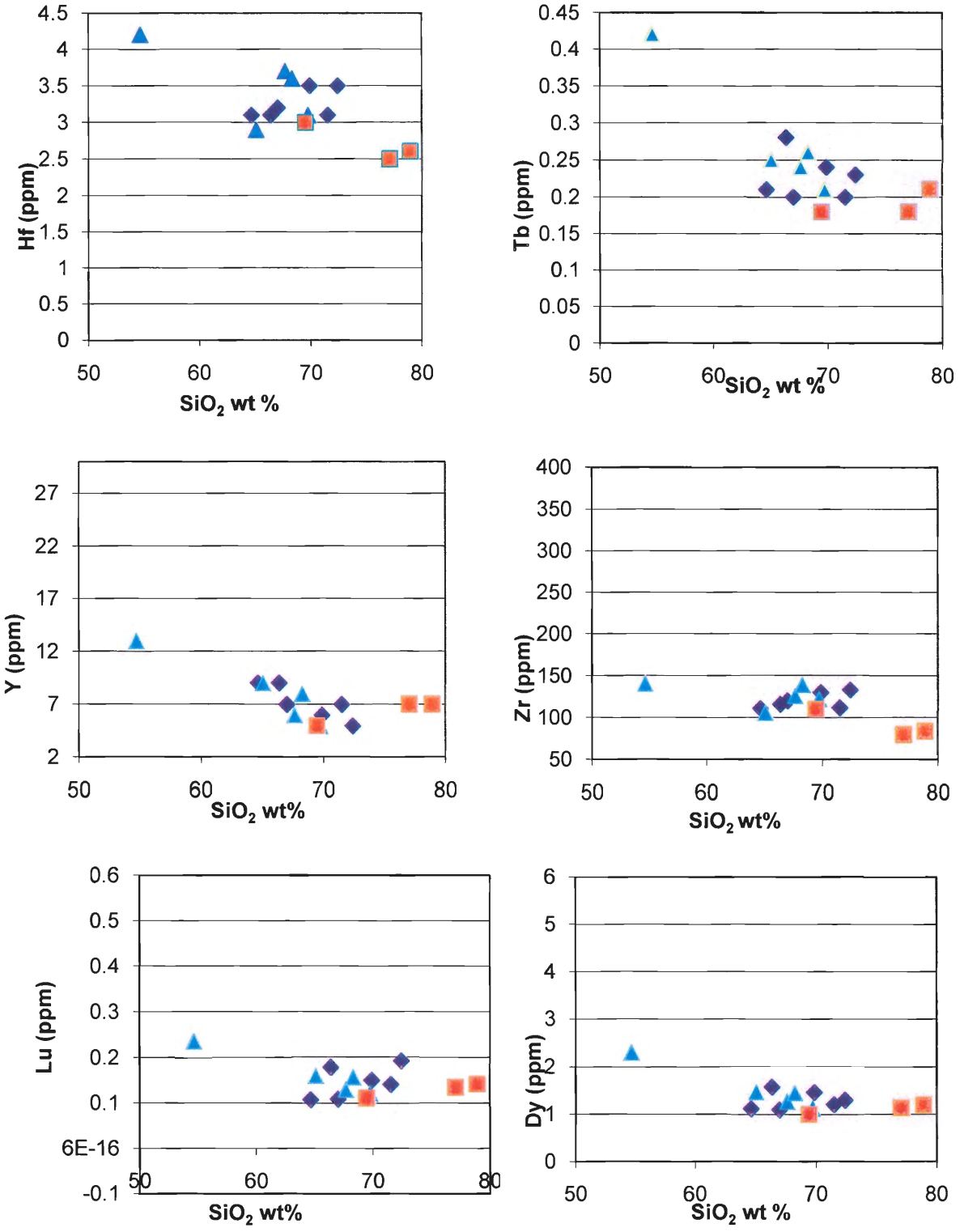


**Figure 5.7** $SiO_2$ wt% vs. trace elements plot containing values from MM Granodiorite, MM Porphyry and MM Quartz Porphyry. The legend for these diagrams are the same as Fig. 5.3 and 5.8

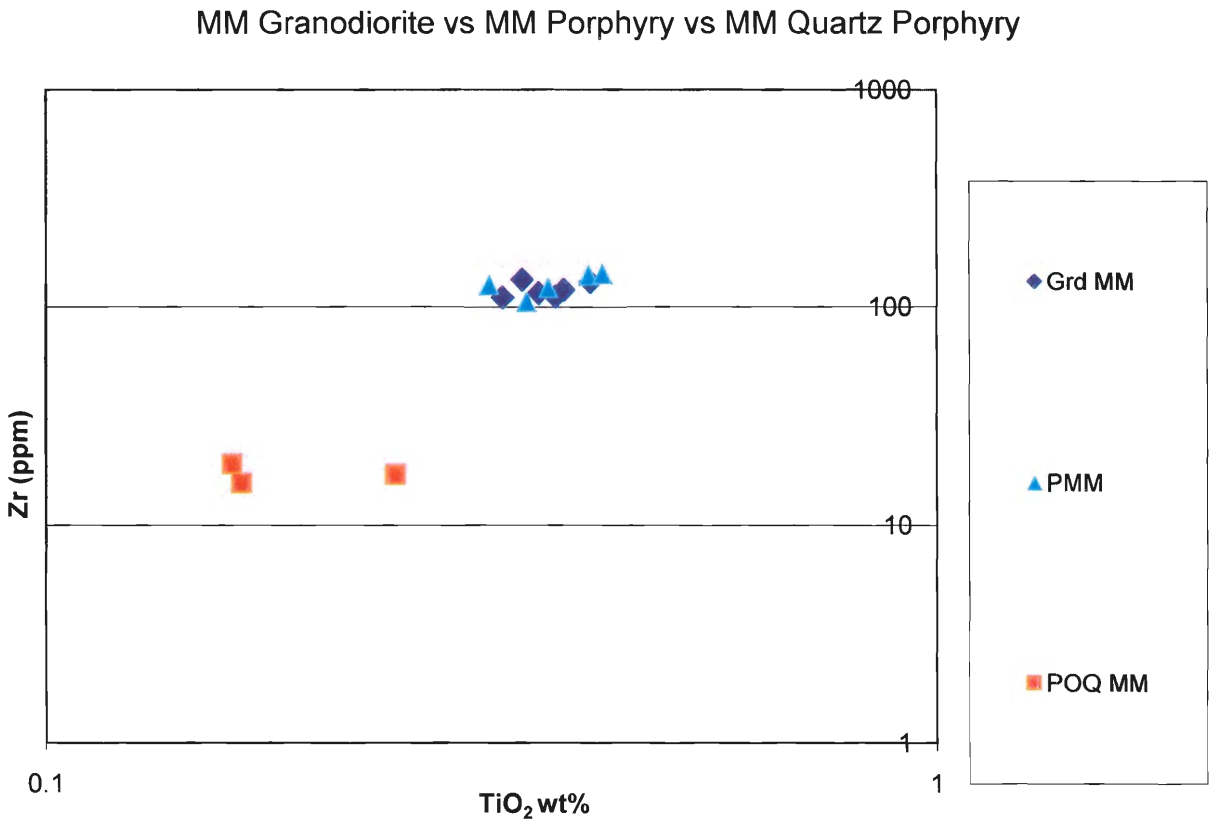


**Figure 5.8** Comparison of the Zr and $TiO_2$ values between the MM Granodiorite (Grd MM), MM Porphyry (PMM) and the MM Quartz Porphyry (POQ MM). To emphasis the spatial arrangement of the data values, the X and Y axis of this plot are log-scale.

## 5.4 Comparisons with other Intrusive Complexes in the Region

Geochemical comparisons between MMH, Chuquicamata, El Abra and Fortuna were done by comparing the data from various units within the deposits in trace element geochemical plots.

Figure 5.9 compares the geochemistry of intrusive units within the Chuquicamata Intrusive Complex (CIC) with the units of MMH. The points denoted EsteK, EsteSer and Este 2 were all taken from the Este Porphyry (see Chapter 3). For the samples Banco 2 and Este 2 the whole rock geochemistry was done together with the MMH samples in this study. The rest of the data from Chuquicamata is from from Arnott (2003). Ester (a

representative sample of Este Porphyry), Este 2 (ditto.), Este K (potassically altered Este porphyry) and Banco2 plot within the same compositional field as data from MMH. EsteSer (Este Porphyry in the Q-Ser alteration zone), Banco and Fiesta plot outside of the MMH compositional field.

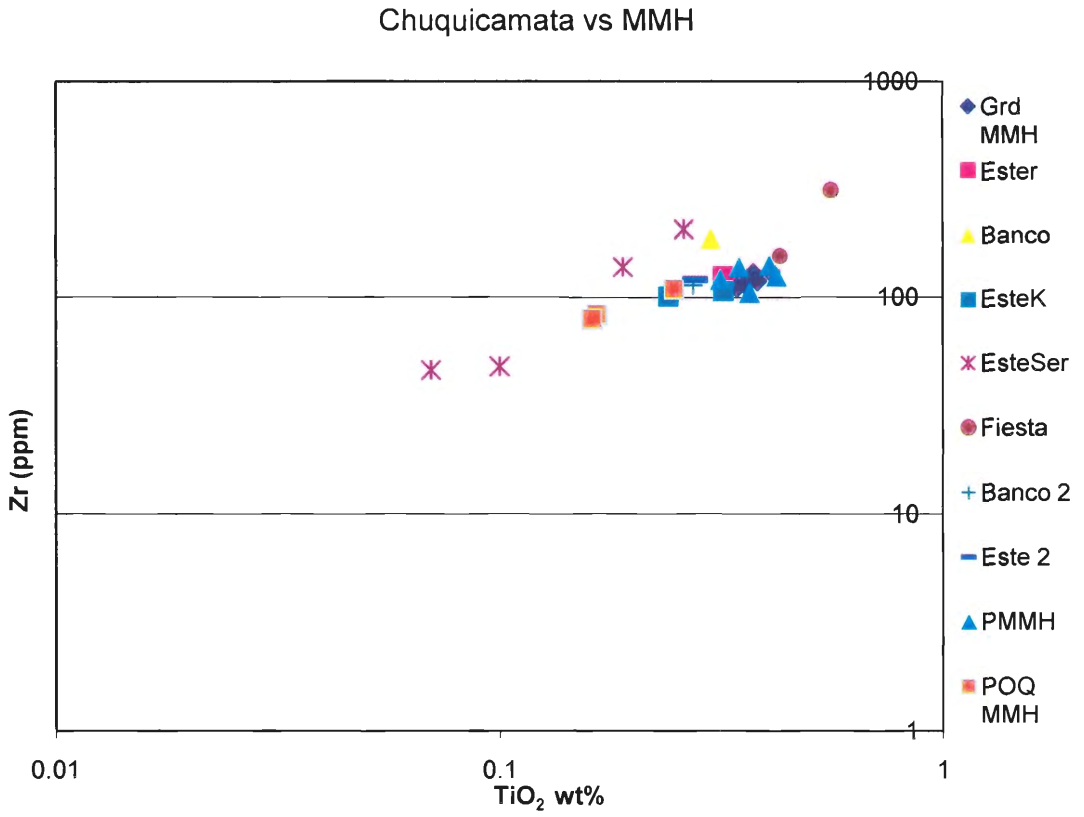


**Figure 5.9** Comparison of intrusive rocks from the Chuquicamata mine with the MMH deposit using a $TiO_2$ vs. Zr diagram. Ester, Banco, EsteK, EsteSer, Fiesta, Banco 2 and Este 2 are all part of the Chuquicamata Intrusive Complex (CIC). Data from the CIC comes from Arnott (2003) except for Banco 2 and Este 2 which were analyzed along with the MMH samples.

Figure 5.10 compares the geochemistry of units from within the El Abra Intrusive Complex to those from MMH. The Zr and $TiO_2$ values from the El Abra Apolo Leucogranite and the El Abra Mine Porphyry show a strong correlation with those from the MM Granodiorite and the MM Porphyry. Values from the El Abra Aplite have similar $TiO_2$ values but show Zr values higher than the rest of the units.

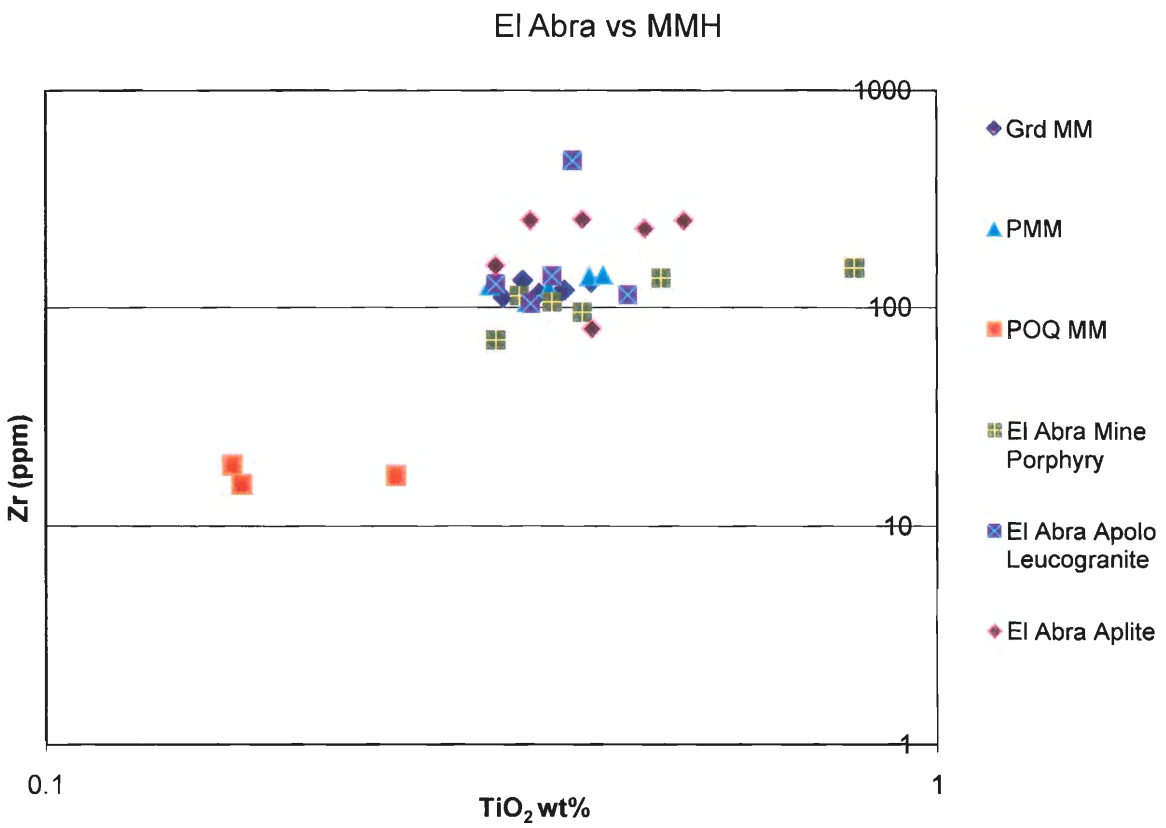


**Figure 5.10** Comparison of intrusive rocks from the El Abra Intrusive Complex and MMH using a Zr vs. $TiO_2$ plot. Data for El Abra from Ballard (2001).

Fig 5.11 compares the geochemistry of San Lorenzo Porphyry and the Fortuna Leucocratic Intrusion to that of the lithologic units within MMH. The Zr and $TiO_2$ values from the San Lorenzo Porphyry show a strong correlation with those from the MM Granodiorite and MM Porphyry. The geochemical field from the Fortuna Leucrocratic Intrusion encompasses the MM Granodiorite and MM Porphyry but has much more variability in terms of $TiO_2$ values.

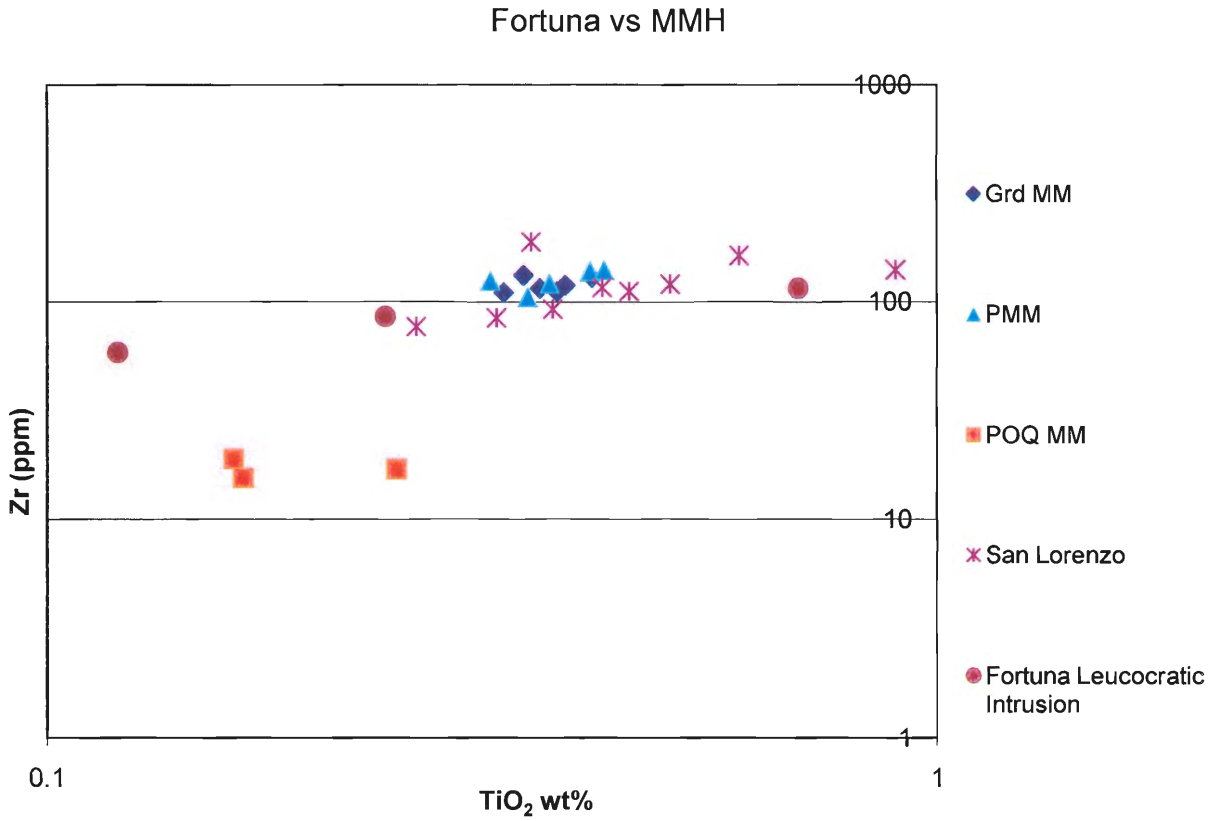


**Figure 5.11** Comparison between the Fortuna Igneous Complex and MMH on a Zr vs. $TiO_2$ plot. Data from Fortuna is from Ballard (2001).

## 5.5 Discussion

The major element geochemical data from MMH is less a reflection of igneous geochemical character and more a reflection of hydrothermal alteration processes. Taking this into consideration, the Le Maitre (1989) and Rickwood (1989) classification diagram shown in Fig. 5.2 may not indicate that many of the samples are shoshonite/high K calc-alkaline rocks but that these samples underwent potassic alteration. While the $SiO_2$ wt% vs. major element vaguely follow the fractional crystallization model, deviations from that trend are indicative of hydrothermal alteration.

The classification of the samples from MMH as andesite and rhyodacite is typical of sub-volcanic rocks within this region of the Andes. On the topic of adakite classification, the conclusion is not as clear. The results show that within each lithologic

unit, less than half of samples have both Sr/Y and La/Yb ratios that meet the adakitic classification level ($\geq 20$). Considering, however, that some of the ratios do meet the adakite standard, it is fair to say that the composition of Triassic MM Granodiorite, and the Eocene MM Porphyry and MM Quartz Porphyry are similar to adakites or sub-adakitic.

The $SiO_2$ wt % vs. trace element diagrams all indicate that the MM Granodiorite and the MM Porphyry have very similar trace element geochemistry. This is further supported with similar results in the Zr vs. $TiO_2$ diagram (Fig. 5.8), the $TiO_2$ vs. $SiO_2$ and $Fe_2O_3$ vs. $SiO_2$ (Fig. 5.3) and the chondrite-normalized diagram (Fig. 5.5). Assuming that the immobile elements used in these comparisons are reflective of the geochemical conditions at crystallization, these findings indicate that there were geochemical and possibly tectonic similarities in the genesis of both the MM Granodiorite and the MM Porphyry. Strengthening this argument is the findings that half of the MM Granodiorite measurements plot in the productive field of the Baldwin & Pearce (1982) diagram (Fig. 5.6). This finding implies a connection between productive copper porphyry deposits and MM Granodiorite.

The result from the geochemical comparison between MMH and the Chuquicamata Intrusive Complex (CIC) is uncertain. Although the two units seem to be similar in their geochemistry, the results from the data obtained from Arnott (2003) as well as this study are not conclusive. For example, although the data from Este 2 and Este K plot within close range of the MMH units, EsteSer, which belongs to the same lithologic unit as the aforementioned, plots in its own distinguishable geochemical field; this result probably reflects the intense high sulphidation alteration (and hydration)

produced by the quartz-sericite phase in Chuquicamata (Ossandón et al. 2001). Because the Este Porphyry is established as the largest contributor of ore within the CIC, this unit is the most essential in terms of finding a geochemical match. The correlation between MMH and the Banco porphyry is inconclusive as one of the data points fits in the MMH geochemical field (Banco) whereas the other does not (Banco 2). Overall, the findings from this comparison indicate that the CIC and MMH lithological units are geochemically similar but it does not confirm a relationship.

The comparison between intrusive units from El Albra and MMH show that the El Abra Mine Porphyry and the El Abra Leucogranite plot in similar geochemical fields in the Zr vs. $TiO_2$ diagram as the MM Porphyry and the MM Granodiorite. The El Abra Aplite porphyry has similar $TiO_2$ values as the MM Porphyry and MM Granodiorite but higher Zr values. As discussed earlier in section 5.4, geochemical comparisons using Zr and $TiO_2$ are reflective of conditions during crystallization as Zr and Ti are both immobile elements. The correlation of the El Abra Mine Porphyry and the MM Porphyry is significant because both these units are considered to be the major contributors of ore in their respective deposits. This similarity indicates that El Abra and MMH formed under similar geochemical and possibly tectonic conditions.

As is the case with El Abra, the most prominent porphyry unit within the Fortuna Igneous Complex, the San Lorenzo Porphyry, falls into the same geochemical field as the MM Porphyry and MM Granodiorite. The geochemical field of the Fortuna Leucocratic Intrusion encompasses the data from the MM Porphyry and MM Granodiorite but is much more variable in its proportion of $TiO_2$. This comparison between the Fortuna

Igneous Complex and MMH indicates that the two units formed under similar geochemical and possibly tectonic conditions.

# CHAPTER 6: DISCUSSION AND CONCLUSIONS

Whole rock geochemical analysis and petrographic analysis have proven effective methods of evaluating the petrology of the MMH deposit. The trace element geochemical analysis has given insight into the igneous geochemical conditions that existed before the hydrothermal alteration overprint. This analysis allows for comparison of lithologic units within the MMH deposit as well as comparisons between MMH and other deposits in the region. Due to the tectonic implications of the West Fault (ie truncation of major ore deposits), these geochemical comparisons can be used as a tool to correlate deposits that may have been cogenetic. The major element geochemical analysis, the EMP analysis as well as the optical microscopy have been instructive on both the primary igneous conditions of the deposit as well as the subsequent hydrothermal alteration processes.

A trace element geochemical comparison was done between the lithologic units within the MMH deposit to see if the units had distinct geochemical signatures. The results showed that while the MM Quartz Porphyry has a different compositional field from the MM Porphyry and the MM Granodiorite. These two units overlapped and thus they are not distinguishable using trace element geochemistry. This finding implies a petrologic and tectonic connection between the two units which is unusual since the MM Granodiorite has been dated as Triassic (237-222 Ma) (Boric et al. 2009) and the MM Porphyry has been dated as 39 Ma (Eocene; Boric et al. 2009). There are two possible explanations for this coincidence: 1) there was an error in the logging of the core and the samples obtained all belong to the MM Granodiorite, and 2) the MM Granodiorite formed under extremely similar petrologic/tectonic conditions as the MM Porphyry .

Logging nomenclature at MMH has evolved over more than 2 decades by very competent geologists, and consists of two stages: a first fast logging preceding splitting and sampling for grade and physical properties, and a second, more careful logging with analytical data on hand. It is however possible that where the largely barren (unmineralized) host MM Granodiorite starts to show extensive veining, alteration and mineralization, the geologists needed to describe a new rock type. Locally, the alteration can develop large feldspar crystals, silicified rock can look like quartz phenocrysts, and the crosscutting veins characteristic of porphyry deposits led to the designation of the rock as porphyry. Thus it is possible that an alteration overprint caused what was primarily MM Granodiorite to be called MM Porphyry. Although this scenario is plausible, the petrographic evaluation conducted on the MMH samples (Chapter 4) indicate that the MM Porphyry and the MM Granodiorite are distinctive rock types with independent primary igneous features. Definite evidence is the drastic difference between the preserved calcic plagioclase (oligoclase-andesine) in MM Porphyry, compared to pure albite in MM Granodiorite. With this consideration, it is implausible that an error occurred in the logging.

In the very likely case that the samples obtained are true to the lithologic units they have been ascribed, the findings of this study imply that the MM Granodiorite formed under almost identical geochemical and tectonic conditions ~200 million years before MM Porphyry in the Triassic. The geochemical similarities between the MM Porphyry and the MM Granodiorite indicate that the MM Granodiorite could have shared a parental source at depth. As is suggested by the Baldwin & Pearce (1982) diagram, the common parental magma source may have been enriched in copper, or the petrogentic

conditions to form both magma suites were very similar. This implies that productive copper porphyries may have been produced in the Triassic. In this respect it is interesting to note that the Permo-Triassic basement contains metallic mineralization of Triassic age elsewhere in the region (e.g. Maksaev 1990; Camus 2003).

As stated in section 5.5, the results from this study show a relationship between MMH and Chuquicamata but do not indicate a cogenetic relationship. In following with the hypothesis of 35 km of sinistral displacement along the west fault, the location of MMH and Chuquicamata relative to each other indicate that MMH is not a "missing portion" of Chuquicamata. Furthermore, the earliest date for copper porphyry intrusion at Chuquicamata is the Este Porphyry at 34 Ma (see table 3.1), 5 My later than the emplacement of the MM Porphyry. The date of 34 Ma does however compare to the age of the MM Quartz Porphyry (Boric et al. 2009). This date relationship in combination with the geochemical correlation between Chuquicamata and the MM Quartz Porphyry indicates that these two units could have both been related to the same magmatic event and both may share a parental source at depth. This analogy has been used to explain the Late Oligocene-Early Eocene Cu-porphyry mineralization phenomena in the northern Chilean Andes (e.g. Sillitoe 2010).

Figures 5.10 and 5.11 show that geochemical fields of the porphyry units from MMH, Fortuna and El Abra overlap. Dilles et al. (1997) argue that El Abra and Fortuna are one cogenetic igneous complex that intruded 39-37 Ma and was subsequently divided and displaced during the 35 km of post mineralization sinistral displacement along the West Fault. The evidence from this geochemical study strengthens this argument and also indicates that MMH was part of this igneous complex. As discussed in chapter 3.2,

the MM Porphyry has been dated as 39 Ma (Boric et al. 2009). As seen in Fig. 1.1, the MMH deposit is very elongate. Although the main concentration of ore is in the southern region of the deposit, away from Fortuna, the MMH igneous complex extends north within close proximity to Fortuna. The age and location of the deposit together with the geochemical evidence from this study indicate the MMH could be closely linked to the Fortuna-El Abra cogenetic igneous complex, possibly even cogenetic.

The discovery that the MM Granodiorite of Triassic age (e.g. Boric et al. 2009) has characteristics indistinguishable from the Fortuna and El Abra igneous suite of Eocene age, leads to the conclusion that there might be something more than a simple spatial coincidence, and that the MM Granodiorite is not merely a passive host to the Tertiary porphyries. The question that arises is: what tectonic/petrologic conditions could have led to the generation of identical magmas in the Triassic and in the Eocene? The answer could have implications to possibly explain that both magma suites have a common source, either in the crust or mantle. A full discussion of this issue is out of the scope of this thesis, yet some analysis follows.

The existence of giant porphyry copper deposits in the Central Andes in northern Chile has traditionally been associated with the "Andean" orogenic cycle (e.g. Maksaev 1990; Sillitoe 2010), and "Andean" has generally implied Jurassic to Holocene, ca. 200 My, of which only the Eocene-Oligocene generated giant ore deposits of the likes of Chuquicamata and Escondida. However, copper and molybdenum mineralization, mostly in non-economic concentrations, is known to occur in the pre-Jurassic basement of the Domeyko Cordillera, and even CODELCO, the company that owns Chuquicamata and MMH has developed prospects of Triassic and Carboniferous age (e.g. Marquartdt et al.

1997). Several workers, among them Cornejo et al. (1997), have pointed out that directly south of Chuquicamata District and the town of Calama in the Sierra Limón Verde ( Lat. 22°30'- 24°S) the metamorphic basement is intruded by a volcano-plutonic complex of Permo-Carboniferous age, in turn intruded by Triassic, Cretaceous and Eocene plutons. At the Lila prospect, Cu-Mo mineralization is associated to hydrothermal alteration with K-Ar ages of 213 to 195 Ma (Marquardt et al., 1997; Camus, 2003), thus is similar to the Triassic-Jurassic like MM Granodiorite. North of Chuquicamata, Tomlinson et al., (2001) gives K-Ar ages of hydrothermal alteration in Cu-Mo mineralization in the Loa prospect as 223 ± 5 Ma for sericite and 239 ± 7 Ma for biotite (Triassic). More recently, Munizaga et al., (2006) have published (SHRIMP U-Pb) geochronological data that recognize Permian to Triassic magmatic activity, with the Triassic being associated with minor porphyry type Cu-Mo mineralization in the region of Collahuasi (lat. 20° to 22°S; Fig. 1.2) . This Permo-Triassic magmatism (Collahuasi Group) was generated before the "Andean" cycle, along the western margin of the Gondwana supercontinent, and is correlative with an extensive belt of volcanic and subvolcanic rocks throughout the main Andes of Chile, the Frontal Cordillera of Argentina (Choiyoi Group or Choiyoi Granite-Rhyolite Province), and the Eastern Cordillera of Peru. In fact all large porphyry coppers of Chile, including the Eocene-Oligocene in northern Chile, and the Neogene in central Chile, may have a basement that includes this Choiyoi complex. Zentilli et al. (1988) pointed out the remarkable similarity in lead isotopes of all porphyry copper deposits in Chile that suggested a common source for the magmas. If the same source region for the magmas was tapped in the Triassic and

the Eocene, the remarkable similarity between Triassic and Eocene igneous rocks can be explained.

# CHAPTER 7: FUTURE WORK

Although this study indicates the tectonic and compositional similarities between the MM Porphyry and MM Granodiorite as well as the cogenetic relationship between MMH, El Abra and Fortuna, there is still work that could be done to confirm these conclusions. For instance, a more thorough age evaluation of the MM Granodiorite and MM Porphyry would solve the question of whether or not MM Porphyry and MM Granodiorite are in fact distinct lithologic units that formed 250 My apart. Comparisons between MMH, El Abra and Fortuna using other evaluative methods such as isotope geochemistry could add to the hypothesis of cogenetic correlation between the three units. Finally, a more thorough investigation into the characteristics of Triassic plutonic rocks, specifically their potential as parental magma sources to Cu porphyries, could give insights into the Cu anomaly that exists in the northern Chilean Eocene-Oligocene magmatic arc.

As a first step, samples of representative lithologies should be collected and analyzed chemically, and U-Pb dating of zircons should be done from exactly the same rocks. This way, any differences and similarities between Triassic and Eocene rocks can be corroborated.

REFERENCES

Actlabs. 2010. 4E-exploration-INAA, total digestion-ICP, lithium Metaborate/Tetraborate fusion-ICP [online]. Available from http://www.actlabs.com/page.aspx?page=522&app=226&cat1=549&tp=12&lk=no&menu=64&print=yes [cited 03/14 2011].

Alvarez, O. and Miranda, M.J. 1991. Primeras consideraciones geológicas del yacimiento mansa mina. In 6th Congreso Geológico Chileno, Viña del Mar, Vol. 6, pp. 7.

Ambrus, W.J. 1979. Emplazamiento y mineralizacion de los porfidos cuperiferos de Chile. translated title: Emplacement and mineralization of the porphyry copper deposits of chile. Ph.D, Universidad de Salamanca, Spain.

Arnott, A.M. 2003. Evolution of the hydrothermal alteration at the Chuquicamata porphyry copper system, northern Chile. PhD, Dalhousie University, Halifax, Nova Scotia.

Ballard, J.R. 2001. A comparative study between the geochemistry of the ore-bearing and barren calc-alkaline intrusions. PhD, The Australian National University, Canberra, Australia.

Barra, F., Ruiz, M., Ryan, M., and Titley, S. 2002. A Re-Os study of sulfide minerals from the bagdad porphyry Cu-Mo deposit, northern Arizona, USA, Mineralium Deposita, 38: 585-596.

Boric, R., Diaz, J., Becerra, H., and Zentilli, M. 2009. Geology of the Ministro Hales Mine (MMH), Chuquicamata district, Chile. In Congresso Geologico Chileno, Santiago, Chile, Vol. 12, pp. 1-4.

Burnham, W.C. 1979. Magmas and hydrothermal fluids. In Geochemistry of Hydrothermal Ore Deposits Edited by H.L. Barnes. John Wiley & Sons, Inc., Toronto, pp. 107-123.

Camus, F. 2003. Geologica de los porfirico en los andes de chile. In Servico National de Geologiay Mineria, 267, Santiago, Chile, pp. 267.

Camus, F. and Dilles, J. 1997. A special issue devoted to porphyry copper deposit of northern Chile: Preface, Economic Geology, 96: 233-237.

Candela, P.A. and Piccoli, M. 2005. Magmatic processes in the development of porphyry-type ore systems, Economic Geology, 100: 25-37.

Castillo, P.R. 2006. An overview of adakite petrogenesis, Chinese Science Bulletin, 51: 257-268.

Camus, F. and Dilles, J. 1997. A special issue devoted to porphyry copper deposit of northern Chile: Preface, Economic Geology, 96: 233-237.

Candela, P.A. and Piccoli, M. 2005. Magmatic processes in the development of porphyry-type ore systems, Economic Geology, 100: 25-37.

Castillo, P.R. 2006. An overview of adakite petrogenesis, Chinese Science Bulletin, 51: 257-268.

Corbett, G. 2009. Anatomy of porphyry-related Au-Cu-Ag-Mo minerlised systems: Some exploration implications. In Australian Institue fo Geoscientists North Queensland Exploration Conference, Queensland, Australia, Vol. 1, pp. 1-13.

Cornejo, P., Matthews, S., Marinovic, N., Perez de Arce, C., Bassa, M., Alfero, J., and Navarro, M. 1997. Alteración hidrothermal y mineralización recurrente de Cu y Cu-Mo durante el pérmico yel triásico en la cordillera de Domeyko (zona de Zaldívar-Salar de los morros): Antecedentes geocronológicas-U-pb, 40Ar/39Ar, re-os. In Congresso Geologico Chileno, Antofagasta, Vol. 2, pp. 219-222.

Deer, W.A., Howie, R.A., and Zussman, J. 1992. An introduction to the rock-forming minerals. Addison Wesley Longman Ltd, Essex, England.

Dilles, J.H., Tomlinson, A.J., Martin, M.W., and Blanco, N. ACTAS. El Abra and Fortuna complexes: A prophry copper batholith sinistrally displaced by the Falla Oeste, ACTAS, 3: 1883-1887.

Goldstein, J., Newbury, D., Joy, D., Lyman, C., Echlin, P., Lifshin, E., Sawyer, L., and Micheal, J. 2003. Scanning electron microscopy and X-ray microanalysis. Kluwer Academic Publishers, New York.

Guilbert, J.M. and Park, C.F. 1986. Porphyry copper deposits. W.H. Freeman and Company, New York.

Gustafson, L.B. and Hunt, J.P. 1975. The porphyry copper deposit at El Salvador, Chile, Economic Geology, 70: 857-912.

Le Maitre, R.W., Bateman, P., Dudek, A., Keller, J., Lameyre Le Bas, M.J., Sabine, P.A., Schmid, R., Sorensen, H., and Streckeisen, A. 1989. A classification of igneous rock and glossary terms. Blackwell, Oxford, UK.

Lindsay, D.D. 1997. Structural control and anisotrophy of mineralization within the Chuquicamata porphyry copper district, northern Chile. PhD, Dalhousie University, Halifax, NS.

Lowell, J.D. and Guilbert, J.M. 1970. Lateral and verticle alteration-mineralization zoning in porphyry ore deposits, Econoic Geology, 65: 373-408.

Maksaev, V. 1990. Metallogeny , geological evolution and thermochronology of the Andes between latitudes 21° and 26° south, and the origin of major porphyry copper deposits. PhD, Dalhousie University, Halifax, Nova Scotia.

Maksaev, V. and Zentilli, M. 1999. Fission track thermochronology of the Domeyko Cordillera, northern Chile: Implications for Andean tectonics and porphyry copper metallogenesis. , Exploration and Mining Geology, 8: 65-89.

Marquardt, J.C., Pizarro, J., Gomez, M., and Martinez, A. 1997. Prospecto Lila, descubrimiento de un porfido cuprifero triasico superior-jurasico inferior, en la cordillera de Domeyko, II region, Chile. In Congresso Geologico Chileno N 8 Actas, Antofagasta, Vol. 8, pp. 1048-1053.

McInnes, B., Farley, K., Sillitoe, R.H., and Kohn, B. 1999. Application of apatite (U-Th)/He thermochronometry to the determination and sense and amount of verticle displacement at the Chuquicamata porphyry depoist, Chile, Economic Geology, 94: 937-948.

Müller G., Quiroga J. (2003) Geology of the MM Copper Deposit, Chuquicamata District – An Update. *Actas, X Congreso Geológico Chileno*, Concepción.

Munizaga, F., Maksaev, V., Fanning, C.M., Giglio, S., Yaxley, G., and Tassinan, C.C.G. 2008. Late paleozoic-early triassic magmatism on the western margin of gondwana: Collahuasi area, northern chile, Gondwana Research, 13: 407-427.

Ossandón, G.C., Freraut, R.C., Gustafson, L.B., Lindsay, D.D., and Zentilli, M. 2001. Geology of Chuquicamata mine: A progress report, Economic Geology, 96: 249-270.

Proffett, J. 2008. Geologic report of the MM deposit: Chuquicamata district, Chile. Unpublished internal report for CODELCO.

Reynolds, P., Ravenhurst, C., Zentilli, M., and Lindsay, D. 1998. High-precision/dating of two consecutive hydrothermal events in the Chuquicamata porphyry copper system, Chile, Chemical Geology, 148: 45-60.

Reynolds, P., Ravenhurst, C., Zentilli, M., and Lindsay, D. 1998. High-precision $^{40}Ar/^{39}Ar$ dating of two consecutive hydrothermal events in the Chuquicamata porphyry copper system, Chile, Isotope Geoscience, 148: 45-60.

Richards, J.P. 2002. Discussion on "giant versus small prophyry copper deposits of Cenozoic age in northern Chile: Adakitic versus normal calc-alkaline magmatism by oyarzun et al. Mineralium Deposita, 37: 788-790.

Rickwood, P.C. 1989. Boundary lines within petrologic diagrams which oxides of major and minor elements, Lithos, 22: 247-263.

Sibson, R.H. 2001. Seismogenic framework for hydrothermal transport and ore deposition, Society of Economic Geologists Reviews, 14: 25-50.

Sillitoe, R.H. 2010. Copper porphyry systems, Economic Geology, 105: 3-41.

Sillitoe, R.H. 1973. The tops and bottoms of porphyry copper deposits, Economic Geology, 68: 799-815.

Sillitoe, R.H. and McKee, E.H. 1996. Age of supergene oxidation and enrichment in the Chilean porphyry copper province, Economic Geology, 91: 164-179.

Sillitoe, R.H., Marquardt, J.C., Ramiez, F., Becerra, H., and Gomez, M. 1996. Geology of the concealed MM porphyry copper deposit, Chuquicamata district, northern Chile. In Andean Copper Deposits: New Discoveries, Mineralization, styles and Metallogeny Edited by S. P. Citizen Printing Co., Fort Collins CO, pp. 59-68.

Sillitoe, R.H. and McKee, E.H. 1996. Age of supergene oxidation and enrichment in the Chilean porphyry copper province, Econoic Geology, 91: 164-179.

Sun, S.S. and McDonough, W.F. 1989. Chemical and isotopic systematics of oceanic basalts: Implications for mantle composition and processes. In Magmatism in ocean basins Edited by A.D. Saunders and M.J. Norry. Geological Society of America, , pp. 313-345.

Tobey, E.F. 2005. Interim report on mineralogy and geochemistry at Mansa Mina. Geovectra, Santiago, Chile. Confidential report for CODELCO.

Tomlinson, A.J. and Blanco, N. 1997. Structural evolution and displacement history of the West Fault System, Precordillera, Chile: Part 2, postmineral history, ACTAS, 3: 1878-1882.

Tomlinson, A.J., Blanco, N., Maksaev, V., Dilles, J., Grunder, A.L., and Ladino, M. 2001. Geologia de la Precordillera Andina de Quebra de Blanca-Chuquicamata regions I y II. Servicio National de Geologia y Mineria, Santiago.

Zentilli, M., Lindsay, D., and Graves, M.C. 1994. Geological investigations at the Mansa Mina deposit. Unpublished report for CODELCO by Cuesta Research Ltd., Halifax, NS.

Zentilli, M., Doe, B.R., and Hedge, L.E. 1988. Lead isotopes in porphyry copper deposits as compared with other Andean mineral deposits. In Chilean Geological Congress, Santiago, Vol. 1, pp. 13331-13369.

Zentilli, M., Graves, M., Lindsay, D., Ossandón, G., and Camus, F. 1995. Recurrent mineralization in the Chuquicamata porphyry copper system: Restrictions on genesis from mineralogical, geochronological and isotopic studies. In Proceedings of Conference

on Giant Ore Deposits: Controls on the Scale of Orogenic Magmatic-Hydrothermal Mineralization Edited by A.H. Clark. Queen's University, Kingston, Ont, pp. 86-100.

Actlabs. 2010. 4E-exploration-INAA, total digestion-ICP, lithium metaborate/Tetraborate fusion-ICP [online]. Available from http://www.actlabs.com/page.aspx?page=522&app=226&cat1=549&tp=12&lk=no&menu=64&print=yes [cited 03/14 2011].

Ambrus, W.J. 1979. Emplazamiento y mineralización de los pórfidos cupríferos de Chile. translated title: Emplacement and mineralization of the porphyry copper deposits of Chile. Ph.D, Universidad de Salamanca, Spain.

Arnott, A.M. 2003. Evolution of the hydrothermal alteration at the Chuquicamata porphyry copper system, northern Chile. PhD, Dalhousie University, Halifax, Nova Scotia.

Ballard, J.R. 2001. A comparative study between the geochemistry of the ore-bearing and barren calc-alkaline intrusions. PhD, The Australian National University, Canberra, Australia.

Barra, F., Ruiz, M., Ryan, M., and Titley, S. 2002. A Re-Os study of sulfide minerals from the Bagdad porphyry Cu-Mo deposit, northern Arizona, USA, Mineralium Deposita, 38: 585-596.

Boric, R. 2009. Geology of the Ministro Hales mine (MMH), Chuquicamata District, Chile. In Congreso Geologico Chileno, Santiago, Chile, Vol. 12, pp. 1-4.

Burnham, W.C. 1979. Magmas and hydrothermal fluids. In Geochemistry of Hydrothermal Ore Deposits Edited by H.L. Barnes. John Wiley & Sons, Inc., Toronto, pp. 107-123.

Camus, F. 2003. Geologica de los sistemas porfiricos en los Andes de Chile. In Servicio Nacional de Geologiay Mineria, 267, Santiago, Chile, pp. 267.

Camus, F. and Dilles, J. 1997. A special issue devoted to porphyry copper deposits of northern Chile: Preface, Economic Geology, 96: 233-237.

Candela, P.A. and Piccoli, M. 2005. Magmatic processes in the development of porphyry-type ore systems, Economic Geology, 100: 25-37.

Castillo, P.R. 2006. An overview of adakite petrogenesis, Chinese Science Bulletin, 51: 257-268.

Corbett, G. 2009. Anatomy of porphyry-related Au-Cu-Ag-Mo mineralised systems: Some exploration implications. In Australian Institute of Geoscientists North Queensland Exploration Conference, Queensland, Australia, Vol. 1, pp. 1-13.

Cornejo, P., Matthews, S., Marinovic, N., Perez de Arce, C., Bassa, M., Alfaro, J., and Navarro, M. 1997. Alteración hidrotermal y mineralización recurrente de Cu y Cu-Mo durante el Pérmico y el Triásico en la cordillera de Domeyko (zona de Zaldívar-Salar de los Morros): Antecedentes geocronológicas-U-Pb, 40Ar/39Ar, Re-Os. In Congreso Geológico Chileno, Antofagasta, Vol. 2, pp. 219-222.

Deer, W.A., Howie, R.A., and Zussman, J. 1992. An introduction to the rock-forming minerals. Addison Wesley Longman Ltd, Essex, England.

Dilles, J.H., Tomlinson, A.J., Martin, M.W., and Blanco, N. 1997. El Abra and Fortuna complexes: A porphyry copper batholith sinistrally displaced by the Falla Oeste, In Congreso Geologico Chileno No 8. ACTAS. 3: 1883-1887.

Goldstein, J., Newbury, D., Joy, D., Lyman, C., Echlin, P., Lifshin, E., Sawyer, L., and Michael, J. 2003. Scanning electron microscopy and X-ray microanalysis. Kluwer Academic Publishers, New York.

Guilbert, J.M. and Park, C.F. 1983. Porphyry copper deposits. W.H. Freeman and Company, New York.

Gustafson, L.B. and Hunt, J.P. 1975. The porphyry copper deposit at El Salvador, Chile, Economic Geology, 70: 857-912.

Le Maitre, R.W., Bateman, P., Dudek, A., Keller, J., Lameyre Le Bas, M.J., Sabine, P.A., Schmid, R., Sorensen, H., and Streckeisen, A. 1989. A classification of igneous rocks and glossary terms. Blackwell, Oxford, UK.

Lindsay, D.D. 1997. Structural control and anisotropy of mineralization within the Chuquicamata porphyry copper district, northern Chile. PhD, Dalhousie University, Halifax, NS.

Lowell, J.D. and Guilbert, J.M. 1970. Lateral and vertical alteration-mineralization zoning in porphyry ore deposits, Economic Geology, 65: 373-408.

Maksaev, V. and Zentilli, M. 1999. Fission track thermochronology of the Domeyko cordillera, northern Chile: Implications for Andean tectonics and porphyry copper metallogenesis., Exploration and Mining Geology, 8: 65-89.

Marquardt, J.C., Pizarro, J., Gomez, M., and Martínez, A. 1997. Prospecto Lila, descubrimiento de un pórfido cuprífero Triásico superior-Jurásico inferior, en la cordillera de Domeyko, II Región, Chile. In Congreso Geológico Chileno N 8 Actas, Antofagasta, Vol. 8, pp. 1048-1053.

McInnes, B., Farley, K., Sillitoe, R.H., and Kohn, B. 1999. Application of apatite (U-Th)/He thermochronometry to the determination and sense and amount of vertical

displacement at the Chuquicamata porphyry deposit, Chile, Economic Geology, 94: 937-948.

Munizaga, F., Maksaev, V., Fanning, C.M., Giglio, S., Yaxley, G., and Tassinan, C.C.G. 2008. Late Paleozoic-early Triassic magmatism on the western margin of Gondwana: Collahuasi area, northern Chile, Gondwana Research, 13: 407-427.

Ossandón, G.C., Fréraut, R.C., Gustafson, L.B., Lindsay, D.D., and Zentilli, M. 2001. Geology of Chuquicamata mine: A progress report, Economic Geology, 96: 249-270.

Proffett, J. 2008. Geologic report of the MM deposit: Chuquicamata district, Chile. Unpublished internal report for CODELCO.

Reynolds, P., Ravenhurst, C., Zentilli, M., and Lindsay, D. 1998. High-precision $^{40}Ar/^{39}Ar$ dating of two consecutive hydrothermal events in the Chuquicamata porphyry copper system, Chile, Chemical Geology, Isotope Geoscience, 148: 45-60.

Richards, J.P. 2002. Discussion on "giant versus small prophyry copper deposits of Cenozoic age in northern Chile: Adakitic versus normal calc-alkaline magmatism" by Oyarzún et al. Mineralium Deposita, 37: 788-790.

Rickwood, P.C. 1989. Boundary lines within petrologic diagrams which oxides of major and minor elements, Lithos, 22: 247-263.

Sibson, R.H. 2001. Seismogenic framework for hydrothermal transport and ore deposition, Society of Economic Geologists Reviews, 14: 25-50.

Sillitoe, R.H. 2010. Copper porphyry systems, Economic Geology, 105: 3-41.

Sillitoe, R.H. 1973. The tops and bottoms of porphyry copper deposits, Economic Geology, 68: 799-815.

Sillitoe, R.H. and McKee, E.H. 1996. Age of supergene oxidation and enrichment in the Chilean porphyry copper province, Economic Geology, 91: 164-179.

Sillitoe, R.H., Marquardt, J.C., Ramírez, F., Becerra, H., and Gómez, M. 1996. Geology of the concealed MM porphyry copper deposit, Chuquicamata district, northern Chile. In Andean
Copper Deposits: New Discoveries, Mineralization, Styles and Metallogeny Edited by F. Camus, R.H.Sillitoe and R.Petersen. Society of Economic Geologists, Special Publication No. 5, Citizen Printing Co., Fort Collins CO, pp. 59-68.

Sillitoe, R.H. and McKee, E.H. 1996. Age of supergene oxidation and enrichment in the Chilean porphyry copper province, Economic Geology, 91: 164-179.

Sun, S.S. and McDonough, W.F. 1989. Chemical and isotopic systematics of oceanic basalts: Implications for mantle composition and processes. In Magmatism in ocean basins Edited by
A.D. Saunders and M.J. Norry. Geological Society of America, pp. 313-345.

Tomlinson, A.J. and Blanco, N. 1997. Structural evolution and displacement history of the West Fault system, precordillera, Chile: Part 2, postmineral history, In Congreso Geologico Chileno No 8. ACTAS, 3: 1878-1882.

Tomlinson, A.J., Blanco, N., Maksaev, V., Dilles, J., Grunder, A.L., and Ladino, M. 2001. Geologia de la Precordillera Andina de Quebrada Blanca-Chuquicamata regions I y II. Unpublished; CODELCO and Servicio Nacional de Geologia y Mineria, Santiago. pp. 444

Zentilli, M., Doe, B.R., and Hedge, L.E. 1988. Lead isotopes in porphyry copper deposits as compared with other Andean mineral deposits. In Chilean Geological Congress, Santiago, Vol. 1, pp. 13331-13369.

Zentilli, M., Graves, M., Lindsay, D., Ossandón, G., and Camus, F. 1995. Recurrent mineralization in the Chuquicamata porphyry copper system: Restrictions on genesis from mineralogical, geochronological and isotopic studies. In Proceedings of Conference on Giant Ore Deposits: Controls on the Scale of Orogenic Magmatic-Hydrothermal Mineralization Edited by A.H. Clark. Queen's University, Kingston, Ontario, pp. 86-100.

# Appendix 1 EMP Images and Data

This appendix includes EMP data tables from samples ZMMH-10 (MM Granodiorite), ZMMH-11 (MM Quartz Porphyry) and ZMMH-14 (MM Porphyry) (table 4.1) for analysis on both silicates and sulphides. Included with the data are backscatter images of the locations where the points were taken. These images are brighter in locations with high electron density and darker in locations of low electron density. The exact location of each point is marked in red.

## ZMMH-10 Silicates (MM Granodiorite)

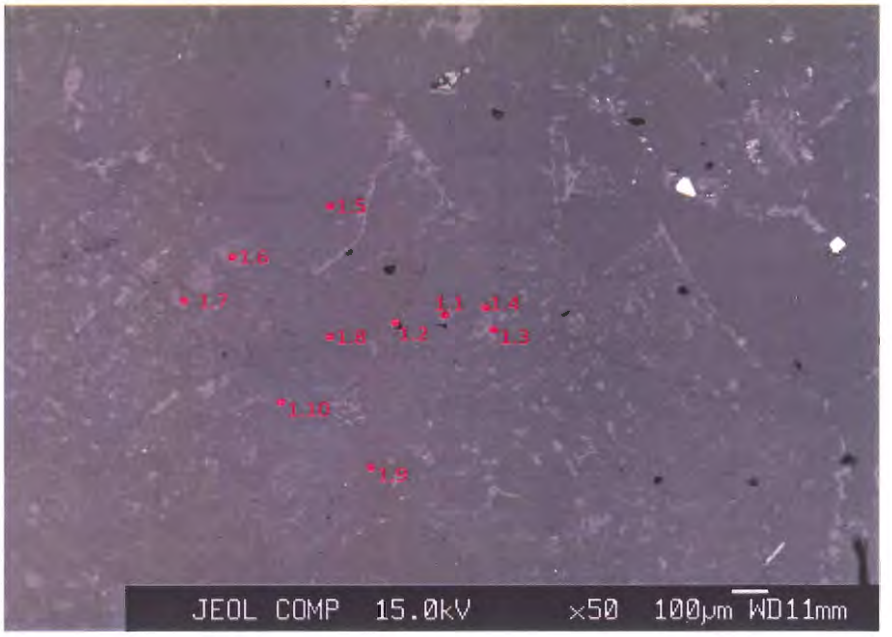


**Mass %**

| No. | $K_2O$ | $Cr_2O_3$ | $Na_2O$ | $Al_2O_3$ | MnO | CaO | $TiO_2$ | MgO | $SiO_2$ | FeO | $P_2O_5$ | Cl | F | NiO | $SO_3$ | Total | Mineral type |
|---|---|---|---|---|---|---|---|---|---|---|---|---|---|---|---|---|---|
| 1.1 | 10.36 | 0.00 | 0.27 | 34.42 | 0.003 | 0.01 | 0.06 | 0.65 | 48.11 | 2.13 | 0.01 | 0.00 | 0.00 | 0.03 | 0.03 | 96.08 | K-feldspar |
| 1.2 | 0.14 | 0.00 | 7.75 | 19.12 | 0 | 0.39 | 0.00 | 0.00 | 69.16 | 0.03 | 0.00 | 0.06 | 0.00 | 0.01 | 0.00 | 96.65 | Albite |
| 1.3 | 10.10 | 0.03 | 0.19 | 33.16 | 0.012 | 0.03 | 0.06 | 0.95 | 46.31 | 2.68 | 0.00 | 0.00 | 0.00 | 0.04 | 0.00 | 93.57 | K-feldspar |
| 1.4 | 0.15 | 0.00 | 6.54 | 19.71 | 0 | 0.19 | 0.00 | 0.00 | 71.33 | 0.03 | 0.00 | 0.03 | 0.00 | 0.00 | 0.00 | 97.97 | Albite |
| 1.5 | 0.37 | 0.00 | 8.05 | 19.13 | 0 | 0.18 | 0.00 | 0.00 | 69.80 | 0.05 | 0.00 | 0.02 | 0.00 | 0.02 | 0.00 | 97.63 | Albite |
| 1.6 | 4.79 | 0.01 | 0.09 | 28.63 | 0.355 | 0.06 | 0.02 | 9.22 | 39.00 | 9.34 | 0.00 | 0.01 | 0.01 | 0.06 | 0.02 | 91.61 | K-feldspar |
| 1.7 | 4.20 | 0.00 | 0.08 | 33.68 | 0.007 | 0.09 | 0.01 | 1.66 | 52.07 | 2.49 | 0.01 | 0.00 | 0.01 | 0.01 | 0.01 | 94.32 | K-feldspar |
| 1.8 | 0.11 | 0.00 | 12.17 | 19.12 | 0 | 0.13 | 0.00 | 0.00 | 68.50 | 0.04 | 0.00 | 0.00 | 0.00 | 0.02 | 0.01 | 100.10 | Albite |
| 1.9 | 0.23 | 0.00 | 11.71 | 19.41 | 0 | 0.26 | 0.00 | 0.00 | 68.14 | 0.10 | 0.00 | 0.03 | 0.00 | 0.03 | 0.01 | 99.91 | Albite |
| 1.10 | 0.16 | 0.00 | 10.34 | 19.38 | 0 | 0.41 | 0.00 | 0.00 | 69.61 | 0.05 | 0.01 | 0.00 | 0.00 | 0.00 | 0.00 | 99.96 | Albite |

**Cation Total**

| No. | K | Cr | Na | Al | Mn | Ca | Ti | Mg | Si | Fe | P | Cl | F | Ni | S | Total | Mineral type |
|---|---|---|---|---|---|---|---|---|---|---|---|---|---|---|---|---|---|
| 1.1 | 0.0792 | 0 | 0.0031 | 0.2431 | 0 | 0 | 0.0003 | 0.0058 | 0.2882 | 0.0107 | 0.0001 | 0 | 0 | 0.0001 | 0.0001 | 0.6308 | K-feldspar |
| 1.2 | 0.001 | 0 | 0.0834 | 0.1251 | 0 | 0.0023 | 0 | 0 | 0.3839 | 0.0001 | 0 | 0.0006 | 0 | 0.0001 | 0 | 0.5966 | Albite |
| 1.3 | 0.0797 | 0.0001 | 0.0023 | 0.2417 | 0.0001 | 0.0002 | 0.0003 | 0.0087 | 0.2863 | 0.0139 | 0 | 0 | 0 | 0.0002 | 0 | 0.6335 | K-feldspar |
| 1.4 | 0.001 | 0 | 0.0689 | 0.1262 | 0 | 0.0011 | 0 | 0 | 0.3873 | 0.0001 | 0 | 0.0003 | 0 | 0 | 0 | 0.585 | Albite |
| 1.5 | 0.0026 | 0 | 0.0859 | 0.1241 | 0 | 0.0011 | 0 | 0 | 0.3841 | 0.0002 | 0 | 0.0002 | 0 | 0.0001 | 0 | 0.5983 | Albite |
| 1.6 | 0.0397 | 0 | 0.0011 | 0.2194 | 0.002 | 0.0004 | 0.0001 | 0.0894 | 0.2535 | 0.0508 | 0 | 0.0001 | 0.0002 | 0.0003 | 0.0001 | 0.6572 | K-feldspar |
| 1.7 | 0.0313 | 0 | 0.0009 | 0.2319 | 0 | 0.0006 | 0 | 0.0144 | 0.3042 | 0.0121 | 0.0001 | 0 | 0.0002 | 0 | 0 | 0.5957 | K-feldspar |
| 1.8 | 0.0008 | 0 | 0.129 | 0.1232 | 0 | 0.0008 | 0 | 0 | 0.3746 | 0.0002 | 0 | 0 | 0 | 0.0001 | 0 | 0.6287 | Albite |
| 1.9 | 0.0016 | 0 | 0.1244 | 0.1254 | 0 | 0.0016 | 0 | 0 | 0.3734 | 0.0005 | 0 | 0.0003 | 0 | 0.0001 | 0 | 0.6274 | Albite |
| 1.10 | 0.0011 | 0 | 0.1089 | 0.1241 | 0 | 0.0024 | 0 | 0 | 0.3781 | 0.0002 | 0 | 0 | 0 | 0 | 0 | 0.6148 | Albite |

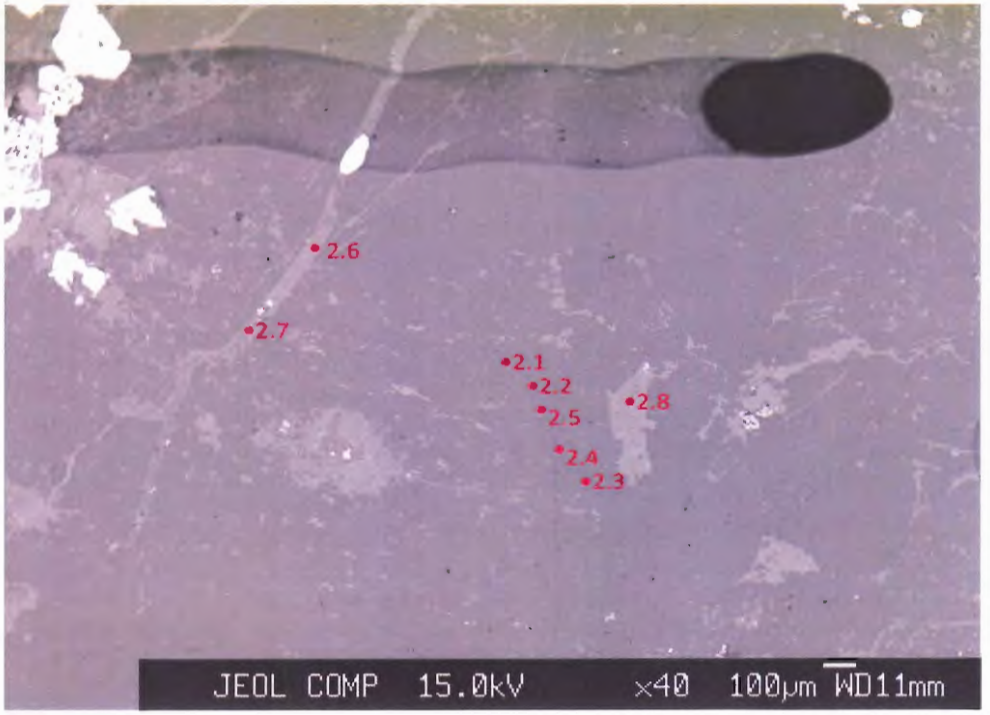


**Mass %**

| | $K_2O$ | $Cr_2O_3$ | $Na_2O$ | $Al_2O_3$ | MnO | CaO | $TiO_2$ | MgO | $SiO_2$ | FeO | $P_2O_5$ | Cl | F | NiO | $SO_3$ | Total | Mineral type |
|---|---|---|---|---|---|---|---|---|---|---|---|---|---|---|---|---|---|
| 2.1 | 5.20 | 0.00 | 4.93 | 24.27 | 0.007 | 0.46 | 0.02 | 0.97 | 58.00 | 1.57 | 0.03 | 0.00 | 0.00 | 0.01 | 0.00 | 95.47 | unstable |
| 2.2 | 0.48 | 0.00 | 10.24 | 19.59 | 0.005 | 1.15 | 0.00 | 0.00 | 65.21 | 0.08 | 0.00 | 0.15 | 0.00 | 0.01 | 0.00 | 96.88 | Albite |
| 2.3 | 0.10 | 0.00 | 6.30 | 19.65 | 0 | 0.25 | 0.00 | 0.00 | 70.79 | 0.08 | 0.00 | 0.00 | 0.00 | 0.04 | 0.01 | 97.20 | Albite |
| 2.4 | 0.64 | 0.00 | 10.43 | 19.33 | 0 | 0.54 | 0.00 | 0.00 | 68.18 | 0.06 | 0.00 | 0.00 | 0.00 | 0.01 | 0.01 | 99.20 | Albite |
| 2.5 | 0.14 | 0.00 | 11.99 | 19.39 | 0 | 0.35 | 0.00 | 0.00 | 68.22 | 0.03 | 0.00 | 0.00 | 0.00 | 0.02 | 0.01 | 100.14 | Albite |
| 2.6 | 16.35 | 0.01 | 0.42 | 17.80 | 0 | 0.01 | 0.01 | 0.00 | 64.35 | 0.03 | 0.00 | 0.00 | 0.00 | 0.07 | 0.02 | 99.07 | K-feldspar |
| 2.7 | 9.06 | 0.00 | 0.09 | 30.20 | 0.008 | 0.20 | 0.06 | 1.24 | 50.51 | 2.46 | 0.00 | 0.01 | 0.06 | 0.06 | 0.03 | 93.97 | K-feldspar |
| 2.8 | 0.02 | 0.02 | 0.01 | 19.24 | 0.729 | 0.04 | 0.08 | 21.14 | 27.91 | 17.11 | 0.00 | 0.01 | 0.02 | 0.07 | 0.01 | 86.40 | unstable |

**Cation Total**

| No. | K | Cr | Na | Al | Mn | Ca | Ti | Mg | Si | Fe | P | Cl | F | Ni | S | Total | Mineral type |
|---|---|---|---|---|---|---|---|---|---|---|---|---|---|---|---|---|---|
| 2.1 | 0.0389 | 0 | 0.0561 | 0.1679 | 0 | 0.0029 | 0.0001 | 0.0085 | 0.3404 | 0.0077 | 0.0001 | 0 | 0 | 0.0001 | 0 | 0.6228 | Andesine |
| 2.2 | 0.0034 | 0 | 0.1124 | 0.1307 | 0 | 0.007 | 0 | 0 | 0.3692 | 0.0004 | 0 | 0.0014 | 0 | 0.0001 | 0 | 0.6247 | Albite |
| 2.3 | 0.0007 | 0 | 0.0668 | 0.1267 | 0 | 0.0015 | 0 | 0 | 0.3871 | 0.0004 | 0 | 0 | 0 | 0.0002 | 0 | 0.5835 | Albite |
| 2.4 | 0.0045 | 0 | 0.1113 | 0.1254 | 0 | 0.0032 | 0 | 0 | 0.3752 | 0.0003 | 0 | 0 | 0 | 0 | 0 | 0.6199 | Albite |
| 2.5 | 0.0009 | 0 | 0.1271 | 0.125 | 0 | 0.0021 | 0 | 0 | 0.3731 | 0.0002 | 0 | 0 | 0 | 0.0001 | 0 | 0.6286 | Albite |
| 2.6 | 0.1219 | 0 | 0.0047 | 0.1226 | 0 | 0.0001 | 0 | 0 | 0.376 | 0.0002 | 0 | 0 | 0 | 0.0003 | 0.0001 | 0.6259 | K-feldspar |
| 2.7 | 0.0702 | 0 | 0.0011 | 0.2162 | 0 | 0.0013 | 0.0003 | 0.0112 | 0.3068 | 0.0125 | 0 | 0.0001 | 0.0011 | 0.0003 | 0.0001 | 0.6213 | K-feldspar |
| 2.8 | 0.0002 | 0.0001 | 0.0001 | 0.1661 | 0.0045 | 0.0003 | 0.0005 | 0.2308 | 0.2044 | 0.1048 | 0 | 0.0001 | 0.0006 | 0.0004 | 0 | 0.7129 | unstable |

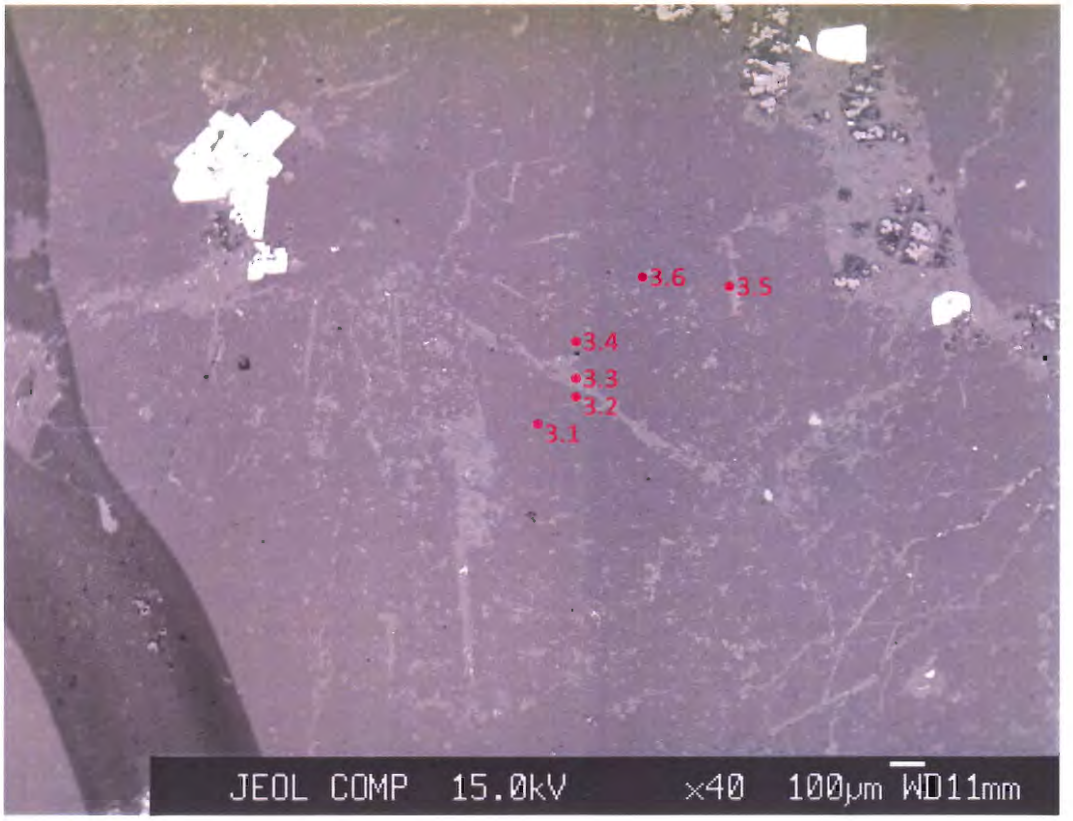


**Mass %**

| No. | $K_2O$ | $Cr_2O_3$ | $Na_2O$ | $Al_2O_3$ | MnO | CaO | $TiO_2$ | MgO | $SiO_2$ | FeO | $P_2O_5$ | Cl | F | NiO | $SO_3$ | Total | Mineral type |
|---|---|---|---|---|---|---|---|---|---|---|---|---|---|---|---|---|---|
| 3.1 | 0.16 | 0.00 | 10.97 | 19.28 | 0 | 0.18 | 0.00 | 0.00 | 68.42 | 0.05 | 0.01 | 0.03 | 0.00 | 0.01 | 0.00 | 99.10 | Albite |
| 3.2 | 9.30 | 0.00 | 3.85 | 18.40 | 0.004 | 0.22 | 0.04 | 0.00 | 65.18 | 0.15 | 0.01 | 0.01 | 0.00 | 0.04 | 0.00 | 97.20 | K-feldspar |
| 3.3 | 0.03 | 0.02 | 0.00 | 19.37 | 0.684 | 0.02 | 0.08 | 21.69 | 27.84 | 15.72 | 0.05 | 0.00 | 0.00 | 0.00 | 0.02 | 85.53 | ? |
| 3.4 | 0.17 | 0.00 | 11.80 | 19.01 | 0 | 0.44 | 0.00 | 0.00 | 67.95 | 0.03 | 0.01 | 0.01 | 0.00 | 0.00 | 0.01 | 99.42 | Albite |
| 3.5 | 1.43 | 0.03 | 0.01 | 3.61 | 1.786 | 50.54 | 0.00 | 0.33 | 7.07 | 0.77 | 0.06 | 0.00 | 0.00 | 0.05 | 0.05 | 65.72 | ? |
| 3.6 | 0.45 | 0.00 | 0.49 | 8.08 | 0.375 | 37.45 | 0.00 | 0.09 | 22.86 | 0.18 | 0.06 | 0.01 | 0.00 | 0.01 | 0.10 | 70.14 | ? |

**Cation Total**

| No. | K | Cr | Na | Al | Mn | Ca | Ti | Mg | Si | Fe | P | Cl | F | Ni | S | Total | Mineral type |
|---|---|---|---|---|---|---|---|---|---|---|---|---|---|---|---|---|---|
| 3.1 | 0.0012 | 0 | 0.1169 | 0.1249 | 0 | 0.0011 | 0 | 0 | 0.3761 | 0.0002 | 0 | 0.0003 | 0 | 0 | 0 | 0.6208 | Albite |
| 3.2 | 0.0685 | 0 | 0.0431 | 0.1254 | 0 | 0.0014 | 0.0002 | 0 | 0.3767 | 0.0007 | 0 | 0.0001 | 0 | 0.0002 | 0 | 0.6163 | K-feldspar |
| 3.3 | 0.0003 | 0.0001 | 0 | 0.1674 | 0.0042 | 0.0002 | 0.0005 | 0.2371 | 0.2042 | 0.0964 | 0.0003 | 0 | 0.0001 | 0 | 0.0001 | 0.711 | ? |
| 3.4 | 0.0012 | 0 | 0.126 | 0.1234 | 0 | 0.0026 | 0 | 0 | 0.3742 | 0.0001 | 0.0001 | 0.0001 | 0 | 0 | 0 | 0.6278 | Albite |
| 3.5 | 0.0232 | 0.0003 | 0.0002 | 0.0542 | 0.0193 | 0.6893 | 0 | 0.0062 | 0.09 | 0.0082 | 0.0007 | 0 | 0 | 0.0005 | 0.0005 | 0.8927 | ? |
| 3.6 | 0.0056 | 0 | 0.0093 | 0.0935 | 0.0031 | 0.394 | 0 | 0.0014 | 0.2245 | 0.0015 | 0.0005 | 0.0002 | 0 | 0.0001 | 0.0007 | 0.7345 | ? |

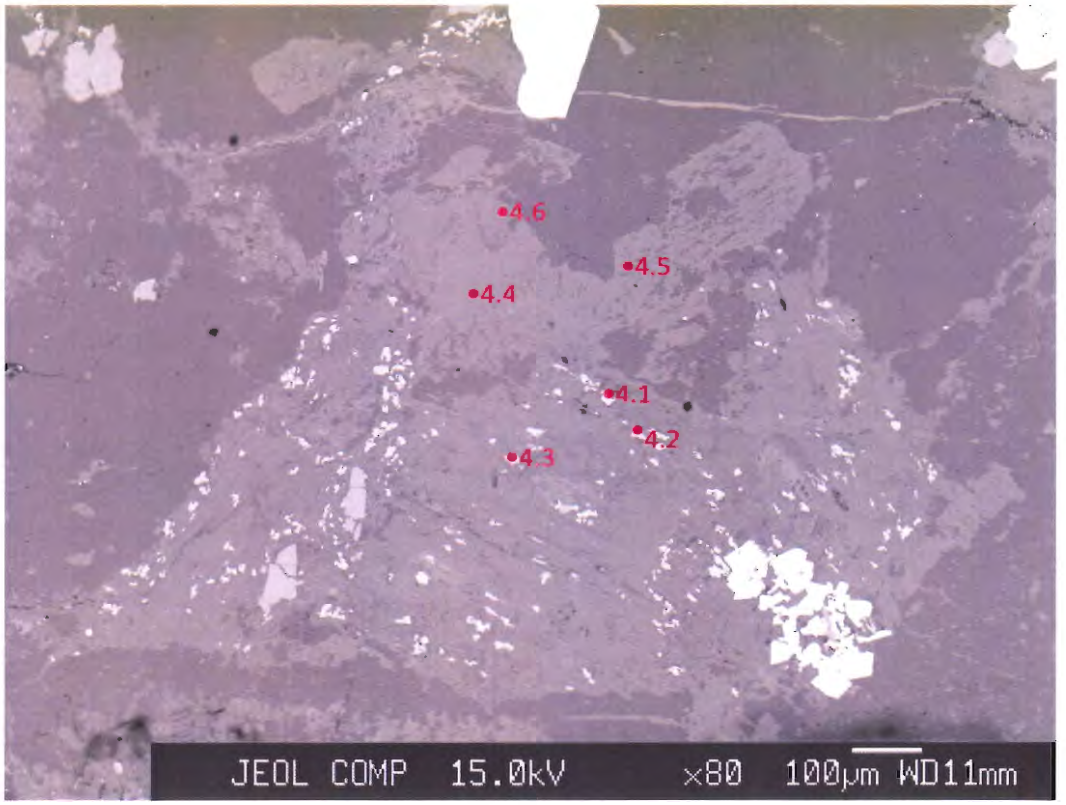


**Mass %**

| No. | $K_2O$ | $Cr_2O_3$ | $Na_2O$ | $Al_2O_3$ | MnO | CaO | $TiO_2$ | MgO | $SiO_2$ | FeO | $P_2O_5$ | Cl | F | NiO | $SO_3$ | Total | Comment |
|---|---|---|---|---|---|---|---|---|---|---|---|---|---|---|---|---|---|
| 4.1 | 0.13 | 0.15 | 0.01 | 0.07 | 0.078 | 0.07 | 94.46 | 0.00 | 0.23 | 0.62 | 0.05 | 0.02 | 0.00 | 0.11 | 0.04 | 96.04 | rutile |
| 4.2 | 0.10 | 0.12 | 0.03 | 0.43 | 0.099 | 1.71 | 88.87 | 0.00 | 2.52 | 0.94 | 0.07 | 0.02 | 0.00 | 0.13 | 0.05 | 95.08 | rutile |
| 4.3 | 0.23 | 0.17 | 0.02 | 0.41 | 0.137 | 0.48 | 90.79 | 0.00 | 1.31 | 1.47 | 0.03 | 0.03 | 0.00 | 0.11 | 0.07 | 95.25 | rutile |
| 4.4 | 15.676 | 0 | 0.4241 | 17.476 | 0.012 | 0.017 | 0.05 | 0 | 62.9 | 0.076 | 0.003 | 0.043 | 0 | 0.023 | 0.018 | 96.704 | K-feldspar |
| 4.5 | 15.788 | 0 | 0.3349 | 17.58 | 0.004 | 0 | 0.014 | 0 | 62.67 | 0.012 | 0.049 | 0.068 | 0 | 0 | 0.011 | 96.516 | K-feldspar |
| 4.6 | 13.776 | 0.0043 | 0.4482 | 17.76 | 0 | 0.026 | 0 | 0 | 65.07 | 0.066 | 0.016 | 0.027 | 0 | 0 | 0.002 | 97.186 | K-feldspar |

**Cation Total**

| No. | K | Cr | Na | Al | Mn | Ca | Ti | Mg | Si | Fe | P | Cl | F | Ni | S | Total | Mineral type |
|---|---|---|---|---|---|---|---|---|---|---|---|---|---|---|---|---|---|
| 4.1 | 0.0011 | 0.0008 | 0.0001 | 0.0006 | 0.0005 | 0.0005 | 0.4937 | 0 | 0.0016 | 0.0036 | 0.0003 | 0.0002 | 0 | 0.0006 | 0.0002 | 0.5038 | rutile |
| 4.2 | 0.0009 | 0.0007 | 0.0004 | 0.0036 | 0.0006 | 0.0128 | 0.4681 | 0 | 0.0177 | 0.0055 | 0.0004 | 0.0002 | 0 | 0.0007 | 0.0003 | 0.512 | rutile |
| 4.3 | 0.0021 | 0.0009 | 0.0003 | 0.0034 | 0.0008 | 0.0036 | 0.4794 | 0 | 0.0092 | 0.0086 | 0.0002 | 0.0003 | 0 | 0.0006 | 0.0003 | 0.5097 | rutile |
| 4.4 | 0.1195 | 0 | 0.0049 | 0.1231 | 0.0001 | 0.0001 | 0.0002 | 0 | 0.3759 | 0.0004 | 0 | 0.0004 | 0 | 0.0001 | 0.0001 | 0.6249 | K-feldspar |
| 4.5 | 0.1206 | 0 | 0.0039 | 0.1241 | 0 | 0 | 0.0001 | 0 | 0.3753 | 0.0001 | 0.0002 | 0.0007 | 0 | 0 | 0.0001 | 0.6252 | K-feldspar |
| 4.6 | 0.1029 | 0 | 0.0051 | 0.1225 | 0 | 0.0002 | 0 | 0 | 0.3808 | 0.0003 | 0.0001 | 0.0003 | 0 | 0 | 0 | 0.6123 | K-feldspar |

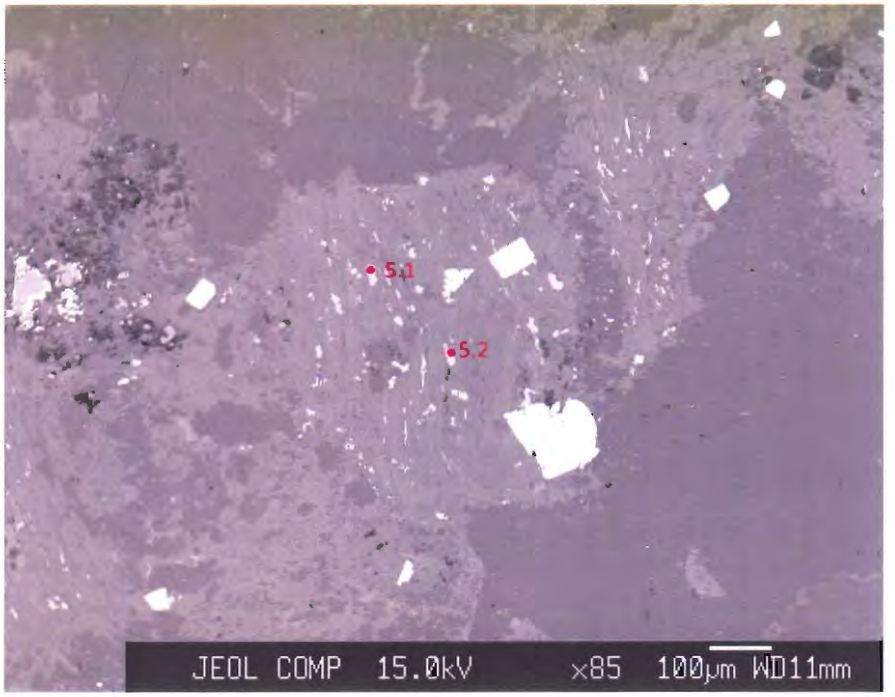


**Mass %**

| No. | $K_2O$ | $Cr_2O_3$ | $Na_2O$ | $Al_2O_3$ | MnO | CaO | $TiO_2$ | MgO | $SiO_2$ | FeO | $P_2O_5$ | Cl | F | NiO | $SO_3$ | Total | Mineral type |
|---|---|---|---|---|---|---|---|---|---|---|---|---|---|---|---|---|---|
| 5.1 | 0.56 | 0.12 | 0.02 | 1.68 | 0.11 | 0.12 | 89.93 | 0.46 | 3.01 | 1.12 | 0.05 | 0.02 | 0.00 | 0.10 | 0.05 | 97.35 | rutile |
| 5.2 | 0.07 | 0.15 | 0.00 | 0.55 | 0.114 | 0.32 | 94.50 | 0.48 | 1.10 | 1.01 | 0.05 | 0.02 | 0.00 | 0.14 | 0.07 | 98.58 | rutile |

**Cation Total**

| No. | K | Cr | Na | Al | Mn | Ca | Ti | Mg | Si | Fe | P | Cl | F | Ni | S | Total | Mineral type |
|---|---|---|---|---|---|---|---|---|---|---|---|---|---|---|---|---|---|
| 5.1 | 0.0048 | 0.0006 | 0.0002 | 0.0135 | 0.0006 | 0.0009 | 0.4603 | 0.0047 | 0.0205 | 0.0064 | 0.0003 | 0.0002 | 0 | 0.0006 | 0.0002 | 0.5138 | rutile |
| 5.2 | 0.0006 | 0.0008 | 0 | 0.0044 | 0.0007 | 0.0023 | 0.4805 | 0.0048 | 0.0075 | 0.0057 | 0.0003 | 0.0003 | 0 | 0.0008 | 0.0003 | 0.5091 | rutile |

**ZMMH 11 Silicates (MM Quartz Porphyry)**

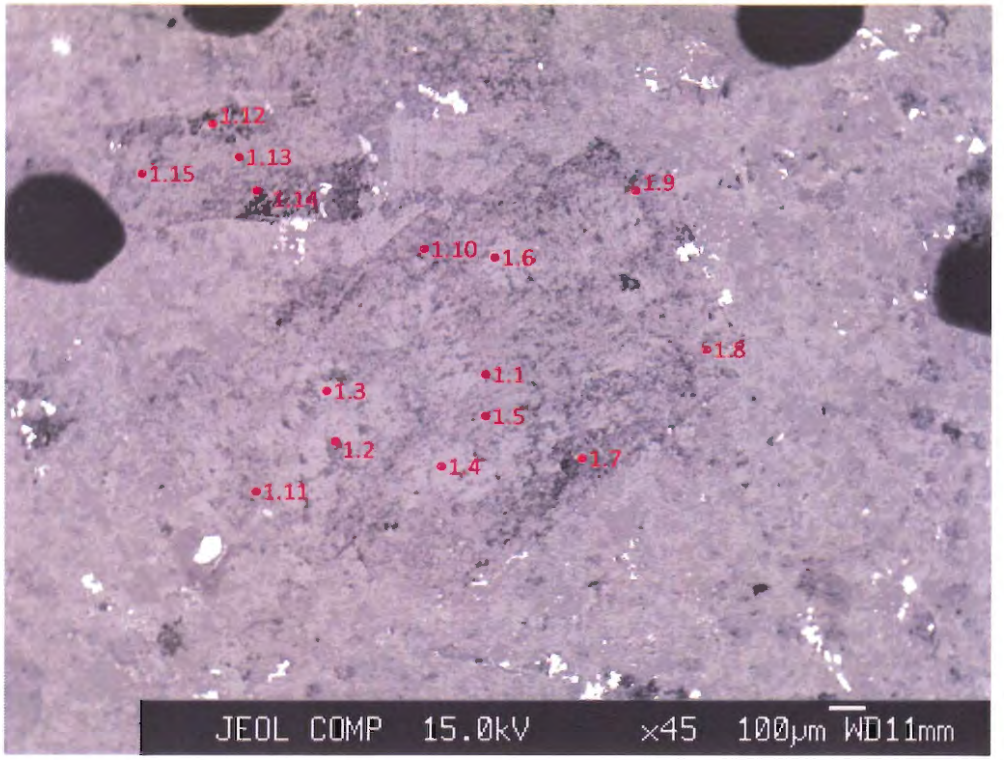

**Mass %**

| No. | $K_2O$ | $Cr_2O_3$ | $Na_2O$ | $SiO_2$ | MnO | CaO | $TiO_2$ | MgO | $Al_2O_3$ | FeO | BaO | Total | Mineal type |
|---|---|---|---|---|---|---|---|---|---|---|---|---|---|
| 1.1 | 9.29 | 0.00 | 0.20 | 48.71 | 0.011 | 0.00 | 0.06 | 2.59 | 28.88 | 1.38 | 0.00 | 91.11 | K-feldspar |
| 1.2 | 0.26 | 0.00 | 0.05 | 44.95 | 0 | 0.00 | 0.00 | 0.14 | 35.56 | 0.05 | 0.00 | 81.01 | K-feldspar |
| 1.3 | 15.18 | 0.00 | 0.53 | 63.53 | 0 | 0.00 | 0.13 | 0.00 | 18.04 | 0.04 | 1.19 | 98.64 | K-feldspar |
| 1.4 | 15.37 | 0.00 | 0.53 | 63.78 | 0 | 0.00 | 0.05 | 0.00 | 17.84 | 0.03 | 0.66 | 98.26 | K-feldspar |
| 1.5 | 15.39 | 0.00 | 0.28 | 63.50 | 0 | 0.00 | 0.12 | 0.02 | 18.24 | 0.10 | 1.55 | 99.20 | K-feldspar |
| 1.6 | 10.28 | 0.00 | 0.10 | 47.33 | 0.095 | 0.00 | 0.04 | 3.04 | 29.52 | 2.17 | 0.00 | 92.58 | K-feldspar |
| 1.7 | 0.50 | 0.00 | 0.03 | 47.87 | 0 | 0.00 | 0.00 | 0.19 | 37.65 | 0.04 | 0.00 | 86.27 | K-feldspar |
| 1.8 | 10.35 | 0.00 | 0.25 | 48.98 | 0.036 | 0.16 | 0.14 | 2.46 | 26.76 | 2.69 | 0.03 | 91.86 | K-feldspar |
| 1.9 | 3.55 | 0.00 | 0.30 | 46.61 | 0 | 0.59 | 0.00 | 1.22 | 30.30 | 0.53 | 0.00 | 83.10 | K-feldspar |
| 1.10 | 9.08 | 0.00 | 0.24 | 48.89 | 0.03 | 0.05 | 0.08 | 2.51 | 27.25 | 2.27 | 0.00 | 90.40 | K-feldspar |
| 1.11 | 14.15 | 0.00 | 0.33 | 61.45 | 0 | 1.12 | 0.00 | 0.06 | 16.75 | 0.12 | 0.00 | 93.99 | K-feldspar |
| 1.12 | 7.92 | 0.00 | 0.11 | 35.80 | 0 | 0.00 | 0.00 | 0.86 | 14.37 | 0.40 | 0.00 | 59.46 | K-feldspar |
| 1.13 | 9.32 | 0.00 | 0.12 | 47.92 | 0.019 | 0.00 | 0.08 | 2.49 | 29.11 | 1.61 | 0.00 | 90.67 | K-feldspar |
| 1.14 | 0.07 | 0.00 | 0.08 | 45.21 | 0 | 0.29 | 0.00 | 0.10 | 36.55 | 0.02 | 0.00 | 82.32 | unstable |
| 1.15 | 3.09 | 0.00 | 0.07 | 46.32 | 0 | 0.00 | 0.01 | 0.68 | 34.14 | 0.58 | 0.00 | 84.88 | K-feldspar |

**Cation Total**

| No. | K | Cr | Na | Si | Mn | Ca | Ti | Mg | Al | Fe | Ba | Total | Mineral type |
|---|---|---|---|---|---|---|---|---|---|---|---|---|---|
| 1.1 | 0.0742 | 0 | 0.0024 | 0.305 | 0.0001 | 0 | 0.0003 | 0.0242 | 0.2131 | 0.0072 | 0 | 0.6266 | K-feldspar |
| 1.2 | 0.0022 | 0 | 0.0006 | 0.2934 | 0 | 0 | 0 | 0.0013 | 0.2735 | 0.0003 | 0 | 0.5713 | K-feldspar |
| 1.3 | 0.114 | 0 | 0.006 | 0.374 | 0 | 0 | 0.0006 | 0 | 0.1252 | 0.0002 | 0.0027 | 0.6227 | K-feldspar |
| 1.4 | 0.1155 | 0 | 0.006 | 0.3756 | 0 | 0 | 0.0002 | 0 | 0.1239 | 0.0002 | 0.0015 | 0.6229 | K-feldspar |
| 1.5 | 0.1153 | 0 | 0.0032 | 0.373 | 0 | 0 | 0.0005 | 0.0002 | 0.1263 | 0.0005 | 0.0036 | 0.6227 | K-feldspar |
| 1.6 | 0.082 | 0 | 0.0013 | 0.2958 | 0.0005 | 0 | 0.0002 | 0.0283 | 0.2175 | 0.0113 | 0 | 0.637 | K-feldspar |
| 1.7 | 0.0039 | 0 | 0.0003 | 0.2938 | 0 | 0 | 0 | 0.0017 | 0.2723 | 0.0002 | 0 | 0.5723 | K-feldspar |
| 1.8 | 0.0833 | 0 | 0.0031 | 0.3091 | 0.0002 | 0.0011 | 0.0006 | 0.0232 | 0.1991 | 0.0142 | 0.0001 | 0.6341 | K-feldspar |
| 1.9 | 0.0298 | 0 | 0.0038 | 0.3062 | 0 | 0.0042 | 0 | 0.012 | 0.2346 | 0.0029 | 0 | 0.5936 | K-feldspar |
| 1.10 | 0.0734 | 0 | 0.0029 | 0.3098 | 0.0002 | 0.0004 | 0.0004 | 0.0237 | 0.2035 | 0.012 | 0 | 0.6264 | K-feldspar |
| 1.11 | 0.1106 | 0 | 0.004 | 0.3764 | 0 | 0.0074 | 0 | 0.0006 | 0.1209 | 0.0006 | 0 | 0.6205 | K-feldspar |
| 1.12 | 0.0974 | 0 | 0.0021 | 0.345 | 0 | 0 | 0 | 0.0124 | 0.1632 | 0.0032 | 0 | 0.6234 | K-feldspar |
| 1.13 | 0.075 | 0 | 0.0015 | 0.3022 | 0.0001 | 0 | 0.0004 | 0.0234 | 0.2164 | 0.0085 | 0 | 0.6275 | K-feldspar |
| 1.14 | 0.0005 | 0 | 0.001 | 0.2905 | 0 | 0.002 | 0 | 0.001 | 0.2768 | 0.0001 | 0 | 0.572 | unstable |
| 1.15 | 0.0252 | 0 | 0.0008 | 0.2959 | 0 | 0 | 0 | 0.0065 | 0.257 | 0.0031 | 0 | 0.5885 | K-feldspar |

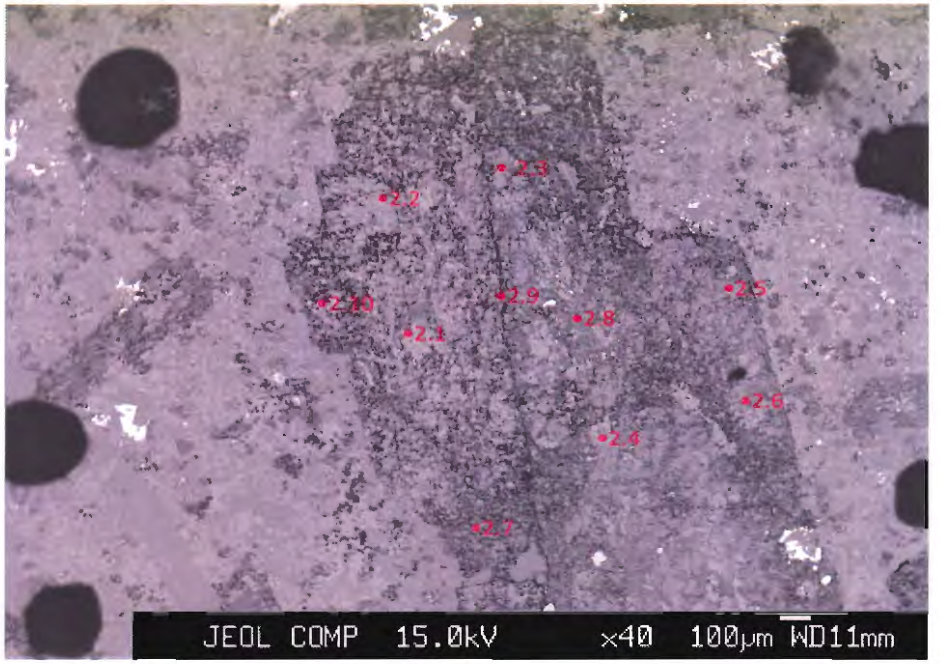


**Mass %**

| No. | $K_2O$ | $Cr_2O_3$ | $Na_2O$ | $SiO_2$ | MnO | CaO | $TiO_2$ | MgO | $Al_2O_3$ | FeO | BaO | Total | Mineral Type |
|---|---|---|---|---|---|---|---|---|---|---|---|---|---|
| 2.1 | 15.32 | 0.00 | 0.33 | 64.15 | 0 | 0.01 | 0.07 | 0.03 | 18.43 | 0.06 | 0.77 | 99.16 | K-feldspar |
| 2.2 | 8.83 | 0.00 | 0.13 | 48.80 | 0.022 | 0.00 | 0.00 | 2.07 | 29.39 | 2.83 | 0.00 | 92.07 | K-feldspar |
| 2.3 | 8.55 | 0.00 | 0.13 | 50.78 | 0.021 | 0.00 | 0.00 | 1.65 | 31.77 | 1.29 | 0.00 | 94.19 | K-feldspar |
| 2.4 | 8.52 | 0.00 | 0.11 | 48.73 | 0.008 | 0.00 | 0.00 | 2.05 | 30.03 | 1.11 | 0.00 | 90.56 | K-feldspar |
| 2.5 | 6.26 | 0.00 | 0.20 | 51.97 | 0.005 | 0.01 | 0.02 | 0.24 | 30.48 | 0.13 | 0.20 | 89.52 | K-feldspar |
| 2.6 | 5.45 | 0.00 | 0.22 | 42.12 | 0.022 | 0.00 | 0.01 | 1.56 | 26.13 | 1.53 | 0.03 | 77.07 | K-feldspar |
| 2.7 | 7.83 | 0.00 | 0.09 | 37.48 | 0 | 0.00 | 0.00 | 0.00 | 10.54 | 0.00 | 0.00 | 55.95 | K-feldspar |
| 2.8 | 15.50 | 0.05 | 0.25 | 63.60 | 0.033 | 0.03 | 0.08 | 0.01 | 18.08 | 0.12 | 0.87 | 98.63 | K-feldspar |
| 2.9 | 14.50 | 0.00 | 0.29 | 58.65 | 0 | 0.04 | 0.02 | 0.03 | 16.55 | 0.06 | 0.32 | 90.45 | K-feldspar |
| 2.10 | 10.18 | 0.04 | 0.23 | 47.16 | 0.058 | 0.20 | 0.02 | 1.61 | 23.08 | 1.47 | 0.18 | 84.23 | K-feldspar |

**Cation Total**

| No. | K | Cr | Na | Si | Mn | Ca | Ti | Mg | Al | Fe | Ba | Total | Mineral |
|---|---|---|---|---|---|---|---|---|---|---|---|---|---|
| 2.1 | 0.114 | 0 | 0.0037 | 0.3741 | 0 | 0 | 0.0003 | 0.0002 | 0.1267 | 0.0003 | 0.0018 | 0.6212 | K-feldspar |
| 2.2 | 0.0701 | 0 | 0.0015 | 0.3035 | 0.0001 | 0 | 0 | 0.0192 | 0.2154 | 0.0147 | 0 | 0.6245 | K-feldspar |
| 2.3 | 0.0653 | 0 | 0.0015 | 0.3043 | 0.0001 | 0 | 0 | 0.0147 | 0.2244 | 0.0065 | 0 | 0.6169 | K-feldspar |
| 2.4 | 0.0679 | 0 | 0.0014 | 0.3044 | 0 | 0 | 0 | 0.0191 | 0.2211 | 0.0058 | 0 | 0.6198 | K-feldspar |
| 2.5 | 0.0491 | 0 | 0.0024 | 0.3196 | 0 | 0.0001 | 0.0001 | 0.0022 | 0.2209 | 0.0007 | 0.0005 | 0.5956 | K-feldspar |
| 2.6 | 0.0504 | 0 | 0.0031 | 0.3057 | 0.0001 | 0 | 0.0001 | 0.0168 | 0.2235 | 0.0093 | 0.0001 | 0.6091 | K-feldspar |
| 2.7 | 0.1013 | 0 | 0.0017 | 0.3798 | 0 | 0 | 0 | 0.0001 | 0.1259 | 0 | 0 | 0.6089 | K-feldspar |
| 2.8 | 0.1163 | 0.0002 | 0.0029 | 0.3741 | 0.0002 | 0.0002 | 0.0004 | 0.0001 | 0.1254 | 0.0006 | 0.002 | 0.6224 | K-feldspar |
| 2.9 | 0.1183 | 0 | 0.0035 | 0.3751 | 0 | 0.0003 | 0.0001 | 0.0003 | 0.1247 | 0.0003 | 0.0008 | 0.6234 | K-feldspar |
| 2.1 | 0.089 | 0.0002 | 0.0031 | 0.3233 | 0.0003 | 0.0015 | 0.0001 | 0.0165 | 0.1865 | 0.0084 | 0.0005 | 0.6295 | K-feldspar |

## ZMMH-14 Silicates (MM Porphyry)

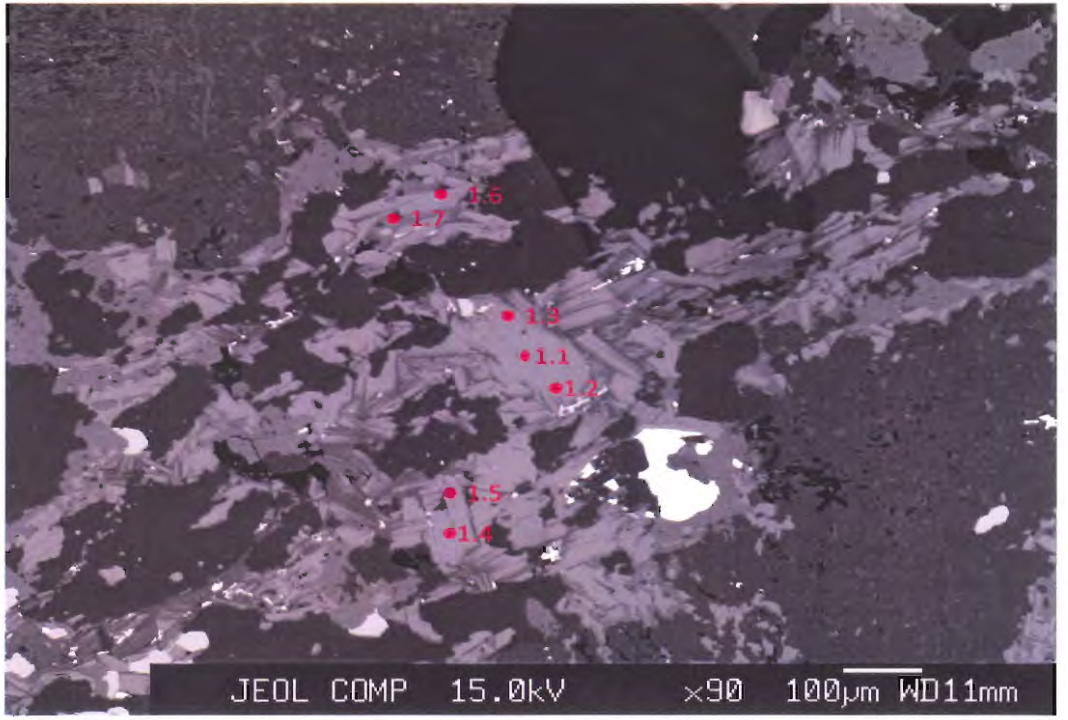


**Mass %**

| No. | $K_2O$ | $Cr_2O_3$ | $Na_2O$ | $Al_2O_3$ | MnO | CaO | $TiO_2$ | MgO | $SiO_2$ | FeO | $P_2O_5$ | Cl | F | NiO | $SO_3$ | Total | Mineral type |
|---|---|---|---|---|---|---|---|---|---|---|---|---|---|---|---|---|---|
| 1.1 | 8.70 | 0.00 | 0.17 | 14.25 | 0.05 | 0.00 | 2.96 | 16.69 | 38.01 | 11.16 | 0.03 | 0.13 | 0.96 | 0.05 | 0.04 | 92.78 | biotite |
| 1.2 | 8.17 | 0.00 | 0.18 | 14.37 | 0.08 | 0.03 | 2.78 | 16.23 | 37.97 | 10.37 | 0.02 | 0.14 | 1.01 | 0.06 | 0.03 | 90.99 | biotite |
| 1.3 | 8.92 | 0.01 | 0.08 | 14.21 | 0.084 | 0.02 | 2.96 | 17.07 | 38.26 | 10.95 | 0.00 | 0.13 | 1.13 | 0.02 | 0.00 | 93.33 | biotite |
| 1.4 | 9.63 | 0.03 | 0.18 | 14.93 | 0.077 | 0.00 | 3.00 | 17.18 | 38.58 | 10.89 | 0.00 | 0.14 | 1.03 | 0.02 | 0.00 | 95.23 | biotite |
| 1.7 | 15.57 | 0.00 | 0.72 | 18.03 | 0 | 0.01 | 0.00 | 0.00 | 64.38 | 0.14 | 0.02 | 0.01 | 0.00 | 0.00 | 0.00 | 98.88 | K-feldspar |
| 1.5 | 9.81 | 0.05 | 0.17 | 15.41 | 0.085 | 0.00 | 2.86 | 16.44 | 37.62 | 11.05 | 0.00 | 0.13 | 0.99 | 0.02 | 0.00 | 94.19 | biotite |
| 1.6 | 9.68 | 0.01 | 0.16 | 14.62 | 0.104 | 0.00 | 2.86 | 17.03 | 38.72 | 10.78 | 0.01 | 0.12 | 1.13 | 0.02 | 0.00 | 94.74 | biotite |

**Cation Total**

| No. | K2O | Cr2O3 | Na2O | Al2O3 | MnO | CaO | TiO2 | MgO | SiO2 | FeO | P2O5 | Cl | F | NiO | SO3 | Total | Mineral type |
|---|---|---|---|---|---|---|---|---|---|---|---|---|---|---|---|---|---|
| 1.1 | 0.0761 | 0 | 0.0023 | 0.1151 | 0.0003 | 0 | 0.0153 | 0.1706 | 0.2607 | 0.064 | 0.0002 | 0.0015 | 0.0204 | 0.0003 | 0.0002 | 0.727 | biotite |
| 1.2 | 0.0723 | 0 | 0.0024 | 0.1176 | 0.0005 | 0.0002 | 0.0145 | 0.168 | 0.2636 | 0.0602 | 0.0001 | 0.0016 | 0.0217 | 0.0003 | 0.0001 | 0.7232 | biotite |
| 1.3 | 0.0776 | 0.0001 | 0.0011 | 0.1142 | 0.0005 | 0.0001 | 0.0152 | 0.1736 | 0.261 | 0.0625 | 0 | 0.0014 | 0.0238 | 0.0001 | 0 | 0.7313 | biotite |
| 1.4 | 0.0823 | 0.0001 | 0.0024 | 0.1179 | 0.0004 | 0 | 0.0151 | 0.1716 | 0.2585 | 0.061 | 0 | 0.0015 | 0.0214 | 0.0001 | 0 | 0.7324 | biotite |
| 1.5 | 0.0832 | 0.0001 | 0.002 | 0.1161 | 0.0006 | 0 | 0.0145 | 0.171 | 0.2608 | 0.0608 | 0 | 0.0014 | 0.0235 | 0.0001 | 0 | 0.7342 | K-feldspar |
| 1.6 | 0.0851 | 0.0003 | 0.0022 | 0.1235 | 0.0005 | 0 | 0.0146 | 0.1666 | 0.2557 | 0.0628 | 0 | 0.0015 | 0.0209 | 0.0001 | 0 | 0.7339 | biotite |
| 1.7 | 0.1158 | 0 | 0.0081 | 0.1239 | 0 | 0.0001 | 0 | 0 | 0.3755 | 0.0007 | 0.0001 | 0.0001 | 0 | 0 | 0 | 0.6244 | biotite |

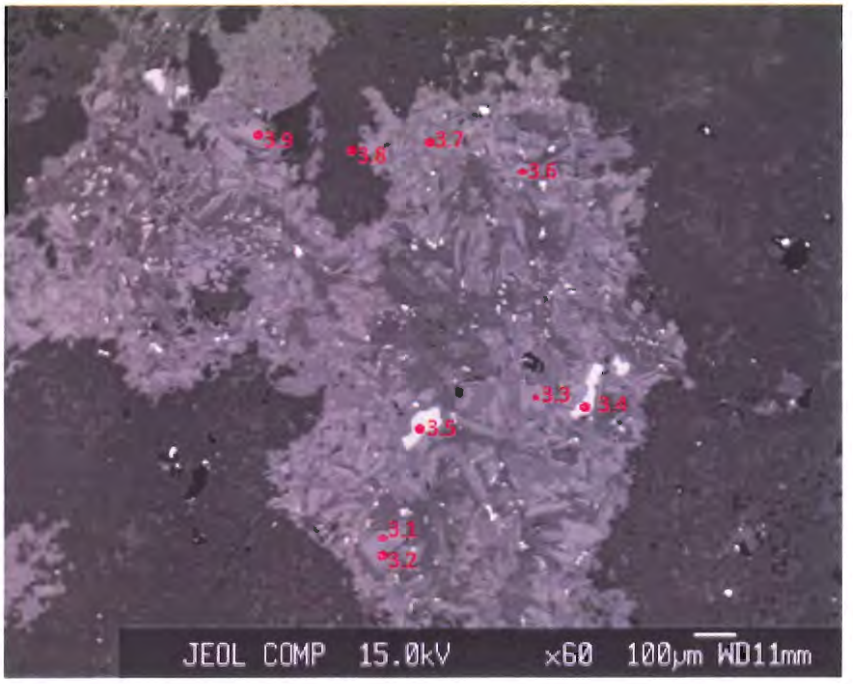


**Mass %**

| No. | $K_2O$ | $Cr_2O_3$ | $Na_2O$ | $Al_2O_3$ | MnO | CaO | $TiO_2$ | MgO | $SiO_2$ | FeO | $P_2O_5$ | Cl | F | NiO | $SO_3$ | Total | Mineral type |
|---|---|---|---|---|---|---|---|---|---|---|---|---|---|---|---|---|---|
| 3.1 | 7.77 | 0.01 | 0.17 | 14.59 | 0.134 | 0.28 | 2.89 | 15.97 | 36.80 | 11.41 | 0.00 | 0.16 | 0.85 | 0.04 | 0.04 | 90.72 | biotite |
| 3.2 | 7.79 | 0.02 | 0.21 | 14.48 | 0.09 | 0.28 | 2.72 | 15.82 | 36.90 | 10.74 | 0.00 | 0.14 | 0.87 | 0.02 | 0.00 | 89.67 | biotite |
| 3.3 | 9.02 | 0.01 | 0.21 | 14.92 | 0.05 | 0.01 | 3.04 | 16.39 | 37.52 | 11.19 | 0.00 | 0.13 | 0.88 | 0.01 | 0.00 | 92.97 | biotite |
| 3.4 | 0.10 | 0.05 | 0.19 | 0.00 | 0.209 | 54.15 | 0.01 | 0.11 | 0.10 | 0.44 | 41.27 | 0.66 | 3.33 | 0.08 | 0.03 | 99.18 | apatite |
| 3.5 | 0.05 | 0.06 | 0.19 | 0.00 | 0.209 | 54.13 | 0.03 | 0.11 | 0.07 | 0.33 | 41.39 | 0.75 | 3.82 | 0.04 | 0.05 | 99.46 | apatite |
| 3.6 | 8.94 | 0.03 | 0.08 | 15.12 | 0.2 | 0.01 | 2.40 | 17.20 | 37.40 | 10.98 | 0.02 | 0.12 | 1.16 | 0.03 | 0.04 | 93.19 | biotite |
| 3.7 | 15.81 | 0.00 | 0.73 | 17.86 | 0 | 0.03 | 0.00 | 0.00 | 64.08 | 0.10 | 0.00 | 0.00 | 0.00 | 0.00 | 0.00 | 98.62 | K-feldspar |
| 3.8 | 1.31 | 0.58 | 1.25 | 7.54 | 0.215 | 0.51 | 0.45 | 0.59 | 24.61 | 1.00 | 0.32 | 1.00 | 0.21 | 0.58 | 1.37 | 41.22 | chlorite? |
| 3.9 | 8.75 | 0.00 | 0.23 | 14.42 | 0.014 | 0.07 | 2.95 | 16.27 | 37.59 | 10.99 | 0.00 | 0.14 | 0.98 | 0.05 | 0.00 | 92.00 | biotite |

**Cation Total**

| No. | K | Cr | Na | Al | Mn | Ca | Ti | Mg | Si | Fe | P | Cl | F | Ni | S | Total | Mineral type |
|---|---|---|---|---|---|---|---|---|---|---|---|---|---|---|---|---|---|
| 3.1 | 0.0694 | 0.0001 | 0.0023 | 0.1204 | 0.0008 | 0.0021 | 0.0152 | 0.1667 | 0.2578 | 0.0668 | 0 | 0.0018 | 0.0185 | 0.0002 | 0.0002 | 0.7224 | biotite |
| 3.2 | 0.0702 | 0.0001 | 0.0028 | 0.1205 | 0.0005 | 0.0021 | 0.0145 | 0.1665 | 0.2605 | 0.0634 | 0 | 0.0016 | 0.019 | 0.0001 | 0 | 0.7219 | biotite |
| 3.3 | 0.0789 | 0.0001 | 0.0027 | 0.1206 | 0.0003 | 0.0001 | 0.0157 | 0.1675 | 0.2573 | 0.0642 | 0 | 0.0014 | 0.0187 | 0.0001 | 0 | 0.7277 | biotite |
| 3.4 | 0.023 | 0.0064 | 0.0334 | 0.1223 | 0.0025 | 0.0075 | 0.0047 | 0.0121 | 0.3388 | 0.0115 | 0.0037 | 0.0227 | 0.0088 | 0.0064 | 0.0142 | 0.6181 | apatite |
| 3.5 | 0.0781 | 0.0001 | 0.0011 | 0.122 | 0.0012 | 0 | 0.0124 | 0.1755 | 0.256 | 0.0628 | 0.0001 | 0.0013 | 0.0244 | 0.0002 | 0.0002 | 0.7354 | apatite |
| 3.6 | 0.0004 | 0.0003 | 0.0026 | 0 | 0.0012 | 0.395 | 0.0002 | 0.0011 | 0.0005 | 0.0019 | 0.2386 | 0.0079 | 0.0754 | 0.0002 | 0.0002 | 0.7255 | biotite |
| 3.7 | 0.1182 | 0 | 0.0083 | 0.1233 | 0 | 0.0002 | 0 | 0 | 0.3755 | 0.0005 | 0 | 0 | 0 | 0 | 0 | 0.626 | K-feldspar |
| 3.8 | 0.0773 | 0 | 0.003 | 0.1176 | 0.0001 | 0.0005 | 0.0154 | 0.1679 | 0.2602 | 0.0636 | 0 | 0.0016 | 0.021 | 0.0003 | 0 | 0.7286 | chlorite? |
| 3.9 | 0.0009 | 0.0002 | 0.0025 | 0 | 0.0012 | 0.3954 | 0.0001 | 0.0012 | 0.0007 | 0.0025 | 0.2381 | 0.007 | 0.0664 | 0.0004 | 0.0002 | 0.7168 | biotite |

** There is no location 2 for the ZMMH-14 EMP analysis

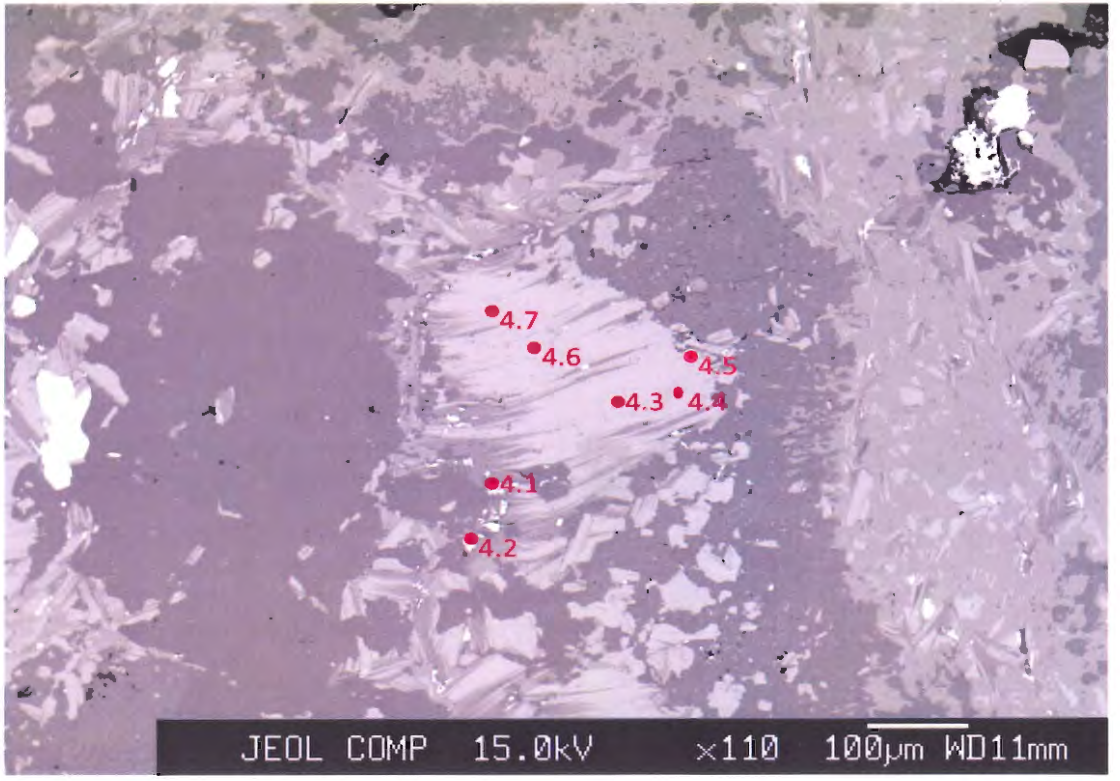


**Mass %**

| No. | $K_2O$ | $Cr_2O_3$ | $Na_2O$ | $Al_2O_3$ | MnO | CaO | $TiO_2$ | MgO | $SiO_2$ | FeO | $P_2O_5$ | Cl | F | NiO | $SO_3$ | Total | Mineral type |
|---|---|---|---|---|---|---|---|---|---|---|---|---|---|---|---|---|---|
| 4.1 | 0.07 | 0.12 | 0.01 | 0.16 | 0.035 | 1.11 | 93.12 | 0.04 | 1.48 | 0.73 | 0.02 | 0.01 | 0.00 | 0.10 | 0.01 | 97.02 | rutile |
| 4.2 | 0.10 | 0.00 | 0.00 | 0.03 | 0.002 | 0.01 | 95.12 | 0.00 | 0.09 | 1.13 | 0.02 | 0.00 | 0.03 | 0.03 | 0.00 | 96.57 | rutile |
| 4.3 | 9.30 | 0.02 | 0.25 | 14.84 | 0.066 | 0.02 | 3.11 | 17.09 | 38.94 | 11.38 | 0.00 | 0.14 | 1.07 | 0.03 | 0.02 | 95.79 | biotite |
| 4.4 | 9.23 | 0.02 | 0.21 | 14.52 | 0.034 | 0.01 | 3.09 | 16.80 | 38.56 | 11.59 | 0.00 | 0.14 | 1.06 | 0.02 | 0.02 | 94.81 | biotite |
| 4.5 | 8.97 | 0.00 | 0.23 | 14.32 | 0.026 | 0.06 | 3.08 | 16.59 | 38.35 | 11.07 | 0.00 | 0.11 | 0.92 | 0.04 | 0.01 | 93.38 | biotite |
| 4.6 | 9.42 | 0.02 | 0.14 | 14.59 | 0.083 | 0.02 | 3.03 | 16.78 | 38.52 | 11.30 | 0.00 | 0.12 | 1.04 | 0.03 | 0.01 | 94.63 | biotite |
| 4.7 | 9.42 | 0.02 | 0.20 | 14.40 | 0.056 | 0.01 | 3.20 | 16.92 | 38.28 | 11.52 | 0.00 | 0.15 | 0.96 | 0.04 | 0.00 | 94.75 | biotite |

**Cation Total**

| No. | K | Cr | Na | Al | Mn | Ca | Ti | Mg | Si | Fe | P | Cl | F | Ni | S | Total | Mineral type |
|---|---|---|---|---|---|---|---|---|---|---|---|---|---|---|---|---|---|
| 4.1 | 0.0006 | 0.0007 | 0.0001 | 0.0013 | 0.0002 | 0.0081 | 0.4812 | 0.0004 | 0.0102 | 0.0042 | 0.0001 | 0.0002 | 0 | 0.0006 | 0.0001 | 0.5081 | rutile |
| 4.2 | 0.0009 | 0 | 0 | 0.0002 | 0 | 0.0001 | 0.4954 | 0 | 0.0007 | 0.0066 | 0.0001 | 0 | 0.0007 | 0.0002 | 0 | 0.5049 | rutile |
| 4.3 | 0.079 | 0.0001 | 0.0032 | 0.1165 | 0.0004 | 0.0002 | 0.0156 | 0.1697 | 0.2594 | 0.0634 | 0 | 0.0015 | 0.0221 | 0.0002 | 0.0001 | 0.7314 | biotite |
| 4.4 | 0.0794 | 0.0001 | 0.0028 | 0.1153 | 0.0002 | 0.0001 | 0.0157 | 0.1688 | 0.2599 | 0.0653 | 0 | 0.0016 | 0.022 | 0.0001 | 0.0001 | 0.7315 | biotite |
| 4.5 | 0.078 | 0 | 0.0031 | 0.115 | 0.0002 | 0.0004 | 0.0158 | 0.1685 | 0.2613 | 0.0631 | 0 | 0.0013 | 0.0195 | 0.0002 | 0.0001 | 0.7265 | biotite |
| 4.6 | 0.0811 | 0.0001 | 0.0018 | 0.1161 | 0.0005 | 0.0001 | 0.0154 | 0.1688 | 0.26 | 0.0638 | 0 | 0.0013 | 0.0216 | 0.0002 | 0 | 0.7308 | biotite |
| 4.7 | 0.0812 | 0.0001 | 0.0026 | 0.1147 | 0.0003 | 0.0001 | 0.0163 | 0.1704 | 0.2586 | 0.0651 | 0 | 0.0017 | 0.02 | 0.0002 | 0 | 0.7313 | biotite |

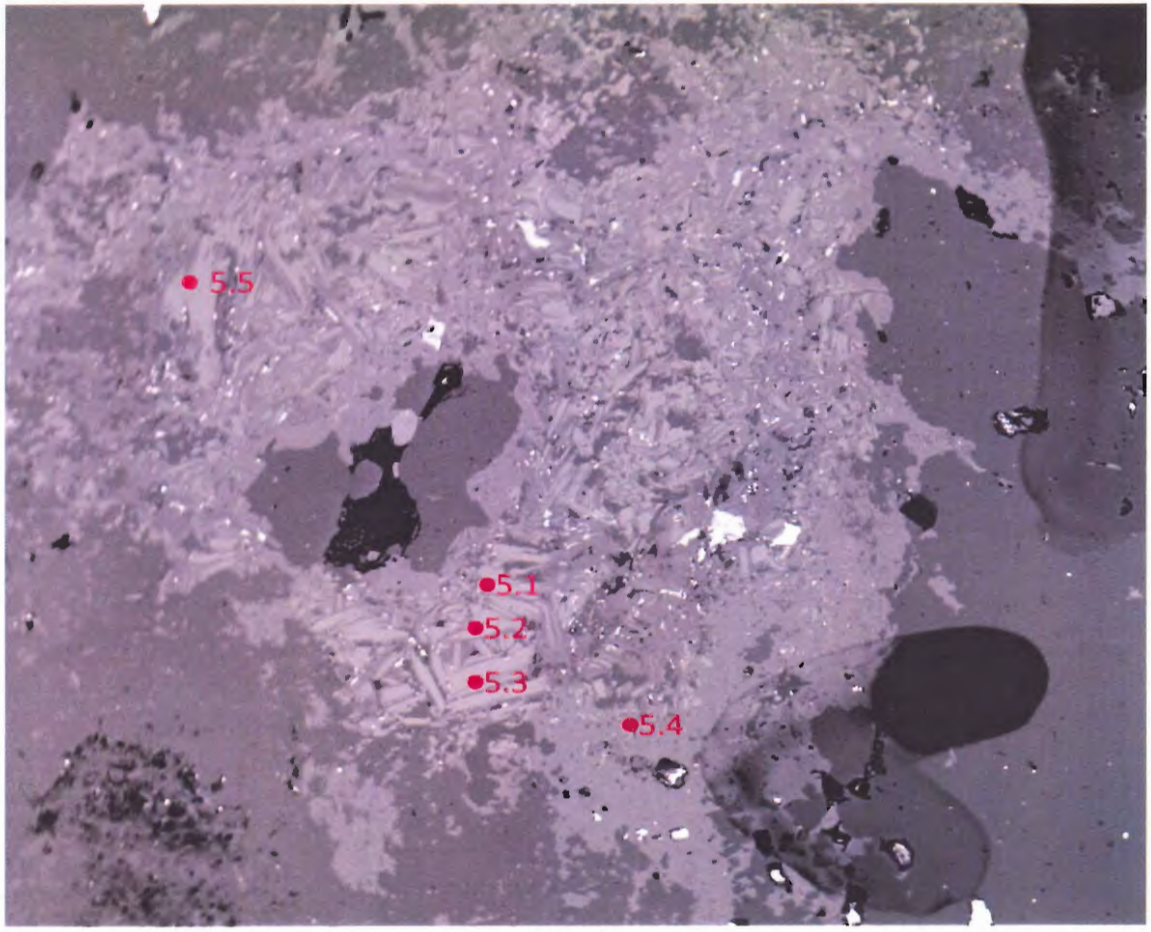


**Mass %**

| No. | $K_2O$ | $Cr_2O_3$ | $Na_2O$ | $Al_2O_3$ | MnO | CaO | $TiO_2$ | MgO | $SiO_2$ | FeO | $P_2O_5$ | Cl | F | NiO | $SO_3$ | Total | Mineral type |
|---|---|---|---|---|---|---|---|---|---|---|---|---|---|---|---|---|---|
| 5.1 | 9.58 | 0.05 | 0.23 | 14.92 | 0.036 | 0.00 | 3.28 | 16.52 | 37.93 | 11.59 | 0.01 | 0.12 | 0.92 | 0.02 | 0.02 | 94.80 | K-feldspar |
| 5.2 | 9.78 | 0.00 | 0.15 | 14.49 | 0.116 | 0.01 | 2.99 | 16.88 | 38.41 | 11.18 | 0.02 | 0.14 | 1.07 | 0.04 | 0.03 | 94.82 | K-feldspar |
| 5.3 | 9.59 | 0.05 | 0.25 | 14.76 | 0.048 | 0.03 | 3.28 | 16.57 | 38.62 | 11.54 | 0.00 | 0.13 | 0.99 | 0.02 | 0.00 | 95.43 | K-feldspar |
| 5.4 | 16.22 | 0.00 | 0.47 | 18.01 | 0 | 0.02 | 0.00 | 0.00 | 64.38 | 0.14 | 0.07 | 0.00 | 0.00 | 0.02 | 0.00 | 99.32 | K-feldspar |
| 5.5 | 9.35 | 0.01 | 0.29 | 14.58 | 0.043 | 0.03 | 3.30 | 16.55 | 38.31 | 11.46 | 0.00 | 0.12 | 0.99 | 0.02 | 0.02 | 94.61 | K-feldspar |

**Cation Total**

| No. | K | Cr | Na | Al | Mn | Ca | Ti | Mg | Si | Fe | P | Cl | F | Ni | S | Total | Mineral type |
|---|---|---|---|---|---|---|---|---|---|---|---|---|---|---|---|---|---|
| 5.1 | 0.0826 | 0.0003 | 0.003 | 0.1189 | 0.0002 | 0 | 0.0167 | 0.1664 | 0.2563 | 0.0655 | 0.0001 | 0.0014 | 0.0192 | 0.0001 | 0.0001 | 0.7309 | K-feldspar |
| 5.2 | 0.0842 | 0 | 0.002 | 0.1154 | 0.0007 | 0.0001 | 0.0152 | 0.1699 | 0.2594 | 0.0631 | 0.0001 | 0.0016 | 0.0222 | 0.0002 | 0.0001 | 0.7343 | K-feldspar |
| 5.3 | 0.082 | 0.0003 | 0.0033 | 0.1166 | 0.0003 | 0.0002 | 0.0165 | 0.1657 | 0.259 | 0.0647 | 0 | 0.0014 | 0.0205 | 0.0001 | 0 | 0.7307 | K-feldspar |
| 5.4 | 0.1206 | 0 | 0.0053 | 0.1236 | 0 | 0.0001 | 0 | 0 | 0.375 | 0.0007 | 0.0003 | 0 | 0 | 0.0001 | 0 | 0.6258 | K-feldspar |
| 5.5 | 0.0806 | 0 | 0.0038 | 0.1161 | 0.0002 | 0.0002 | 0.0168 | 0.1667 | 0.2589 | 0.0647 | 0 | 0.0014 | 0.0208 | 0.0001 | 0.0001 | 0.7305 | K-feldspar |

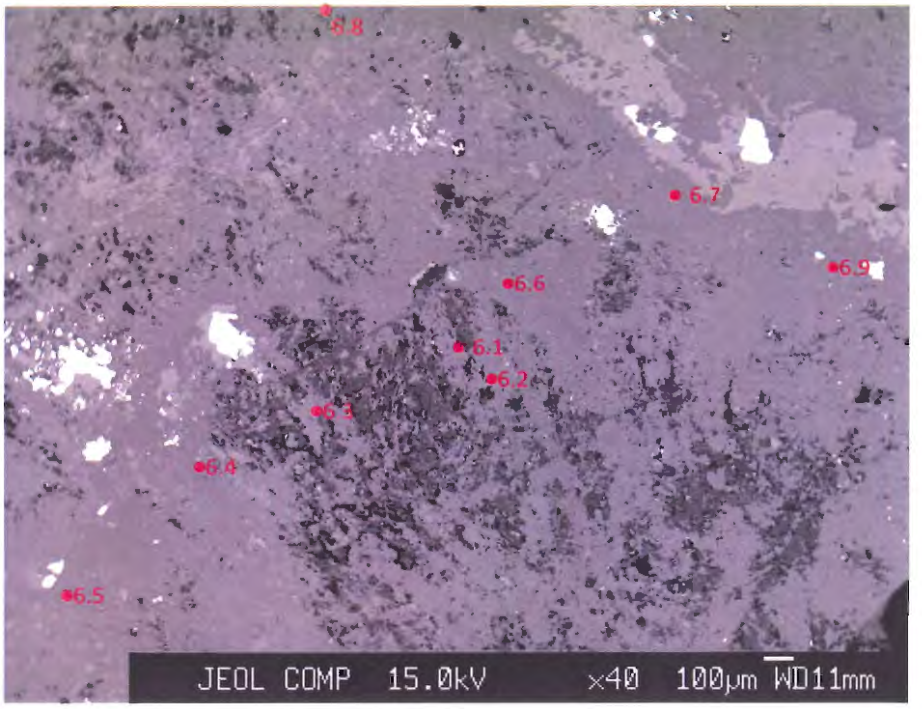


**Mass %**

| No. | $K_2O$ | $Cr_2O_3$ | $Na_2O$ | $Al_2O_3$ | MnO | CaO | $TiO_2$ | MgO | $SiO_2$ | FeO | $P_2O_5$ | Cl | F | NiO | $SO_3$ | Total | Mineral type |
|---|---|---|---|---|---|---|---|---|---|---|---|---|---|---|---|---|---|
| 6.1 | 0.23 | 0.00 | 7.92 | 24.66 | 0 | 6.89 | 0.00 | 0.00 | 60.09 | 0.01 | 0.00 | 0.01 | 0.02 | 0.00 | 0.00 | 99.81 | Andesine |
| 6.2 | 0.24 | 0.00 | 7.50 | 24.68 | 0 | 6.75 | 0.00 | 0.00 | 60.37 | 0.00 | 0.00 | 0.00 | 0.00 | 0.00 | 0.00 | 99.55 | Andesine |
| 6.3 | 0.20 | 0.00 | 9.09 | 21.81 | 0 | 3.43 | 0.00 | 0.00 | 65.74 | 0.00 | 0.01 | 0.07 | 0.00 | 0.00 | 0.00 | 100.34 | Oligoclase |
| 6.4 | 0.27 | 0.00 | 9.51 | 21.56 | 0 | 3.24 | 0.00 | 0.00 | 65.23 | 0.00 | 0.03 | 0.04 | 0.00 | 0.00 | 0.00 | 99.88 | Oligoclase |
| 6.5 | 0.42 | 0.00 | 4.74 | 20.37 | 0 | 1.60 | 0.00 | 0.01 | 68.03 | 0.03 | 0.28 | 0.00 | 0.01 | 0.00 | 0.02 | 95.51 | Oligoclase |
| 6.6 | 0.17 | 0.00 | 5.30 | 21.52 | 0 | 2.17 | 0.00 | 0.00 | 68.96 | 0.00 | 0.02 | 0.00 | 0.01 | 0.00 | 0.00 | 98.13 | Oligoclase |
| 6.7 | 0.34 | 0.01 | 9.92 | 21.63 | 0.006 | 3.33 | 0.00 | 0.00 | 64.23 | 0.06 | 0.00 | 0.00 | 0.00 | 0.01 | 0.02 | 99.56 | Oligoclase |
| 6.8 | 0.29 | 0.00 | 9.74 | 21.79 | 0 | 3.36 | 0.00 | 0.00 | 64.10 | 0.03 | 0.00 | 0.00 | 0.00 | 0.01 | 0.01 | 99.33 | Oligoclase |
| 6.9 | 1.75 | 0.00 | 1.86 | 24.27 | 0.011 | 2.04 | 0.01 | 0.43 | 64.97 | 0.47 | 0.00 | 0.01 | 0.04 | 0.01 | 0.00 | 95.83 | unstable |

**Cation Total**

| No. | K | Cr | Na | Al | Mn | Ca | Ti | Mg | Si | Fe | P | Cl | F | Ni | S | Total | Mineral type |
|---|---|---|---|---|---|---|---|---|---|---|---|---|---|---|---|---|---|
| 6.1 | 0.0016 | 0 | 0.0857 | 0.1624 | 0 | 0.0412 | 0 | 0 | 0.3357 | 0.0001 | 0 | 0.0001 | 0.0003 | 0 | 0 | 0.6272 | Andesine |
| 6.2 | 0.0017 | 0 | 0.0813 | 0.1625 | 0 | 0.0404 | 0 | 0 | 0.3372 | 0 | 0 | 0 | 0 | 0 | 0 | 0.6231 | Andesine |
| 6.3 | 0.0014 | 0 | 0.0965 | 0.1407 | 0 | 0.0201 | 0 | 0 | 0.3599 | 0 | 0 | 0.0006 | 0 | 0 | 0 | 0.6192 | Oligoclase |
| 6.4 | 0.0019 | 0 | 0.1016 | 0.14 | 0 | 0.0191 | 0 | 0 | 0.3594 | 0 | 0.0002 | 0.0004 | 0 | 0 | 0 | 0.6226 | Oligoclase |
| 6.5 | 0.003 | 0 | 0.0512 | 0.1339 | 0 | 0.0096 | 0 | 0.0001 | 0.3794 | 0.0001 | 0.0013 | 0 | 0.0001 | 0 | 0.0001 | 0.5789 | Oligoclase |
| 6.6 | 0.0012 | 0 | 0.056 | 0.1382 | 0 | 0.0126 | 0 | 0 | 0.3757 | 0 | 0.0001 | 0 | 0.0001 | 0 | 0 | 0.584 | Oligoclase |
| 6.7 | 0.0024 | 0.0001 | 0.1068 | 0.1414 | 0 | 0.0198 | 0 | 0 | 0.3564 | 0.0003 | 0 | 0 | 0 | 0 | 0.0001 | 0.6274 | Oligoclase |
| 6.8 | 0.002 | 0 | 0.1049 | 0.1427 | 0 | 0.02 | 0 | 0 | 0.3561 | 0.0002 | 0 | 0 | 0 | 0 | 0 | 0.6259 | Oligoclase |
| 6.9 | 0.0125 | 0 | 0.0201 | 0.1598 | 0.0001 | 0.0122 | 0 | 0.0035 | 0.363 | 0.0022 | 0 | 0.0001 | 0.0007 | 0 | 0 | 0.5743 | unstable |

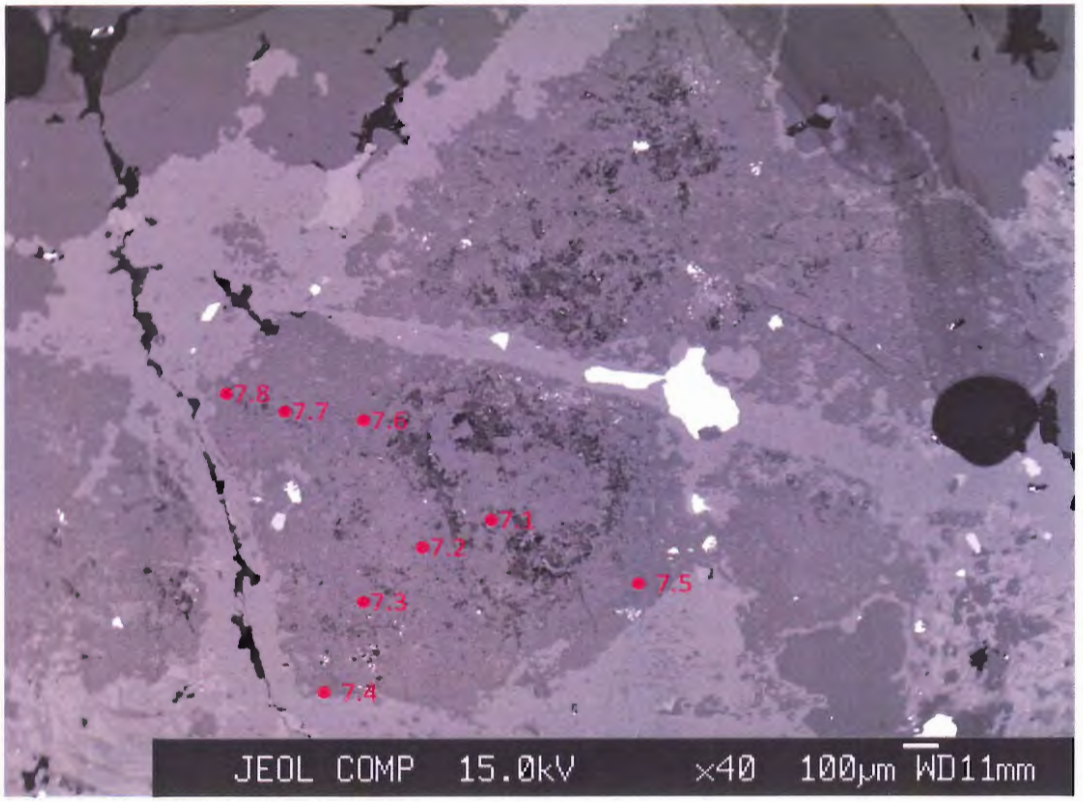


**Mass %**

| No. | $K_2O$ | $Cr_2O_3$ | $Na_2O$ | $Al_2O_3$ | MnO | CaO | $TiO_2$ | MgO | $SiO_2$ | FeO | $P_2O_5$ | Cl | F | NiO | $SO_3$ | Total | Mineral type |
|---|---|---|---|---|---|---|---|---|---|---|---|---|---|---|---|---|---|
| 7.1 | 5.53 | 0.00 | 3.98 | 27.43 | 0 | 1.91 | 0.01 | 0.63 | 57.19 | 0.84 | 0.75 | 0.01 | 0.18 | 0.00 | 0.04 | 98.42 | K-feldspar |
| 7.2 | 4.65 | 0.00 | 4.42 | 24.52 | 0 | 4.03 | 0.00 | 0.29 | 58.02 | 0.24 | 0.00 | 0.03 | 0.03 | 0.03 | 0.03 | 96.27 | unstable |
| 7.3 | 0.47 | 0.00 | 9.76 | 21.56 | 0 | 3.13 | 0.00 | 0.01 | 64.65 | 0.06 | 0.01 | 0.00 | 0.00 | 0.01 | 0.02 | 99.68 | Oligoclase |
| 7.4 | 0.37 | 0.00 | 2.69 | 21.30 | 0 | 1.89 | 0.00 | 0.03 | 69.68 | 0.03 | 0.00 | 0.04 | 0.02 | 0.00 | 0.02 | 96.06 | unstable |
| 7.5 | 0.37 | 0.00 | 7.59 | 21.10 | 0 | 2.13 | 0.00 | 0.00 | 68.30 | 0.09 | 0.00 | 0.00 | 0.00 | 0.01 | 0.02 | 99.62 | Anorthoclase |
| 7.6 | 0.24 | 0.00 | 8.62 | 24.24 | 0 | 5.93 | 0.00 | 0.01 | 61.24 | 0.05 | 0.00 | 0.00 | 0.00 | 0.00 | 0.02 | 100.35 | Andesine |
| 7.7 | 8.21 | 0.02 | 1.36 | 30.97 | 0 | 0.67 | 0.02 | 1.15 | 52.50 | 1.16 | 0.00 | 0.01 | 0.12 | 0.03 | 0.05 | 96.22 | K-feldspar |
| 7.8 | 0.52 | 0.00 | 4.98 | 23.83 | 0.008 | 4.41 | 0.00 | 0.02 | 64.98 | 0.06 | 0.00 | 0.01 | 0.00 | 0.04 | 0.03 | 98.89 | Oligoclase |

**Cation total**

| No. | K | Cr | Na | Al | Mn | Ca | Ti | Mg | Si | Fe | P | Cl | F | Ni | S | Total | Mineral type |
|---|---|---|---|---|---|---|---|---|---|---|---|---|---|---|---|---|---|
| 7.1 | 0.0402 | 0 | 0.044 | 0.1841 | 0 | 0.0116 | 0.0001 | 0.0053 | 0.3256 | 0.004 | 0.0036 | 0.0001 | 0.0032 | 0 | 0.0002 | 0.622 | K-feldspar |
| 7.2 | 0.0345 | 0 | 0.0499 | 0.1683 | 0 | 0.0251 | 0 | 0.0025 | 0.3379 | 0.0012 | 0 | 0.0002 | 0.0005 | 0.0001 | 0.0002 | 0.6205 | unstable |
| 7.3 | 0.0033 | 0 | 0.1048 | 0.1407 | 0 | 0.0186 | 0 | 0 | 0.3578 | 0.0003 | 0.0001 | 0 | 0 | 0.0001 | 0.0001 | 0.6259 | Oligoclase |
| 7.4 | 0.0026 | 0 | 0.0287 | 0.1379 | 0 | 0.0111 | 0 | 0.0002 | 0.3828 | 0.0002 | 0 | 0.0004 | 0.0003 | 0 | 0.0001 | 0.5644 | unstable |
| 7.5 | 0.0025 | 0 | 0.08 | 0.1352 | 0 | 0.0124 | 0 | 0 | 0.3713 | 0.0004 | 0 | 0 | 0 | 0.0001 | 0.0001 | 0.6021 | Anorthoclase |
| 7.6 | 0.0017 | 0 | 0.0927 | 0.1584 | 0 | 0.0353 | 0 | 0.0001 | 0.3397 | 0.0002 | 0 | 0 | 0 | 0 | 0.0001 | 0.6283 | Andesine |
| 7.7 | 0.0616 | 0.0001 | 0.0156 | 0.2148 | 0 | 0.0042 | 0.0001 | 0.0101 | 0.309 | 0.0057 | 0 | 0.0001 | 0.0022 | 0.0002 | 0.0002 | 0.6239 | K-feldspar |
| 7.8 | 0.0037 | 0 | 0.053 | 0.1542 | 0 | 0.026 | 0 | 0.0002 | 0.3567 | 0.0003 | 0 | 0.0001 | 0 | 0.0002 | 0.0001 | 0.5946 | Oligoclase |

## ZMMH-10 Sulphides (MM Granodiorite)

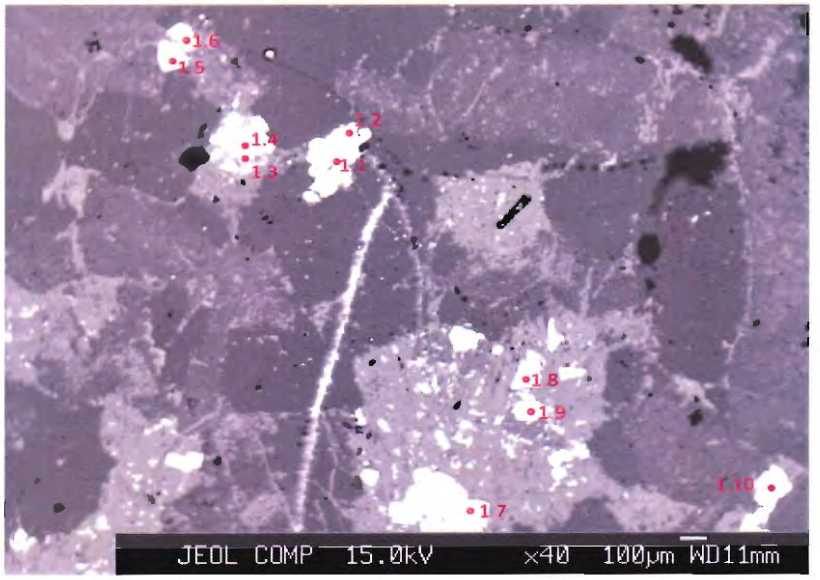


**Mass Percent**

| No. | Mo | S | As | Fe | Pb | Ag | Co | Ti | Ca | Cu | Sn | Sb | Mn | Zn | W | Total | Mineral |
|---|---|---|---|---|---|---|---|---|---|---|---|---|---|---|---|---|---|
| 1.1 | 0.0072 | 50.2275 | 0.0153 | 43.9959 | 0.2043 | 0.0741 | 0.3078 | 0.1203 | 0.0458 | 0.269 | 0.1362 | 0.1062 | 0.1487 | 0.4393 | 0.9603 | 97.0579 | pyrite |
| 1.2 | 0.0184 | 51.3077 | 0.0498 | 43.1368 | 0.2411 | 0.0437 | 0.3065 | 0.099 | 0.0096 | 0.2723 | 0.1494 | 0.1172 | 0.1079 | 0.4171 | 0.8029 | 97.0795 | pyrite |
| 1.3 | 0 | 31.3435 | 0.0494 | 30.7517 | 0.0558 | 0.0138 | 0.0126 | 0.1141 | 0.057 | 0.1292 | 0.1118 | 0.0487 | 0.3447 | 0.2137 | 0.452 | 63.6981 | pyrite |
| 1.4 | 0 | 27.8536 | 0 | 24.4639 | 0 | 0 | 0.1074 | 0.0594 | 1.633 | 0.0933 | 0.0468 | 0.0015 | 0.0605 | 0.1974 | 0.4246 | 54.9414 | pyrite |
| 1.5 | 0.0092 | 51.4537 | 0.0354 | 43.4407 | 0.2028 | 0.0646 | 0.2247 | 0.1068 | 0.0291 | 0.255 | 0.1524 | 0.1016 | 0.1069 | 0.4923 | 1.0286 | 97.7038 | pyrite |
| 1.6 | 0.0072 | 52.1252 | 0.0283 | 43.7317 | 0.2023 | 0.0454 | 0.1671 | 0.1156 | 0.0243 | 0.2602 | 0.1621 | 0.1211 | 0.1083 | 0.4297 | 0.9519 | 98.4805 | pyrite |
| 1.7 | 0 | 52.1629 | 0.0655 | 43.8929 | 0.1745 | 0.0638 | 0.0536 | 0.0978 | 0.0329 | 0.2875 | 0.1354 | 0.1035 | 0.1042 | 0.4066 | 0.8859 | 98.467 | pyrite |
| 1.8 | 0 | 51.391 | 0.071 | 43.9334 | 0.1302 | 0.0553 | 0.2331 | 0.1944 | 0.0162 | 0.228 | 0.1096 | 0.1023 | 0.0943 | 0.4416 | 0.8927 | 97.8931 | pyrite |
| 1.9 | 0.0123 | 51.6535 | 0.0608 | 43.6425 | 0.1648 | 0.047 | 0.2571 | 0.118 | 0.0084 | 0.2409 | 0.1697 | 0.1078 | 0.1173 | 0.4258 | 0.9795 | 98.0054 | pyrite |
| 1.10 | 0 | 6.239 | 0 | 4.1785 | 0 | 0 | 0.0186 | 0.0075 | 0.9174 | 0 | 0.0352 | 0.0622 | 0 | 0 | 0 | 11.4584 | pyrite |
| 1.11 | 0.0525 | 52.3401 | 0.052 | 44.0553 | 0.2127 | 0.0542 | 0.3695 | 0.1229 | 0.0395 | 0.3062 | 0.16 | 0.1114 | 0.1226 | 0.4655 | 0.9692 | 99.4336 | pyrite |

**Atomic Ratio**

| No. | Mo | S | As | Fe | Pb | Ag | Co | Ti | Ca | Cu | Sn | Sb | Mn | Zn | W | Total | Mineral |
|---|---|---|---|---|---|---|---|---|---|---|---|---|---|---|---|---|---|
| 1.1 | 0.0031 | 65.6568 | 0.0086 | 33.0134 | 0.0413 | 0.0288 | 0.2189 | 0.1052 | 0.0479 | 0.1774 | 0.0481 | 0.0365 | 0.1134 | 0.2816 | 0.2189 | 100 | pyrite |
| 1.2 | 0.008 | 66.6295 | 0.0277 | 32.1568 | 0.0485 | 0.0169 | 0.2165 | 0.086 | 0.01 | 0.1784 | 0.0524 | 0.0401 | 0.0818 | 0.2657 | 0.1818 | 100 | pyrite |
| 1.3 | 0 | 63.1265 | 0.0426 | 35.5528 | 0.0174 | 0.0083 | 0.0138 | 0.1537 | 0.0919 | 0.1313 | 0.0608 | 0.0258 | 0.4052 | 0.2111 | 0.1588 | 100 | pyrite |
| 1.4 | 0 | 63.932 | 0 | 32.2332 | 0 | 0 | 0.1341 | 0.0913 | 2.9982 | 0.108 | 0.029 | 0.0009 | 0.081 | 0.2222 | 0.17 | 100 | pyrite |
| 1.5 | 0.004 | 66.5156 | 0.0196 | 32.2362 | 0.0406 | 0.0248 | 0.158 | 0.0924 | 0.0301 | 0.1663 | 0.0532 | 0.0346 | 0.0806 | 0.3121 | 0.2319 | 100 | pyrite |
| 1.6 | 0.0031 | 66.7221 | 0.0155 | 32.1336 | 0.0401 | 0.0173 | 0.1164 | 0.0991 | 0.0249 | 0.168 | 0.0561 | 0.0408 | 0.0809 | 0.2698 | 0.2125 | 100 | pyrite |
| 1.7 | 0 | 66.7235 | 0.0359 | 32.2294 | 0.0345 | 0.0242 | 0.0373 | 0.0838 | 0.0337 | 0.1855 | 0.0468 | 0.0349 | 0.0778 | 0.2551 | 0.1976 | 100 | pyrite |
| 1.8 | 0 | 66.2715 | 0.0392 | 32.5218 | 0.026 | 0.0212 | 0.1635 | 0.1678 | 0.0167 | 0.1483 | 0.0382 | 0.0347 | 0.0709 | 0.2793 | 0.2008 | 100 | pyrite |
| 1.9 | 0.0053 | 66.5252 | 0.0335 | 32.2654 | 0.0328 | 0.018 | 0.1802 | 0.1017 | 0.0086 | 0.1565 | 0.059 | 0.0365 | 0.0881 | 0.269 | 0.22 | 99.9998 | pyrite |
| 1.1 | 0 | 66.2844 | 0 | 25.4836 | 0 | 0 | 0.1075 | 0.0531 | 7.7963 | 0 | 0.1009 | 0.1741 | 0 | 0 | 0 | 100 | pyrite |
| 1.11 | 0.0223 | 66.4812 | 0.0283 | 32.1221 | 0.0418 | 0.0204 | 0.2553 | 0.1045 | 0.0402 | 0.1962 | 0.0549 | 0.0373 | 0.0908 | 0.29 | 0.2147 | 100 | pyrite |

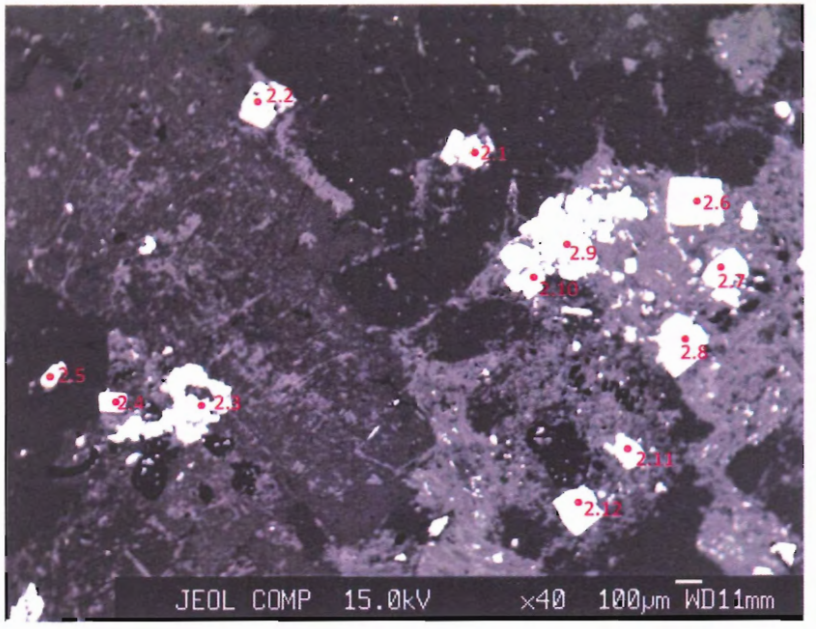


**Mass Percent**

| No. | Mo | S | As | Fe | Pb | Ag | Co | Ti | Ca | Cu | Sn | Sb | Mn | Zn | W | Total | Mineral |
|---|---|---|---|---|---|---|---|---|---|---|---|---|---|---|---|---|---|
| 2.1 | 0 | 52.0586 | 0.0511 | 44.0582 | 0.213 | 0.0462 | 0.1187 | 0.108 | 0.1285 | 0.281 | 0.1589 | 0.1272 | 0.107 | 0.4399 | 1.0512 | 98.9476 | pyrite |
| 2.2 | 0.0073 | 49.4516 | 0.0425 | 45.1898 | 0.1772 | 0.0521 | 0.1548 | 0.1081 | 0.0453 | 0.2686 | 0.156 | 0.0865 | 0.1357 | 0.4379 | 0.957 | 97.2705 | pyrite |
| 2.3 | 0 | 51.0961 | 0.0269 | 42.0204 | 0.1927 | 0.0614 | 0.1934 | 0.0975 | 0.5997 | 0.2378 | 0.1464 | 0.1091 | 0.1134 | 0.3861 | 0.9376 | 96.2186 | pyrite |
| 2.4 | 0 | 50.7116 | 0.0556 | 43.3694 | 0.1273 | 0.0419 | 0.0801 | 0.1106 | 0.0161 | 0.2624 | 0.1758 | 0.1004 | 0.1311 | 0.4106 | 0.9913 | 96.5843 | pyrite |
| 2.5 | 0 | 52.6324 | 0.0428 | 44.1574 | 0.2437 | 0.0521 | 0.1421 | 0.0923 | 0.0091 | 0.3587 | 0.1537 | 0.1122 | 0.1079 | 0.4531 | 1.014 | 99.5716 | pyrite |
| 2.6 | 0 | 52.1416 | 0.0484 | 44.0801 | 0.2162 | 0.055 | 0.1428 | 0.1236 | 0.0188 | 0.2972 | 0.1631 | 0.1224 | 0.1127 | 0.4546 | 0.9401 | 98.9167 | pyrite |
| 2.7 | 0 | 52.2434 | 0.0454 | 44.0068 | 0.1779 | 0.055 | 0.1508 | 0.1041 | 0.027 | 0.2736 | 0.1718 | 0.097 | 0.1157 | 0.4009 | 0.8298 | 98.6993 | pyrite |
| 2.8 | 0 | 52.315 | 0.0437 | 44.0905 | 0.1919 | 0.0391 | 0.1022 | 0.1021 | 0.0144 | 0.2362 | 0.1592 | 0.0903 | 0.1293 | 0.4149 | 0.8925 | 98.8214 | pyrite |
| 2.9 | 0 | 52.4284 | 0.0669 | 44.3483 | 0.2264 | 0.0575 | 0.1829 | 0.1072 | 0.0199 | 0.2616 | 0.1557 | 0.0977 | 0.114 | 0.4654 | 0.9473 | 99.4793 | pyrite |
| 2.10 | 0 | 52.1503 | 0.0467 | 43.9622 | 0.2058 | 0.0483 | 0.1914 | 0.1013 | 0.0354 | 0.225 | 0.1867 | 0.1081 | 0.1148 | 0.4449 | 1.0207 | 98.8417 | pyrite |
| 2.11 | 0.0273 | 52.3065 | 0.0446 | 44.0718 | 0.2195 | 0.0517 | 0.2236 | 0.0971 | 0.0254 | 0.2636 | 0.1333 | 0.0927 | 0.1197 | 0.4041 | 0.9863 | 99.0672 | pyrite |
| 2.12 | 0 | 51.7876 | 0.0129 | 44.2807 | 0.1324 | 0.0023 | 0 | 0.0485 | 0.0193 | 0 | 0 | 0 | 0 | 0.0243 | 0 | 96.3081 | pyrite |

**Atomic Ratio**

| No. | Mo | S | As | Fe | Pb | Ag | Co | Ti | Ca | Cu | Sn | Sb | Mn | Zn | W | Total | Mineral |
|---|---|---|---|---|---|---|---|---|---|---|---|---|---|---|---|---|---|
| 2.1 | 0 | 66.4542 | 0.0279 | 32.2848 | 0.0421 | 0.0175 | 0.0824 | 0.0922 | 0.1312 | 0.1809 | 0.0548 | 0.0427 | 0.0797 | 0.2754 | 0.234 | 99.9999 | pyrite |
| 2.2 | 0.0032 | 64.8037 | 0.0239 | 33.9938 | 0.0359 | 0.0203 | 0.1104 | 0.0948 | 0.0474 | 0.1776 | 0.0552 | 0.0299 | 0.1038 | 0.2814 | 0.2187 | 100 | pyrite |
| 2.3 | 0 | 66.7622 | 0.015 | 31.5169 | 0.039 | 0.0238 | 0.1375 | 0.0852 | 0.6268 | 0.1568 | 0.0517 | 0.0375 | 0.0865 | 0.2474 | 0.2136 | 99.9999 | pyrite |
| 2.4 | 0 | 66.3324 | 0.0311 | 32.5643 | 0.0258 | 0.0163 | 0.057 | 0.0968 | 0.0169 | 0.1732 | 0.0621 | 0.0346 | 0.1001 | 0.2634 | 0.2261 | 100 | pyrite |
| 2.5 | 0 | 66.6974 | 0.0232 | 32.1217 | 0.0478 | 0.0196 | 0.098 | 0.0783 | 0.0092 | 0.2293 | 0.0526 | 0.0374 | 0.0798 | 0.2816 | 0.2241 | 100 | pyrite |
| 2.6 | 0 | 66.5325 | 0.0265 | 32.2874 | 0.0427 | 0.0208 | 0.0991 | 0.1055 | 0.0192 | 0.1913 | 0.0562 | 0.0411 | 0.0839 | 0.2845 | 0.2092 | 99.9999 | pyrite |
| 2.7 | 0 | 66.6707 | 0.0248 | 32.2377 | 0.0351 | 0.0209 | 0.1047 | 0.0889 | 0.0276 | 0.1762 | 0.0592 | 0.0326 | 0.0861 | 0.2509 | 0.1847 | 100 | pyrite |
| 2.8 | 0 | 66.6938 | 0.0239 | 32.2659 | 0.0379 | 0.0148 | 0.0709 | 0.0871 | 0.0147 | 0.1519 | 0.0548 | 0.0303 | 0.0962 | 0.2594 | 0.1984 | 100 | pyrite |
| 2.9 | 0 | 66.522 | 0.0364 | 32.301 | 0.0444 | 0.0217 | 0.1262 | 0.091 | 0.0202 | 0.1674 | 0.0534 | 0.0326 | 0.0844 | 0.2896 | 0.2096 | 100 | pyrite |
| 2.10 | 0 | 66.5961 | 0.0255 | 32.2264 | 0.0407 | 0.0183 | 0.133 | 0.0866 | 0.0362 | 0.1449 | 0.0644 | 0.0364 | 0.0855 | 0.2786 | 0.2273 | 100 | pyrite |
| 2.11 | 0.0116 | 66.6127 | 0.0243 | 32.2183 | 0.0433 | 0.0196 | 0.1549 | 0.0828 | 0.0259 | 0.1693 | 0.0459 | 0.0311 | 0.089 | 0.2524 | 0.219 | 100 | pyrite |
| 2.12 | 0 | 67.0017 | 0.0072 | 32.8863 | 0.0265 | 0.0009 | 0 | 0.042 | 0.02 | 0 | 0 | 0 | 0 | 0.0154 | 0 | 100 | pyrite |

## ZMMH-11 Sulphides (MM Quartz Porphyry)

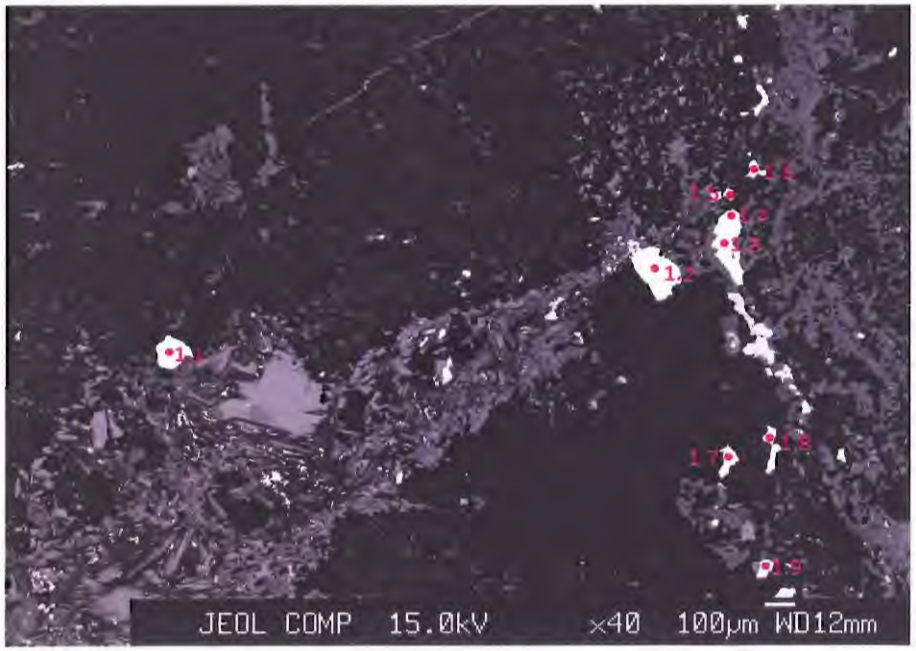


**Mass Percent**

| No. | Mo | S | As | Fe | Pb | Ag | Co | Ti | Ca | Cu | Sn | Sb | Mn | Zn | W | Total | Mineral |
|---|---|---|---|---|---|---|---|---|---|---|---|---|---|---|---|---|---|
| 1.1 | 0 | 33.7854 | 0 | 28.9219 | 0 | 0.038 | 0.0873 | 0.0029 | 0.0149 | 34.035 | 0.0145 | 0.0114 | 0 | 0.0835 | 0.1233 | 97.1181 | chalcopyrite |
| 1.2 | 0 | 33.9183 | 0 | 28.6683 | 0 | 0.0121 | 0.0723 | 0.0072 | 0.0074 | 34.1029 | 0.0392 | 0.0107 | 0 | 0.1273 | 0.0693 | 97.035 | chalcopyrite |
| 1.3 | 0 | 25.7118 | 0 | 11.0056 | 0 | 0.152 | 0.097 | 0.0432 | 0.0275 | 60.4177 | 0.0142 | 0.0319 | 0.0245 | 0.2496 | 0.405 | 98.1801 | bornite |
| 1.4 | 0 | 34.0818 | 0 | 28.7392 | 0 | 0.0436 | 0.0202 | 0.013 | 0.0034 | 33.8964 | 0 | 0 | 0.0078 | 0.1047 | 0.2588 | 97.1689 | chalcopyrite |
| 1.5 | 0 | 25.0454 | 0 | 10.3951 | 0 | 0.0292 | 0.151 | 0.0524 | 0.0211 | 61.9548 | 0.0202 | 0.0525 | 0.0241 | 0.247 | 0.4244 | 98.4173 | bornite |
| 1.6 | 0 | 25.4532 | 0 | 10.2796 | 0 | 0.0992 | 0.1506 | 0.0168 | 0.0205 | 62.0918 | 0.0605 | 0.056 | 0 | 0.2031 | 0.3668 | 98.7982 | bornite |
| 1.7 | 0 | 25.074 | 0 | 10.6574 | 0 | 0.1069 | 0.0234 | 0.0218 | 0.0162 | 62.7147 | 0.0292 | 0.0546 | 0.0352 | 0.2369 | 0.4634 | 99.4338 | bornite |
| 1.8 | 0 | 24.9874 | 0 | 10.2942 | 0.0861 | 0.1326 | 0.0637 | 0.0401 | 0.0281 | 62.2888 | 0.0473 | 0.0772 | 0.0214 | 0.2732 | 0.499 | 98.8392 | bornite |
| 1.9 | 0 | 25.1131 | 0 | 10.6564 | 0 | 0.129 | 0.0837 | 0.0321 | 0.0414 | 62.9525 | 0.0152 | 0.0291 | 0.0055 | 0.2262 | 0.5141 | 99.7983 | bornite |

**Atomic Ratio**

| No. | Mo | S | As | Fe | Pb | Ag | Co | Ti | Ca | Cu | Sn | Sb | Mn | Zn | W | Total | Mineral |
|---|---|---|---|---|---|---|---|---|---|---|---|---|---|---|---|---|---|
| 1.1 | 0 | 49.9047 | 0 | 24.5233 | 0 | 0.0167 | 0.0702 | 0.0028 | 0.0176 | 25.3622 | 0.0058 | 0.0044 | 0 | 0.0605 | 0.0318 | 100 | chalcopyrite |
| 1.2 | 0 | 50.0854 | 0 | 24.3007 | 0 | 0.0053 | 0.0581 | 0.0072 | 0.0088 | 25.4048 | 0.0156 | 0.0042 | 0 | 0.0922 | 0.0178 | 100 | chalcopyrite |
| 1.3 | 0 | 40.8918 | 0 | 10.0475 | 0 | 0.0718 | 0.0839 | 0.0459 | 0.035 | 48.4748 | 0.0061 | 0.0134 | 0.0227 | 0.1947 | 0.1123 | 99.9999 | bornite |
| 1.4 | 0 | 50.2564 | 0 | 24.3268 | 0 | 0.0191 | 0.0162 | 0.0128 | 0.004 | 25.2157 | 0 | 0 | 0.0067 | 0.0757 | 0.0666 | 100 | chalcopyrite |
| 1.5 | 0 | 39.9837 | 0 | 9.5263 | 0 | 0.0138 | 0.1311 | 0.056 | 0.027 | 49.8974 | 0.0087 | 0.0221 | 0.0224 | 0.1934 | 0.1182 | 100 | bornite |
| 1.6 | 0 | 40.3941 | 0 | 9.3647 | 0 | 0.0468 | 0.13 | 0.0179 | 0.026 | 49.7117 | 0.0259 | 0.0234 | 0 | 0.1581 | 0.1015 | 100 | bornite |
| 1.7 | 0 | 39.7104 | 0 | 9.6888 | 0 | 0.0503 | 0.0202 | 0.0231 | 0.0205 | 50.1069 | 0.0125 | 0.0228 | 0.0325 | 0.184 | 0.128 | 100 | bornite |
| 1.8 | 0 | 39.8373 | 0 | 9.4211 | 0.0212 | 0.0628 | 0.0552 | 0.0428 | 0.0358 | 50.0987 | 0.0204 | 0.0324 | 0.02 | 0.2136 | 0.1387 | 100 | bornite |
| 1.9 | 0 | 39.6463 | 0 | 9.6572 | 0 | 0.0605 | 0.0719 | 0.0339 | 0.0522 | 50.1376 | 0.0065 | 0.0121 | 0.0051 | 0.1751 | 0.1415 | 100 | bornite |

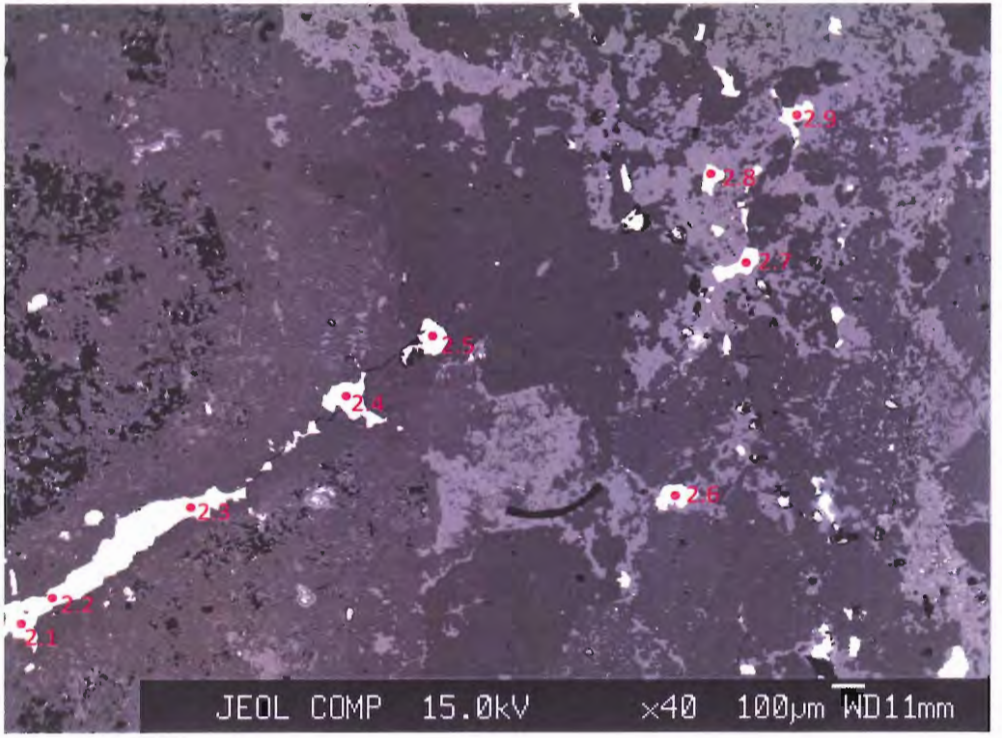


**Mass Percent**

| No. | Mo | S | As | Fe | Pb | Ag | Co | Ti | Ca | Cu | Sn | Sb | Mn | Zn | W | Total | Mineral |
|---|---|---|---|---|---|---|---|---|---|---|---|---|---|---|---|---|---|
| 2.1 | 0 | 25.4042 | 0 | 10.7624 | 0 | 0.1652 | 0.0701 | 0.0118 | 0.025 | 62.4988 | 0.0232 | 0.06 | 0.0226 | 0.2291 | 0.43 | 99.7025 | bornite |
| 2.2 | 0 | 8.557 | 0 | 10.3364 | 0 | 0 | 0.11 | 0 | 0 | 62.202 | 0 | 0 | 0.0405 | 0.2451 | 0.4299 | 81.921 | bornite |
| 2.3 | 0 | 25.3515 | 0 | 10.7277 | 0 | 0.1047 | 0.0364 | 0.0324 | 0.0305 | 62.6739 | 0.0281 | 0.066 | 0.0085 | 0.2449 | 0.4517 | 99.7563 | bornite |
| 2.4 | 0 | 25.2397 | 0 | 10.8631 | 0 | 0.0978 | 0.1441 | 0.0411 | 0.0284 | 62.7318 | 0.0856 | 0.0488 | 0.0059 | 0.2451 | 0.5742 | 100.106 | bornite |
| 2.5 | 0 | 18.9846 | 0 | 7.8408 | 0.6628 | 0.2747 | 0 | 0.0135 | 0.0653 | 45.4342 | 0.0284 | 0.0071 | 0.0141 | 0.1424 | 0.1127 | 73.5807 | bornite |
| 2.6 | 0 | 33.9644 | 0 | 28.8563 | 0.0322 | 0.0108 | 0 | 0.0035 | 0.0157 | 34.2971 | 0 | 0.0124 | 0.0039 | 0.09 | 0.0443 | 97.3307 | chalcopyrite |
| 2.7 | 0 | 31.9853 | 0 | 27.5755 | 0 | 0.0014 | 0.0082 | 0.0123 | 0.0014 | 33.116 | 0.0103 | 0.0424 | 0 | 0.0566 | 0.0719 | 92.8814 | chalcopyrite |
| 2.8 | 0 | 24.9419 | 0 | 10.7461 | 0 | 0.0649 | 0.1241 | 0.038 | 0.0371 | 62.8049 | 0.0603 | 0.0836 | 0.0115 | 0.2599 | 0.5137 | 99.6861 | bornite |
| 2.9 | 0 | 25.297 | 0 | 10.7407 | 0 | 0.1454 | 0 | 0.0338 | 0.0275 | 62.9608 | 0.0856 | 0.0593 | 0.0244 | 0.2072 | 0.3142 | 99.896 | bornite |

**Atomic Ratio**

| No. | Mo | S | As | Fe | Pb | Ag | Co | Ti | Ca | Cu | Sn | Sb | Mn | Zn | W | Total | Mineral |
|---|---|---|---|---|---|---|---|---|---|---|---|---|---|---|---|---|---|
| 2.1 | 0 | 40.0384 | 0 | 9.7369 | 0 | 0.0774 | 0.0601 | 0.0125 | 0.0315 | 49.6924 | 0.0099 | 0.0249 | 0.0208 | 0.1771 | 0.1182 | 100 | bornite |
| 2.2 | 0 | 18.5421 | 0 | 12.8572 | 0 | 0 | 0.1297 | 0 | 0 | 67.9968 | 0 | 0 | 0.0513 | 0.2605 | 0.1624 | 100 | bornite |
| 2.3 | 0 | 39.953 | 0 | 9.7049 | 0 | 0.049 | 0.0312 | 0.0341 | 0.0385 | 49.8287 | 0.012 | 0.0274 | 0.0078 | 0.1893 | 0.1241 | 100 | bornite |
| 2.4 | 0 | 39.7224 | 0 | 9.814 | 0 | 0.0457 | 0.1233 | 0.0432 | 0.0357 | 49.8067 | 0.0364 | 0.0202 | 0.0054 | 0.1892 | 0.1576 | 99.9999 | bornite |
| 2.5 | 0 | 40.6009 | 0 | 9.6257 | 0.2193 | 0.1746 | 0 | 0.0193 | 0.1116 | 49.019 | 0.0164 | 0.004 | 0.0176 | 0.1494 | 0.042 | 99.9999 | bornite |
| 2.6 | 0 | 50.0125 | 0 | 24.3913 | 0.0073 | 0.0047 | 0 | 0.0035 | 0.0184 | 25.4777 | 0 | 0.0048 | 0.0033 | 0.065 | 0.0114 | 100 | chalcopyrite |
| 2.7 | 0 | 49.5208 | 0 | 24.5076 | 0 | 0.0006 | 0.0069 | 0.0127 | 0.0017 | 25.8657 | 0.0043 | 0.0173 | 0 | 0.043 | 0.0194 | 100 | chalcopyrite |
| 2.8 | 0 | 39.4659 | 0 | 9.7607 | 0 | 0.0305 | 0.1068 | 0.0403 | 0.047 | 50.1341 | 0.0258 | 0.0348 | 0.0106 | 0.2017 | 0.1417 | 99.9999 | bornite |
| 2.9 | 0 | 39.8237 | 0 | 9.7061 | 0 | 0.068 | 0 | 0.0356 | 0.0346 | 50.0023 | 0.0364 | 0.0246 | 0.0224 | 0.16 | 0.0863 | 100 | bornite |

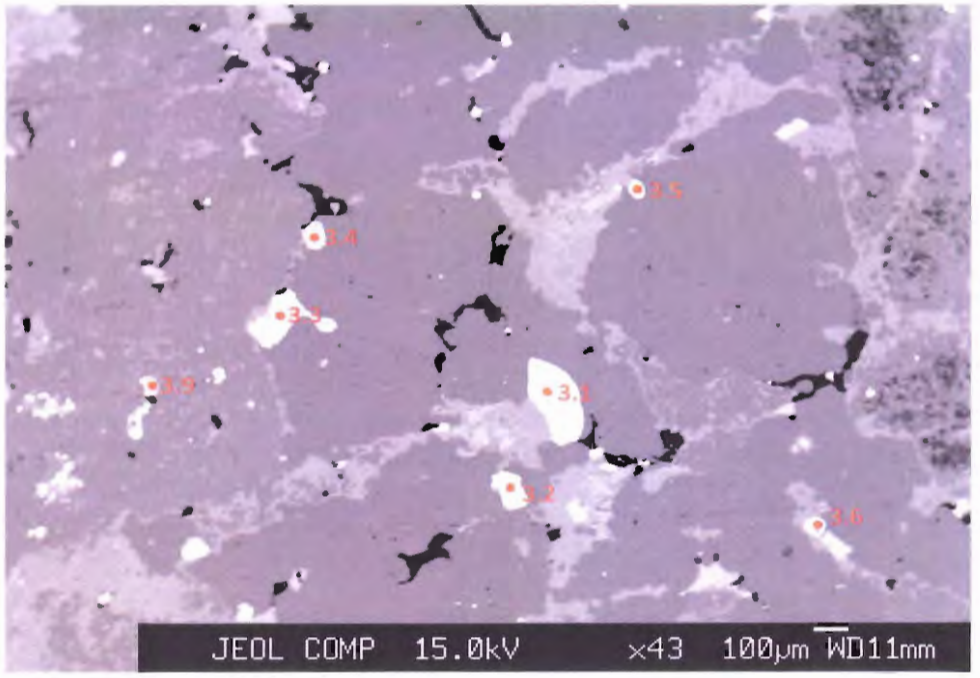


**Mass Percent**

| No. | Mo | S | As | Fe | Pb | Ag | Co | Ti | Ca | Cu | Sn | Sb | Mn | Zn | W | Total | Mineral |
|---|---|---|---|---|---|---|---|---|---|---|---|---|---|---|---|---|---|
| 3 | 0.0448 | 34.1344 | 0 | 28.7132 | 0.0139 | 0.0024 | 0 | 0.011 | 0.0145 | 34.3811 | 0 | 0 | 0.0097 | 0.1288 | 0.2284 | 97.6823 | chalcopyrite |
| 3.1 | 0 | 34.1069 | 0 | 29.2585 | 0 | 0.0008 | 0 | 0.0012 | 0.0027 | 34.442 | 0.0166 | 0 | 0 | 0.1414 | 0.1468 | 98.117 | chalcopyrite |
| 3.2 | 0 | 34.0181 | 0 | 28.9445 | 0 | 0.0108 | 0.1091 | 0.0045 | 0.0102 | 34.2642 | 0 | 0.0262 | 0.0144 | 0.0943 | 0.2394 | 97.7358 | chalcopyrite |
| 3.3 | 0 | 25.3308 | 0 | 10.8286 | 0 | 0.0726 | 0.0432 | 0.0155 | 0.0295 | 63.7064 | 0.0262 | 0.0426 | 0.0444 | 0.2357 | 0.3114 | 100.687 | bornite |
| 3.4 | 0 | 25.4149 | 0 | 10.6887 | 0.0031 | 0.0212 | 0 | 0.0411 | 0.0193 | 63.0256 | 0.0564 | 0.0644 | 0.0355 | 0.273 | 0.4525 | 100.096 | bornite |
| 3.5 | 0 | 34.2284 | 0 | 28.7625 | 0.0719 | 0.0092 | 0.0644 | 0.0214 | 0.0173 | 34.0917 | 0.036 | 0.0248 | 0 | 0.1249 | 0.2019 | 97.6545 | chalcopyrite |
| 3.6 | 0.2834 | 0.349 | 0.0733 | 0.4101 | 84.381 | 0.0875 | 0.6414 | 0.2866 | 0.4566 | 1.0202 | 0.392 | 1.1207 | 0.3282 | 1.3839 | 3.261 | 94.475 | ??? |
| 3.9 | 0.0749 | 23.4471 | 0.0546 | 4.4176 | 0.0886 | 0.1605 | 0.1973 | 0.1774 | 0.0604 | 73.0209 | 0.2181 | 0.1955 | 0.1518 | 0.8043 | 1.8528 | 104.922 | bornite |

**Atomic Ratio**

| No. | Mo | S | As | Fe | Pb | Ag | Co | Ti | Ca | Cu | Sn | Sb | Mn | Zn | W | Total | Mineral |
|---|---|---|---|---|---|---|---|---|---|---|---|---|---|---|---|---|---|
| 3 | 0.022 | 50.1188 | 0 | 24.2008 | 0.0032 | 0.0011 | 0 | 0.0108 | 0.017 | 25.4669 | 0 | 0 | 0.0083 | 0.0927 | 0.0585 | 100 | chalcopyrite |
| 3.1 | 0 | 49.8782 | 0 | 24.5618 | 0 | 0.0004 | 0 | 0.0011 | 0.0032 | 25.4099 | 0.0066 | 0 | 0 | 0.1014 | 0.0374 | 100 | chalcopyrite |
| 3.2 | 0 | 49.956 | 0 | 24.3997 | 0 | 0.0047 | 0.0872 | 0.0045 | 0.012 | 25.3844 | 0 | 0.0101 | 0.0123 | 0.0679 | 0.0613 | 100 | chalcopyrite |
| 3.3 | 0 | 39.5925 | 0 | 9.7157 | 0 | 0.0337 | 0.0367 | 0.0162 | 0.0369 | 50.2336 | 0.0111 | 0.0176 | 0.0405 | 0.1807 | 0.0849 | 100 | bornite |
| 3.4 | 0 | 39.9219 | 0 | 9.6381 | 0.0008 | 0.0099 | 0 | 0.0432 | 0.0243 | 49.9445 | 0.0239 | 0.0266 | 0.0326 | 0.2103 | 0.124 | 100 | bornite |
| 3.5 | 0 | 50.2415 | 0 | 24.235 | 0.0163 | 0.004 | 0.0514 | 0.021 | 0.0204 | 25.2448 | 0.0143 | 0.0096 | 0 | 0.0899 | 0.0517 | 99.9999 | chalcopyrite |
| 3.6 | 0.5554 | 2.0463 | 0.1839 | 1.3802 | 76.562 | 0.1525 | 2.0462 | 1.125 | 2.1415 | 3.0178 | 0.6208 | 1.7304 | 1.1232 | 3.9799 | 3.3345 | 100 | ??? |
| 3.9 | 0.039 | 36.5666 | 0.0364 | 3.9548 | 0.0214 | 0.0744 | 0.1674 | 0.1852 | 0.0753 | 57.4501 | 0.0919 | 0.0803 | 0.1381 | 0.6152 | 0.5039 | 100 | bornite |

## ZMMH-14 Sulphides (MM Porphyry)

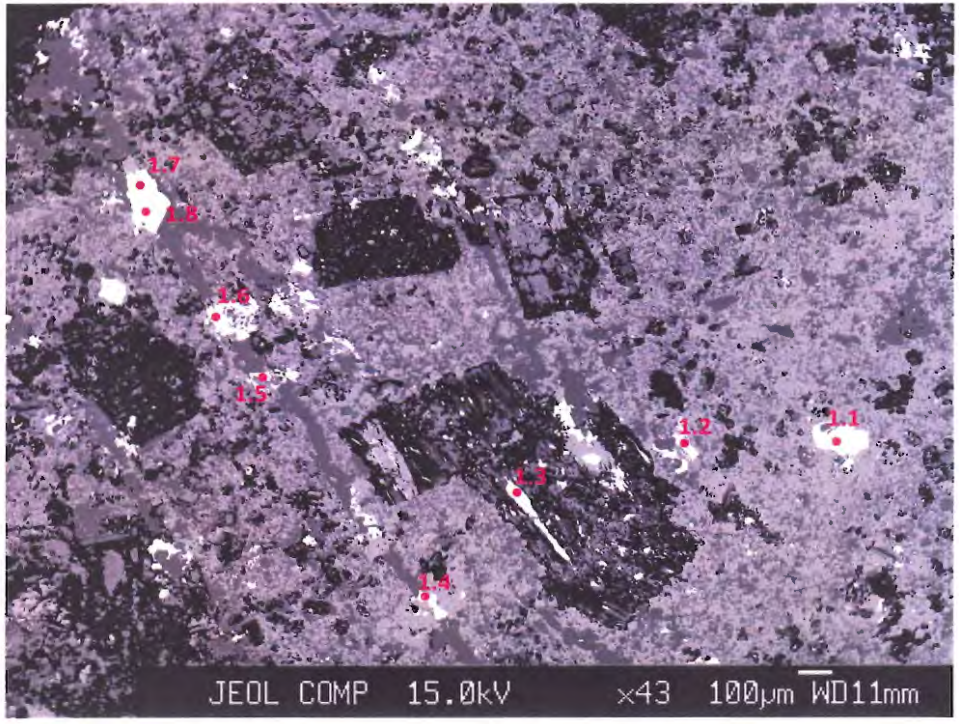


**Mass Percent**

| No. | Mo | S | As | Fe | Pb | Ag | Co | Ti | Ca | Cu | Sn | Sb | Mn | Zn | W | Total | Mineral |
|---|---|---|---|---|---|---|---|---|---|---|---|---|---|---|---|---|---|
| 1.1 | 0 | 35.1452 | 0.0108 | 28.8937 | 0 | 0.0659 | 0.0039 | 0.0412 | 0.0052 | 34.2039 | 0.0468 | 0.0823 | 0.0214 | 0.1353 | 0.3833 | 99.0389 | chalcopyrite |
| 1.2 | 0.0183 | 25.1428 | 0 | 10.5293 | 0 | 0.1344 | 0 | 0.0605 | 0.0497 | 62.1406 | 0.0538 | 0.1031 | 0.0414 | 0.3282 | 0.5793 | 99.1815 | bornite |
| 1.3 | 0 | 34.1697 | 0 | 28.8313 | 0 | 0.0483 | 0.0497 | 0.0523 | 0.0181 | 34.0941 | 0.0314 | 0.0626 | 0.0113 | 0.2485 | 0.2589 | 97.8763 | chalcopyrite |
| 1.4 | 0 | 34.2483 | 0 | 28.5306 | 0 | 0.0686 | 0.02 | 0.0257 | 0.024 | 34.5086 | 0.0262 | 0.0778 | 0.0295 | 0.2673 | 0.4148 | 98.2415 | chalcopyrite |
| 1.5 | 0.0019 | 25.4927 | 0.0271 | 10.2518 | 0 | 0.0706 | 0.0162 | 0.0643 | 0.0396 | 61.5839 | 0.065 | 0.0815 | 0.0278 | 0.375 | 0.6401 | 98.7375 | bornite |
| 1.6 | 0 | 25.52 | 3.4071 | 8.4763 | 0.0259 | 0.1866 | 0.0299 | 0.0615 | 0.0609 | 57.5389 | 0.051 | 0.1298 | 0.059 | 0.7099 | 0.521 | 96.7779 | bornite |
| 1.7 | 0.0061 | 25.9352 | 0 | 10.7544 | 0 | 0.1173 | 0.0022 | 0.0506 | 0.0379 | 62.6309 | 0.0891 | 0.0983 | 0.0504 | 0.2976 | 0.5607 | 100.631 | bornite |
| 1.8 | 0 | 34.524 | 0 | 29.0048 | 0 | 0.057 | 0 | 0.024 | 0.0102 | 34.6069 | 0.0387 | 0.0329 | 0.028 | 0.1473 | 0.3472 | 98.821 | chalcopyrite |

**Atomic Ratio**

| No. | Mo | S | As | Fe | Pb | Ag | Co | Ti | Ca | Cu | Sn | Sb | Mn | Zn | W | Total | Mineral |
|---|---|---|---|---|---|---|---|---|---|---|---|---|---|---|---|---|---|
| 1.1 | 0 | 50.7698 | 0.0067 | 23.9598 | 0 | 0.0283 | 0.0031 | 0.0399 | 0.006 | 24.9266 | 0.0182 | 0.0313 | 0.018 | 0.0958 | 0.0966 | 100 | chalcopyrite |
| 1.2 | 0.0097 | 39.9154 | 0 | 9.5955 | 0 | 0.0634 | 0 | 0.0643 | 0.0632 | 49.768 | 0.0231 | 0.0431 | 0.0384 | 0.2555 | 0.1604 | 100 | bornite |
| 1.3 | 0 | 50.0953 | 0 | 24.2639 | 0 | 0.021 | 0.0397 | 0.0514 | 0.0212 | 25.2164 | 0.0124 | 0.0242 | 0.0096 | 0.1787 | 0.0662 | 100 | chalcopyrite |
| 1.4 | 0 | 50.1066 | 0 | 23.9611 | 0 | 0.0298 | 0.0159 | 0.0251 | 0.0281 | 25.4701 | 0.0104 | 0.03 | 0.0252 | 0.1918 | 0.1058 | 100 | chalcopyrite |
| 1.5 | 0.001 | 40.5204 | 0.0184 | 9.354 | 0 | 0.0334 | 0.014 | 0.0684 | 0.0504 | 49.3826 | 0.0279 | 0.0341 | 0.0258 | 0.2924 | 0.1774 | 100 | bornite |
| 1.6 | 0 | 41.4567 | 2.3685 | 7.9042 | 0.0065 | 0.0901 | 0.0264 | 0.0669 | 0.0792 | 47.1546 | 0.0224 | 0.0555 | 0.056 | 0.5656 | 0.1476 | 100 | bornite |
| 1.7 | 0.0032 | 40.4414 | 0 | 9.6264 | 0 | 0.0544 | 0.0019 | 0.0528 | 0.0472 | 49.269 | 0.0375 | 0.0404 | 0.0458 | 0.2276 | 0.1525 | 100 | bornite |
| 1.8 | 0 | 50.1498 | 0 | 24.1856 | 0 | 0.0246 | 0 | 0.0233 | 0.0118 | 25.3605 | 0.0152 | 0.0126 | 0.0237 | 0.1049 | 0.088 | 100 | chalcopyrite |

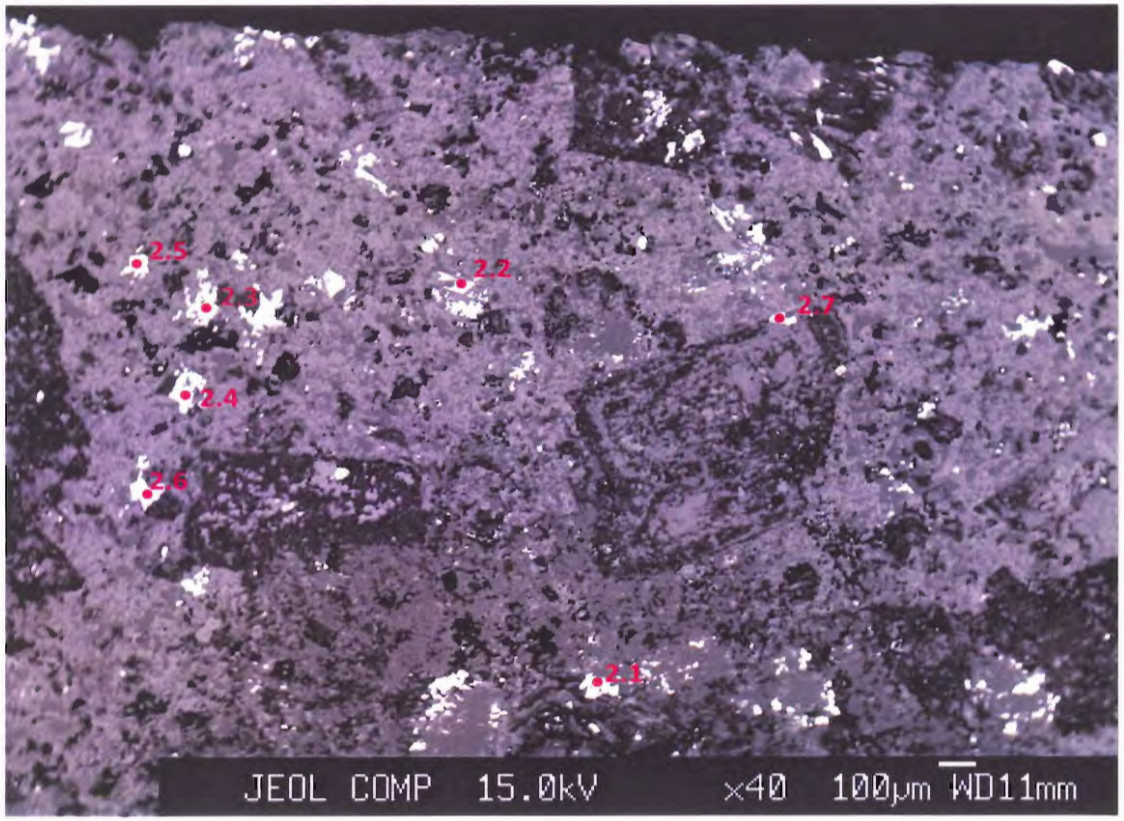


**Mass Percent**

| No. | Mo | S | As | Fe | Pb | Ag | Co | Ti | Ca | Cu | Sn | Sb | Mn | Zn | W | Total | Mineral |
|---|---|---|---|---|---|---|---|---|---|---|---|---|---|---|---|---|---|
| 2.1 | 0 | 34.1049 | 0.0064 | 28.0119 | 0 | 0.0628 | 0 | 0.0915 | 0.0405 | 33.429 | 0.0293 | 0.0909 | 0.0093 | 0.2095 | 0.4523 | 96.5384 | chalcopyrite |
| 2.2 | 0 | 34.2452 | 0.0011 | 28.4041 | 0 | 0.0295 | 0 | 0.0314 | 0.0429 | 33.8787 | 0.018 | 0.0525 | 0.019 | 0.2098 | 0.4007 | 97.3329 | chalcopyrite |
| 2.3 | 0 | 34.492 | 0.006 | 28.3696 | 0 | 0.0579 | 0 | 0.0122 | 0.0266 | 34.1822 | 0.0037 | 0.0595 | 0.0291 | 0.1963 | 0.3747 | 97.8099 | chalcopyrite |
| 2.4 | 0 | 34.2232 | 0.0164 | 28.7472 | 0 | 0.034 | 0 | 0.0422 | 0.0123 | 33.6642 | 0.0365 | 0.0723 | 0.0303 | 0.2342 | 0.3501 | 97.463 | chalcopyrite |
| 2.5 | 0 | 34.2973 | 0 | 28.1732 | 0.0464 | 0.0212 | 0.0421 | 0.0085 | 0.0287 | 33.4263 | 0.0642 | 0.0827 | 0.0105 | 0.1877 | 0.3639 | 96.7527 | chalcopyrite |
| 2.6 | 0 | 33.9901 | 0 | 28.0206 | 0 | 0.0556 | 0 | 0.0348 | 0.0238 | 33.1062 | 0 | 0.0768 | 0.0051 | 0.1873 | 0.3254 | 95.8258 | chalcopyrite |
| 2.7 | 0 | 34.2066 | 0 | 28.1391 | 0 | 0.0516 | 0.0274 | 0.0267 | 0.0305 | 33.3935 | 0.0109 | 0.046 | 0.0194 | 0.1909 | 0.3762 | 96.5189 | chalcopyrite |

**Atomic Ratio**

| No. | Mo | S | As | Fe | Pb | Ag | Co | Ti | Ca | Cu | Sn | Sb | Mn | Zn | W | Total | Mineral |
|---|---|---|---|---|---|---|---|---|---|---|---|---|---|---|---|---|---|
| 2.1 | 0 | 50.6134 | 0.0041 | 23.8634 | 0 | 0.0277 | 0 | 0.0909 | 0.048 | 25.0277 | 0.0117 | 0.0355 | 0.0081 | 0.1525 | 0.117 | 100 | chalcopyrite |
| 2.2 | 0 | 50.4283 | 0.0007 | 24.0102 | 0 | 0.0129 | 0 | 0.0309 | 0.0506 | 25.168 | 0.0072 | 0.0204 | 0.0163 | 0.1515 | 0.1029 | 99.9999 | chalcopyrite |
| 2.3 | 0 | 50.5258 | 0.0038 | 23.8555 | 0 | 0.0252 | 0 | 0.0119 | 0.0311 | 25.2606 | 0.0014 | 0.0229 | 0.0249 | 0.141 | 0.0957 | 99.9999 | chalcopyrite |
| 2.4 | 0 | 50.3386 | 0.0103 | 24.2726 | 0 | 0.0149 | 0 | 0.0416 | 0.0145 | 24.9803 | 0.0145 | 0.028 | 0.026 | 0.1689 | 0.0898 | 100 | chalcopyrite |
| 2.5 | 0 | 50.7366 | 0 | 23.9243 | 0.0106 | 0.0093 | 0.0339 | 0.0084 | 0.034 | 24.9458 | 0.0257 | 0.0322 | 0.0091 | 0.1362 | 0.0939 | 100 | chalcopyrite |
| 2.6 | 0 | 50.7261 | 0 | 24.0047 | 0 | 0.0247 | 0 | 0.0348 | 0.0284 | 24.9251 | 0 | 0.0302 | 0.0044 | 0.1371 | 0.0847 | 100 | chalcopyrite |
| 2.7 | 0 | 50.7034 | 0 | 23.943 | 0 | 0.0227 | 0.0221 | 0.0265 | 0.0362 | 24.9711 | 0.0044 | 0.018 | 0.0168 | 0.1388 | 0.0972 | 100 | chalcopyrite |

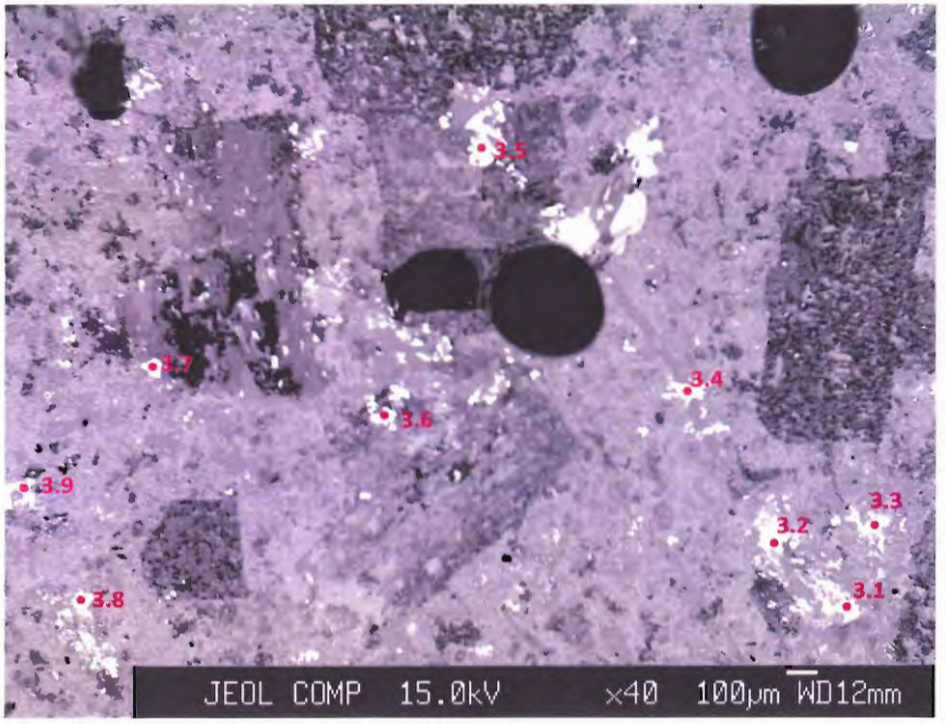


**Mass Percent**

| No. | Mo | S | As | Fe | Pb | Ag | Co | Ti | Ca | Cu | Sn | Sb | Mn | Zn | W | Total | Mineral |
|---|---|---|---|---|---|---|---|---|---|---|---|---|---|---|---|---|---|
| 3.1 | 0 | 34.3127 | 0.0294 | 28.1762 | 0 | 0.0304 | 0.042 | 0.0317 | 0.0209 | 33.6142 | 0.0067 | 0.0892 | 0.0256 | 0.2285 | 0.3623 | 96.9698 | chalcopyrite |
| 3.2 | 0 | 34.3256 | 0.012 | 28.5121 | 0.0101 | 0.0603 | 0.1013 | 0.0135 | 0.0301 | 33.9874 | 0.0437 | 0.0622 | 0.0039 | 0.1931 | 0.3485 | 97.7039 | chalcopyrite |
| 3.3 | 0 | 20.5339 | 0.1312 | 7.9407 | 0 | 0.1092 | 0 | 0.0279 | 0.0176 | 53.7881 | 0.0022 | 0.1677 | 0.0107 | 0.2814 | 0.309 | 83.3196 | bornite |
| 3.4 | 0 | 34.0149 | 0.0154 | 28.627 | 0 | 0.0467 | 0 | 0.0472 | 0.023 | 33.5406 | 0.0304 | 0.0463 | 0.0128 | 0.1679 | 0.3981 | 96.9704 | chalcopyrite |
| 3.5 | 0 | 34.0455 | 0 | 28.29 | 0 | 0.0431 | 0 | 0.0179 | 0.0273 | 33.6357 | 0.0283 | 0.0688 | 0 | 0.2433 | 0.3097 | 96.7097 | chalcopyrite |
| 3.6 | 0 | 26.4013 | 0.0131 | 11.0672 | 0 | 0.0705 | 0 | 0.0567 | 0.0351 | 60.5895 | 0.0368 | 0.1191 | 0.0316 | 0.3793 | 0.6593 | 99.4596 | bornite |
| 3.7 | 0 | 34.4408 | 0 | 28.4827 | 0 | 0.0491 | 0.0123 | 0.0544 | 0.0195 | 33.9806 | 0 | 0.0588 | 0.0276 | 0.2714 | 0.3626 | 97.7599 | chalcopyrite |
| 3.8 | 0 | 26.0869 | 0 | 10.7029 | 0 | 0.1123 | 0.1032 | 0.0533 | 0.0442 | 60.9184 | 0.0065 | 0.0941 | 0.0382 | 0.3542 | 0.6664 | 99.1807 | bornite |
| 3.9 | 0 | 34.273 | 0.0027 | 28.3445 | 0 | 0.0508 | 0 | 0.0226 | 0.0127 | 33.6845 | 0.0088 | 0.064 | 0.0288 | 0.243 | 0.3336 | 97.0691 | chalcopyrite |

**Atomic Ratio**

| No. | Mo | S | As | Fe | Pb | Ag | Co | Ti | Ca | Cu | Sn | Sb | Mn | Zn | W | Total | Mineral |
|---|---|---|---|---|---|---|---|---|---|---|---|---|---|---|---|---|---|
| 3.1 | 0 | 50.6516 | 0.0186 | 23.8759 | 0 | 0.0133 | 0.0337 | 0.0314 | 0.0246 | 25.0327 | 0.0027 | 0.0347 | 0.0221 | 0.1655 | 0.0933 | 100 | chalcopyrite |
| 3.2 | 0 | 50.3769 | 0.0076 | 24.0206 | 0.0023 | 0.0263 | 0.0808 | 0.0133 | 0.0354 | 25.1639 | 0.0173 | 0.0241 | 0.0033 | 0.139 | 0.0892 | 100 | chalcopyrite |
| 3.3 | 0 | 39.0439 | 0.1068 | 8.6673 | 0 | 0.0617 | 0 | 0.0355 | 0.0268 | 51.5961 | 0.0012 | 0.084 | 0.0119 | 0.2625 | 0.1025 | 100 | bornite |
| 3.4 | 0 | 50.304 | 0.0097 | 24.3024 | 0 | 0.0205 | 0 | 0.0467 | 0.0272 | 25.0237 | 0.0121 | 0.018 | 0.0111 | 0.1218 | 0.1027 | 100 | chalcopyrite |
| 3.5 | 0 | 50.4382 | 0 | 24.0587 | 0 | 0.019 | 0 | 0.0178 | 0.0324 | 25.1391 | 0.0113 | 0.0268 | 0 | 0.1767 | 0.08 | 100 | chalcopyrite |
| 3.6 | 0 | 41.3982 | 0.0088 | 9.9617 | 0 | 0.0329 | 0 | 0.0595 | 0.0441 | 47.9293 | 0.0156 | 0.0492 | 0.0289 | 0.2917 | 0.1803 | 100 | bornite |
| 3.7 | 0 | 50.474 | 0 | 23.9616 | 0 | 0.0214 | 0.0098 | 0.0533 | 0.0228 | 25.1231 | 0 | 0.0227 | 0.0236 | 0.195 | 0.0927 | 100 | chalcopyrite |
| 3.8 | 0 | 41.106 | 0 | 9.6811 | 0 | 0.0526 | 0.0885 | 0.0562 | 0.0557 | 48.426 | 0.0028 | 0.0391 | 0.0351 | 0.2738 | 0.1831 | 100 | bornite |
| 3.9 | 0 | 50.5561 | 0.0017 | 24.0011 | 0 | 0.0223 | 0 | 0.0224 | 0.015 | 25.0668 | 0.0035 | 0.0249 | 0.0248 | 0.1758 | 0.0858 | 100 | chalcopyrite |

# Appendix 2 Petrographic Descriptions

The following section contains petrographic descriptions of each core chip sample obtained from MMH (table 4.1). Photos of the core chip sample and photos taken with a microscopic camera are also included. The petrographic descriptions were done by observations using optical and reflected light microscopy.

**ZMMH-4**

**DDH 3173 888.5-888.63 m**

PHb (Hornblende Porphyry)


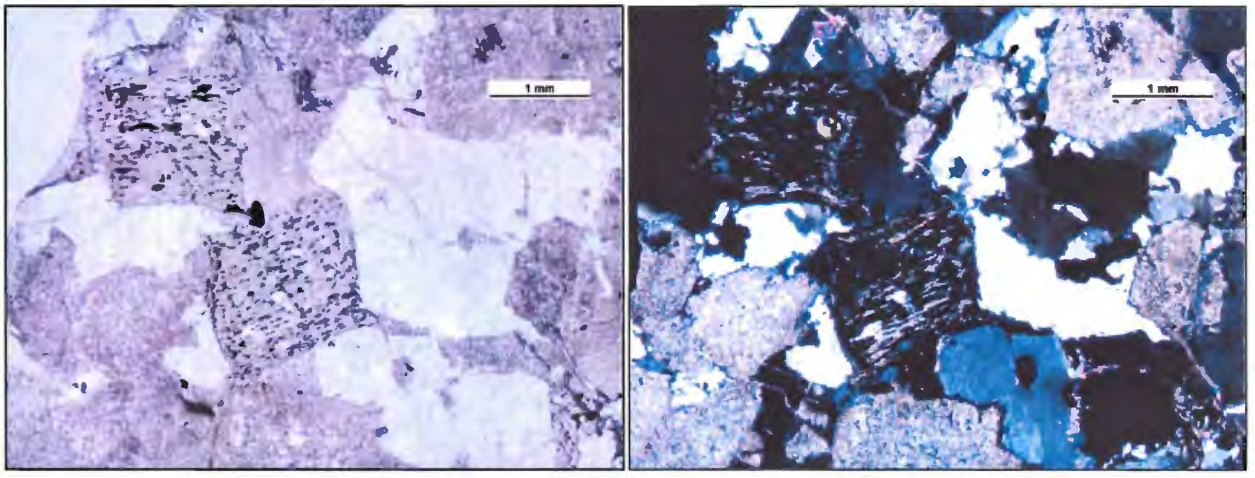


Observations

*Rock Chip*

The sample has a light-green to light-grey colour with a pink colouring surrounding the veins. There are also dark green hornblende phenocrysts as well as quartz phenocrysts.

*Thin Section/Polished Section*

The sample has a porphyritic texture with feldspar phenocrysts that have been entirely altered to sericite. These phenocrysts range in size from 2.5-0.5mm and are euhedral to subhedral prismatic. Hornblende phenocrysts are rectangular and have undergone chloritization. The hornblende is poikilitic and chloritized with inclusions of quartz, chalcopyrite and

molybdenite and occasionally zircon and apatite. Quartz phenocrysts are massive and anhedral with sutured boundaries. The quartz is interstitial between feldspar phenocrysts. Veins are common in the thin section. They are <0.25mm thick and mostly comprised of quartz and anhydrite with inclusions of chalcopyrite and chalcocite. The veins contain halos of chlorite.

Discussion

Due to the poikiloblastic nature of the hornblende phenocrysts, it is possible that they replace some other pre-existing mafic mineral. The chalcocite + chalcopyrite + molybdenite sulphide assemblage as well as the pink colour observed in the rock chip indicates that this sample has undergone potassic alteration. The presence of chalcopyrite and anhydrite in the veins indicate that the sample contains A- and/or B-type quartz veins. The latter is the most probably as there was no feldspar (or sericite) observed in the veins. The overprinting of feldspar phenocrysts by sericite and the light green colour of the rock chip indicate a later alteration phase such as chlorite-sericite alteration affected the sample.

**ZMMH-5**

**DDH 3173 853.75-853.86m**

**Grd MM** (MM Granodiorite)

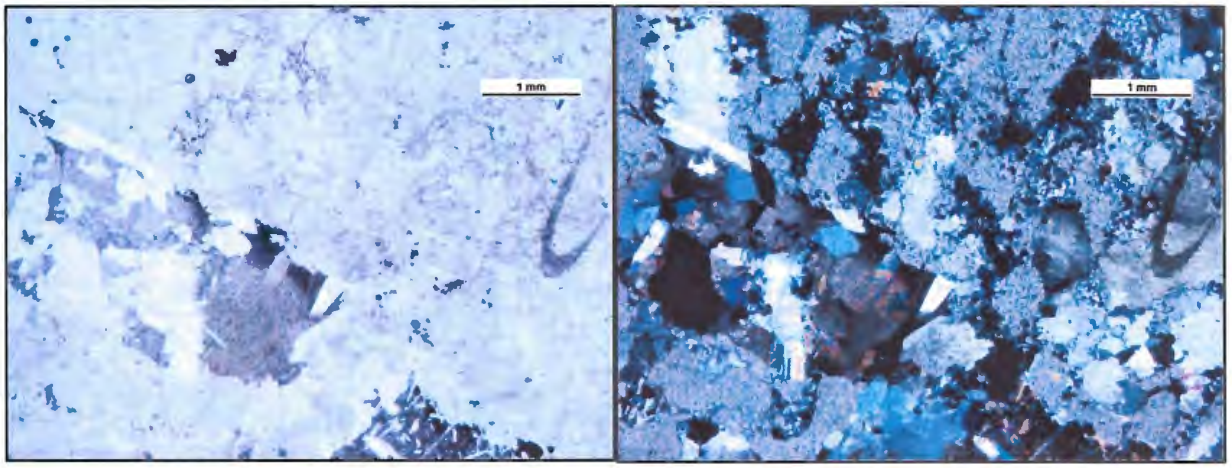


Observations

*Rock Chip*

The sample has a dark- to medium-green colour as well as portions that are light-grey to light-pink. Quartz phenocrysts are visible as well as disseminated chalcopyrite and pyrite.

*Thin Section/Polished Section*

The sample has a generally equigranular, hypidiomorphic texture. Feldspars show a prismatic shape and have been almost entirely altered to sericite. Chloritized remnants of biotite and/or amphibole are poikiloblastic with inclusions of quartz, apatite, chalcopyrite and rutile. There is one evident vein that is 1.5 mm thick. It contains euhedral, prismatic quartz, anhydrite, sericite and pyrite. It does not appear to have a chloritic halo. The thin sections contain sulphides such as pyrite and chalcocite which are disseminated as well as a small amount of what appear to be galena (not confirmed).

Discussion

The presence of chalcopyrite within the altered biotite and hornblende, the presence of chalcocite as well as the pink colour observed in the rock chip indicates that the sample had initially undergone potassic alteration. The sericitization of the feldspars, the chloritization of the hornblende/biotite and the pyrite indicates that the sample was later affected by a higher sulphidation alteration phase, likely chlorite-sericite. It is difficult to classify this vein as it has characteristics of both A- and B-type veins however; the euhedral quartz and central channel indicates that it is more of a B-type vein. It is likely that this vein was formed during conditions that were transitional from A-type quartz vein formation to B-type.

**ZMMH-7**

**DDH 4903 1012.0-1012.25m**

**PMM** (MM Porphyry)


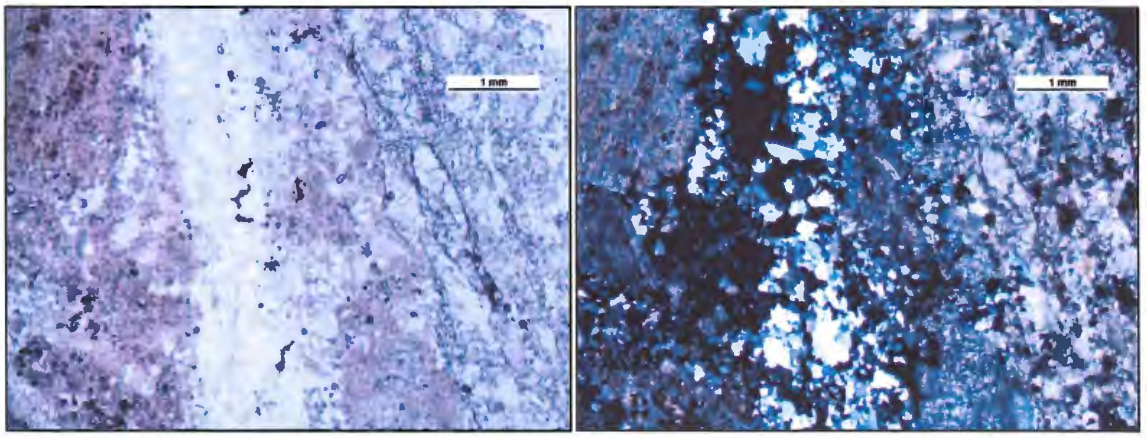


Observations

*Rock Chip*

The sample is light- to dark- grey with a carbonate vein on the edge.

*Thin Section/Polished Section*

The sample is vuggy and porphyritic with feldspar phenocrysts that have been partially sericitized. These feldspars are plagioclase and are up to 4 mm in length. There are also large quartz phenocrysts with embayed grain boundaries. Less commonly, there are smaller phenocrysts (1 mm in length) of biotite that has been thoroughly chloritized. These phenocrysts are poikilitic with inclusions of carbonate, euhedral quartz, chalcopyrite and chalcocite. Apatite and rare zircon crystals typically appear within close proximity of these chloritized biotite

phenocrysts. Occasionally they appear elsewhere in the sample. The groundmass is fine-grained quartz with embayed and sub-grain boundaries, much like the quartz phenocrysts. There is an aplitic quartz vein that is 1.5 mm thick which contains chalcopyrite and bornite. This vein does not have a chloritized halo. There is also a carbonate vein at the edge of the slide with an undeterminable thickness. Beyond the sulphides that occur in the vein, a small amount of disseminated chalcopyrite, bornite and chalcocite occur in other regions of the thin section.

Discussion

The chalcopyrite-bornite assemblage within the aplitic vein indicates that it is likely an A-type quartz vein. The carbonate vein likely occurred much late with respect to the rest of the sample. The presence of plagioclase is indicative of preservation of primary feldspars or albitization of primary feldspars. If the latter is true than this is indication of potassic alteration. The partial sericitization and chloritization indicates that the sample later underwent less pervasive phyllic alteration.

**ZMMH-9**

**DDH 4884 158.9-159.0m**

**PMM** (MM Porphyry)

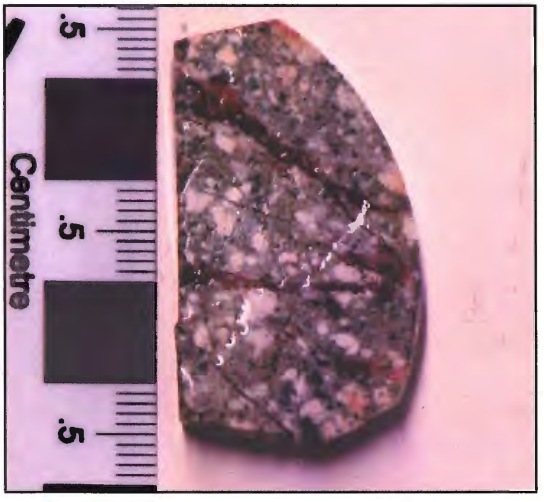

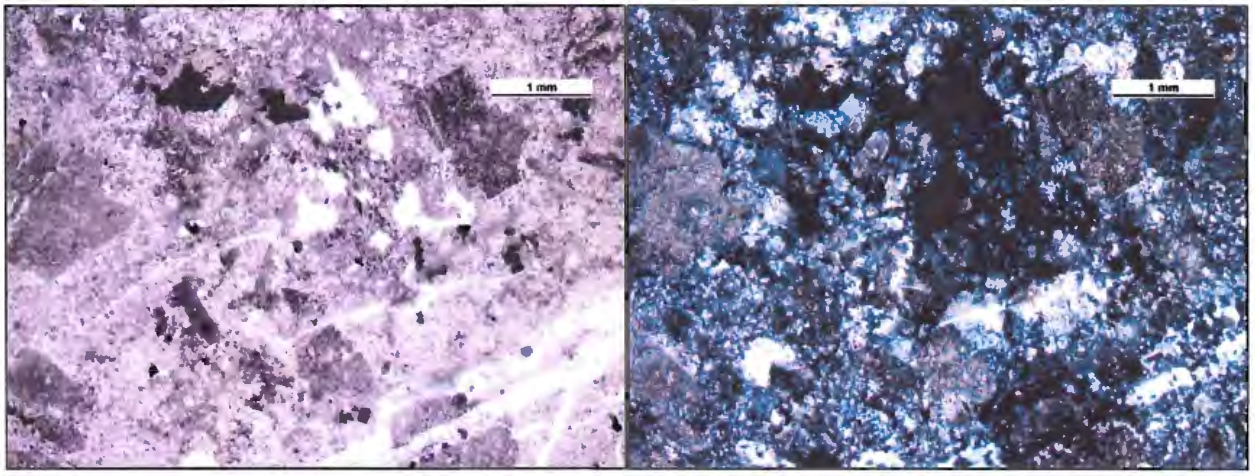


Observations

*Rock Chip*

The sample is porphyritic with a green-grey groundmass and white feldspar phenocrysts. Iron oxide is visible in the veins.

*Thin Section/Polished Section*

The sample is porphyritic and has undergone pervasive veining. The feldspar phenocrysts have been entirely sericitized and in some cases have an alteration rim around the outside. One of the feldspar phenocrysts show blurred microcline twinning suggesting it was originally plagioclase. These phenocrysts range in size from 4.5 mm to 1 mm. The groundmass is aplitic and contains quartz and sericite.

The sample is vuggy and has undergone pervasive veining. The thickness of the veins is $\leq 1$ mm. Many open spaces occur within the veins. The veins also contain prismatic quartz, carbonate and iron-oxide.

Suphides are disseminated throughout the sample. The most common sulphide is chalcopyrite followed by chalcocite, pyrite and rare instances of bornite.

The sample contains no chloritized biotite, apatites or zircons.

Discussion

The chalcopyrite-chalcocite-bornite sulphide assemblage indicates that the sample originally underwent potassic alteration. The sericitization of the feldspars and pyrite indicate that the sample later underwent phyllic alteration. The vuggy texture, carbonate, iron oxide within the veins and the shallow depth of the sample indicate advanced weathering has occurred;

this observation is consistent with the shallow provenance of the sample in the drill-hole (159 m). The spaces that occur within the veins as well as the euhedral quartz, carbonate and iron-oxide indicate these veins are D-type quartz veins. The chalcopyrite + bornite sulphide assemblage could have been in part contributed to by the presence of these veins.

**ZMMH-10**

**DDH 5014 161.0-161.2m**

**Grd MM**

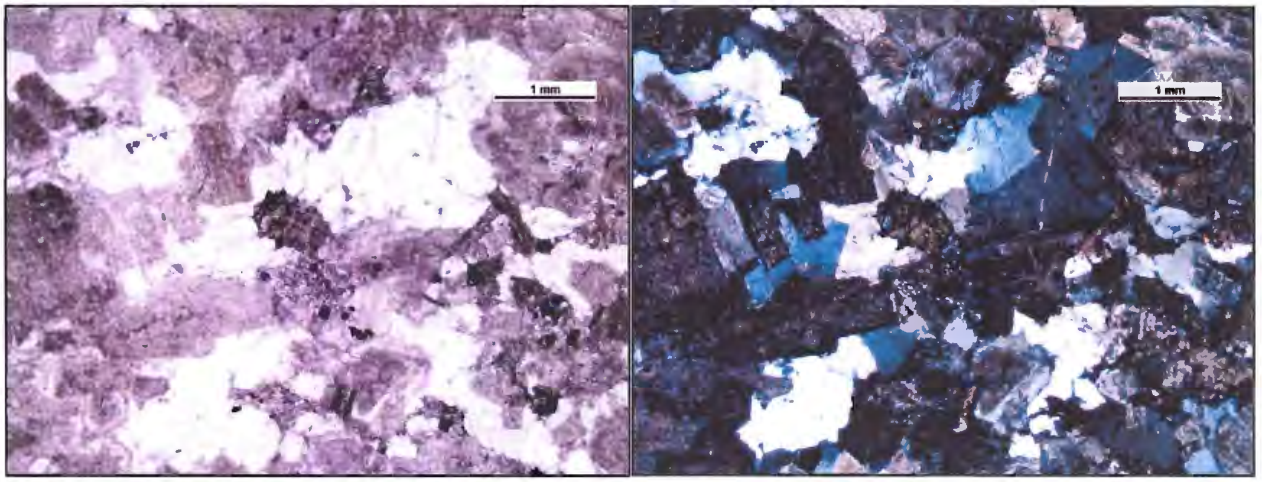


Observations

*Rock Chip*

The rock is coarse-grained equigranular with white to light-green feldspar, dark green chlorite and quartz.

*Thin Section*

The sample is equigranular and hypidiomorphic. It contains euhedral to subhedral feldspars which have undergone light to moderate sericitization (with respect to other samples). Most of these feldspars are plagioclase, however there are a few K-feldspars. These feldspars are intergrown and a few show zoning patterns with sericitized centers. In some places there are remnants of biotite that have been chloritized. This chloritized biotite is poikilitic with inclusions of sulphides and prismatic quartz. Anhedral quartz occurs interstitially between feldspar and chloritized biotite. Veining is not pervasive and the veins that do exist < 0.2 mm. These veins are comprised of quartz. Carbonate exists in one region of the thin section.

The polished section had been carbon coated for use in the electron microprobe and therefore sulphides cannot be correctly identified under reflected light.

Discussion

The classification of alteration in this sample is limited by the fact that sulphides are not observable due to use of the polished section in the electron microprobe. EMP results show that the plagioclase is albite and thus, there are two conclusions that could be drawn. The first is that the albite and K-feldspar are primary, the second is that the sample has been affected by potassic alteration whereby the primary feldspars were altered to K-feldspar and albite. Tobey (2004) states that albitization has not thoroughly affected MMH although the latter situation seems more likely than the former. Since the veining is not pervasive and is composed only of quartz than it is difficult to categorize them with respect to Gustafson & Hunt's (1975) quartz vein classification model.

The amount of sericitization and chloritization indicate that the sample has not gone pervasive phyllic alteration. Due to the shallow depth of the sample, the carbonate could have originated from potassic alteration or, more likely from weathering and precipitation processes.

**ZMMH-11**

**DDH 4976 897.87 – 898.00 m**

POQ MM

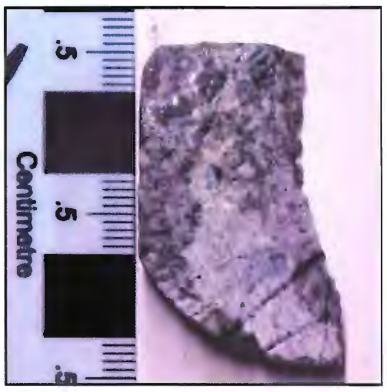


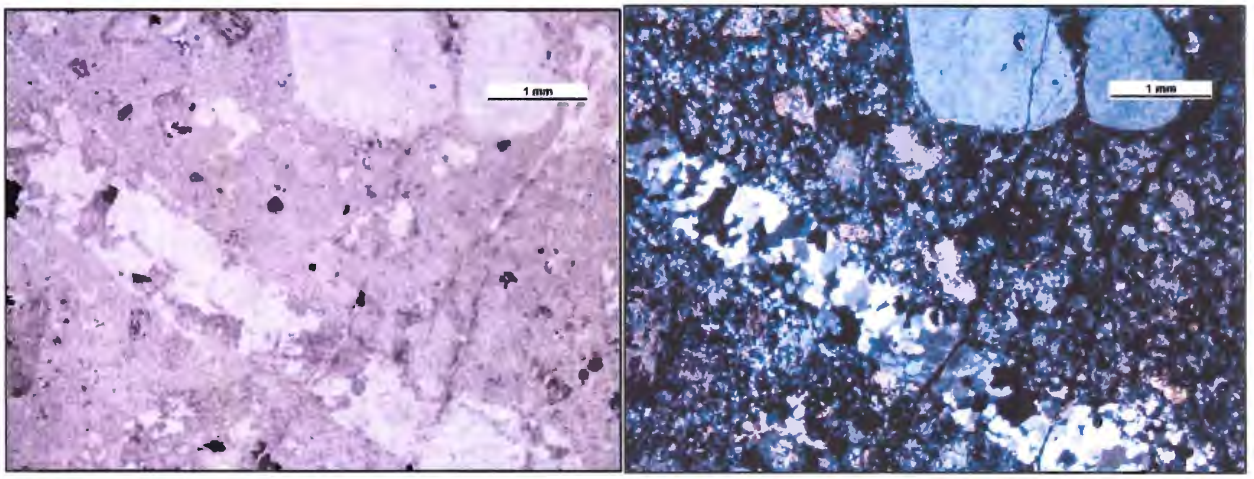


Observation

*Rock Chip*

Quartz phenocrysts are present in the rock chip as well as a milky white groundmass. Veining is visible with the veins containing vugs.

*Thin Section:*

The sample is porphyritic with phenocrysts of quartz and feldspar. The feldspar phenocrysts are zoned with the centers having been more heavily altered to quartz with the outsides containing more sericite. Sericitization is more prominent along cleavage planes. These feldspar phenocrysts are 0.5 mm to 4.25 mm. The quartz phenocrysts are spheroid with a diameter of 2.5-6mm. The groundmass aplitic and is mostly comprised of quartz and sericite (the sericite has presumably replaced feldspars). The veins are < 1 mm thick and comprised of

quartz and sulphides. All of the veins in the sample run parallel to one another. The sample is vuggy with most of the open spaces occurring along the veins. The sample does not contain chlorite, apatites or zircons.

The polished section had been carbon coated for use in the electron microprobe and therefore sulphides cannot be properly identified.

Discussion

The EMP results show that the feldspars of this section are K-feldspar indicating that the section has undergone potassic alteration. The sericitization of these K-feldspars indicate that the sample underwent phyllic alteration subsequent to the potassic alteration. The open spaces within the veins indicate that these veins are D-type quartz veins.

**ZMMH-12**

**1128.0-1128.12 m**

POQ MM (Quartz Porphyry)


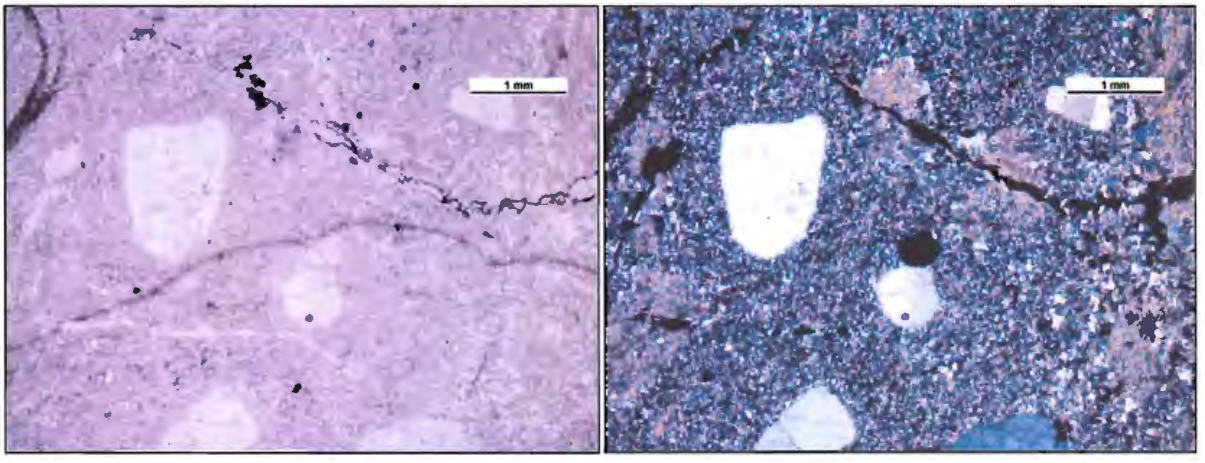

Observations

*Rock Chip*

The sample is milky white with visible quartz phenocrysts. The veins contain most of the sulphides.

*Thin Section/Polished Section*

The sample is porphyritic with quartz and feldspar phenocrysts. The feldspar phenocrysts are < 1mm and have been completely sericitized. The quartz phenocrysts are spheroidal and <2.5 mm in diameter. The groundmass is aplitic and consists of quartz and sericite (presumably the sericite is result of altered feldspar). The veins occur in various directions with some cross-cutting each other. These veins contain empty spaces (vugs) and are comprised of pyrite and chalcopyrite. There is a quartz phenocryst that cuts through a vein (alternatively, the vein did not fracture the phenocryst). The sample contains a small amount of zircon and apatite (<10) as well as rutile.

Discussion

The sericitization of the feldspars indicates that the sample underwent phyllic alteration. It is possible that potassic alteration preceded the phyllic alteration but was completely overprinted. The quartz phenocrysts that seem to truncate the veins indicate that the formation of these phenocrysts occurred after the formation of the veins, or that the fractures where the veins were emplaced did not rupture the quartz crystals. The open spaces within the veins along with the chalcopyrite + pyrite sulphide assemblage indicates they are D-type veins.

**ZMMH-13**

**DDH 4976 1123.78-1123.90 m**

POQ MM (Quartz Porphyry)

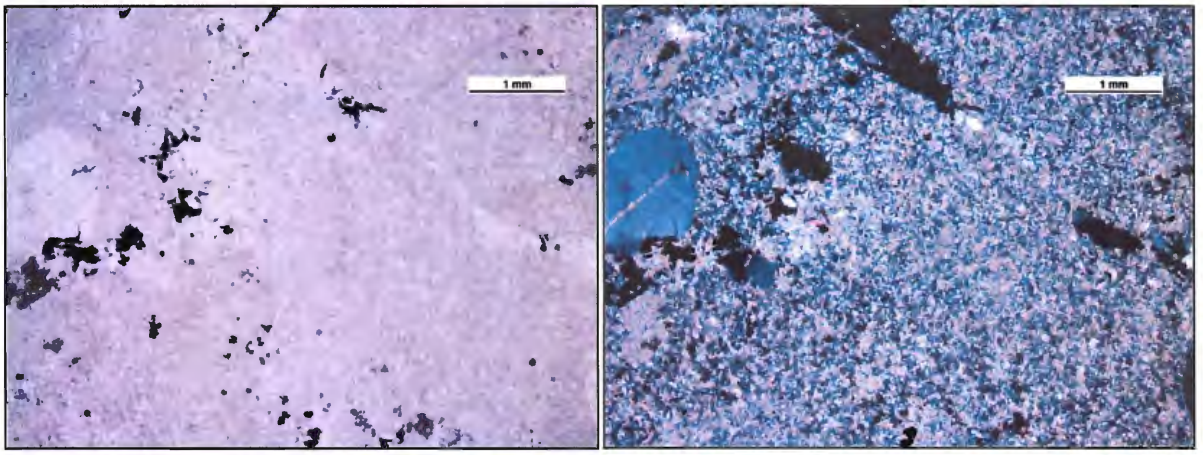


*Rock Chips*

The sample is white with quartz phenocrysts and a milky groundmass. There are sulphides visible as well as dark green areas which contain sulphides.

*Thin Section/Polished Section*

The sample is porphyritic with quartz and feldspar phenocrysts. The feldspar phenocrysts are completely sericitized and <2.5 mm. The quartz phenocrysts are spheroidal and also <2.5 mm. Some of these quartz phenocrysts ("quartz eyes") have internal sub-grain boundaries. The groundmass is aplitic and consists of quartz and sericite (presumably altered feldspar). The veins occur in many directions. They consist of quartz as well as pyrite and chalcopyrite and all contain empty spaces (vugs). The veins cut through the feldspar phenocrysts but the quartz phenocrysts are not affected by the veins. Pyrite is the most common sulphide with occasional chalcopyrite and bornite. The chalcopyrite that occurs forms a halo around pyrite. The sample also contains rutile. There were no apatites or zircons seen in the sample.

Discussion

The sericitization of the feldspar phenocrysts, the vuggy texture as well as the presence of pyrite indicates that the sample underwent phyllic alteration. It is possible that potassic alteration preceded the phyllic alteration but was entirely overprinted. The apparent truncation of veins by quartz phenocrysts indicates that the phenocrysts post-date the veins, or the fracturing did not crack the quartz crystals. The open spaces within the veins as well as the sulphide assemblage of pyrite + chalcopyrite indicate that they are D-type quartz veins.

**ZMMH-14**

**DDH 4976 1241.00-1241.12m**

PMM

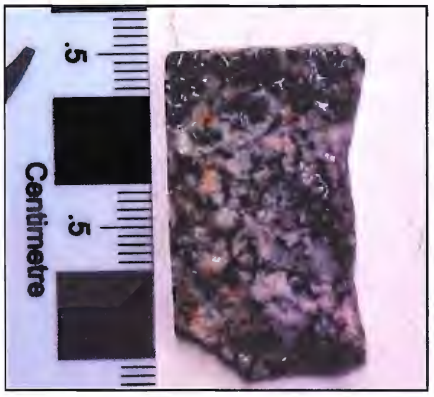


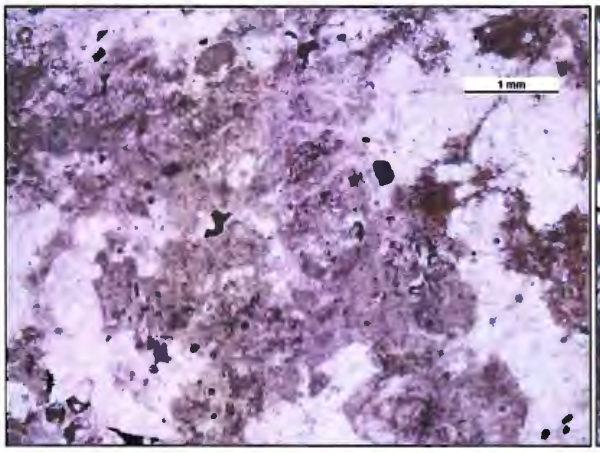


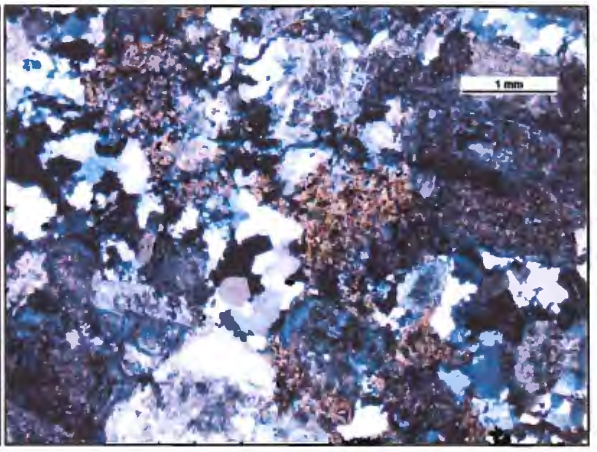


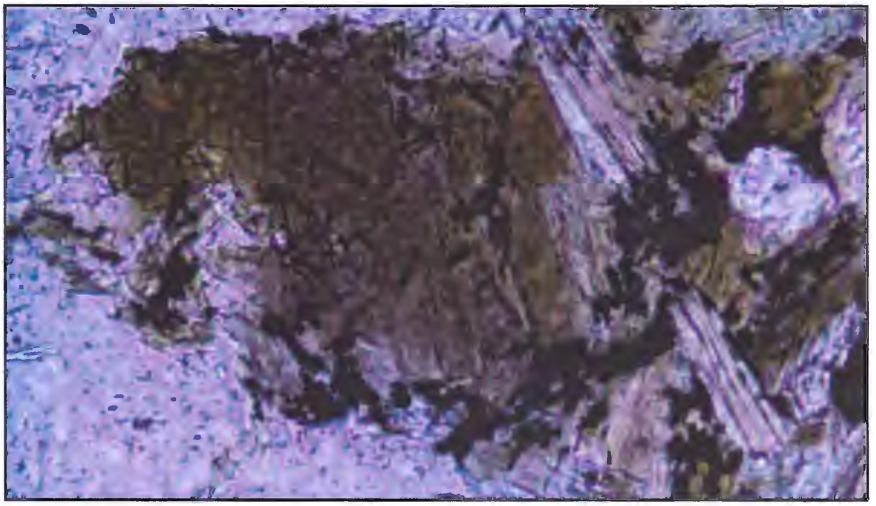

Observations

*Rock Chips*

The rock chip has a milky-white groundmass with quartz phenocrysts, pink feldspar phenocrysts as well as dark phenocrysts visible. There is also iron-oxide staining

*Thin Section*

The sample is vuggy and porphyritic with plagioclase and K-feldspar phenocrysts. The plagioclase phenocrysts are euhedral to subhedral with alteration rims around the outside. The size of the phenocrysts ranges from 5 mm to 2.5 mm. The K-feldspar phenocrysts are subhedral to euhedral and also have alteration rims as well as penetrative alteration veins. The size of these phenocrysts is approximately 2 mm. These feldspar phenocrysts have undergone moderate sericitization (relative to other samples). There are vugs which occur within these phenocrysts. The interstitial minerals are biotite and quartz. The quartz is anhedral with embayed boundaries. In some places it looks as though quartz has entirely replaced the feldspar phenocryst (see photo) and the quartz has subgrains. The biotite has undergone minimal chloritization and occurs as pockets of accumulated fine-grained elongated grains. Some of these biotites contain microlath inclusions of exsolved rutile ("sagenitic"). These crystals occur at angles of 60°-120° (see photo above). The veins are 0.25 mm-0.5 mm thick and are mostly comprised of quartz with some carbonate and sulphides. These veins show an aplitic texture in some places. The sulphides occur mostly within the veins but also within the interstitial quartz and occasionally within the feldspar phenocrysts.

The polished section had been carbon coated for use in the electron microprobe and therefore sulphides cannot be correctly determined.

Discussion

The occurrence of K-feldspar and albite (as indicated by EMP data) as well as carbonate indicate that the sample has undergone potassic alteration. The phyllic alteration was likely confined to the veins and halos observed in the feldspar phenocrysts. The sagenitic biotite suggests that the secondary titanium minerals were exsolved during alteration.

**ZMMH-15**

**DDH 4976 1286.47-1286.60 m**

PMM

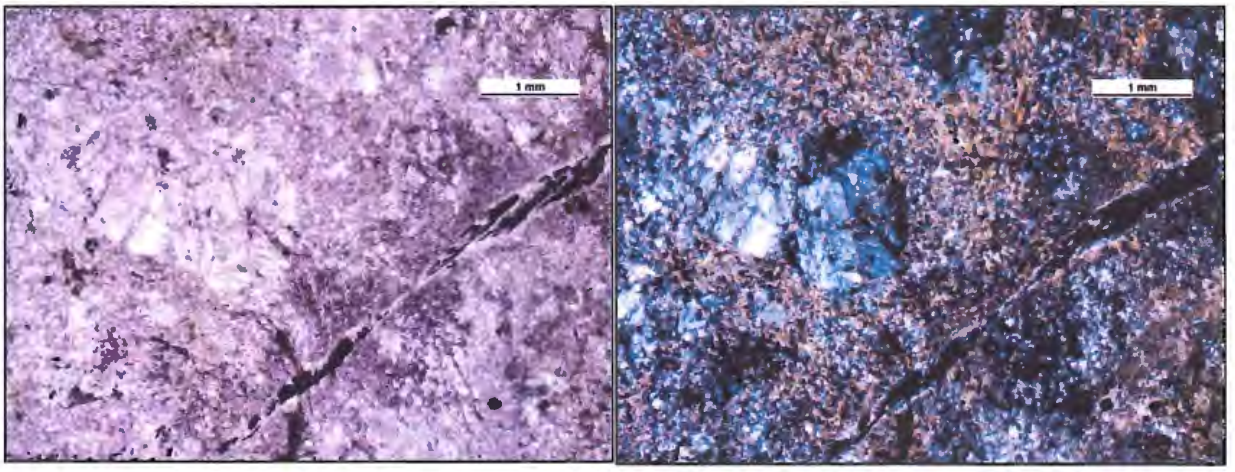


Observations

*Rock Chips*

The samples has greenish tint with black portions of biotite as well as visible feldspar phenocrysts that are light green. There are visible veins that have a pinkish colour.

*Thin Section/Polished Section*

The sample is porphyritic and has been heavily sericitized. There are few K-feldspar and plagioclase phenocrysts which still show relic characteristics. These phenocrysts are 2.5 mm and 1.5 mm respectively. These phenocrysts are subhedral. The groundmass is comprised of quartz, biotite and sericite. The biotite is shreddy and occurs in concentrated regions as subparallel and elongate grains. Veins are 0.5 to 1 mm thick and are comprised of carbonate, quartz and chalcopyrite.

Discussion

The presence of K-feldspar as well as the pink coloured veins indicates that the sample has undergone potassic alteration. The sericitization of the feldspars as well as the green colour of the rock chips indicates that the sample underwent subsequent phyllic alteration. The shredded texture of the biotite may indicate it is secondary. The carbonate in the veins indicates that these are D-type quartz veins

**ZMMH-17**

**DDH 4976 855.40 – 855.50 m**

Grd MM

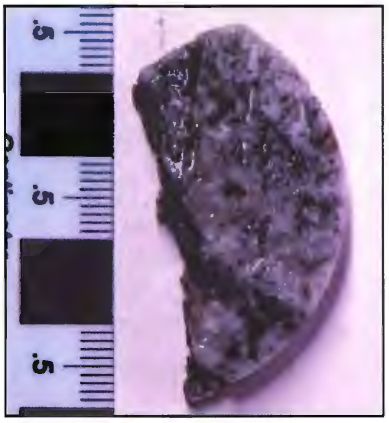

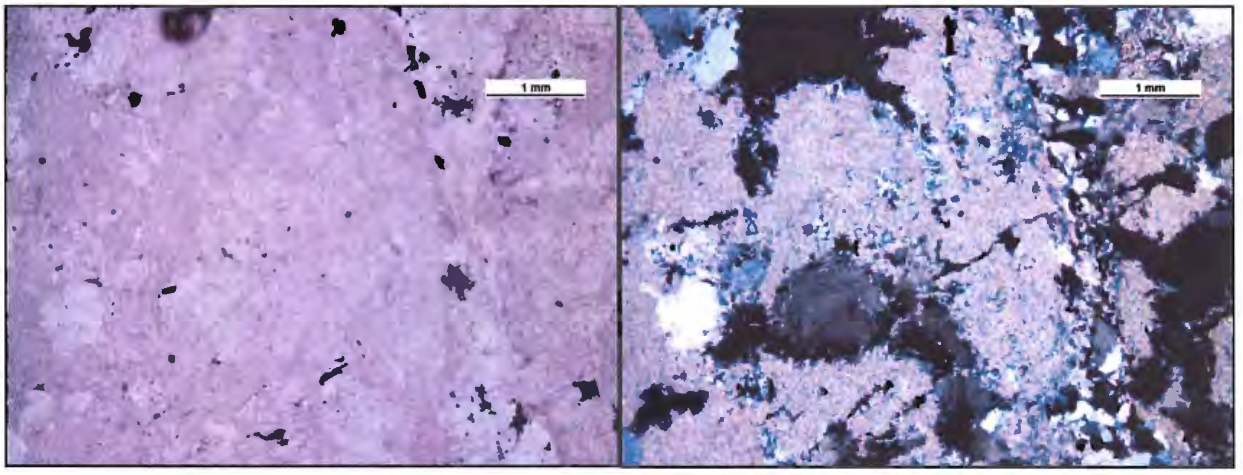


Observations

*Rock Chips*

The sample has a milk-white groundmass with visible quartz phenocrysts. Molybdenite can be indentified within the veins as well as disseminated pyritic sulphides

*Thin Section/Polished Section*

The sample is vuggy and has been completely sericitized. There are quartz phenocrysts as well as quartz veins that contain molybdenite, chalcopyrite and pyrite. These veins run subparallel to one another. There is also chalcopyrite and pyrite disseminated throughout the sample.

Discussion

The veins that contain molybdenite indicate that the veins are B-type quartz veins and that the sample underwent metasomatism with magmatic brine in the initial phases of alteration. The pervasive sericitization as well as the presence of pyrite indicates that the sample underwent phyllic alteration, likely sericitic. The presence of chalcopyrite indicates that perhaps the sample underwent potassic alteration at one time, but this cannot be proven from the observations.

**ZMMH-18**

**DDH 4976 845.85-845.95 m**

Grd MM

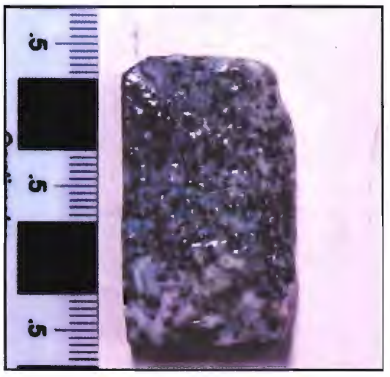

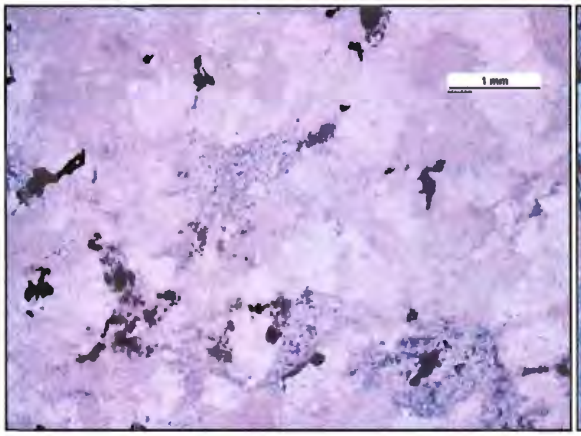


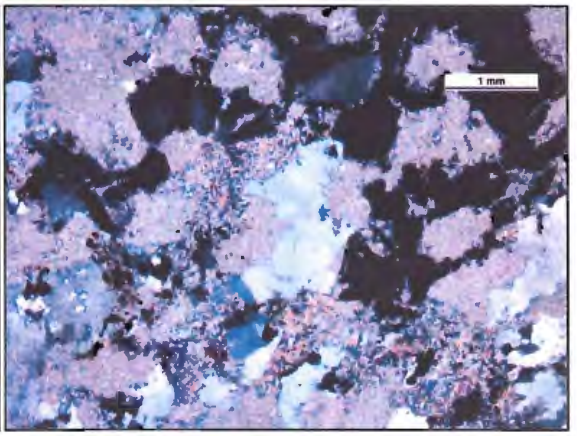

Observations

*Rock Chips*

The sample has a milky-white groundmass with quartz phenocrysts. Pyritic sulphides are visible as well a brownish mineral with staining which is probably rutile.

*Thin Section/Polished Section*

The sample is vuggy and has been completely sericitized. There are some quartz phenocrysts that are <1.5 mm. There are microlaths of rutile that occur in concentrated areas of the thin section. The sample does not have veining. Pyrite, bornite and chalcocite are disseminated throughout the sample.

Discussion

The presence of chalcocite indicates that the sample was strongly mineralized. The microlaths of rutile indicate that biotite was likely originally present in the rock, rutile having exsolved during alteration. The vuggy texture, complete sericitization and missing biotites indicate that the sample has undergone pervasive phyllic alteration, likely sericitic. The chalcopyrite and bornite could have originated in earlier alteration phases but it is difficult to confirm this.

**ZMMH-20**

**DDH 4976 870.90 – 871.05 m**

Grd MM

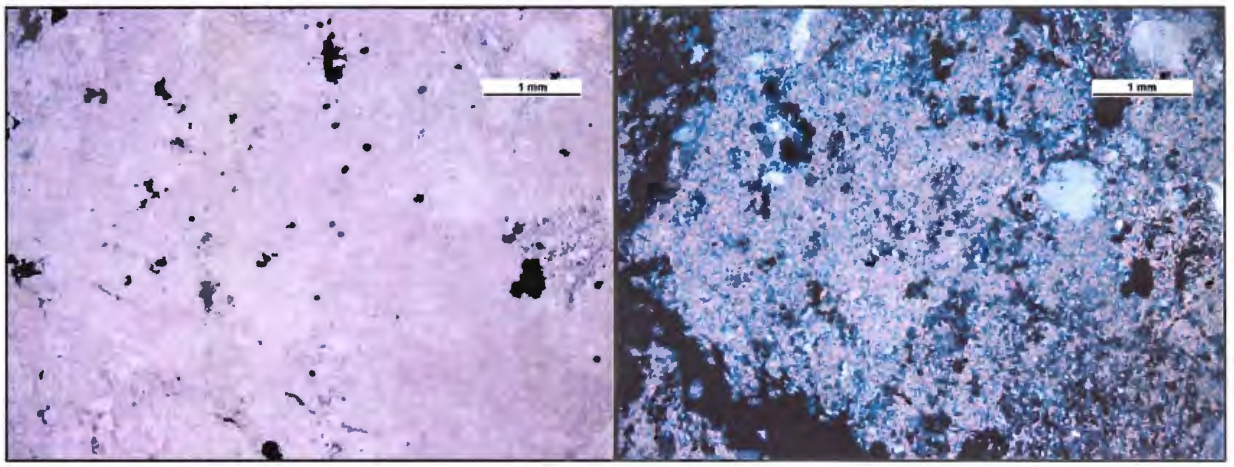


Observations

*Rock Chip*

The sample is vuggy with many spaces occurring within a vein. The groundmass is milky-white and quartz phenocrysts are visible. Sulphides appear to be disseminated throughout the sample as well as a brown mineral that stains the sample which is likely rutile.

*Thin Section/Polished Section*

The sample has been completely sericitized with remnant quartz phenocrysts. The sample is vuggy with spaces occurring disseminated throughout the sample as well as along sub parallel veins. The sulphides that occur are pyrite, chalcopyrite and bornite and are dispersed throughout the sample. Rutile occurs within concentrated areas within the sample as well.

Discussion

The vuggy texture, the complete sericitization as well as the pyrite indicates that the sample underwent phyllic alteration, likely sericitic. The presence of bornite and chalcopyrite could be indicators of previous potassic alteration although these sulphides assemblages do occur in phyllic alteration zones as well. The presence of rutile indicates that biotite was initially present but was likely altered beyond recognition.

**ZMMH-21**

**DDH 4976 883.20 – 883.24 m**

PMM

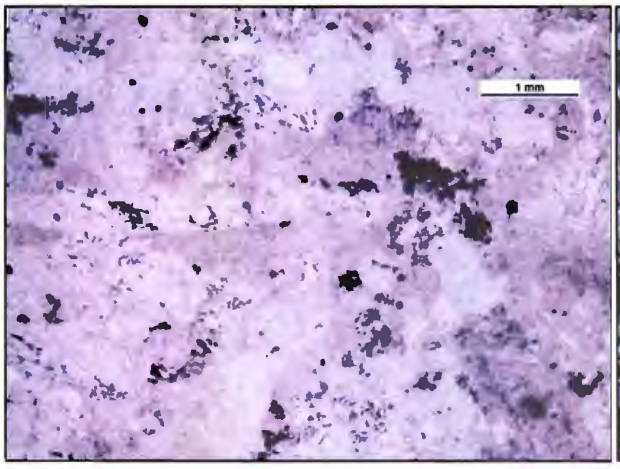


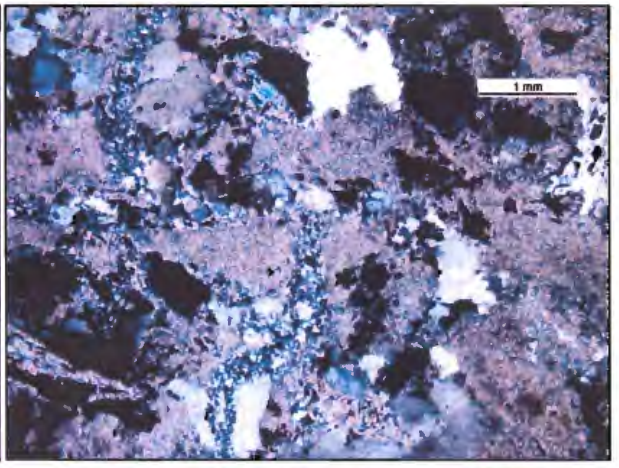


Observations

*Rock Chips*

The sample has quartz phenocrysts as well as light-green phenocrysts and much smaller dark green areas. Sulphides appear dispersed throughout the sample.

*Thin Section/Polished Section*

The sample is vuggy and has been completely sericitized. The sample contains quartz phenocrysts. There are two generations of veins with a younger, medium grained quartz vein cutting an aplitic quartz vein (see photo). Chlorite occurs in some regions indicating chloritization of biotite or hornblende. The sulphides that occur are chalcopyrite, pyrite and chalcocite and are disseminated throughout the sample.

Discussion

The appearance of chalcocite suggests that the sample was heavily mineralized. The complete sericitization and chloritization, vuggy texture and presence of pyrite indicate the sample later underwent phyllic alteration, possibly both chlorite-sericite and sericitic alteration. The aplitic vein that is displaced is likely an A-type quartz vein with the younger, coarser grained vein likely a B-type vein.

**ZMMH-23**

**DDH 4976 1064.00 – 1064.15 m**

Grd MM

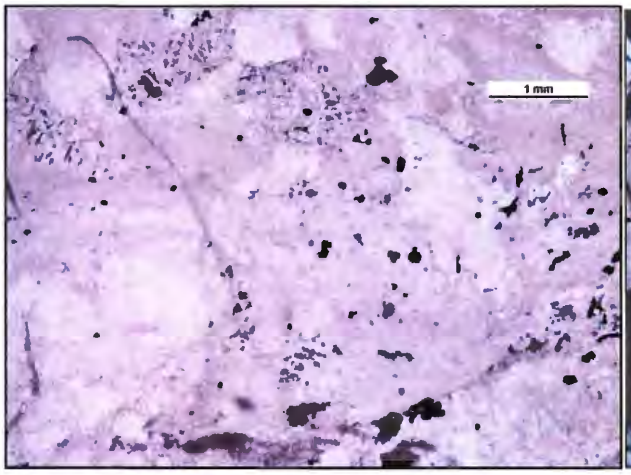


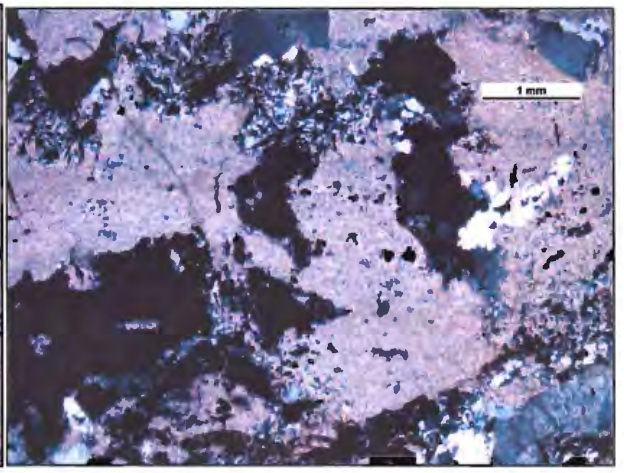


Observations

*Rock Chips*

The sample has phenocrysts of quartz, feldspar and a green mineral, likely chlorite. The sample has a vuggy texture, especially close to the veins.

*Thin Section/Polished Section*

The sample is vuggy and heavily altered with the feldspars completely sericitized and the biotite and/or hornblende completely chloritized. The remnants of the biotite/hornblende are poikiloblastic with inclusions of sulphides. There is one vein in the sample that is 1.25 mm thick and comprised of mainly quartz with some sulphides as well. The sulphides that occur in the sample are chalcopyrite, chalcocite and pyrite. The chalcopyrite has in some places undergone alteration to chalcocite. The sulphides that do not occur in the veins are disseminated throughout the sample.

Discussion

The occurrence of chalcocite indicates that the sample was heavily mineralized. The vuggy texture, sericitization and chloritization as well as the presence of pyrite indicates that the sample subsequently underwent phyllic alteration, possibly both sericitic and chlorite-sericite type. The Chalcopyrite could have origins in potassic and/or phyllic alteration phases. The vugs within the vein as well as the pyrite + chalcopyrite sulphide assemblage is indicative that it is a D-type quartz vein.

# Appendix 3 Activation Laboratories Quality Control

The following table outlines the tests for quality control conducted by Activation Laboratories in Ancaster, Ontario where the whole-rock geochemical analysis was preformed.

| Analyte Symbol | SiO2 | Al2O3 | Fe2O3(T) | MnO | MgO | CaO | Na2O | K2O | TiO2 | P2O5 | LOI | Total | Au | Ag | Ag | As | Ba | Be | Bi | Br | Cd | Co | Cr | Cs | Cu | Ga | Ge | Hf | Hg | In | Ir |
|---|---|---|---|---|---|---|---|---|---|---|---|---|---|---|---|---|---|---|---|---|---|---|---|---|---|---|---|---|---|---|---|
| Unit Symbol | % | % | % | % | % | % | % | % | % | % | % | % | ppb | ppm | ppm | ppm | ppm | ppm | ppm | ppm | ppm | ppm | ppm | ppm | ppm | ppm | ppm | ppm | ppm | ppm | ppm | ppb |
| Detection Limit | 0.01 | 0.01 | 0.01 | 0.001 | 0.01 | 0.01 | 0.01 | 0.01 | 0.001 | 0.01 | | 0.01 | 1 | 0.5 | 5 | 1 | 1 | 1 | 0.1 | 0.5 | 0.5 | 0.1 | 0.5 | 0.1 | 1 | 1 | 0.5 | 0.1 | 1 | 0.1 | 1 |
| Analysis Method | FUS-ICP | FUS-ICP | FUS-ICP | FUS-ICP | FUS-ICP | FUS-ICP | FUS-ICP | FUS-ICP | FUS-ICP | FUS-ICP | FUS-ICP | FUS-ICP | INAA | TD-ICP | INAA | INAA | FUS-ICP | FUS-ICP | FUS-MS | INAA | TD-ICP | INAA | INAA | FUS-MS | TD-ICP | FUS-MS | FUS-MS | FUS-MS | INAA | FUS-MS | INAA |
| GXR-1 Meas | | | | | | | | | | | | | | 30.4 | | | | | | | 3.3 | | | | 1320 | | | | | | |
| GXR-1 Cert | | | | | | | | | | | | | | 31 | | | | | | | 3.3 | | | | 1110 | | | | | | |
| WMG-1 Meas | | | | | | | | | | | | | 132 | | < 5 | 8 | | | | | | 199 | 829 | 0.4 | | 8 | | 1.3 | | | 50 |
| WMG-1 Cert | | | | | | | | | | | | | 110 | | 2.7 | 7 | | | | | | 200 | 770 | 0.48 | | 10.3 | | 1.3 | | | 46 |
| NIST 694 Meas | 10.94 | 1.87 | 0.74 | 0.013 | 0.34 | 42.51 | 0.88 | 0.55 | 0.114 | 30.17 | | | | | | | | | | | | | | | | | | | | | |
| NIST 694 Cert | 11.2 | 1.8 | 0.79 | 0.0116 | 0.33 | 43.6 | 0.86 | 0.51 | 0.11 | 30.2 | | | | | | | | | | | | | | | | | | | | | |
| DNC-1 Meas | 47.23 | 18.25 | 9.7 | 0.148 | 10.22 | 11.56 | 1.93 | 0.23 | 0.471 | 0.09 | | | | < 0.5 | | | 108 | < 1 | < 0.1 | | | | | 0.2 | 108 | 14 | 1.6 | 1.1 | | | |
| DNC-1 Cert | 47 | 18.3 | 9.93 | 0.149 | 10.1 | 11.3 | 1.87 | 0.234 | 0.48 | 0.09 | | | | 0.027 | | | 114 | 1 | 0.02 | | | | | 0.34 | 96 | 15 | 1.3 | 1.01 | | | |
| BIR-1 Meas | | | | | | | | | | | | | | | | | | | | | | | | | | | | | | | |
| BIR-1 Cert | | | | | | | | | | | | | | | | | | | | | | | | | | | | | | | |
| GBW 07113 Meas | 71.34 | 12.27 | 3.07 | 0.139 | 0.14 | 0.6 | 2.48 | 5.42 | 0.267 | 0.04 | | | | | | | 495 | 4 | | | | | | | | | | | | | |
| GBW 07113 Cert | 72.8 | 13 | 3.21 | 0.14 | 0.16 | 0.59 | 2.57 | 5.43 | 0.3 | 0.05 | | | | | | | 506 | 4 | | | | | | | | | | | | | |
| MICA-FE Meas | | | | | | | | | | | | | | | | | | | | | | | | | | | | | | | |
| MICA-FE Cert | | | | | | | | | | | | | | | | | | | | | | | | | | | | | | | |
| GXR-4 Meas | | | | | | | | | | | | | | 3.2 | | | | | | | < 0.5 | | | | 6310 | | | | | | |
| GXR-4 Cert | | | | | | | | | | | | | | 4 | | | | | | | 0.86 | | | | 6520 | | | | | | |
| GXR-2 Meas | | | | | | | | | | | | | | 18.4 | | | | | < 0.1 | | 4.4 | | | 5.3 | 92 | 34 | | 6 | | < 0.1 | |
| GXR-2 Cert | | | | | | | | | | | | | | 17 | | | | | 0.69 | | 4.1 | | | 5.2 | 76 | 37 | | 8.3 | | 0.252 | |
| SDC-1 Meas | | | | | | | | | | | | | | < 0.5 | | | | | | | < 0.5 | | | | 31 | | | | | | |
| SDC-1 Cert | | | | | | | | | | | | | | 0.041 | | | | | | | 0.08 | | | | 30 | | | | | | |
| SCO-1 Meas | | | | | | | | | | | | | | < 0.5 | | | | | | | < 0.5 | | | | 28 | | | | | | |
| SCO-1 Cert | | | | | | | | | | | | | | 0.134 | | | | | | | 0.14 | | | | 28.7 | | | | | | |
| GXR-6 Meas | | | | | | | | | | | | | | 0.5 | | | | | | | < 0.5 | | | | 71 | | | | | | |
| GXR-6 Cert | | | | | | | | | | | | | | 1.3 | | | | | | | 1 | | | | 66 | | | | | | |
| NIST 1633b Meas | 48.53 | 28.62 | 11.29 | 0.019 | 0.76 | 2.2 | 0.27 | 2.34 | 1.3 | 0.55 | | | | | | | 719 | | | | | | | | | | | | | | |
| NIST 1633b Cert | 49.2 | 28.4 | 11.1 | 0.02 | 0.8 | 2.11 | 0.27 | 2.35 | 1.32 | 0.53 | | | | | | | 709 | | | | | | | | | | | | | | |
| SY-3 Meas | | | | | | | | | | | | | | | | | | | | | | | | | | | | | | | |
| SY-3 Cert | | | | | | | | | | | | | | | | | | | | | | | | | | | | | | | |
| BE-N Meas | | | | | | | | | | | | | | | | | | | | | | | | | | | | | | | |
| BE-N Cert | | | | | | | | | | | | | | | | | | | | | | | | | | | | | | | |
| AC-E Meas | | | | | | | | | | | | | | | | | | | | | | | | | | | | | | | |
| AC-E Cert | | | | | | | | | | | | | | | | | | | | | | | | | | | | | | | |
| W-2a Meas | 52.34 | 15.52 | 10.64 | 0.167 | 6.26 | 11.1 | 2.24 | 0.63 | 1.082 | 0.15 | | | | | | | 180 | < 1 | < 0.1 | | | | | 0.9 | | 17 | 1.7 | 2.6 | | | |
| W-2a Cert | 52.4 | 15.4 | 10.7 | 0.163 | 6.37 | 10.9 | 2.14 | 0.626 | 1.06 | 0.13 | | | | | | | 182 | 1.3 | 0.03 | | | | | 0.99 | | 17 | 1 | 2.6 | | | |
| OREAS 13P Meas | | | | | | | | | | | | | | | | | | | | | | | | | 2870 | | | | | | |
| OREAS 13P Cert | | | | | | | | | | | | | | | | | | | | | | | | | 2500 | | | | | | |
| SY-4 Meas | 50.33 | 20.53 | 6.15 | 0.109 | 0.5 | 8.26 | 7.05 | 1.71 | 0.291 | 0.13 | | | | | | | 358 | 3 | | | | | | | | | | | | | |
| SY-4 Cert | 49.9 | 20.69 | 6.21 | 0.108 | 0.54 | 8.05 | 7.1 | 1.66 | 0.287 | 0.131 | | | | | | | 340 | 2.6 | | | | | | | | | | | | | |
| CTA-AC-1 Meas | | | | | | | | | | | | | | | | | | | | | | | | | | | | 1.7 | | | |
| CTA-AC-1 Cert | | | | | | | | | | | | | | | | | | | | | | | | | | | | 1.13 | | | |
| BIR-1a Meas | 47.82 | 15.7 | 11.24 | 0.17 | 9.6 | 13.51 | 1.84 | 0.02 | 0.981 | 0.03 | | | | | | | 10 | < 1 | < 0.1 | | | | | < 0.1 | | 15 | 1.7 | 0.6 | | | |
| BIR-1a Cert | 47.8 | 15.4 | 11.3 | 0.171 | 9.68 | 13.2 | 1.75 | 0.03 | 0.96 | 0.05 | | | | | | | 7 | 0.58 | 0.02 | | | | | 0.005 | | 16 | 1.5 | 0.6 | | | |
| NCS DC86312 Meas | | | | | | | | | | | | | | | | | | | | | | | | | | | | | | | |
| NCS DC86312 Cert | | | | | | | | | | | | | | | | | | | | | | | | | | | | | | | |
| VS-N Meas | | | | | | | | | | | | | | | | | | | | | | | | | | | | | | | |
| VS-N Cert | | | | | | | | | | | | | | | | | | | | | | | | | | | | | | | |
| NCS DC70014 Meas | | | | | | | | | | | | | | | | | | | 80.3 | | | | | | | 26 | | | | | |
| NCS DC70014 Cert | | | | | | | | | | | | | | | | | | | 80.3 | | | | | | | 25.2 | | | | | |
| NCS DC70009 (GBW07241) Meas | | | | | | | | | | | | | | | | | | | 116 | | | | | 43.6 | | 16 | 11 | | | 1.3 | |
| NCS DC70009 (GBW07241) Cert | | | | | | | | | | | | | | | | | | | 680 | | | | | 41 | | 16.5 | 11.2 | | | 1.3 | |
| OREAS 100a (Fusion) Meas | | | | | | | | | | | | | | | | | | | | | | | | | | | | | | | |
| OREAS 100a (Fusion) Cert | | | | | | | | | | | | | | | | | | | | | | | | | | | | | | | |
| OREAS 101a (Fusion) Meas | | | | | | | | | | | | | | | | | | | | | | | | | | | | | | | |
| OREAS 101a (Fusion) Cert | | | | | | | | | | | | | | | | | | | | | | | | | | | | | | | |
| JR-1 Meas | | | | | | | | | | | | | | | | | | | 0.5 | | | | | 20.8 | | 16 | 2.7 | 5.1 | | < 0.1 | |
| JR-1 Cert | | | | | | | | | | | | | | | | | | | 0.56 | | | | | 20.8 | | 16.1 | 1.88 | 4.51 | | 0.028 | |
| ZMMH 15Q Orig | 54.78 | 21.79 | 3.05 | 0.084 | 3.29 | 1.95 | 4.59 | 4.61 | 0.423 | 0.11 | 4.2 | 98.88 | | | | | 587 | 3 | 0.1 | | | | | 11.1 | | 29 | 2.2 | 4.2 | | < 0.1 | |
| ZMMH 15Q Dup | 54.7 | 21.67 | 3.06 | 0.084 | 3.32 | 1.95 | 4.56 | 4.61 | 0.421 | 0.11 | 4.2 | 98.69 | | | | | 589 | 3 | 0.2 | | | | | 11.1 | | 29 | 2.2 | 4.2 | | < 0.1 | |
| ZMMH 17Q Orig | | | | | | | | | | | | | | 0.5 | | | | | | | < 0.5 | | | | 7200 | | | | | | |
| ZMMH 17Q Dup | | | | | | | | | | | | | | < 0.5 | | | | | | | < 0.5 | | | | 7150 | | | | | | |
| Method Blank Method Blank | | | | | | | | | | | | | | < 0.5 | | | | | | | < 0.5 | | | | < 1 | | | | | | |
| Method Blank Method Blank | | | | | | | | | | | | | < 1 | | < 5 | < 1 | | | | < 0.5 | | < 0.1 | < 0.5 | | | | | | < 1 | | < 1 |
| Method Blank Method Blank | | | | | | | | | | | | | | | | | | | | | | | | | | | | | | | |

| Analyte Symbol | Mo | Nb | Ni | Pb | Rb | S | Sb | Sc | Se | Sn | Sr | Ta | Th | U | V | W | Y | Zn | Zn | Zr | La | Ce | Pr | Nd | Sm | Eu | Gd | Tb | Dy | Ho | Er |
|---|---|---|---|---|---|---|---|---|---|---|---|---|---|---|---|---|---|---|---|---|---|---|---|---|---|---|---|---|---|---|---|
| Unit Symbol | ppm | ppm | ppm | ppm | ppm | % | ppm | ppm | ppm | ppm | ppm | ppm | ppm | ppm | ppm | ppm | ppm | ppm | ppm | ppm | ppm | ppm | ppm | ppm | ppm | ppm | ppm | ppm | ppm | ppm | ppm | ppm |
| Detection Limit | 2 | 0.2 | 1 | 5 | 1 | 0.001 | 0.1 | 0.01 | 0.5 | 1 | 2 | 0.01 | 0.05 | 0.01 | 5 | 1 | 1 | 1 | 50 | 1 | 0.05 | 0.05 | 0.01 | 0.05 | 0.01 | 0.005 | 0.01 | 0.01 | 0.01 | 0.01 | 0.01 |
| Analysis Method | FUS-MS | FUS-MS | TD-ICP | TD-ICP | FUS-MS | TD-ICP | INAA | INAA | INAA | FUS-MS | FUS-ICP | FUS-MS | FUS-MS | FUS-MS | FUS-ICP | INAA | FUS-ICP | TD-ICP | INAA | FUS-MS | FUS-MS | FUS-MS | FUS-MS | FUS-MS | FUS-MS | FUS-MS | FUS-MS | FUS-MS | FUS-MS | FUS-MS | FUS-MS | FUS-MS |
| GXR-1 Meas | | | 43 | 725 | | 0.251 | | | | | | | | | | | | 744 | | | | | | | | | | | | | |
| GXR-1 Cert | | | 41 | 730 | | 0.257 | | | | | | | | | | | | 760 | | | | | | | | | | | | | |
| WMG-1 Meas | < 2 | 5 | | | | | 2.3 | 27.1 | 15.2 | 2 | | 0.24 | 1.09 | 0.66 | | < 1 | | | 140 | 47 | 7.61 | 15.5 | | 8.21 | 2.02 | 0.614 | | 0.35 | 2.02 | 0.42 | |
| WMG-1 Cert | 1.4 | 6 | | | | | 1.8 | 26 | 15 | 2.2 | | 0.5 | 1.1 | 0.65 | | 1.3 | | | 110 | 43 | 8.2 | 16 | | 9 | 2.3 | 0.82 | | 0.3 | 2.8 | 0.5 | |
| NIST 694 Meas | | | | | | | | | | | | | | | 1660 | | | | | | | | | | | | | | | | |
| NIST 694 Cert | | | | | | | | | | | | | | | 1740 | | | | | | | | | | | | | | | | |
| DNC-1 Meas | < 2 | 1.6 | 240 | 6 | 4 | 0.052 | | | | | 144 | 0.08 | 0.31 | 0.1 | 158 | | 17 | 54 | | 39 | 4.7 | 9.66 | 1.21 | 5.24 | 1.48 | 0.584 | 2.04 | 0.42 | 2.78 | 0.64 | 1.83 |
| DNC-1 Cert | 0.7 | 3 | 247 | 6.3 | 4.5 | 0.039 | | | | | 145 | 0.098 | 0.2 | 0.1 | 148 | | 18 | 66 | | 41 | 3.8 | 10.6 | 1.3 | 4.9 | 1.38 | 0.59 | 2 | 0.41 | 2.7 | 0.62 | 2 |
| BIR-1 Meas | | | | | | | | | | | | | | | | | | | | | | | | | | | | | | | |
| BIR-1 Cert | | | | | | | | | | | | | | | | | | | | | | | | | | | | | | | |
| GBW 07113 Meas | | | | | | | | | | | 40 | | | | < 5 | | 46 | | | | | | | | | | | | | | |
| GBW 07113 Cert | | | | | | | | | | | 43 | | | | 5 | | 43 | | | | | | | | | | | | | | |
| MICA-FE Meas | | | | | | | | | | | | | | | | | | | | | | | | | | | | | | | |
| MICA-FE Cert | | | | | | | | | | | | | | | | | | | | | | | | | | | | | | | |
| GXR-4 Meas | | | 47 | 46 | | 1.77 | | | | | | | | | | | | 69 | | | | | | | | | | | | | |
| GXR-4 Cert | | | 42 | 52 | | 1.77 | | | | | | | | | | | | 73 | | | | | | | | | | | | | |
| GXR-2 Meas | < 2 | 10.1 | 20 | 706 | 75 | 0.036 | | | | 2 | | 0.73 | 8.23 | 2.88 | | | | 545 | | 226 | 28.4 | 54.3 | | 19.6 | 3.6 | 0.694 | 3.01 | 0.49 | 2.8 | | |
| GXR-2 Cert | 2.1 | 11 | 21 | 690 | 78 | 0.0313 | | | | 1.7 | | 0.9 | 8.8 | 2.9 | | | | 530 | | 269 | 25.6 | 51.4 | | 19 | 3.5 | 0.81 | 3.3 | 0.48 | 3.3 | | |
| SDC-1 Meas | | | 36 | 22 | | 0.067 | | | | | | | | | | | | 97 | | | | | | | | | | | | | |
| SDC-1 Cert | | | 38 | 25 | | 0.065 | | | | | | | | | | | | 103 | | | | | | | | | | | | | |
| SCO-1 Meas | | | 28 | 26 | | | | | | | | | | | | | | 97 | | | | | | | | | | | | | |
| SCO-1 Cert | | | 27 | 31 | | | | | | | | | | | | | | 103 | | | | | | | | | | | | | |
| GXR-6 Meas | | | 26 | 90 | | 0.017 | | | | | | | | | | | | 125 | | | | | | | | | | | | | |
| GXR-6 Cert | | | 27 | 101 | | 0.016 | | | | | | | | | | | | 118 | | | | | | | | | | | | | |
| NIST 1633b Meas | | | | | | | | | | | 1044 | | | | 311 | | | | | | | | | | | | | | | | |
| NIST 1633b Cert | | | | | | | | | | | 1040 | | | | 296 | | | | | | | | | | | | | | | | |
| SY-3 Meas | | | | | | | | | | | | | | | | | | | | | | | | | | | | | | | |
| SY-3 Cert | | | | | | | | | | | | | | | | | | | | | | | | | | | | | | | |
| BE-N Meas | | | | | | | | | | | | | | | | | | | | | | | | | | | | | | | |
| BE-N Cert | | | | | | | | | | | | | | | | | | | | | | | | | | | | | | | |
| AC-E Meas | | | | | | | | | | | | | | | | | | | | | | | | | | | | | | | |
| AC-E Cert | | | | | | | | | | | | | | | | | | | | | | | | | | | | | | | |
| W-2a Meas | < 2 | 8.3 | | | 20 | | | | | | 194 | 0.45 | 2.23 | 0.52 | 285 | | 20 | | | 95 | 11.7 | 25 | | 13 | 3.34 | 1.09 | | 0.65 | 3.82 | 0.79 | 2.11 |
| W-2a Cert | 0.6 | 7.9 | | | 21 | | | | | | 190 | 0.5 | 2.4 | 0.53 | 262 | | 24 | | | 94 | 10 | 23 | | 13 | 3.3 | 1 | | 0.63 | 3.6 | 0.76 | 2.5 |
| OREAS 13P Meas | | | 2170 | | | | | | | | | | | | | | | | | | | | | | | | | | | | |
| OREAS 13P Cert | | | 2260 | | | | | | | | | | | | | | | | | | | | | | | | | | | | |
| SY-4 Meas | | | | | | | | | | | 1187 | | | | 5 | | 119 | | | | | | | | | | | | | | |
| SY-4 Cert | | | | | | | | | | | 1191 | | | | 8 | | 119 | | | | | | | | | | | | | | |
| CTA-AC-1 Meas | | | | | | | | | | | | 2.56 | 23.3 | 4.28 | | | | | | | 2290 | 3000 | | 1120 | 163 | 44.7 | 125 | 14.5 | | | |
| CTA-AC-1 Cert | | | | | | | | | | | | 2.65 | 21.8 | 4.4 | | | | | | | 2176 | 3326 | | 1087 | 162 | 46.7 | 124 | 13.9 | | | |
| BIR-1a Meas | < 2 | 0.6 | | | < 1 | | | | | < 1 | 110 | 0.02 | 0.08 | 0.02 | 343 | | 14 | | | 15 | 1.25 | 2.98 | 0.47 | 2.69 | 1.13 | 0.524 | 1.84 | 0.39 | 2.54 | 0.56 | 1.6 |
| BIR-1a Cert | 0.5 | 0.6 | | | 0.25 | | | | | 0.65 | 108 | 0.04 | 0.03 | 0.01 | 313 | | 16 | | | 16 | 0.62 | 1.95 | 0.38 | 2.5 | 1.1 | 0.54 | 1.85 | 0.36 | 2.5 | 0.57 | 1.7 |
| NCS DC86312 Meas | | | | | | | | | | | | | 26 | | | | | | | | | | | | | | | | | | |
| NCS DC86312 Cert | | | | | | | | | | | | | 23.6 | | | | | | | | | | | | | | | | | | |
| VS-N Meas | | | | | | | | | | | | | | | | | | | | | | | | | | | | | | | |
| VS-N Cert | | | | | | | | | | | | | | | | | | | | | | | | | | | | | | | |
| NCS DC70014 Meas | > 100 | | | | | | | | | | | | | | | | | | | | 50.4 | 92.6 | 10.5 | 38.2 | 7.92 | 1.66 | 7.16 | 1.17 | 6.43 | 1.27 | 3.44 |
| NCS DC70014 Cert | 270 | | | | | | | | | | | | | | | | | | | | 45.3 | 87 | 10.8 | 39.9 | 8 | 1.8 | 7.4 | 1.1 | 6.7 | 1.3 | 3.5 |
| NCS DC70009 (GBW07241) Meas | > 100 | | | | 505 | | | | | > 1000 | | | 28.4 | | | | | | | | 26.8 | 64 | 8.16 | 32.2 | 12.6 | 0.117 | 15 | 3.44 | 21.6 | 4.52 | 13.1 |
| NCS DC70009 (GBW07241) Cert | 980 | | | | 500 | | | | | 1700 | | | 28.3 | | | | | | | | 23.7 | 60.3 | 7.9 | 32.9 | 12.5 | 0.16 | 14.8 | 3.3 | 20.7 | 4.5 | 13.4 |
| OREAS 100a (Fusion) Meas | 23 | | | | | | | | | | | | 50.4 | 137 | | | | | | | 288 | 485 | 47 | 149 | 24.1 | 3.59 | 20.5 | 3.69 | 22.6 | 4.84 | 14.1 |
| OREAS 100a (Fusion) Cert | 24.1 | | | | | | | | | | | | 51.6 | 135 | | | | | | | 260 | 463 | 47.1 | 152 | 23.6 | 3.71 | 23.6 | 3.8 | 23.2 | 4.81 | 14.9 |
| OREAS 101a (Fusion) Meas | 20 | | | | | | | | | | | | 36 | 421 | | | | | | | 855 | 1410 | 133 | 398 | 50.7 | 8.09 | 35.8 | 5.46 | 32 | 6.58 | 19.2 |
| OREAS 101a (Fusion) Cert | 21.9 | | | | | | | | | | | | 36.6 | 422 | | | | | | | 816 | 1396 | 134 | 403 | 48.8 | 8.06 | 43.4 | 5.92 | 33.3 | 6.46 | 19.5 |
| JR-1 Meas | 3 | 17.8 | | | 248 | | | | | 3 | | 1.71 | 26.5 | 9.2 | | | | | 100 | 23.1 | 52 | 6.2 | 23.9 | 5.91 | 0.284 | 5.62 | 1.04 | 6.3 | 1.34 | 3.91 |
| JR-1 Cert | 3.25 | 15.2 | | | 257 | | | | | 2.86 | | 1.86 | 26.7 | 8.88 | | | | | 99.9 | 19.7 | 47.2 | 5.58 | 23.3 | 6.03 | 0.3 | 5.06 | 1.01 | 5.69 | 1.11 | 3.61 |
| ZMMH 15Q Orig | 7 | 5.7 | | | 164 | | | | | 2 | 373 | 0.5 | 5.83 | 1.85 | 127 | | 12 | | 141 | 31.8 | 59 | 5.69 | 20.1 | 3.64 | 1.01 | 2.81 | 0.41 | 2.29 | 0.44 | 1.3 |
| ZMMH 15Q Dup | 7 | 4.8 | | | 163 | | | | | 2 | 373 | 0.47 | 5.75 | 1.88 | 126 | | 13 | | 141 | 31.2 | 58.8 | 5.63 | 20 | 3.61 | 1 | 2.93 | 0.42 | 2.3 | 0.44 | 1.32 |
| ZMMH 17Q Orig | | | 25 | < 5 | | 1.58 | | | | | | | | | | | | 21 | | | | | | | | | | | | | |
| ZMMH 17Q Dup | | | 22 | < 5 | | 1.58 | | | | | | | | | | | | 21 | | | | | | | | | | | | | |
| Method Blank Method Blank | | | < 1 | < 5 | | < 0.001 | | | | | | | | | | | | < 1 | | | | | | | | | | | | | |
| Method Blank Method Blank | | | | | | | < 0.1 | < 0.01 | < 0.5 | | | | | | | < 1 | | | < 50 | | | | | | | | | | | | |
| Method Blank Method Blank | | | | | | | | | | | | | | | | | | | | | | | | | | | | | | | |

| Analyte Symbol | Tl | Tm | Yb | Lu | Mass | Ga | Pb | Sn | Nb | Rb |
|---|---|---|---|---|---|---|---|---|---|---|
| Unit Symbol | ppm | ppm | ppm | ppm | g | ppm | ppm | ppm | ppm | ppm |
| Detection Limit | 0.05 | 0.005 | 0.01 | 0.002 | | 5 | 5 | 5 | 1 | 2 |
| Analysis Method | FUS-MS | FUS-MS | FUS-MS | FUS-MS | INAA | PPXRF | PPXRF | PPXRF | PPXRF | PPXRF |
| GXR-1 Meas | | | | | | | | | | |
| GXR-1 Cert | | | | | | | | | | |
| WMG-1 Meas | | 0.171 | 1.08 | 0.152 | | | | | | |
| WMG-1 Cert | | 0.2 | 1.3 | 0.21 | | | | | | |
| NIST 694 Meas | | | | | | | | | | |
| NIST 694 Cert | | | | | | | | | | |
| DNC-1 Meas | < 0.05 | 0.313 | 1.98 | 0.288 | | | | | | |
| DNC-1 Cert | 0.026 | 0.38 | 2.01 | 0.32 | | | | | | |
| BIR-1 Meas | | | | | | 17 | < 5 | < 5 | < 1 | 3 |
| BIR-1 Cert | | | | | | 16 | 3 | 0.65 | 0.6 | 0.25 |
| GBW 07113 Meas | | | | | | | | | | |
| GBW 07113 Cert | | | | | | | | | | |
| MICA-FE Meas | | | | | | 98 | 25 | 85 | 295 | 2190 |
| MICA-FE Cert | | | | | | 95 | 13 | 70 | 270 | 2200 |
| GXR-4 Meas | | | | | | | | | | |
| GXR-4 Cert | | | | | | | | | | |
| GXR-2 Meas | 0.69 | 0.264 | 1.74 | 0.249 | | | | | | |
| GXR-2 Cert | 1.03 | 0.3 | 2.04 | 0.27 | | | | | | |
| SDC-1 Meas | | | | | | | | | | |
| SDC-1 Cert | | | | | | | | | | |
| SCO-1 Meas | | | | | | | | | | |
| SCO-1 Cert | | | | | | | | | | |
| GXR-6 Meas | | | | | | | | | | |
| GXR-6 Cert | | | | | | | | | | |
| NIST 1633b Meas | | | | | | | | | | |
| NIST 1633b Cert | | | | | | | | | | |
| SY-3 Meas | | | | | | 28 | 150 | 13 | 155 | 214 |
| SY-3 Cert | | | | | | 27 | 133 | 6.5 | 148 | 206 |
| BE-N Meas | | | | | | 17 | 6 | 8 | 104 | 60 |
| BE-N Cert | | | | | | 17 | 4 | 2 | 105 | 47 |
| AC-E Meas | | | | | | 42 | 41 | 14 | 108 | 157 |
| AC-E Cert | | | | | | 39 | 39 | 13 | 110 | 152 |
| W-2a Meas | < 0.05 | 0.329 | 2.09 | 0.29 | | | | | | |
| W-2a Cert | 0.2 | 0.38 | 2.1 | 0.33 | | | | | | |
| OREAS 13P Meas | | | | | | | | | | |
| OREAS 13P Cert | | | | | | | | | | |
| SY-4 Meas | | | | | | | | | | |
| SY-4 Cert | | | | | | | | | | |
| CTA-AC-1 Meas | | | 10.6 | 1.07 | | | | | | |
| CTA-AC-1 Cert | | | 11.4 | 1.08 | | | | | | |
| BIR-1a Meas | < 0.05 | 0.264 | 1.65 | 0.239 | | | | | | |
| BIR-1a Cert | 0.01 | 0.26 | 1.65 | 0.26 | | | | | | |
| NCS DC86312 Meas | | | | | | | | | | |
| NCS DC86312 Cert | | | | | | | | | | |
| VS-N Meas | | | | | | 387 | > 1000 | 810 | 741 | 825 |
| VS-N Cert | | | | | | 400 | 1000 | 800 | 700 | 800 |
| NCS DC70014 Meas | | 0.53 | 3.41 | 0.477 | | | | | | |
| NCS DC70014 Cert | | 0.57 | 3.3 | 0.5 | | | | | | |
| NCS DC70009 (GBW07241) Meas | 2.15 | 2.43 | 16.4 | 2.34 | | | | | | |
| NCS DC70009 (GBW07241) Cert | 1.8 | 2.2 | 14.9 | 2.4 | | | | | | |
| OREAS 100a (Fusion) Meas | | 2.34 | 15 | 2.1 | | | | | | |
| OREAS 100a (Fusion) Cert | | 2.31 | 14.9 | 2.26 | | | | | | |
| OREAS 101a (Fusion) Meas | | 2.97 | 18.2 | 2.51 | | | | | | |
| OREAS 101a (Fusion) Cert | | 2.9 | 17.5 | 2.66 | | | | | | |
| JR-1 Meas | 1.28 | 0.696 | 4.65 | 0.692 | | | | | | |
| JR-1 Cert | 1.56 | 0.67 | 4.55 | 0.71 | | | | | | |
| ZMMH 15Q Orig | 0.84 | 0.203 | 1.41 | 0.234 | | | | | | |
| ZMMH 15Q Dup | 0.86 | 0.201 | 1.38 | 0.238 | | | | | | |
| ZMMH 17Q Orig | | | | | | | | | | |
| ZMMH 17Q Dup | | | | | | | | | | |
| Method Blank Method Blank | | | | | | | | | | |
| Method Blank Method Blank | | | | | 1 | | | | | |
| Method Blank Method Blank | | | | | | < 5 | < 5 | < 5 | < 1 | < 2 |

# Appendix 4 Whole-rock Geochemical Data for MMH Samples

The following section contains the data table for the whole-rock geochemical analysis preformed on the MMH and Chuquicamata samples by Activation Labs in Ancaster, Ontario.

| MMH | | | | | | | | | | | | |
|---|---|---|---|---|---|---|---|---|---|---|---|---|
| **Analyte Symbol** | SiO2 | Al2O3 | Fe2O3(T) | MnO | MgO | CaO | Na2O | K2O | TiO2 | P2O5 | LOI | Total |
| **Unit Symbol** | % | % | % | % | % | % | % | % | % | % | % | % |
| **Detection Limit** | 0.01 | 0.01 | 0.01 | 0.001 | 0.01 | 0.01 | 0.01 | 0.01 | 0.001 | 0.01 | | 0.01 |
| **Analysis Method** | FUS-ICP | FUS-ICP | FUS-ICP | FUS-ICP | FUS-ICP | FUS-ICP | FUS-ICP | FUS-ICP | FUS-ICP | FUS-ICP | FUS-ICP | FUS-ICP |
| ZMMH 04Q | 64.18 | 15.29 | 2.34 | 0.293 | 1.02 | 2.16 | 0.36 | 9.51 | 0.336 | 0.16 | 4.5 | 100.1 |
| ZMMH 05Q | 64.77 | 15.58 | 2.8 | 0.54 | 1.5 | 1.57 | 0.09 | 5.67 | 0.326 | 0.14 | 4.76 | 97.74 |
| ZMMH 07Q | 67.73 | 15.42 | 2.02 | 0.219 | 0.89 | 1.83 | 2.9 | 5.54 | 0.315 | 0.15 | 3.61 | 100.6 |
| ZMMH 09Q | 65.17 | 14.57 | 3.45 | 1.89 | 1.04 | 0.23 | 0.14 | 8.16 | 0.347 | 0.12 | 4.47 | 99.59 |
| ZMMH 10Q | 67.1 | 15 | 3.53 | 0.201 | 1.4 | 1.97 | 5.09 | 2.19 | 0.382 | 0.1 | 3.39 | 100.4 |
| ZMMH 11Q | 69.55 | 15.63 | 1.87 | 0.02 | 0.58 | 0.16 | 0.16 | 7.53 | 0.247 | 0.1 | 2.73 | 98.58 |
| ZMMH 12Q | 79.01 | 12.71 | 1.02 | 0.015 | 0.36 | 0.05 | 0.09 | 3.82 | 0.166 | 0.04 | 1.97 | 99.27 |
| ZMMH 13Q | 77.17 | 11.79 | 3.37 | 0.012 | 0.22 | 0.05 | 0.08 | 3.22 | 0.162 | 0.03 | 3.12 | 99.23 |
| ZMMH 14Q | 68.36 | 15.98 | 1.98 | 0.055 | 1.78 | 2.19 | 4.47 | 3.26 | 0.407 | 0.12 | 2.22 | 100.8 |
| ZMMH 15Q | 54.74 | 21.73 | 3.06 | 0.084 | 3.3 | 1.95 | 4.58 | 4.61 | 0.422 | 0.11 | 4.2 | 98.78 |
| ZMMH 17Q | 71.57 | 14.8 | 2.55 | 0.017 | 0.75 | 0.18 | 0.09 | 4.59 | 0.343 | 0.1 | 3.04 | 98.02 |
| ZMMH 18Q | 72.46 | 16.36 | 3.57 | 0.006 | 0.05 | 0.06 | 0.09 | 1.77 | 0.409 | 0.06 | 4.49 | 99.32 |
| ZMMH 20Q | 69.95 | 15.55 | 3.35 | 0.012 | 0.51 | 0.08 | 0.08 | 4.46 | 0.374 | 0.07 | 3.78 | 98.23 |
| ZMMH 21Q | 69.79 | 15.54 | 2.39 | 0.027 | 1.1 | 0.18 | 0.1 | 5.56 | 0.367 | 0.09 | 3.1 | 98.24 |
| ZMMH 23Q | 66.48 | 17.2 | 3.18 | 0.205 | 2.8 | 0.16 | 0.09 | 4.85 | 0.358 | 0.09 | 3.78 | 99.21 |
| Cu-1333 Banco 2 | 69.27 | 17.1 | 1.65 | 0.01 | 0.32 | 1.91 | 4.96 | 2.74 | 0.273 | 0.04 | 0.96 | 99.22 |
| Cu-2022 Este 2 | 68.65 | 16.18 | 2.49 | 0.03 | 0.61 | 2.87 | 4.68 | 3 | 0.276 | 0.09 | 0.34 | 99.23 |

| MMH | | | | | | | | | | | | |
|---|---|---|---|---|---|---|---|---|---|---|---|---|
| **Analyte Symbol** | Au | Ag | As | Ba | Be | Bi | Br | Cd | Co | Cr | Cs | Cu |
| **Unit Symbol** | ppb | ppm | ppm | ppm | ppm | ppm | ppm | ppm | ppm | ppm | ppm | ppm |
| **Detection Limit** | 1 | 0.5 | 1 | 1 | 1 | 0.1 | 0.5 | 0.5 | 0.1 | 0.5 | 0.1 | 1 |
| **Analysis Method** | INAA | INAA / TD-ICP | INAA | FUS-ICP | FUS-ICP | FUS-MS | INAA | TD-ICP | INAA | INAA | FUS-MS | TD-ICP |
| ZMMH 04Q | 14 | 6.8 | < 1 | 1262 | 2 | 1 | < 0.5 | 3.7 | 2.2 | 6.7 | 2.3 | 5080 |
| ZMMH 05Q | 3 | 5.3 | 1 | 790 | 2 | 0.6 | 1.1 | 30 | 3.3 | 9.9 | 4.6 | 5220 |
| ZMMH 07Q | 5 | 1.2 | 4 | 842 | 2 | < 0.1 | < 0.5 | 0.9 | 2.7 | 6.9 | 7 | 3310 |
| ZMMH 09Q | < 1 | 0.8 | 12 | 1815 | 1 | < 0.1 | < 0.5 | 6.9 | 8.3 | 12.7 | 6.9 | 118 |
| ZMMH 10Q | < 1 | < 0.5 | 15 | 455 | 1 | < 0.1 | < 0.5 | 3.6 | 12.1 | 12.3 | 7.2 | 33 |
| ZMMH 11Q | 21 | 2.6 | 118 | 922 | 2 | 0.7 | < 0.5 | 0.5 | 1.7 | 5.1 | 2.6 | 7510 |
| ZMMH 12Q | 4 | 0.9 | 12 | 253 | 1 | 0.1 | < 0.5 | < 0.5 | 0.8 | 7.7 | 0.9 | 2770 |
| ZMMH 13Q | 13 | 3 | 8 | 130 | < 1 | 0.2 | < 0.5 | < 0.5 | 3.3 | 10.5 | 5.1 | 6210 |
| ZMMH 14Q | 15 | 1.6 | < 1 | 504 | 2 | 0.2 | < 0.5 | < 0.5 | 4.2 | 13.1 | 3 | 3610 |
| ZMMH 15Q | 24 | 0.6 | 2 | 588 | 3 | 0.2 | < 0.5 | < 0.5 | 7.3 | 11.4 | 11.1 | 4810 |
| ZMMH 17Q | 3 | < 0.5 | 4 | 706 | 1 | < 0.1 | < 0.5 | < 0.5 | 8.1 | 13.4 | 2.2 | 7170 |
| ZMMH 18Q | 70 | 2.6 | 51 | 79 | < 1 | 0.5 | 1.2 | < 0.5 | 7.2 | 22.6 | 1.2 | 7100 |
| ZMMH 20Q | 30 | 5.9 | 37 | 307 | 1 | 0.7 | 1.2 | < 0.5 | 4 | 23.6 | 1.9 | > 10000 |
| ZMMH 21Q | 9 | 1.4 | 118 | 404 | 2 | < 0.1 | 1.3 | < 0.5 | 2.4 | 16.2 | 4.2 | 9470 |
| ZMMH 23Q | 5 | 1.8 | 2 | 544 | 2 | 0.2 | 1.2 | 3.8 | 6.8 | 15.2 | 4 | 7030 |
| Cu-1333 Banco 2 | < 1 | < 0.5 | 9 | 790 | 2 | < 0.1 | 0.9 | < 0.5 | 2.8 | 6 | 2.2 | 1560 |
| Cu-2022 Este 2 | < 1 | < 0.5 | 2 | 791 | 2 | < 0.1 | < 0.5 | < 0.5 | 3.6 | 5.1 | 0.7 | 306 |

| MMH | | | | | | | | | | | | |
|---|---|---|---|---|---|---|---|---|---|---|---|---|
| **Analyte Symbol** | Ga | Ge | Hf | Hg | In | Ir | Mo | Nb | Ni | Pb | Rb | S |
| **Unit Symbol** | ppm | ppm | ppm | ppm | ppm | ppb | ppm | ppm | ppm | ppm | ppm | % |
| **Detection Limit** | 1 | 0.5 | 0.1 | 1 | 0.1 | 1 | 2 | 0.2 | 1 | 5 | 1 | 0.001 |
| **Analysis Method** | FUS-MS | FUS-MS | FUS-MS | INAA | FUS-MS | INAA | FUS-MS | FUS-MS | TD-ICP | TD-ICP | FUS-MS | TD-ICP |
| ZMMH 04Q | 18 | 2.4 | 3 | < 1 | < 0.1 | < 1 | 16 | 8 | 5 | 76 | 231 | 1.57 |
| ZMMH 05Q | 18 | 1.4 | 3.1 | < 1 | < 0.1 | < 1 | 67 | 7.6 | 11 | 1970 | 227 | 1.48 |
| ZMMH 07Q | 17 | 1.8 | 3.7 | < 1 | < 0.1 | < 1 | 21 | 9.4 | 4 | 73 | 132 | 0.28 |
| ZMMH 09Q | 14 | 3 | 2.9 | < 1 | < 0.1 | < 1 | < 2 | 4 | 14 | 374 | 220 | 1.69 |
| ZMMH 10Q | 15 | 0.9 | 3.2 | < 1 | < 0.1 | < 1 | < 2 | 4.5 | 19 | 369 | 58 | 1.06 |
| ZMMH 11Q | 17 | 4.3 | 3 | < 1 | < 0.1 | < 1 | > 100 | 6.3 | 6 | 12 | 191 | 0.714 |
| ZMMH 12Q | 10 | 1.6 | 2.6 | < 1 | < 0.1 | < 1 | 28 | 5.2 | 2 | < 5 | 88 | 0.355 |
| ZMMH 13Q | 8 | 1.4 | 2.5 | < 1 | < 0.1 | < 1 | 27 | 6.9 | 5 | 6 | 92 | 2.53 |
| ZMMH 14Q | 18 | 2.3 | 3.6 | < 1 | < 0.1 | < 1 | 2 | 5.6 | 16 | < 5 | 78 | 0.219 |
| ZMMH 15Q | 29 | 2.2 | 4.2 | < 1 | < 0.1 | < 1 | 7 | 5.2 | 23 | < 5 | 163 | 0.408 |
| ZMMH 17Q | 16 | 1.9 | 3.1 | < 1 | < 0.1 | < 1 | > 100 | 3.7 | 23 | < 5 | 133 | 1.58 |
| ZMMH 18Q | 9 | 1.8 | 3.5 | < 1 | < 0.1 | < 1 | 18 | 4.7 | 17 | 14 | 46 | 3.15 |
| ZMMH 20Q | 21 | 1.9 | 3.5 | < 1 | < 0.1 | < 1 | 20 | 65.1 | 11 | < 5 | 114 | 3.03 |
| ZMMH 21Q | 15 | 4.4 | 3.1 | < 1 | 0.1 | < 1 | 60 | 3.7 | 6 | 5 | 220 | 0.917 |
| ZMMH 23Q | 19 | 1.6 | 3.1 | < 1 | 0.3 | < 1 | 2 | 4.9 | 20 | < 5 | 159 | 1.46 |
| Cu-1333 Banco 2 | 22 | 1.6 | 3.2 | < 1 | < 0.1 | < 1 | < 2 | 5.7 | 3 | 5 | 69 | 0.164 |
| Cu-2022 Este 2 | 20 | 1.3 | 3.6 | < 1 | < 0.1 | < 1 | < 2 | 9.8 | 4 | 8 | 66 | 0.039 |

| MMH | | | | | | | | | | | | |
|---|---|---|---|---|---|---|---|---|---|---|---|---|
| **Analyte Symbol** | Sb | Sc | Se | Sn | Sr | Ta | Th | U | V | W | Y | Zn |
| **Unit Symbol** | ppm | ppm | ppm | ppm | ppm | ppm | ppm | ppm | ppm | ppm | ppm | ppm |
| **Detection Limit** | 0.1 | 0.01 | 0.5 | 1 | 2 | 0.01 | 0.05 | 0.01 | 5 | 1 | 1 | 1 |
| **Analysis Method** | INAA | INAA | INAA | FUS-MS | FUS-ICP | FUS-MS | FUS-MS | FUS-MS | FUS-ICP | INAA | FUS-ICP | INAA / TD-ICP |
| ZMMH 04Q | 0.6 | 3.88 | < 0.5 | 2 | 307 | 0.54 | 5.48 | 0.95 | 46 | 10 | 6 | 906 |
| ZMMH 05Q | 0.8 | 3.68 | < 0.5 | 2 | 106 | 0.52 | 5.88 | 2.17 | 45 | 9 | 7 | 6210 |
| ZMMH 07Q | 0.5 | 3.73 | < 0.5 | 1 | 244 | 0.7 | 9.68 | 1.7 | 41 | 5 | 6 | 227 |
| ZMMH 09Q | 2.5 | 6.66 | < 0.5 | < 1 | 137 | 0.31 | 4.36 | 1.34 | 54 | 13 | 9 | 1660 |
| ZMMH 10Q | 0.8 | 6.72 | < 0.5 | 1 | 207 | 0.28 | 4.17 | 0.73 | 63 | < 1 | 5 | 730 |
| ZMMH 11Q | 2.5 | 2.93 | < 0.5 | 3 | 132 | 0.43 | 4.14 | 1.97 | 27 | 13 | 5 | 93 |
| ZMMH 12Q | 1.9 | 2.54 | < 0.5 | 7 | 58 | 0.48 | 5.23 | 0.91 | 22 | 11 | 7 | 21 |
| ZMMH 13Q | 1.5 | 2.43 | 3.8 | 17 | 56 | 0.47 | 5.11 | 0.96 | 36 | 18 | 7 | 22 |
| ZMMH 14Q | 0.3 | 8.12 | < 0.5 | 2 | 370 | 0.32 | 4.46 | 1.04 | 75 | 4 | 8 | 55 |
| ZMMH 15Q | 0.5 | 8.65 | < 0.5 | 2 | 373 | 0.48 | 5.79 | 1.86 | 126 | < 1 | 13 | 45 |
| ZMMH 17Q | 0.3 | 7.57 | < 0.5 | 4 | 26 | 0.31 | 3.5 | 1.12 | 73 | 13 | 6 | 21 |
| ZMMH 18Q | 1.5 | 7.4 | 5.5 | 11 | 214 | 0.31 | 4.91 | 0.98 | 85 | 17 | 7 | 16 |
| ZMMH 20Q | 0.4 | 7.87 | 5.4 | 6 | 168 | 58.4 | 4.45 | 3.57 | 70 | 15 | 9 | 35 |
| ZMMH 21Q | 2.2 | 5.75 | < 0.5 | 3 | 37 | 0.23 | 3.84 | 0.91 | 54 | 17 | 5 | 98 |
| ZMMH 23Q | 0.4 | 7.8 | < 0.5 | 2 | 12 | 0.39 | 4.77 | 1.35 | 66 | 15 | 9 | 1250 |
| Cu-1333 Banco 2 | 0.3 | 2.95 | < 0.5 | 2 | 640 | 0.38 | 4.46 | 5.06 | 27 | 8 | 11 | 343 |
| Cu-2022 Este 2 | < 0.1 | 3.19 | < 0.5 | 1 | 647 | 0.61 | 7.22 | 2.72 | 33 | < 1 | 5 | 121 |

| MMH | | | | | | | | | | | | |
|---|---|---|---|---|---|---|---|---|---|---|---|---|
| **Analyte Symbol** | Zr | La | Ce | Pr | Nd | Sm | Eu | Gd | Tb | Dy | Ho | Er |
| **Unit Symbol** | ppm | ppm | ppm | ppm | ppm | ppm | ppm | ppm | ppm | ppm | ppm | ppm |
| **Detection Limit** | 1 | 0.05 | 0.05 | 0.01 | 0.05 | 0.01 | 0.005 | 0.01 | 0.01 | 0.01 | 0.01 | 0.01 |
| **Analysis Method** | FUS-MS | FUS-MS | FUS-MS | FUS-MS | FUS-MS | FUS-MS | FUS-MS | FUS-MS | FUS-MS | FUS-MS | FUS-MS | FUS-MS |
| ZMMH 04Q | 107 | 21.4 | 41.4 | 4.21 | 15.5 | 2.59 | 0.641 | 1.81 | 0.24 | 1.23 | 0.23 | 0.64 |
| ZMMH 05Q | 111 | 24.5 | 45.6 | 4.34 | 15.1 | 2.44 | 0.804 | 1.56 | 0.21 | 1.12 | 0.21 | 0.63 |
| ZMMH 07Q | 126 | 25.7 | 47.7 | 4.69 | 16.5 | 2.65 | 0.666 | 1.76 | 0.24 | 1.27 | 0.24 | 0.7 |
| ZMMH 09Q | 106 | 18.4 | 35.4 | 3.49 | 12.3 | 2.17 | 0.733 | 1.65 | 0.25 | 1.47 | 0.29 | 0.87 |
| ZMMH 10Q | 120 | 17.3 | 32.2 | 3.15 | 11.5 | 1.88 | 0.581 | 1.36 | 0.2 | 1.1 | 0.22 | 0.63 |
| ZMMH 11Q | 110 | 17.1 | 32.8 | 3.3 | 11.6 | 1.98 | 0.526 | 1.3 | 0.18 | 1 | 0.19 | 0.55 |
| ZMMH 12Q | 84 | 15.6 | 28.6 | 2.69 | 9.37 | 1.59 | 0.439 | 1.34 | 0.21 | 1.19 | 0.24 | 0.74 |
| ZMMH 13Q | 80 | 19 | 36.2 | 3.42 | 11.4 | 1.76 | 0.379 | 1.14 | 0.18 | 1.13 | 0.24 | 0.75 |
| ZMMH 14Q | 139 | 17.1 | 32.4 | 3.16 | 11.9 | 2.14 | 0.618 | 1.64 | 0.26 | 1.45 | 0.29 | 0.85 |
| ZMMH 15Q | 141 | 31.5 | 58.9 | 5.66 | 20.1 | 3.63 | 1.01 | 2.87 | 0.42 | 2.3 | 0.44 | 1.31 |
| ZMMH 17Q | 112 | 12.6 | 24.9 | 2.47 | 8.94 | 1.48 | 0.325 | 1.24 | 0.2 | 1.21 | 0.25 | 0.76 |
| ZMMH 18Q | 133 | 20.7 | 40 | 3.9 | 14 | 2.56 | 0.627 | 1.75 | 0.23 | 1.3 | 0.27 | 0.89 |
| ZMMH 20Q | 130 | 19 | 35.4 | 3.35 | 11.6 | 2.01 | 0.499 | 1.66 | 0.24 | 1.46 | 0.28 | 0.83 |
| ZMMH 21Q | 122 | 16.4 | 29.7 | 2.89 | 10.4 | 1.84 | 0.581 | 1.42 | 0.21 | 1.13 | 0.23 | 0.68 |
| ZMMH 23Q | 116 | 17.4 | 33.3 | 3.22 | 11.8 | 2.09 | 0.404 | 1.72 | 0.28 | 1.57 | 0.31 | 0.91 |
| Cu-1333 Banco 2 | 115 | 14.1 | 26.2 | 2.43 | 8.58 | 1.57 | 0.537 | 1.42 | 0.28 | 1.8 | 0.36 | 1.05 |
| Cu-2022 Este 2 | 122 | 19.5 | 37.5 | 3.77 | 13.6 | 2.32 | 0.61 | 1.55 | 0.2 | 1.07 | 0.21 | 0.61 |

| MMH | | | | | | | | | | |
|---|---|---|---|---|---|---|---|---|---|---|
| **Analyte Symbol** | Tl | Tm | Yb | Lu | Mass | Ga | Pb | Sn | Nb | Rb |
| **Unit Symbol** | ppm | ppm | ppm | ppm | g | ppm | ppm | ppm | ppm | ppm |
| **Detection Limit** | 0.05 | 0.005 | 0.01 | 0.002 | | 5 | 5 | 5 | 1 | 2 |
| **Analysis Method** | FUS-MS | FUS-MS | FUS-MS | FUS-MS | INAA | PPXRF | PPXRF | PPXRF | PPXRF | PPXRF |
| ZMMH 04Q | 1.56 | 0.096 | 0.64 | 0.107 | 1.362 | 17 | 73 | 9 | 6 | 244 |
| ZMMH 05Q | 1.94 | 0.095 | 0.64 | 0.108 | 1.2 | 23 | > 1000 | 7 | 6 | 197 |
| ZMMH 07Q | 0.95 | 0.11 | 0.79 | 0.13 | 1.426 | 17 | 73 | 5 | 7 | 140 |
| ZMMH 09Q | 3.12 | 0.136 | 0.95 | 0.16 | 1.418 | 14 | 350 | 6 | 3 | 225 |
| ZMMH 10Q | 0.58 | 0.097 | 0.65 | 0.109 | 1.479 | 15 | 346 | 9 | 4 | 54 |
| ZMMH 11Q | 1.18 | 0.086 | 0.64 | 0.111 | 1.223 | 15 | 14 | 12 | 7 | 207 |
| ZMMH 12Q | 0.49 | 0.118 | 0.84 | 0.141 | 1.344 | 9 | < 5 | 18 | 5 | 96 |
| ZMMH 13Q | 0.65 | 0.118 | 0.82 | 0.134 | 1.409 | 7 | < 5 | 17 | 5 | 99 |
| ZMMH 14Q | 0.37 | 0.131 | 0.91 | 0.157 | 1.519 | 17 | 8 | 7 | 4 | 85 |
| ZMMH 15Q | 0.85 | 0.202 | 1.4 | 0.236 | 1.34 | 27 | 8 | 10 | 4 | 176 |
| ZMMH 17Q | 0.97 | 0.117 | 0.81 | 0.141 | 1.273 | 14 | < 5 | 17 | 4 | 144 |
| ZMMH 18Q | 0.36 | 0.15 | 1.06 | 0.192 | 1.207 | 8 | 13 | 12 | 4 | 52 |
| ZMMH 20Q | 0.75 | 0.128 | 0.9 | 0.15 | 1.185 | 20 | 9 | 8 | 4 | 122 |
| ZMMH 21Q | 1.19 | 0.104 | 0.72 | 0.122 | 1.136 | 13 | < 5 | 9 | 3 | 237 |
| ZMMH 23Q | 1.22 | 0.146 | 1.04 | 0.178 | 1.24 | 20 | 9 | < 5 | 3 | 173 |
| Cu-1333 Banco 2 | 0.21 | 0.166 | 1.14 | 0.188 | 1.439 | 21 | 10 | 9 | 5 | 79 |
| Cu-2022 Este 2 | 0.12 | 0.095 | 0.67 | 0.116 | 1.669 | 20 | 8 | < 5 | 7 | 76 |

# Appendix 5 Data from Ballard (2001) Thesis

The following section contains data tables from Ballard (2001). This whole-rock geochemical data was used to compare the MMH data with the Fortuna and El Abra igneous complexes.

Los Picos

| Analyte Symbol | SiO2 | Al2O3 | Fe2O3(T) | MnO | MgO | CaO | Na2O |
|---|---|---|---|---|---|---|---|
| Unit Symbol | % | % | % | % | % | % | % |
| 98-518 | 60.6 | 16.6 | 5.88 | 0.09 | 2.81 | 5.03 | 3.75 |
| 98-519 | 62.6 | 16.4 | 5.42 | 0.09 | 2.42 | 4.74 | 3.77 |
| 98-520 | 58.7 | 17 | 6.66 | 0.07 | 3.11 | 5.54 | 3.73 |
| 98-522 | 59.6 | 16.5 | 6.54 | 0.11 | 3.24 | 5.8 | 3.71 |
| 98-524 | 60.9 | 16.5 | 6.21 | 0.1 | 2.86 | 5.27 | 3.74 |
| 98-525 | 68.1 | 14.7 | 3.76 | 0.06 | 1.33 | 2.84 | 3.29 |
| 98-526 | 57.1 | 17.8 | 6.74 | 0.11 | 3.6 | 6.04 | 4.03 |
| 98-527 | 61.7 | 16.7 | 6.13 | 0.09 | 2.45 | 4.87 | 4 |
| 98-540 | 66.7 | 15.2 | 4.26 | 0.08 | 1.54 | 3.22 | 3.36 |
| 98-549 | 61.4 | 16.9 | 5.65 | 0.07 | 2.52 | 4.6 | 3.91 |
| 98-564 | 65.8 | 15.5 | 4.25 | 0.07 | 1.68 | 3.66 | 3.68 |

**Fortuna Gris**

| Analyte Symbol | SiO2 | Al2O3 | Fe2O3(T) | MnO | MgO | CaO | Na2O |
|---|---|---|---|---|---|---|---|
| Unit Symbol | % | % | % | % | % | % | % |
| 98-532 | 64.4 | 16.5 | 4.39 | 0.05 | 1.81 | 4.19 | 4.13 |
| 98-534 | 65.7 | 15.2 | 4.85 | 0.07 | 1.72 | 3.44 | 3.25 |
| 98-544 | 61.2 | 17.1 | 5.89 | 0.1 | 2.81 | 5.18 | 3.77 |
| 98-548 | 73.1 | 14.1 | 1.8 | 0.02 | 0.37 | 1.29 | 3.4 |
| 98-550 | 67.9 | 15.1 | 3.67 | 0.05 | 1.23 | 2.88 | 3.48 |
| 98-551 | 63.5 | 16.8 | 4.93 | 0.06 | 2 | 4.43 | 4.08 |
| 98-552 | 62.6 | 16.9 | 5.4 | 0.09 | 2.31 | 4.9 | 4 |
| 98-553 | 63.7 | 16.7 | 4.77 | 0.06 | 2.07 | 3.63 | 3.97 |
| 98-559 | 64.4 | 16.4 | 4.37 | 0.07 | 1.83 | 4.19 | 4.04 |
| 98-561 | 66.7 | 16.1 | 3.7 | 0.05 | 1.39 | 3.69 | 4.06 |
| 98-566 | 66.7 | 16.9 | 4 | 0.06 | 1.44 | 3.78 | 4.1 |
| 98-576 | 63.4 | 16.7 | 4.83 | 0.07 | 2.21 | 4.65 | 4.11 |

**Fortuna Clara**

| Analyte Symbol | SiO2 | Al2O3 | Fe2O3(T) | MnO | MgO | CaO | Na2O |
|---|---|---|---|---|---|---|---|
| Unit Symbol | % | % | % | % | % | % | % |
| 98-535 | 64.8 | 17.3 | 3.72 | 0.06 | 1.52 | 3.7 | 4.56 |
| 98-536 | 65.3 | 16.8 | 3.8 | 0.08 | 1.68 | 3.96 | 4.42 |
| 98-538 | 66.6 | 16 | 3.57 | 0.06 | 1.43 | 3.69 | 4.27 |
| 98-541 | 65.9 | 16.9 | 3.08 | 0.04 | 1.11 | 3.23 | 4.9 |
| 98-547 | 67.1 | 16.6 | 3.3 | 0.07 | 1.17 | 3.21 | 4.78 |
| 98-554 | 65.6 | 16.9 | 3.76 | 0.03 | 1.5 | 3.89 | 4.63 |
| 98-556 | 66.4 | 16.4 | 3.95 | 0.04 | 1.45 | 3.11 | 4.4 |
| 98-567 | 67.2 | 16.7 | 0.47 | 0.06 | 1.09 | 3.96 | 4.65 |
| 98-570 | 68.2 | 15.7 | 3.46 | 0.02 | 1.26 | 2.97 | 4.02 |
| 98-572 | 65.5 | 17 | 3.91 | 0.05 | 1.47 | 3.85 | 4.34 |
| 98-575 | 66.9 | 16.4 | 3.11 | 0.02 | 1.29 | 3.54 | 4.66 |
| 98-577 | 68.4 | 15.4 | 2.95 | 0.04 | 1.67 | 3.35 | 4.1 |

## San Lorenzo

| Analyte Symbol | SiO2 | Al2O3 | Fe2O3(T) | MnO | MgO | CaO | Na2O |
|---|---|---|---|---|---|---|---|
| Unit Symbol | % | % | % | % | % | % | % |
| 98-531 | 66.7 | 16.2 | 3.23 | 0.04 | 1.36 | 3.62 | 4.19 |
| 98-542 | 65.4 | 16.7 | 3.17 | 0.03 | 1.3 | 3.04 | 4.81 |
| 98-545 | 70.8 | 15 | 2.09 | 0.05 | 0.73 | 2.1 | 4.21 |
| 98-546 | 68.4 | 16 | 2.83 | 0.06 | 0.91 | 3.11 | 4.54 |
| 98-560 | 65.4 | 19.9 | 3.87 | 0 | 0.62 | 0.51 | 1.96 |
| 98-562 | 70.9 | 15.5 | 2.07 | 0.02 | 0.76 | 1.56 | 4.25 |
| 98-563 | 69.9 | 15.6 | 2.33 | 0.04 | 0.85 | 2.7 | 4.12 |
| 98-568 | 64.3 | 15.9 | 8.43 | 0.01 | 0.41 | 0.58 | 4.66 |
| 98-571 | 76.4 | 13.1 | 0.61 | 0.01 | 0.23 | 1.17 | 3.35 |
| 98-573 | 68.1 | 16.1 | 2.79 | 0.03 | 1.29 | 2.24 | 3.11 |

## Fortuna Leucocratic Intrusion

| Analyte Symbol | SiO2 | Al2O3 | Fe2O3(T) | MnO | MgO | CaO | Na2O |
|---|---|---|---|---|---|---|---|
| Unit Symbol | % | % | % | % | % | % | % |
| 98-557 | 77.5 | 12.2 | 0.79 | 0.01 | 0.12 | 0.61 | 2.76 |
| 98-558 | 76.4 | 12.4 | 0.95 | 0.01 | 0.39 | 0.83 | 3.05 |
| 98-569 | 78.1 | 12 | 0.58 | 0.01 | 0.05 | 0.41 | 2.83 |

## Pajonal diorite

| Analyte Symbol | SiO2 | Al2O3 | Fe2O3(T) | MnO | MgO | CaO | Na2O |
|---|---|---|---|---|---|---|---|
| Unit Symbol | % | % | % | % | % | % | % |
| 00-194 | 61 | 15.7 | 6.47 | 0.12 | 2.84 | 5.19 | 3.57 |
| 00-196 | 63.4 | 15.7 | 5.23 | 0.09 | 2.02 | 3.91 | 3.63 |
| 00-197 | 65 | 15.6 | 4.6 | 0.06 | 1.61 | 3.26 | 3.63 |
| 00-199 | 60.9 | 15.9 | 5.89 | 0.1 | 2.44 | 4.52 | 3.62 |
| 00-200 | 58.2 | 15.9 | 6.4 | 0.07 | 3.9 | 5.35 | 4.66 |

## Central Diorite

| Analyte Symbol | SiO2 | Al2O3 | Fe2O3(T) | MnO | MgO | CaO | Na2O |
|---|---|---|---|---|---|---|---|
| Unit Symbol | % | % | % | % | % | % | % |
| 00-128 | 69.1 | 15.2 | 2.79 | 0.01 | 1.7 | 1.41 | 3.19 |
| 00-135 | 65.4 | 15.6 | 4.63 | 0.02 | 2.07 | 2.42 | 3.41 |
| 00-136 | 64.2 | 15.2 | 5.95 | 0.09 | 2.64 | 3.55 | 3.57 |
| 00-178 | 59.8 | 18.8 | 5.84 | 0.05 | 3.62 | 4.21 | 3.37 |
| 00-186 | 63.5 | 17.7 | 5.44 | 0.03 | 2.56 | 2.99 | 3.57 |

## Dark Diorite

| Analyte Symbol | SiO2 | Al2O3 | Fe2O3(T) | MnO | MgO | CaO | Na2O |
|---|---|---|---|---|---|---|---|
| Unit Symbol | % | % | % | % | % | % | % |
| 00-145 | 57.5 | 19.2 | 7.99 | 0.05 | 3.58 | 4.57 | 3.16 |
| 00-160 | 54.4 | 18.1 | 0.86 | 0.14 | 4.65 | 6.67 | 3.64 |
| 00-181 | 66.4 | 15.4 | 4.3 | 0.02 | 1.77 | 2.13 | 3.46 |
| 00-184 | 56.3 | 19.3 | 6.76 | 0.06 | 5.2 | 3.88 | 4 |

## Equis Monzodiorite

| Analyte Symbol | SiO2 | Al2O3 | Fe2O3(T) | MnO | MgO | CaO | Na2O |
|---|---|---|---|---|---|---|---|
| Unit Symbol | % | % | % | % | % | % | % |
| 00-141 | 66.1 | 15.3 | 4.12 | 0.04 | 2.3 | 2.17 | 3.51 |
| 00-146 | 65.3 | 17.5 | 4.97 | 0.01 | 1.84 | 2.01 | 3.35 |
| 00-151 | 70.9 | 14.7 | 1.69 | 0.01 | 0.84 | 1.54 | 3.61 |
| 00-155 | 69.4 | 14.8 | 3.22 | 0.04 | 1.15 | 2.13 | 3.49 |
| 00-173 | 69.1 | 15.7 | 3.11 | 0.01 | 1.74 | 1.1 | 3.05 |

## South Granodiorite

| Analyte Symbol | SiO2 | Al2O3 | Fe2O3(T) | MnO | MgO | CaO | Na2O |
|---|---|---|---|---|---|---|---|
| Unit Symbol | % | % | % | % | % | % | % |
| 00-126 | 57.4 | 22.7 | 2.99 | 0.61 | 4.94 | 3.18 | 0.63 |
| 00-130 | 64.9 | 16.5 | 4.04 | 0.04 | 1.88 | 3.64 | 4.36 |
| 00-156 | 65.7 | 16.8 | 3.52 | 0.04 | 1.94 | 3.29 | 4.28 |
| 00-159 | 66.7 | 16.8 | 2.57 | 0.02 | 1.56 | 3.3 | 4.5 |
| 00-162 | 65.7 | 16.8 | 2.94 | 0.04 | 1.34 | 3.21 | 4.38 |

## El Abra mine porphyry

| Analyte Symbol | SiO2 | Al2O3 | Fe2O3(T) | MnO | MgO | CaO | Na2O |
|---|---|---|---|---|---|---|---|
| Unit Symbol | % | % | % | % | % | % | % |
| 00-138 | 66.7 | 16.9 | 2.83 | 0.04 | 1.25 | 3.07 | 4.55 |
| 00-140 | 70.4 | 17 | 2.16 | 0.01 | 0.7 | 2.14 | 4.95 |
| 00-144 | 68 | 16.4 | 2.38 | 0.02 | 0.8 | 2.33 | 4.63 |
| 00-168 | 60.9 | 16.7 | 6.03 | 0.07 | 2.76 | 4.77 | 3.42 |
| 00-172 | 66.2 | 16.7 | 4.68 | 0.41 | 1.03 | 0.8 | 4.91 |

## El Abra Apolo leucogranite

| Analyte Symbol | SiO2 | Al2O3 | Fe2O3(T) | MnO | MgO | CaO | Na2O |
|---|---|---|---|---|---|---|---|
| Unit Symbol | % | % | % | % | % | % | % |
| 00-120 | 70.9 | 15.3 | 2.55 | 0.02 | 1.02 | 1.11 | 2.66 |
| 00-125 | 70.3 | 15.2 | 1.53 | 0.01 | 1.03 | 1.39 | 4.48 |
| 00-154 | 71.9 | 14.5 | 1.18 | 0.03 | 1.11 | 1.47 | 3.32 |
| 00-171 | 69.3 | 15.1 | 2.93 | 0.01 | 1.15 | 2.23 | 3.9 |
| 00-187 | 72.2 | 14.7 | 1.39 | 0.01 | 1.03 | 0.74 | 3.47 |

## El Abra Aplite

| Analyte Symbol | SiO2 | Al2O3 | Fe2O3(T) | MnO | MgO | CaO | Na2O |
|---|---|---|---|---|---|---|---|
| Unit Symbol | % | % | % | % | % | % | % |
| 00-124 | 70.6 | 14.8 | 2.58 | 0.01 | 0.9 | 1.28 | 3.31 |
| 00-150 | 71.8 | 14.2 | 1.99 | 0.01 | 0.83 | 0.96 | 2.98 |
| 00-158 | 69.7 | 14.7 | 3.29 | 0.02 | 1.25 | 1.94 | 3.58 |
| 00-169 | 74.5 | 13.6 | 1.05 | 0.01 | 0.62 | 0.4 | 2.93 |
| 00-183 | 72.2 | 13.7 | 1.34 | 0.01 | 0.9 | 0.52 | 3.22 |
| 00-188 | 72.9 | 14.2 | 1.93 | 0.01 | 0.69 | 0.65 | 3.31 |

Los Picos

| Analyte Symbol | K2O | TiO2 | P2O5 | LOI | Total | Au | Ag |
|---|---|---|---|---|---|---|---|
| Unit Symbol | % | % | % | % | % | ppb | ppm |
| 98-518 | 2.9 | 0.83 | 0.22 | | 98.68 | | |
| 98-519 | 3.16 | 0.79 | 0.18 | | 99.53 | | |
| 98-520 | 2.88 | 0.89 | 0.21 | | 98.75 | | |
| 98-522 | 2.8 | 0.85 | 0.18 | | 99.37 | | |
| 98-524 | 3.08 | 0.87 | 0.21 | | 99.81 | | |
| 98-525 | 4.87 | 0.6 | 0.11 | | 99.66 | | |
| 98-526 | 1.99 | 0.87 | 0.23 | | 98.56 | | |
| 98-527 | 3.18 | 0.85 | 0.22 | | 100.09 | | |
| 98-540 | 4.6 | 0.64 | 0.14 | | 99.75 | | |
| 98-549 | 2.97 | 0.8 | 0.2 | | 98.96 | | |
| 98-564 | 3.77 | 0.57 | 0.08 | | 99.12 | | |

**Fortuna Gris**

| Analyte Symbol | K2O | TiO2 | P2O5 | LOI | Total | Au | Ag |
|---|---|---|---|---|---|---|---|
| Unit Symbol | % | % | % | % | % | ppb | ppm |
| 98-532 | 2.95 | 0.58 | 0.19 | | 99.14 | | |
| 98-534 | 4.65 | 0.75 | 0.15 | | 99.78 | | |
| 98-544 | 2.88 | 0.75 | 0.19 | | 99.82 | | |
| 98-548 | 5.12 | 0.27 | 0.05 | | 99.51 | | |
| 98-550 | 4.46 | 0.49 | 0.13 | | 99.42 | | |
| 98-551 | 3.12 | 0.63 | 0.2 | | 99.73 | | |
| 98-552 | 2.88 | 0.67 | 0.24 | | 99.97 | | |
| 98-553 | 3.3 | 0.63 | 0.19 | | 99.08 | | |
| 98-559 | 3.16 | 0.59 | 0.18 | | 99.28 | | |
| 98-561 | 3.43 | 0.49 | 0.21 | | 99.84 | | |
| 98-566 | 3.38 | 0.58 | 0.19 | | 101.19 | | |
| 98-576 | 2.95 | 0.64 | 0.19 | | 99.79 | | |

**Fortuna Clara**

| Analyte Symbol | K2O | TiO2 | P2O5 | LOI | Total | Au | Ag |
|---|---|---|---|---|---|---|---|
| Unit Symbol | % | % | % | % | % | ppb | ppm |
| 98-535 | 2.73 | 0.51 | 0.2 | | 99.14 | | |
| 98-536 | 2.84 | 0.53 | 0.19 | | 99.55 | | |
| 98-538 | 3.23 | 0.45 | 0.18 | | 99.45 | | |
| 98-541 | 2.45 | 0.43 | 0.18 | | 98.23 | | |
| 98-547 | 2.88 | 0.42 | 0.24 | | 99.82 | | |
| 98-554 | 2.74 | 0.55 | 0.17 | | 99.7 | | |
| 98-556 | 2.82 | 0.51 | 0.18 | | 99.26 | | |
| 98-567 | 2.57 | 0.47 | 0.06 | | 99.93 | | |
| 98-570 | 3.51 | 0.52 | 0.14 | | 99.73 | | |
| 98-572 | 2.98 | 0.52 | 0.18 | | 99.73 | | |
| 98-575 | 3.02 | 0.42 | 0.16 | | 99.59 | | |
| 98-577 | 3.3 | 0.42 | 0.14 | | 99.79 | | |

## San Lorenzo

| Analyte Symbol | K2O | TiO2 | P2O5 | LOI | Total | Au | Ag |
|---|---|---|---|---|---|---|---|
| Unit Symbol | % | % | % | % | % | ppb | ppm |
| 98-531 | 3.13 | 0.45 | 0.16 | | 99.06 | | |
| 98-542 | 2.67 | 0.42 | 0.19 | | 97.78 | | |
| 98-545 | 3.95 | 0.26 | 0.09 | | 99.34 | | |
| 98-546 | 3.32 | 0.37 | 0.15 | | 99.69 | | |
| 98-560 | 3.17 | 0.9 | 0.07 | | 96.41 | | |
| 98-562 | 3.71 | 0.35 | 0 | | 99.03 | | |
| 98-563 | 3.46 | 0.32 | 0.09 | | 99.42 | | |
| 98-568 | 3.35 | 0.6 | 0.13 | | 98.33 | | |
| 98-571 | 4.91 | 0.15 | 0.14 | | 100.1 | | |
| 98-573 | 4.84 | 0.41 | 0.14 | | 99 | | |

## Fortuna Leucocratic Intrusion

| Analyte Symbol | K2O | TiO2 | P2O5 | LOI | Total | Au | Ag |
|---|---|---|---|---|---|---|---|
| Unit Symbol | % | % | % | % | % | ppb | ppm |
| 98-557 | 6.01 | 0.12 | 0 | | 100.11 | | |
| 98-558 | 5.27 | 0.24 | 0.04 | | 99.67 | | |
| 98-569 | 5.87 | 0.14 | 0.01 | | 99.93 | | |

## Pajonal diorite

| Analyte Symbol | K2O | TiO2 | P2O5 | LOI | Total | Au | Ag |
|---|---|---|---|---|---|---|---|
| Unit Symbol | % | % | % | % | % | ppb | ppm |
| 00-194 | 3.42 | 0.86 | 0.24 | | 99.42 | | |
| 00-196 | 4.27 | 0.85 | 0.18 | | 99.26 | | |
| 00-197 | 4.54 | 0.79 | 0.17 | | 99.24 | | |
| 00-199 | 4.04 | 0.93 | 0.21 | | 98.63 | | |
| 00-200 | 3.68 | 0.84 | 0.25 | | 99.24 | | |

## Central Diorite

| Analyte Symbol | K2O | TiO2 | P2O5 | LOI | Total | Au | Ag |
|---|---|---|---|---|---|---|---|
| Unit Symbol | % | % | % | % | % | ppb | ppm |
| 00-128 | 4.57 | 0.84 | 0.16 | | 98.99 | | |
| 00-135 | 4.2 | 0.85 | 0.24 | | 98.88 | | |
| 00-136 | 2.73 | 0.74 | 0.21 | | 98.86 | | |
| 00-178 | 2.14 | 0.92 | 0.26 | | 99 | | |
| 00-186 | 2.23 | 0.79 | 0.19 | | 99 | | |

## Dark Diorite

| Analyte Symbol | K2O | TiO2 | P2O5 | LOI | Total | Au | Ag |
|---|---|---|---|---|---|---|---|
| Unit Symbol | % | % | % | % | % | ppb | ppm |
| 00-145 | 1.9 | 0.88 | 0.23 | | 98.99 | | |
| 00-160 | 1.41 | 0.86 | 0.23 | | 99 | | |
| 00-181 | 4.03 | 0.79 | 0.16 | | 98.45 | | |
| 00-184 | 2.38 | 0.94 | 0.26 | | 99 | | |

## Equis Monzodiorite

| Analyte Symbol | K2O | TiO2 | P2O5 | LOI | Total | Au | Ag |
|---|---|---|---|---|---|---|---|
| Unit Symbol | % | % | % | % | % | ppb | ppm |
| 00-141 | 4.22 | 0.85 | 0.18 | | 98.85 | | |
| 00-146 | 3.06 | 0.65 | 0.29 | | 98.97 | | |
| 00-151 | 4.61 | 0.35 | 0.04 | | 98.23 | | |
| 00-155 | 4.13 | 0.38 | 0.12 | | 98.77 | | |
| 00-173 | 4.26 | 0.79 | 0.14 | | 99 | | |

## South Granodiorite

| Analyte Symbol | K2O | TiO2 | P2O5 | LOI | Total | Au | Ag |
|---|---|---|---|---|---|---|---|
| Unit Symbol | % | % | % | % | % | ppb | ppm |
| 00-126 | 4.66 | 0.58 | 0.19 | | 97.88 | | |
| 00-130 | 2.74 | 0.58 | 0.21 | | 98.88 | | |
| 00-156 | 2.6 | 0.52 | 0.19 | | 98.83 | | |
| 00-159 | 2.45 | 0.51 | 0.19 | | 98.6 | | |
| 00-162 | 2.98 | 0.45 | 0.19 | | 98.04 | | |

## El Abra mine porphyry

| Analyte Symbol | K2O | TiO2 | P2O5 | LOI | Total | Au | Ag |
|---|---|---|---|---|---|---|---|
| Unit Symbol | % | % | % | % | % | ppb | ppm |
| 00-138 | 2.66 | 0.4 | 0.17 | | 98.64 | | |
| 00-140 | 3.11 | 0.32 | 0.08 | | 100.83 | | |
| 00-144 | 3.11 | 0.34 | 0.11 | | 98.07 | | |
| 00-168 | 2.91 | 0.81 | 0.24 | | 98.67 | | |
| 00-172 | 2.53 | 0.37 | 0.14 | | 97.8 | | |

## El Abra Apolo leucogranite

| Analyte Symbol | K2O | TiO2 | P2O5 | LOI | Total | Au | Ag |
|---|---|---|---|---|---|---|---|
| Unit Symbol | % | % | % | % | % | ppb | ppm |
| 00-120 | 4.88 | 0.45 | 0.07 | | 99 | | |
| 00-125 | 3.51 | 0.37 | 0.13 | | 97.9 | | |
| 00-154 | 4.86 | 0.32 | 0.08 | | 98.8 | | |
| 00-171 | 3.68 | 0.39 | 0.11 | | 98.74 | | |
| 00-187 | 4.98 | 0.35 | 0.06 | | 99 | | |

## El Abra Aplite

| Analyte Symbol | K2O | TiO2 | P2O5 | LOI | Total | Au | Ag |
|---|---|---|---|---|---|---|---|
| Unit Symbol | % | % | % | % | % | ppb | ppm |
| 00-124 | 4.42 | 0.4 | 0.04 | | 98.31 | | |
| 00-150 | 5.63 | 0.47 | 0.03 | | 98.92 | | |
| 00-158 | 4.16 | 0.41 | 0.07 | | 99.11 | | |
| 00-169 | 5.6 | 0.32 | 0.04 | | 99 | | |
| 00-183 | 5.77 | 0.52 | 0.07 | | 98.24 | | |
| 00-188 | 4.86 | 0.35 | 0.09 | | 99 | | |

Los Picos

| Analyte Symbol | As | Ba | Be | Bi | Br | Cd | Co |
|---|---|---|---|---|---|---|---|
| Unit Symbol | ppm | ppm | ppm | ppm | ppm | ppm | ppm |
| 98-518 | | 686 | | | | | |
| 98-519 | | 629 | | | | | |
| 98-520 | | 750 | | | | | |
| 98-522 | | 621 | | | | | |
| 98-524 | | 646 | | | | | |
| 98-525 | | 562 | | | | | |
| 98-526 | | 541 | | | | | |
| 98-527 | | 650 | | | | | |
| 98-540 | | 701 | | | | | |
| 98-549 | | 624 | | | | | |
| 98-564 | | | | | | | |

**Fortuna Gris**

| Analyte Symbol | As | Ba | Be | Bi | Br | Cd | Co |
|---|---|---|---|---|---|---|---|
| Unit Symbol | ppm | ppm | ppm | ppm | ppm | ppm | ppm |
| 98-532 | | 690 | | | | | |
| 98-534 | | 714 | | | | | |
| 98-544 | | 627 | | | | | |
| 98-548 | | 852 | | | | | |
| 98-550 | | 644 | | | | | |
| 98-551 | | 631 | | | | | |
| 98-552 | | 687 | | | | | |
| 98-553 | | 697 | | | | | |
| 98-559 | | 857 | | | | | |
| 98-561 | | 702 | | | | | |
| 98-566 | | 698 | | | | | |
| 98-576 | | 621 | | | | | |

**Fortuna Clara**

| Analyte Symbol | As | Ba | Be | Bi | Br | Cd | Co |
|---|---|---|---|---|---|---|---|
| Unit Symbol | ppm | ppm | ppm | ppm | ppm | ppm | ppm |
| 98-535 | | 738 | | | | | |
| 98-536 | | 870 | | | | | |
| 98-538 | | | | | | | |
| 98-541 | | 812 | | | | | |
| 98-547 | | 832 | | | | | |
| 98-554 | | 635 | | | | | |
| 98-556 | | | | | | | |
| 98-567 | | 663 | | | | | |
| 98-570 | | 686 | | | | | |
| 98-572 | | 719 | | | | | |
| 98-575 | | 568 | | | | | |
| 98-577 | | 795 | | | | | |

## San Lorenzo

| Analyte Symbol | As | Ba | Be | Bi | Br | Cd | Co |
|---|---|---|---|---|---|---|---|
| Unit Symbol | ppm | ppm | ppm | ppm | ppm | ppm | ppm |
| 98-531 | | 705 | | | | | |
| 98-542 | | 717 | | | | | |
| 98-545 | | 472 | | | | | |
| 98-546 | | 688 | | | | | |
| 98-560 | | 439 | | | | | |
| 98-562 | | 787 | | | | | |
| 98-563 | | 630 | | | | | |
| 98-568 | | 928 | | | | | |
| 98-571 | | | | | | | |
| 98-573 | | 870 | | | | | |

## Fortuna Leucocratic Intrusion

| Analyte Symbol | As | Ba | Be | Bi | Br | Cd | Co |
|---|---|---|---|---|---|---|---|
| Unit Symbol | ppm | ppm | ppm | ppm | ppm | ppm | ppm |
| 98-557 | | 98 | | | | | |
| 98-558 | | 296 | | | | | |
| 98-569 | | | | | | | |

## Pajonal diorite

| Analyte Symbol | As | Ba | Be | Bi | Br | Cd | Co |
|---|---|---|---|---|---|---|---|
| Unit Symbol | ppm | ppm | ppm | ppm | ppm | ppm | ppm |
| 00-194 | | 557 | | | | | |
| 00-196 | | 617 | | | | | |
| 00-197 | | 585 | | | | | |
| 00-199 | | 659 | | | | | |
| 00-200 | | 610 | | | | | |

## Central Diorite

| Analyte Symbol | As | Ba | Be | Bi | Br | Cd | Co |
|---|---|---|---|---|---|---|---|
| Unit Symbol | ppm | ppm | ppm | ppm | ppm | ppm | ppm |
| 00-128 | | 618 | | | | | |
| 00-135 | | 599 | | | | | |
| 00-136 | | 650 | | | | | |
| 00-178 | | 487 | | | | | |
| 00-186 | | 462 | | | | | |

## Dark Diorite

| Analyte Symbol | As | Ba | Be | Bi | Br | Cd | Co |
|---|---|---|---|---|---|---|---|
| Unit Symbol | ppm | ppm | ppm | ppm | ppm | ppm | ppm |
| 00-145 | | 503 | | | | | |
| 00-160 | | 411 | | | | | |
| 00-181 | | | | | | | |
| 00-184 | | 335 | | | | | |

## Equis Monzodiorite

| Analyte Symbol | As | Ba | Be | Bi | Br | Cd | Co |
|---|---|---|---|---|---|---|---|
| Unit Symbol | ppm | ppm | ppm | ppm | ppm | ppm | ppm |
| 00-141 | | 574 | | | | | |
| 00-146 | | 811 | | | | | |
| 00-151 | | 466 | | | | | |
| 00-155 | | 625 | | | | | |
| 00-173 | | 753 | | | | | |

## South Granodiorite

| Analyte Symbol | As | Ba | Be | Bi | Br | Cd | Co |
|---|---|---|---|---|---|---|---|
| Unit Symbol | ppm | ppm | ppm | ppm | ppm | ppm | ppm |
| 00-126 | | 405 | | | | | |
| 00-130 | | 749 | | | | | |
| 00-156 | | 693 | | | | | |
| 00-159 | | 654 | | | | | |
| 00-162 | | 788 | | | | | |

## El Abra mine porphyry

| Analyte Symbol | As | Ba | Be | Bi | Br | Cd | Co |
|---|---|---|---|---|---|---|---|
| Unit Symbol | ppm | ppm | ppm | ppm | ppm | ppm | ppm |
| 00-138 | | 758 | | | | | |
| 00-140 | | 952 | | | | | |
| 00-144 | | 855 | | | | | |
| 00-168 | | 689 | | | | | |
| 00-172 | | 770 | | | | | |

## El Abra Apolo leucogranite

| Analyte Symbol | As | Ba | Be | Bi | Br | Cd | Co |
|---|---|---|---|---|---|---|---|
| Unit Symbol | ppm | ppm | ppm | ppm | ppm | ppm | ppm |
| 00-120 | | 482 | | | | | |
| 00-125 | | 402 | | | | | |
| 00-154 | | 455 | | | | | |
| 00-171 | | 506 | | | | | |
| 00-187 | | 517 | | | | | |

## El Abra Aplite

| Analyte Symbol | As | Ba | Be | Bi | Br | Cd | Co |
|---|---|---|---|---|---|---|---|
| Unit Symbol | ppm | ppm | ppm | ppm | ppm | ppm | ppm |
| 00-124 | | 838 | | | | | |
| 00-150 | | 532 | | | | | |
| 00-158 | | 670 | | | | | |
| 00-169 | | 578 | | | | | |
| 00-183 | | 525 | | | | | |
| 00-188 | | 701 | | | | | |

Los Picos

| Analyte Symbol | Cr | Cs | Cu | Ga | Ge | Hf | Hg |
|---|---|---|---|---|---|---|---|
| Unit Symbol | ppm | ppm | ppm | ppm | ppm | ppm | ppm |
| 98-518 | | 4.1 | | | | 4.67 | |
| 98-519 | | 3.47 | | | | 5.18 | |
| 98-520 | | 7.87 | | | | 8.45 | |
| 98-522 | | 4.86 | | | | 4.54 | |
| 98-524 | | 4.81 | | | | 5.79 | |
| 98-525 | | 8.17 | | | | 7.95 | |
| 98-526 | | 1.97 | | | | 3.2 | |
| 98-527 | | 6.58 | | | | 8.96 | |
| 98-540 | | 6.64 | | | | 8.62 | |
| 98-549 | | 4.59 | | | | 5.9 | |
| 98-564 | | | | | | | |

**Fortuna Gris**

| Analyte Symbol | Cr | Cs | Cu | Ga | Ge | Hf | Hg |
|---|---|---|---|---|---|---|---|
| Unit Symbol | ppm | ppm | ppm | ppm | ppm | ppm | ppm |
| 98-532 | | 4.22 | | | | 4.11 | |
| 98-534 | | 7.62 | | | | 10.11 | |
| 98-544 | | 4.51 | | | | 4.67 | |
| 98-548 | | 4.83 | | | | 4.48 | |
| 98-550 | | 8.49 | | | | 5.68 | |
| 98-551 | | 4.45 | | | | 4.37 | |
| 98-552 | | 5.34 | | | | 2.23 | |
| 98-553 | | 6.72 | | | | 4.24 | |
| 98-559 | | 8.27 | | | | 4.18 | |
| 98-561 | | 5.48 | | | | 4.23 | |
| 98-566 | | 5.73 | | | | 4.52 | |
| 98-576 | | 3.98 | | | | 2.1 | |

**Fortuna Clara**

| Analyte Symbol | Cr | Cs | Cu | Ga | Ge | Hf | Hg |
|---|---|---|---|---|---|---|---|
| Unit Symbol | ppm | ppm | ppm | ppm | ppm | ppm | ppm |
| 98-535 | | 4.92 | | | | 2.9 | |
| 98-536 | | 2.71 | | | | 2.99 | |
| 98-538 | | | | | | | |
| 98-541 | | 1.57 | | | | 3.23 | |
| 98-547 | | 3.87 | | | | 4.19 | |
| 98-554 | | 3.47 | | | | 2.93 | |
| 98-556 | | | | | | | |
| 98-567 | | 3.19 | | | | 2.07 | |
| 98-570 | | 8.73 | | | | 4.1 | |
| 98-572 | | 4.81 | | | | 8.25 | |
| 98-575 | | 4.15 | | | | 1.91 | |
| 98-577 | | 8.22 | | | | 3.01 | |

## San Lorenzo

| Analyte Symbol | Cr | Cs | Cu | Ga | Ge | Hf | Hg |
|---|---|---|---|---|---|---|---|
| Unit Symbol | ppm | ppm | ppm | ppm | ppm | ppm | ppm |
| 98-531 | | 4.15 | | | | 3.11 | |
| 98-542 | | 1.26 | | | | 2.8 | |
| 98-545 | | 1.71 | | | | 2.76 | |
| 98-546 | | 1.47 | | | | 3 | |
| 98-560 | | 5.75 | | | | 3.86 | |
| 98-562 | | 8.59 | | | | 5.14 | |
| 98-563 | | 6.72 | | | | 3.19 | |
| 98-568 | | 6.3 | | | | 4.57 | |
| 98-571 | | | | | | | |
| 98-573 | | 3.74 | | | | 2.73 | |

## Fortuna Leucocratic Intrusion

| Analyte Symbol | Cr | Cs | Cu | Ga | Ge | Hf | Hg |
|---|---|---|---|---|---|---|---|
| Unit Symbol | ppm | ppm | ppm | ppm | ppm | ppm | ppm |
| 98-557 | | 4.12 | | | | 2.89 | |
| 98-558 | | 3.75 | | | | 3.43 | |
| 98-569 | | | | | | | |

## Pajonal diorite

| Analyte Symbol | Cr | Cs | Cu | Ga | Ge | Hf | Hg |
|---|---|---|---|---|---|---|---|
| Unit Symbol | ppm | ppm | ppm | ppm | ppm | ppm | ppm |
| 00-194 | | 11.82 | | | | 7.83 | |
| 00-196 | | 6.4 | | | | 8.32 | |
| 00-197 | | 8.54 | | | | 8.43 | |
| 00-199 | | 6.67 | | | | 6.27 | |
| 00-200 | | 4.24 | | | | 4.99 | |

## Central Diorite

| Analyte Symbol | Cr | Cs | Cu | Ga | Ge | Hf | Hg |
|---|---|---|---|---|---|---|---|
| Unit Symbol | ppm | ppm | ppm | ppm | ppm | ppm | ppm |
| 00-128 | | 4.47 | | | | 4.27 | |
| 00-135 | | 5.31 | | | | 7.3 | |
| 00-136 | | 2.49 | | | | 4.69 | |
| 00-178 | | 3.3 | | | | 3.51 | |
| 00-186 | | 4.86 | | | | 5.09 | |

## Dark Diorite

| Analyte Symbol | Cr | Cs | Cu | Ga | Ge | Hf | Hg |
|---|---|---|---|---|---|---|---|
| Unit Symbol | ppm | ppm | ppm | ppm | ppm | ppm | ppm |
| 00-145 | | 6.28 | | | | 2.81 | |
| 00-160 | | 4 | | | | 1.96 | |
| 00-181 | | | | | | | |
| 00-184 | | 14.75 | | | | 2.19 | |

## Equis Monzodiorite

| Analyte Symbol | Cr | Cs | Cu | Ga | Ge | Hf | Hg |
|---|---|---|---|---|---|---|---|
| Unit Symbol | ppm | ppm | ppm | ppm | ppm | ppm | ppm |
| 00-141 | | 6.27 | | | | 8.19 | |
| 00-146 | | 21.35 | | | | 4.65 | |
| 00-151 | | 2.29 | | | | 3.6 | |
| 00-155 | | 8.82 | | | | 5.04 | |
| 00-173 | | 4.02 | | | | 6.29 | |

## South Granodiorite

| Analyte Symbol | Cr | Cs | Cu | Ga | Ge | Hf | Hg |
|---|---|---|---|---|---|---|---|
| Unit Symbol | ppm | ppm | ppm | ppm | ppm | ppm | ppm |
| 00-126 | | 8.8 | | | | 3.37 | |
| 00-130 | | 3.33 | | | | 2.04 | |
| 00-156 | | 2.43 | | | | 2.74 | |
| 00-159 | | 2.65 | | | | 3.12 | |
| 00-162 | | 5.22 | | | | 2.14 | |

## El Abra mine porphyry

| Analyte Symbol | Cr | Cs | Cu | Ga | Ge | Hf | Hg |
|---|---|---|---|---|---|---|---|
| Unit Symbol | ppm | ppm | ppm | ppm | ppm | ppm | ppm |
| 00-138 | | 1.37 | | | | 2.62 | |
| 00-140 | | 1.25 | | | | 1.98 | |
| 00-144 | | 0.97 | | | | 3.11 | |
| 00-168 | | 3.01 | | | | 4.18 | |
| 00-172 | | 1.92 | | | | 2.77 | |

## El Abra Apolo leucogranite

| Analyte Symbol | Cr | Cs | Cu | Ga | Ge | Hf | Hg |
|---|---|---|---|---|---|---|---|
| Unit Symbol | ppm | ppm | ppm | ppm | ppm | ppm | ppm |
| 00-120 | | 4.17 | | | | 3.09 | |
| 00-125 | | 2.59 | | | | 4.75 | |
| 00-154 | | 7.12 | | | | 4.59 | |
| 00-171 | | 9.31 | | | | 12.92 | |
| 00-187 | | 2.13 | | | | 3.37 | |

## El Abra Aplite

| Analyte Symbol | Cr | Cs | Cu | Ga | Ge | Hf | Hg |
|---|---|---|---|---|---|---|---|
| Unit Symbol | ppm | ppm | ppm | ppm | ppm | ppm | ppm |
| 00-124 | | 5.03 | | | | 7.48 | |
| 00-150 | | 3.24 | | | | 6.8 | |
| 00-158 | | 9.24 | | | | 2.53 | |
| 00-169 | | 1.92 | | | | 5.2 | |
| 00-183 | | 1.64 | | | | 7.03 | |
| 00-188 | | 2 | | | | 7.93 | |

Los Picos

| Analyte Symbol | In | Ir | Mo | Nb | Ni | Pb | Rb |
|---|---|---|---|---|---|---|---|
| Unit Symbol | ppm | ppb | ppm | ppm | ppm | ppm | ppm |
| 98-518 | | | | 9.81 | | | 105 |
| 98-519 | | | | 9.35 | | | 121 |
| 98-520 | | | | 11.2 | | | 163 |
| 98-522 | | | | 9.2 | | | 100 |
| 98-524 | | | | 9.76 | | | 113 |
| 98-525 | | | | 13.3 | | | 238 |
| 98-526 | | | | 5.92 | | | 60 |
| 98-527 | | | | 9.74 | | | 117 |
| 98-540 | | | | 12.81 | | | 219 |
| 98-549 | | | | 6.59 | | | 61 |
| 98-564 | | | | | | | |

**Fortuna Gris**

| Analyte Symbol | In | Ir | Mo | Nb | Ni | Pb | Rb |
|---|---|---|---|---|---|---|---|
| Unit Symbol | ppm | ppb | ppm | ppm | ppm | ppm | ppm |
| 98-532 | | | | 8 | | | 94 |
| 98-534 | | | | 11.18 | | | 178 |
| 98-544 | | | | 7.86 | | | 95 |
| 98-548 | | | | 8.81 | | | 160 |
| 98-550 | | | | 11.12 | | | 202 |
| 98-551 | | | | 10.09 | | | 127 |
| 98-552 | | | | 8.47 | | | 88 |
| 98-553 | | | | 8.68 | | | 128 |
| 98-559 | | | | 7.63 | | | 127 |
| 98-561 | | | | 7.27 | | | 83 |
| 98-566 | | | | 9.07 | | | 152 |
| 98-576 | | | | 7.71 | | | 96 |

**Fortuna Clara**

| Analyte Symbol | In | Ir | Mo | Nb | Ni | Pb | Rb |
|---|---|---|---|---|---|---|---|
| Unit Symbol | ppm | ppb | ppm | ppm | ppm | ppm | ppm |
| 98-535 | | | | 6.19 | | | 89 |
| 98-536 | | | | 5.67 | | | 61 |
| 98-538 | | | | | | | |
| 98-541 | | | | 5.89 | | | 51 |
| 98-547 | | | | 7.33 | | | 75 |
| 98-554 | | | | 8.68 | | | 81 |
| 98-556 | | | | | | | |
| 98-567 | | | | 4.61 | | | 52 |
| 98-570 | | | | 11.6 | | | 216 |
| 98-572 | | | | 8.24 | | | 108 |
| 98-575 | | | | 6.34 | | | 108 |
| 98-577 | | | | 8.2 | | | 135 |

## San Lorenzo

| Analyte Symbol | In | Ir | Mo | Nb | Ni | Pb | Rb |
|---|---|---|---|---|---|---|---|
| Unit Symbol | ppm | ppb | ppm | ppm | ppm | ppm | ppm |
| 98-531 | | | | 7.7 | | | 87 |
| 98-542 | | | | 6.63 | | | 55 |
| 98-545 | | | | 6.48 | | | 125 |
| 98-546 | | | | 6.78 | | | 73 |
| 98-560 | | | | 6.86 | | | 77 |
| 98-562 | | | | 8.59 | | | 162 |
| 98-563 | | | | 6.73 | | | 112 |
| 98-568 | | | | 8.65 | | | 110 |
| 98-571 | | | | | | | |
| 98-573 | | | | 6.19 | | | 121 |

## Fortuna Leucocratic Intrusion

| Analyte Symbol | In | Ir | Mo | Nb | Ni | Pb | Rb |
|---|---|---|---|---|---|---|---|
| Unit Symbol | ppm | ppb | ppm | ppm | ppm | ppm | ppm |
| 98-557 | | | | 9.95 | | | 162 |
| 98-558 | | | | 11.31 | | | 144 |
| 98-569 | | | | | | | |

## Pajonal diorite

| Analyte Symbol | In | Ir | Mo | Nb | Ni | Pb | Rb |
|---|---|---|---|---|---|---|---|
| Unit Symbol | ppm | ppb | ppm | ppm | ppm | ppm | ppm |
| 00-194 | | | | 13.05 | | | 179 |
| 00-196 | | | | 13.01 | | | 148 |
| 00-197 | | | | 13.26 | | | 180 |
| 00-199 | | | | 12.81 | | | 153 |
| 00-200 | | | | 8.29 | | | 130 |

## Central Diorite

| Analyte Symbol | In | Ir | Mo | Nb | Ni | Pb | Rb |
|---|---|---|---|---|---|---|---|
| Unit Symbol | ppm | ppb | ppm | ppm | ppm | ppm | ppm |
| 00-128 | | | | 11.66 | | | 105 |
| 00-135 | | | | 10.73 | | | 132 |
| 00-136 | | | | 8.19 | | | 70 |
| 00-178 | | | | 8.85 | | | 78 |
| 00-186 | | | | 9.61 | | | 108 |

## Dark Diorite

| Analyte Symbol | In | Ir | Mo | Nb | Ni | Pb | Rb |
|---|---|---|---|---|---|---|---|
| Unit Symbol | ppm | ppb | ppm | ppm | ppm | ppm | ppm |
| 00-145 | | | | 5.08 | | | 72 |
| 00-160 | | | | 4.33 | | | 69 |
| 00-181 | | | | | | | |
| 00-184 | | | | 5.32 | | | 188 |

## Equis Monzodiorite

| Analyte Symbol | In | Ir | Mo | Nb | Ni | Pb | Rb |
|---|---|---|---|---|---|---|---|
| Unit Symbol | ppm | ppb | ppm | ppm | ppm | ppm | ppm |
| 00-141 | | | | 13.11 | | | 140 |
| 00-146 | | | | 10.4 | | | 240 |
| 00-151 | | | | 10.96 | | | 95 |
| 00-155 | | | | 9.67 | | | 163 |
| 00-173 | | | | 11.45 | | | 130 |

## South Granodiorite

| Analyte Symbol | In | Ir | Mo | Nb | Ni | Pb | Rb |
|---|---|---|---|---|---|---|---|
| Unit Symbol | ppm | ppb | ppm | ppm | ppm | ppm | ppm |
| 00-126 | | | | 5.97 | | | 286 |
| 00-130 | | | | 8.59 | | | 79 |
| 00-156 | | | | 5.73 | | | 69 |
| 00-159 | | | | 7.06 | | | 67 |
| 00-162 | | | | 8.59 | | | 87 |

## El Abra mine porphyry

| Analyte Symbol | In | Ir | Mo | Nb | Ni | Pb | Rb |
|---|---|---|---|---|---|---|---|
| Unit Symbol | ppm | ppb | ppm | ppm | ppm | ppm | ppm |
| 00-138 | | | | 5.92 | | | 46 |
| 00-140 | | | | 5.97 | | | 50 |
| 00-144 | | | | 6.26 | | | 39 |
| 00-168 | | | | 8.57 | | | 96 |
| 00-172 | | | | 6.02 | | | 51 |

## El Abra Apolo leucogranite

| Analyte Symbol | In | Ir | Mo | Nb | Ni | Pb | Rb |
|---|---|---|---|---|---|---|---|
| Unit Symbol | ppm | ppb | ppm | ppm | ppm | ppm | ppm |
| 00-120 | | | | 3.42 | | | 104 |
| 00-125 | | | | 11.37 | | | 103 |
| 00-154 | | | | 11.08 | | | 156 |
| 00-171 | | | | 10.59 | | | 156 |
| 00-187 | | | | 8.55 | | | 101 |

## El Abra Aplite

| Analyte Symbol | In | Ir | Mo | Nb | Ni | Pb | Rb |
|---|---|---|---|---|---|---|---|
| Unit Symbol | ppm | ppb | ppm | ppm | ppm | ppm | ppm |
| 00-124 | | | | 12.6 | | | 152 |
| 00-150 | | | | 9.9 | | | 129 |
| 00-158 | | | | 12.45 | | | 236 |
| 00-169 | | | | 11.52 | | | 114 |
| 00-183 | | | | 12.4 | | | 92 |
| 00-188 | | | | 13.63 | | | 161 |

Los Picos

| Analyte Symbol | S | Sb | Sc | Se | Sn | Sr | Ta |
|---|---|---|---|---|---|---|---|
| Unit Symbol | % | ppm | ppm | ppm | ppm | ppm | ppm |
| 98-518 | | | | | | 519 | 0.71 |
| 98-519 | | | | | | 692 | 0.64 |
| 98-520 | | | | | | 493 | 0.97 |
| 98-522 | | | | | | 546 | 0.7 |
| 98-524 | | | | | | 461 | 0.72 |
| 98-525 | | | | | | 258 | 1.18 |
| 98-526 | | | | | | 865 | 0.41 |
| 98-527 | | | | | | 416 | 0.74 |
| 98-540 | | | | | | 565 | 1 |
| 98-549 | | | | | | 456 | 0.69 |
| 98-564 | | | | | | | |

**Fortuna Gris**

| Analyte Symbol | S | Sb | Sc | Se | Sn | Sr | Ta |
|---|---|---|---|---|---|---|---|
| Unit Symbol | % | ppm | ppm | ppm | ppm | ppm | ppm |
| 98-532 | | | | | | 562 | 0.61 |
| 98-534 | | | | | | 339 | 0.96 |
| 98-544 | | | | | | 755 | 0.61 |
| 98-548 | | | | | | 230 | 0.86 |
| 98-550 | | | | | | 352 | 0.94 |
| 98-551 | | | | | | 350 | 0.76 |
| 98-552 | | | | | | 595 | 0.71 |
| 98-553 | | | | | | 495 | 0.65 |
| 98-559 | | | | | | 570 | 0.59 |
| 98-561 | | | | | | 479 | 0.9 |
| 98-566 | | | | | | 567 | 0.62 |
| 98-576 | | | | | | 557 | 0.53 |

**Fortuna Clara**

| Analyte Symbol | S | Sb | Sc | Se | Sn | Sr | Ta |
|---|---|---|---|---|---|---|---|
| Unit Symbol | % | ppm | ppm | ppm | ppm | ppm | ppm |
| 98-535 | | | | | | 974 | 0.48 |
| 98-536 | | | | | | 718 | 0.44 |
| 98-538 | | | | | | | |
| 98-541 | | | | | | 798 | 0.44 |
| 98-547 | | | | | | 737 | 0.56 |
| 98-554 | | | | | | 603 | 0.63 |
| 98-556 | | | | | | | |
| 98-567 | | | | | | 495 | 0.35 |
| 98-570 | | | | | | 560 | 1.18 |
| 98-572 | | | | | | 626 | 0.65 |
| 98-575 | | | | | | 608 | 0.41 |
| 98-577 | | | | | | 604 | 0.82 |

## San Lorenzo

| Analyte Symbol | S | Sb | Sc | Se | Sn | Sr | Ta |
|---|---|---|---|---|---|---|---|
| Unit Symbol | % | ppm | ppm | ppm | ppm | ppm | ppm |
| 98-531 | | | | | | 606 | 0.76 |
| 98-542 | | | | | | 726 | 0.45 |
| 98-545 | | | | | | 459 | 0.58 |
| 98-546 | | | | | | 584 | 0.6 |
| 98-560 | | | | | | 254 | 0.46 |
| 98-562 | | | | | | 419 | 0.8 |
| 98-563 | | | | | | 377 | 0.68 |
| 98-568 | | | | | | 357 | 0.72 |
| 98-571 | | | | | | | |
| 98-573 | | | | | | 403 | 0.71 |

## Fortuna Leucocratic Intrusion

| Analyte Symbol | S | Sb | Sc | Se | Sn | Sr | Ta |
|---|---|---|---|---|---|---|---|
| Unit Symbol | % | ppm | ppm | ppm | ppm | ppm | ppm |
| 98-557 | | | | | | 62 | 1.35 |
| 98-558 | | | | | | 115 | 1.36 |
| 98-569 | | | | | | | |

## Pajonal diorite

| Analyte Symbol | S | Sb | Sc | Se | Sn | Sr | Ta |
|---|---|---|---|---|---|---|---|
| Unit Symbol | % | ppm | ppm | ppm | ppm | ppm | ppm |
| 00-194 | | | | | | 411 | 1.06 |
| 00-196 | | | | | | 315 | 1.02 |
| 00-197 | | | | | | 282 | 1.11 |
| 00-199 | | | | | | 364 | 0.96 |
| 00-200 | | | | | | 388 | 0.69 |

## Central Diorite

| Analyte Symbol | S | Sb | Sc | Se | Sn | Sr | Ta |
|---|---|---|---|---|---|---|---|
| Unit Symbol | % | ppm | ppm | ppm | ppm | ppm | ppm |
| 00-128 | | | | | | 276 | 0.94 |
| 00-135 | | | | | | 266 | 0.84 |
| 00-136 | | | | | | 380 | 0.58 |
| 00-178 | | | | | | 461 | 0.53 |
| 00-186 | | | | | | 489 | 0.76 |

## Dark Diorite

| Analyte Symbol | S | Sb | Sc | Se | Sn | Sr | Ta |
|---|---|---|---|---|---|---|---|
| Unit Symbol | % | ppm | ppm | ppm | ppm | ppm | ppm |
| 00-145 | | | | | | 566 | 0.32 |
| 00-160 | | | | | | 650 | 0.27 |
| 00-181 | | | | | | | |
| 00-184 | | | | | | 505 | 0.29 |

## Equis Monzodiorite

| Analyte Symbol | S | Sb | Sc | Se | Sn | Sr | Ta |
|---|---|---|---|---|---|---|---|
| Unit Symbol | % | ppm | ppm | ppm | ppm | ppm | ppm |
| 00-141 | | | | | | 2.57 | 1.06 |
| 00-146 | | | | | | 406 | 0.85 |
| 00-151 | | | | | | 276 | 1.27 |
| 00-155 | | | | | | 317 | 1.01 |
| 00-173 | | | | | | 245 | 0.86 |

## South Granodiorite

| Analyte Symbol | S | Sb | Sc | Se | Sn | Sr | Ta |
|---|---|---|---|---|---|---|---|
| Unit Symbol | % | ppm | ppm | ppm | ppm | ppm | ppm |
| 00-126 | | | | | | 88 | 0.48 |
| 00-130 | | | | | | 605 | 0.68 |
| 00-156 | | | | | | 553 | 0.47 |
| 00-159 | | | | | | 610 | 0.5 |
| 00-162 | | | | | | 698 | 0.69 |

## El Abra mine porphyry

| Analyte Symbol | S | Sb | Sc | Se | Sn | Sr | Ta |
|---|---|---|---|---|---|---|---|
| Unit Symbol | % | ppm | ppm | ppm | ppm | ppm | ppm |
| 00-138 | | | | | | 632 | 0.47 |
| 00-140 | | | | | | 680 | 0.56 |
| 00-144 | | | | | | 618 | 0.54 |
| 00-168 | | | | | | 534 | 0.69 |
| 00-172 | | | | | | 398 | 0.51 |

## El Abra Apolo leucogranite

| Analyte Symbol | S | Sb | Sc | Se | Sn | Sr | Ta |
|---|---|---|---|---|---|---|---|
| Unit Symbol | % | ppm | ppm | ppm | ppm | ppm | ppm |
| 00-120 | | | | | | 12 | 0.3 |
| 00-125 | | | | | | 293 | 1.41 |
| 00-154 | | | | | | 257 | 1.31 |
| 00-171 | | | | | | 347 | 1.32 |
| 00-187 | | | | | | 221 | 0.91 |

## El Abra Aplite

| Analyte Symbol | S | Sb | Sc | Se | Sn | Sr | Ta |
|---|---|---|---|---|---|---|---|
| Unit Symbol | % | ppm | ppm | ppm | ppm | ppm | ppm |
| 00-124 | | | | | | 308 | 1.26 |
| 00-150 | | | | | | 186 | 0.79 |
| 00-158 | | | | | | 366 | 1.25 |
| 00-169 | | | | | | 165 | 1.34 |
| 00-183 | | | | | | 148 | 1.18 |
| 00-188 | | | | | | 265 | 1.53 |

Los Picos

| Analyte Symbol | Th | U | V | W | Y | Zn | Zr |
|---|---|---|---|---|---|---|---|
| Unit Symbol | ppm | ppm | ppm | ppm | ppm | ppm | ppm |
| 98-518 | 14.31 | 3.15 | | | 19.97 | | 167 |
| 98-519 | 13.98 | 4.11 | | | 20.6 | | 208 |
| 98-520 | 30.11 | 8.11 | | | 25.5 | | 285 |
| 98-522 | 14.11 | 3.52 | | | 18.49 | | 157 |
| 98-524 | 16.73 | 4.76 | | | 20.04 | | 210 |
| 98-525 | 57.02 | 14.17 | | | 24.84 | | 279 |
| 98-526 | 5.58 | 1.67 | | | 14.53 | | 126 |
| 98-527 | 21.61 | 4.92 | | | 20.61 | | 360 |
| 98-540 | 28.35 | 5.61 | | | 25.22 | | 359 |
| 98-549 | 17.03 | 4.54 | | | 13.89 | | 162 |
| 98-564 | | | | | | | |

**Fortuna Gris**

| Analyte Symbol | Th | U | V | W | Y | Zn | Zr |
|---|---|---|---|---|---|---|---|
| Unit Symbol | ppm | ppm | ppm | ppm | ppm | ppm | ppm |
| 98-532 | 13.41 | 3.93 | | | 13.82 | | 146 |
| 98-534 | 20.36 | 6.36 | | | 22.53 | | 350 |
| 98-544 | 15.12 | 2.77 | | | 17.39 | | 168 |
| 98-548 | 24.51 | 4.15 | | | 17.18 | | 146 |
| 98-550 | 25.29 | 5.46 | | | 23.51 | | 250 |
| 98-551 | 14.58 | 4.56 | | | 21.93 | | 171 |
| 98-552 | 8.75 | 2.02 | | | 14.56 | | 74 |
| 98-553 | 11.88 | 2.86 | | | 14.88 | | 149 |
| 98-559 | 10.92 | 3.3 | | | 13.18 | | 178 |
| 98-561 | 21.31 | 4.96 | | | 11.72 | | 112 |
| 98-566 | 15.26 | 3.63 | | | 17.61 | | 305 |
| 98-576 | 10.39 | 2.7 | | | 13.09 | | 88 |

**Fortuna Clara**

| Analyte Symbol | Th | U | V | W | Y | Zn | Zr |
|---|---|---|---|---|---|---|---|
| Unit Symbol | ppm | ppm | ppm | ppm | ppm | ppm | ppm |
| 98-535 | 6.7 | 1.91 | | | 8.32 | | 105 |
| 98-536 | 6.28 | 2.58 | | | 8.35 | | 108 |
| 98-538 | | | | | | | |
| 98-541 | 5.64 | 1.64 | | | 7.26 | | 121 |
| 98-547 | 7.48 | 2.64 | | | 8.64 | | 157 |
| 98-554 | 11.12 | 3.19 | | | 13.45 | | 99 |
| 98-556 | | | | | | | |
| 98-567 | 3.25 | 0.91 | | | 6.82 | | 77 |
| 98-570 | 19.97 | 5.81 | | | 13.28 | | 64 |
| 98-572 | 16.05 | 5.87 | | | 11.74 | | 116 |
| 98-575 | 8.3 | 2.38 | | | 8.74 | | 80 |
| 98-577 | 9.6 | 3.28 | | | 10.65 | | 63 |

## San Lorenzo

| Analyte Symbol | Th | U | V | W | Y | Zn | Zr |
|---|---|---|---|---|---|---|---|
| Unit Symbol | ppm | ppm | ppm | ppm | ppm | ppm | ppm |
| 98-531 | 13.32 | 4.01 | | | 10.49 | | 112 |
| 98-542 | 5.52 | 1.79 | | | 7.54 | | 117 |
| 98-545 | 15.68 | 7.02 | | | 5.8 | | 77 |
| 98-546 | 12.95 | 4.3 | | | 7.8 | | 93 |
| 98-560 | 11.76 | 5.02 | | | 7.17 | | 140 |
| 98-562 | 18.45 | 4.39 | | | 12.79 | | 188 |
| 98-563 | 21.89 | 4.41 | | | 9.28 | | 85 |
| 98-568 | 19.14 | 3.11 | | | 6 | | 163 |
| 98-571 | | | | | | | |
| 98-573 | 19.85 | 4.15 | | | 6.42 | | 86 |

## Fortuna Leucocratic Intrusion

| Analyte Symbol | Th | U | V | W | Y | Zn | Zr |
|---|---|---|---|---|---|---|---|
| Unit Symbol | ppm | ppm | ppm | ppm | ppm | ppm | ppm |
| 98-557 | 50.82 | 12.11 | | | 13.39 | | 59 |
| 98-558 | 32.34 | 6.84 | | | 13.91 | | 86 |
| 98-569 | | | | | | | |

## Pajonal diorite

| Analyte Symbol | Th | U | V | W | Y | Zn | Zr |
|---|---|---|---|---|---|---|---|
| Unit Symbol | ppm | ppm | ppm | ppm | ppm | ppm | ppm |
| 00-194 | 38.26 | 11.51 | | | 29.56 | | 291 |
| 00-196 | 28.09 | 8.51 | | | 23.7 | | 330 |
| 00-197 | 32.97 | 7.69 | | | 21.5 | | 317 |
| 00-199 | 24.16 | 6.35 | | | 22.88 | | 242 |
| 00-200 | 26.42 | 7.12 | | | 18.94 | | 183 |

## Central Diorite

| Analyte Symbol | Th | U | V | W | Y | Zn | Zr |
|---|---|---|---|---|---|---|---|
| Unit Symbol | ppm | ppm | ppm | ppm | ppm | ppm | ppm |
| 00-128 | 25.25 | 5.58 | | | 18.8 | | 161 |
| 00-135 | 26.67 | 7.26 | | | 23.21 | | 282 |
| 00-136 | 11.36 | 3.03 | | | 17.73 | | 184 |
| 00-178 | 8.97 | 2.58 | | | 16.49 | | 140 |
| 00-186 | 18.59 | 5.61 | | | 15.25 | | 193 |

## Dark Diorite

| Analyte Symbol | Th | U | V | W | Y | Zn | Zr |
|---|---|---|---|---|---|---|---|
| Unit Symbol | ppm | ppm | ppm | ppm | ppm | ppm | ppm |
| 00-145 | 4.62 | 1.55 | | | 9.8 | | 111 |
| 00-160 | 3.3 | 1.11 | | | 15.7 | | 71 |
| 00-181 | | | | | | | |
| 00-184 | 5.26 | 2.6 | | | 15.73 | | 82 |

## Equis Monzodiorite

| Analyte Symbol | Th | U | V | W | Y | Zn | Zr |
|---|---|---|---|---|---|---|---|
| Unit Symbol | ppm | ppm | ppm | ppm | ppm | ppm | ppm |
| 00-141 | 31.24 | 8.76 | | | 23.3 | | 309 |
| 00-146 | 17.17 | 5.4 | | | 15.9 | | 162 |
| 00-151 | 37.56 | 11.25 | | | 15.8 | | 103 |
| 00-155 | 29.54 | 10.11 | | | 12.1 | | 166 |
| 00-173 | 32.82 | 7.21 | | | 29.7 | | 246 |

## South Granodiorite

| Analyte Symbol | Th | U | V | W | Y | Zn | Zr |
|---|---|---|---|---|---|---|---|
| Unit Symbol | ppm | ppm | ppm | ppm | ppm | ppm | ppm |
| 00-126 | 7.49 | 1.31 | | | 9.83 | | 125 |
| 00-130 | 7.68 | 2.82 | | | 12.93 | | 70 |
| 00-156 | 8.73 | 2.99 | | | 7.65 | | 99 |
| 00-159 | 7.61 | 2.59 | | | 9.27 | | 114 |
| 00-162 | 7.73 | 3.06 | | | 8.61 | | 72 |

## El Abra mine porphyry

| Analyte Symbol | Th | U | V | W | Y | Zn | Zr |
|---|---|---|---|---|---|---|---|
| Unit Symbol | ppm | ppm | ppm | ppm | ppm | ppm | ppm |
| 00-138 | 5.29 | 1.24 | | | 6.61 | | 95 |
| 00-140 | 6.59 | 2.34 | | | 7.9 | | 71 |
| 00-144 | 6.46 | 1.87 | | | 7.95 | | 113 |
| 00-168 | 12.5 | 4.07 | | | 15.35 | | 152 |
| 00-172 | 5.24 | 1.64 | | | 6.2 | | 106 |

## El Abra Apolo leucogranite

| Analyte Symbol | Th | U | V | W | Y | Zn | Zr |
|---|---|---|---|---|---|---|---|
| Unit Symbol | ppm | ppm | ppm | ppm | ppm | ppm | ppm |
| 00-120 | 3.57 | 1.07 | | | 7.42 | | 114 |
| 00-125 | 28.91 | 11.7 | | | 13.74 | | 139 |
| 00-154 | 33.52 | 10.32 | | | 14.22 | | 128 |
| 00-171 | 25.72 | 11.06 | | | 16.44 | | 472 |
| 00-187 | 39.06 | 8.9 | | | 11.21 | | 104 |

## El Abra Aplite

| Analyte Symbol | Th | U | V | W | Y | Zn | Zr |
|---|---|---|---|---|---|---|---|
| Unit Symbol | ppm | ppm | ppm | ppm | ppm | ppm | ppm |
| 00-124 | 31.55 | 20.89 | | | 3.07 | | 251 |
| 00-150 | 59.29 | 25.44 | | | 4.07 | | 228 |
| 00-158 | 39.5 | 11.57 | | | 3.23 | | 80 |
| 00-169 | 65.39 | 20.11 | | | 3.6 | | 155 |
| 00-183 | 65.11 | 7.39 | | | 5.01 | | 248 |
| 00-188 | 72.09 | 19.77 | | | 3.52 | | 249 |

Los Picos

| Analyte Symbol | La | Ce | Pr | Nd | Sm | Eu | Gd |
|---|---|---|---|---|---|---|---|
| Unit Symbol | ppm | ppm | ppm | ppm | ppm | ppm | ppm |
| 98-518 | 25.5 | 53.5 | 6.29 | 24.8 | 4.8 | 1.04 | 4.08 |
| 98-519 | 23.8 | 50.6 | 6.02 | 24.1 | 4.78 | 1.09 | 4.23 |
| 98-520 | 32.6 | 68.3 | 7.89 | 30.2 | 5.92 | 1.2 | 5.05 |
| 98-522 | 23.8 | 51.2 | 6.04 | 23.8 | 4.65 | 1.05 | 3.85 |
| 98-524 | 24.3 | 51.3 | 6.04 | 23.8 | 4.76 | 1.06 | 4.2 |
| 98-525 | 36.1 | 78 | 8.75 | 32.2 | 6.04 | 0.76 | 4.87 |
| 98-526 | 17.8 | 37.5 | 4.49 | 18.5 | 3.71 | 1.05 | 3.16 |
| 98-527 | 27.7 | 59.5 | 6.96 | 27.5 | 5.25 | 1.04 | 4.42 |
| 98-540 | 29.5 | 63.8 | 7.43 | 28.3 | 5.37 | 0.88 | 4.49 |
| 98-549 | 23.3 | 48.8 | 5.65 | 22.4 | 4.51 | 0.98 | 3.81 |
| 98-564 | | | | | | | |

**Fortuna Gris**

| Analyte Symbol | La | Ce | Pr | Nd | Sm | Eu | Gd |
|---|---|---|---|---|---|---|---|
| Unit Symbol | ppm | ppm | ppm | ppm | ppm | ppm | ppm |
| 98-532 | 23.1 | 47.2 | 5.43 | 21 | 3.82 | 0.92 | 3.15 |
| 98-534 | 30.6 | 64.7 | 7.5 | 28.3 | 5.65 | 0.93 | 4.44 |
| 98-544 | 22.5 | 47.4 | 5.53 | 22.1 | 4.39 | 0.95 | 3.64 |
| 98-548 | 24.3 | 49.3 | 5.54 | 20 | 3.58 | 0.47 | 3.08 |
| 98-550 | 30.1 | 63.5 | 7.34 | 28.1 | 5.36 | 0.96 | 4.26 |
| 98-551 | 24.5 | 50.9 | 5.81 | 22.7 | 4.21 | 0.95 | 3.29 |
| 98-552 | 23.4 | 48.8 | 5.76 | 22.9 | 4.38 | 0.96 | 3.38 |
| 98-553 | 24.5 | 49.5 | 5.66 | 21.7 | 3.93 | 0.91 | 3 |
| 98-559 | 29.1 | 55.9 | 6.14 | 22.8 | 3.87 | 0.88 | 3.09 |
| 98-561 | 31.7 | 60.8 | 6.67 | 24.6 | 4.23 | 0.85 | 3.32 |
| 98-566 | 25 | 51.1 | 5.87 | 23 | 4.19 | 0.91 | 3.42 |
| 98-576 | 22.1 | 44.4 | 5.09 | 19.6 | 3.49 | 0.86 | 2.88 |

**Fortuna Clara**

| Analyte Symbol | La | Ce | Pr | Nd | Sm | Eu | Gd |
|---|---|---|---|---|---|---|---|
| Unit Symbol | ppm | ppm | ppm | ppm | ppm | ppm | ppm |
| 98-535 | 21 | 41.5 | 4.71 | 18.1 | 3.1 | 0.83 | 2.13 |
| 98-536 | 20.1 | 39.4 | 4.41 | 16.8 | 2.98 | 0.79 | 2.15 |
| 98-538 | | | | | | | |
| 98-541 | 20.4 | 38.2 | 4.38 | 16.6 | 2.77 | 0.79 | 1.9 |
| 98-547 | 22.7 | 43.2 | 4.84 | 18 | 3.13 | 0.84 | 2.21 |
| 98-554 | 25.6 | 54.5 | 6.37 | 23.8 | 4.28 | 0.95 | 3.21 |
| 98-556 | | | | | | | |
| 98-567 | 16.6 | 31.6 | 3.6 | 13.3 | 2.48 | 0.62 | 1.67 |
| 98-570 | 22.8 | 45.5 | 5.36 | 20.1 | 3.68 | 0.8 | 2.88 |
| 98-572 | 23.9 | 50.2 | 5.77 | 22 | 3.75 | 1.01 | 2.89 |
| 98-575 | 16.1 | 33.5 | 3.98 | 15.5 | 2.79 | 0.74 | 2.03 |
| 98-577 | 17 | 34.3 | 4.08 | 16 | 3.27 | 0.73 | 2.55 |

## San Lorenzo

| Analyte Symbol | La | Ce | Pr | Nd | Sm | Eu | Gd |
|---|---|---|---|---|---|---|---|
| Unit Symbol | ppm | ppm | ppm | ppm | ppm | ppm | ppm |
| 98-531 | 21.6 | 43.8 | 4.94 | 18.3 | 3.19 | 0.81 | 2.35 |
| 98-542 | 18.9 | 36 | 4.09 | 15.6 | 2.67 | 0.69 | 1.84 |
| 98-545 | 17.7 | 29.5 | 3 | 10.4 | 1.78 | 0.45 | 1.3 |
| 98-546 | 24.6 | 44.2 | 4.7 | 17 | 2.73 | 0.73 | 1.94 |
| 98-560 | 30.9 | 60.4 | 6.79 | 25.4 | 4.06 | 0.83 | 2.24 |
| 98-562 | 22.8 | 45.8 | 5.11 | 18.3 | 3.52 | 0.54 | 2.64 |
| 98-563 | 19.8 | 38 | 4.16 | 14 | 2.74 | 0.56 | 2.14 |
| 98-568 | 28.5 | 48.8 | 4.77 | 16 | 2.32 | 0.47 | 1.46 |
| 98-571 | | | | | | | |
| 98-573 | 41.7 | 60.9 | 5.63 | 18.1 | 2.42 | 0.56 | 1.64 |

## Fortuna Leucocratic Intrusion

| Analyte Symbol | La | Ce | Pr | Nd | Sm | Eu | Gd |
|---|---|---|---|---|---|---|---|
| Unit Symbol | ppm | ppm | ppm | ppm | ppm | ppm | ppm |
| 98-557 | 33.5 | 67 | 7.19 | 24.4 | 3.95 | 0.25 | 2.74 |
| 98-558 | 29.3 | 57.5 | 6.06 | 20.2 | 3.29 | 0.34 | 2.45 |
| 98-569 | | | | | | | |

## Pajonal diorite

| Analyte Symbol | La | Ce | Pr | Nd | Sm | Eu | Gd |
|---|---|---|---|---|---|---|---|
| Unit Symbol | ppm | ppm | ppm | ppm | ppm | ppm | ppm |
| 00-194 | 39.1 | 86.1 | 9.95 | 38.4 | 7.42 | 1.07 | 6.13 |
| 00-196 | 31.6 | 69 | 7.83 | 30.4 | 5.68 | 0.94 | 4.84 |
| 00-197 | 28.8 | 61.7 | 7.25 | 27.8 | 5.43 | 0.86 | 4.35 |
| 00-199 | 29.7 | 64.6 | 7.6 | 29.3 | 5.74 | 1.03 | 4.78 |
| 00-200 | 28.8 | 60.4 | 6.94 | 26.7 | 4.97 | 1 | 4.02 |

## Central Diorite

| Analyte Symbol | La | Ce | Pr | Nd | Sm | Eu | Gd |
|---|---|---|---|---|---|---|---|
| Unit Symbol | ppm | ppm | ppm | ppm | ppm | ppm | ppm |
| 00-128 | 27.8 | 60.8 | 6.84 | 25.8 | 4.85 | 0.78 | 4.03 |
| 00-135 | 28.9 | 63.3 | 7.34 | 28.2 | 5.32 | 0.92 | 4.63 |
| 00-136 | 23.5 | 50.4 | 5.87 | 23.2 | 4.5 | 0.94 | 3.71 |
| 00-178 | 22.7 | 47.2 | 5.57 | 22.7 | 4.37 | 1.15 | 3.59 |
| 00-186 | 38.6 | 72.9 | 7.52 | 26.4 | 4.52 | 1 | 3.48 |

## Dark Diorite

| Analyte Symbol | La | Ce | Pr | Nd | Sm | Eu | Gd |
|---|---|---|---|---|---|---|---|
| Unit Symbol | ppm | ppm | ppm | ppm | ppm | ppm | ppm |
| 00-145 | 15.4 | 30.6 | 3.52 | 14.6 | 2.81 | 0.88 | 2.14 |
| 00-160 | 16.7 | 33.7 | 4.08 | 17.4 | 3.61 | 0.95 | 3.31 |
| 00-181 | | | | | | | |
| 00-184 | 26.5 | 50 | 5.59 | 21.6 | 4.31 | 1.04 | 3.51 |

## Equis Monzodiorite

| Analyte Symbol | La | Ce | Pr | Nd | Sm | Eu | Gd |
|---|---|---|---|---|---|---|---|
| Unit Symbol | ppm | ppm | ppm | ppm | ppm | ppm | ppm |
| 00-141 | 32.4 | 70.4 | 7.98 | 30.5 | 5.71 | 0.91 | 4.72 |
| 00-146 | 27.7 | 56.1 | 6.18 | 23.6 | 4.67 | 1.09 | 3.72 |
| 00-151 | 22.9 | 53.2 | 5.88 | 21.7 | 3.91 | 0.65 | 2.94 |
| 00-155 | 28.6 | 64 | 7.09 | 25.7 | 4.17 | 0.71 | 2.66 |
| 00-173 | 26.9 | 58.3 | 6.58 | 25.1 | 5.25 | 1.05 | 5.09 |

## South Granodiorite

| Analyte Symbol | La | Ce | Pr | Nd | Sm | Eu | Gd |
|---|---|---|---|---|---|---|---|
| Unit Symbol | ppm | ppm | ppm | ppm | ppm | ppm | ppm |
| 00-126 | 26.2 | 50.1 | 5.29 | 19.5 | 3.2 | 0.89 | 2.36 |
| 00-130 | 23.9 | 48.6 | 5.31 | 20 | 3.39 | 0.86 | 2.77 |
| 00-156 | 17.4 | 32.8 | 3.57 | 13.4 | 2.34 | 0.68 | 1.73 |
| 00-159 | 20.3 | 41.1 | 4.58 | 17.2 | 2.92 | 0.83 | 2.18 |
| 00-162 | 22.3 | 44 | 4.72 | 17.1 | 2.87 | 0.87 | 2.06 |

## El Abra mine porphyry

| Analyte Symbol | La | Ce | Pr | Nd | Sm | Eu | Gd |
|---|---|---|---|---|---|---|---|
| Unit Symbol | ppm | ppm | ppm | ppm | ppm | ppm | ppm |
| 00-138 | 21.1 | 40.9 | 4.36 | 16.1 | 2.56 | 0.72 | 1.71 |
| 00-140 | 20.7 | 40.5 | 4.3 | 15.3 | 2.7 | 0.87 | 2.11 |
| 00-144 | 21.6 | 41.2 | 4.4 | 15.8 | 2.43 | 0.72 | 1.74 |
| 00-168 | 23.4 | 49.5 | 5.69 | 22 | 4.1 | 0.97 | 3.45 |
| 00-172 | 16.8 | 33.2 | 3.55 | 13 | 2.02 | 0.54 | 1.45 |

## El Abra Apolo leucogranite

| Analyte Symbol | La | Ce | Pr | Nd | Sm | Eu | Gd |
|---|---|---|---|---|---|---|---|
| Unit Symbol | ppm | ppm | ppm | ppm | ppm | ppm | ppm |
| 00-120 | 12.3 | 24.3 | 2.57 | 9.7 | 1.78 | 0.4 | 1.45 |
| 00-125 | 20.5 | 46.1 | 5.12 | 19.1 | 3.44 | 0.63 | 2.63 |
| 00-154 | 28.2 | 57.7 | 6.12 | 21.3 | 3.71 | 0.59 | 2.66 |
| 00-171 | 23 | 52.4 | 6.02 | 21.8 | 3.81 | 0.72 | 2.88 |
| 00-187 | 20.2 | 42.5 | 4.59 | 17 | 3.07 | 0.61 | 2.6 |

## El Abra Aplite

| Analyte Symbol | La | Ce | Pr | Nd | Sm | Eu | Gd |
|---|---|---|---|---|---|---|---|
| Unit Symbol | ppm | ppm | ppm | ppm | ppm | ppm | ppm |
| 00-124 | 29.2 | 65.6 | 7.35 | 27 | 4.76 | 0.85 | 3.77 |
| 00-150 | 30.1 | 66.2 | 7.28 | 26.9 | 5.44 | 0.74 | 4.6 |
| 00-158 | 28.3 | 63.7 | 7.58 | 28.8 | 5.29 | 0.89 | 3.84 |
| 00-169 | 25.1 | 56.7 | 6.38 | 23.2 | 4.41 | 0.49 | 3.76 |
| 00-183 | 35.2 | 76.7 | 8.57 | 31.9 | 6.13 | 0.73 | 4.91 |
| 00-188 | 23.5 | 53.4 | 5.91 | 22.2 | 4.08 | 0.6 | 3.59 |

Los Picos

| Analyte Symbol | Tb | Dy | Ho | Er | Tl | Tm | Yb |
|---|---|---|---|---|---|---|---|
| Unit Symbol | ppm | ppm | ppm | ppm | ppm | ppm | ppm |
| 98-518 | 0.57 | 3.65 | 0.71 | 2.04 | | | 2.02 |
| 98-519 | 0.61 | 3.95 | 0.75 | 2.14 | | | 2.17 |
| 98-520 | 0.74 | 4.71 | 0.93 | 2.61 | | | 2.67 |
| 98-522 | 0.54 | 3.47 | 0.68 | 1.89 | | | 1.95 |
| 98-524 | 0.59 | 3.7 | 0.73 | 2 | | | 2.14 |
| 98-525 | 0.7 | 4.41 | 0.87 | 2.53 | | | 2.72 |
| 98-526 | 0.44 | 2.65 | 0.5 | 1.37 | | | 1.36 |
| 98-527 | 0.63 | 3.94 | 0.75 | 2.22 | | | 2.32 |
| 98-540 | 0.66 | 4.19 | 0.81 | 2.36 | | | 2.44 |
| 98-549 | 0.54 | 3.4 | 0.67 | 1.89 | | | 1.95 |
| 98-564 | | | | | | | |

**Fortuna Gris**

| Analyte Symbol | Tb | Dy | Ho | Er | Tl | Tm | Yb |
|---|---|---|---|---|---|---|---|
| Unit Symbol | ppm | ppm | ppm | ppm | ppm | ppm | ppm |
| 98-532 | 0.41 | 2.6 | 0.48 | 1.33 | | | 1.39 |
| 98-534 | 0.66 | 4.17 | 0.8 | 2.29 | | | 2.43 |
| 98-544 | 0.52 | 3.24 | 0.64 | 1.78 | | | 1.79 |
| 98-548 | 0.45 | 2.96 | 0.61 | 1.8 | | | 1.97 |
| 98-550 | 0.61 | 3.91 | 0.74 | 2.16 | | | 2.29 |
| 98-551 | 0.46 | 2.73 | 0.51 | 1.43 | | | 1.55 |
| 98-552 | 0.46 | 2.89 | 0.53 | 1.4 | | | 1.51 |
| 98-553 | 0.42 | 2.53 | 0.48 | 1.35 | | | 1.37 |
| 98-559 | 0.4 | 2.45 | 0.47 | 1.28 | | | 1.37 |
| 98-561 | 0.47 | 2.81 | 0.52 | 1.48 | | | 1.66 |
| 98-566 | 0.49 | 2.95 | 0.57 | 1.5 | | | 1.55 |
| 98-576 | 0.41 | 2.37 | 0.43 | 1.26 | | | 1.21 |

**Fortuna Clara**

| Analyte Symbol | Tb | Dy | Ho | Er | Tl | Tm | Yb |
|---|---|---|---|---|---|---|---|
| Unit Symbol | ppm | ppm | ppm | ppm | ppm | ppm | ppm |
| 98-535 | 0.27 | 1.6 | 0.3 | 0.84 | | | 0.81 |
| 98-536 | 0.27 | 1.57 | 0.28 | 0.78 | | | 0.82 |
| 98-538 | | | | | | | |
| 98-541 | 0.24 | 1.4 | 0.27 | 0.71 | | | 0.77 |
| 98-547 | 0.28 | 1.58 | 0.31 | 0.82 | | | 0.93 |
| 98-554 | 0.43 | 2.55 | 0.49 | 1.36 | | | 1.44 |
| 98-556 | | | | | | | |
| 98-567 | 0.23 | 1.31 | 0.24 | 0.62 | | | 0.63 |
| 98-570 | 0.4 | 2.42 | 0.47 | 1.32 | | | 1.51 |
| 98-572 | 0.39 | 2.35 | 0.45 | 1.26 | | | 1.43 |
| 98-575 | 0.27 | 1.63 | 0.29 | 0.82 | | | 0.9 |
| 98-577 | 0.35 | 2.19 | 0.39 | 1.2 | | | 1.29 |

## San Lorenzo

| Analyte Symbol | Tb | Dy | Ho | Er | Tl | Tm | Yb |
|---|---|---|---|---|---|---|---|
| Unit Symbol | ppm | ppm | ppm | ppm | ppm | ppm | ppm |
| 98-531 | 0.31 | 1.92 | 0.36 | 1.02 | | | 1.17 |
| 98-542 | 0.23 | 1.37 | 0.25 | 0.68 | | | 0.72 |
| 98-545 | 0.17 | 1.06 | 0.2 | 0.57 | | | 0.74 |
| 98-546 | 0.26 | 1.52 | 0.28 | 0.8 | | | 0.88 |
| 98-560 | 0.28 | 1.48 | 0.25 | 0.74 | | | 0.9 |
| 98-562 | 0.39 | 2.24 | 0.43 | 1.26 | | | 1.58 |
| 98-563 | 0.27 | 1.75 | 0.31 | 0.98 | | | 1.2 |
| 98-568 | 0.19 | 1.16 | 0.22 | 0.67 | | | 0.89 |
| 98-571 | | | | | | | |
| 98-573 | 0.19 | 1.12 | 0.21 | 0.59 | | | 0.6 |

## Fortuna Leucocratic Intrusion

| Analyte Symbol | Tb | Dy | Ho | Er | Tl | Tm | Yb |
|---|---|---|---|---|---|---|---|
| Unit Symbol | ppm | ppm | ppm | ppm | ppm | ppm | ppm |
| 98-557 | 0.38 | 2.24 | 0.44 | 1.3 | | | 1.66 |
| 98-558 | 0.35 | 2.23 | 0.45 | 1.41 | | | 1.86 |
| 98-569 | | | | | | | |

## Pajonal diorite

| Analyte Symbol | Tb | Dy | Ho | Er | Tl | Tm | Yb |
|---|---|---|---|---|---|---|---|
| Unit Symbol | ppm | ppm | ppm | ppm | ppm | ppm | ppm |
| 00-194 | | 5.43 | 1.06 | 2.99 | | | 3.18 |
| 00-196 | | 4.33 | 0.84 | 2.46 | | | 2.56 |
| 00-197 | | 4.07 | 0.79 | 2.19 | | | 2.34 |
| 00-199 | | 4.25 | 0.84 | 2.36 | | | 2.38 |
| 00-200 | | 3.59 | 0.7 | 1.93 | | | 1.96 |

## Central Diorite

| Analyte Symbol | Tb | Dy | Ho | Er | Tl | Tm | Yb |
|---|---|---|---|---|---|---|---|
| Unit Symbol | ppm | ppm | ppm | ppm | ppm | ppm | ppm |
| 00-128 | | 3.68 | 0.67 | 1.94 | | | 2.02 |
| 00-135 | | 4.25 | 0.81 | 2.26 | | | 2.26 |
| 00-136 | | 3.32 | 0.62 | 1.8 | | | 1.84 |
| 00-178 | | 3.14 | 0.61 | 1.74 | | | 1.74 |
| 00-186 | | 2.95 | 0.57 | 1.7 | | | 1.73 |

## Dark Diorite

| Analyte Symbol | Tb | Dy | Ho | Er | Tl | Tm | Yb |
|---|---|---|---|---|---|---|---|
| Unit Symbol | ppm | ppm | ppm | ppm | ppm | ppm | ppm |
| 00-145 | | 1.85 | 0.34 | 1.03 | | | 1.01 |
| 00-160 | | 2.95 | 0.59 | 1.7 | | | 1.71 |
| 00-181 | | | | | | | |
| 00-184 | | 3.15 | 0.6 | 1.65 | | | 1.76 |

## Equis Monzodiorite

| Analyte Symbol | Tb | Dy | Ho | Er | Tl | Tm | Yb |
|---|---|---|---|---|---|---|---|
| Unit Symbol | ppm | ppm | ppm | ppm | ppm | ppm | ppm |
| 00-141 | | 4.35 | 0.84 | 2.39 | | | 2.45 |
| 00-146 | | 2.98 | 0.57 | 1.61 | | | 1.61 |
| 00-151 | | 2.68 | 0.54 | 1.65 | | | 1.86 |
| 00-155 | | 2.13 | 0.41 | 1.28 | | | 1.58 |
| 00-173 | | 5 | 0.99 | 2.8 | | | 2.75 |

## South Granodiorite

| Analyte Symbol | Tb | Dy | Ho | Er | Tl | Tm | Yb |
|---|---|---|---|---|---|---|---|
| Unit Symbol | ppm | ppm | ppm | ppm | ppm | ppm | ppm |
| 00-126 | | 1.9 | 0.34 | 1.02 | | | 1.16 |
| 00-130 | | 2.51 | 0.46 | 1.27 | | | 1.36 |
| 00-156 | | 1.4 | 0.27 | 0.73 | | | 0.84 |
| 00-159 | | 1.72 | 0.32 | 0.95 | | | 0.98 |
| 00-162 | | 1.61 | 0.29 | 0.87 | | | 0.97 |

## El Abra mine porphyry

| Analyte Symbol | Tb | Dy | Ho | Er | Tl | Tm | Yb |
|---|---|---|---|---|---|---|---|
| Unit Symbol | ppm | ppm | ppm | ppm | ppm | ppm | ppm |
| 00-138 | | 1.26 | 0.22 | 0.63 | | | 0.67 |
| 00-140 | | 1.77 | 0.33 | 0.9 | | | 1.05 |
| 00-144 | | 1.36 | 0.25 | 0.73 | | | 0.75 |
| 00-168 | | 2.91 | 0.56 | 1.51 | | | 1.61 |
| 00-172 | | 1.14 | 0.21 | 0.6 | | | 0.66 |

## El Abra Apolo leucogranite

| Analyte Symbol | Tb | Dy | Ho | Er | Tl | Tm | Yb |
|---|---|---|---|---|---|---|---|
| Unit Symbol | ppm | ppm | ppm | ppm | ppm | ppm | ppm |
| 00-120 | | 1.28 | 0.26 | 0.76 | | | 0.9 |
| 00-125 | | 2.34 | 0.47 | 1.38 | | | 1.72 |
| 00-154 | | 2.35 | 0.47 | 1.38 | | | 1.79 |
| 00-171 | | 2.74 | 0.55 | 1.69 | | | 2.11 |
| 00-187 | | 2.2 | 0.42 | 1.15 | | | 1.24 |

## El Abra Aplite

| Analyte Symbol | Tb | Dy | Ho | Er | Tl | Tm | Yb |
|---|---|---|---|---|---|---|---|
| Unit Symbol | ppm | ppm | ppm | ppm | ppm | ppm | ppm |
| 00-124 | | 16.22 | 0.59 | 1.62 | | | 1.84 |
| 00-150 | | 19.5 | 0.76 | 2.03 | | | 2.08 |
| 00-158 | | 17.92 | 0.62 | 1.8 | | | 2.08 |
| 00-169 | | 20.79 | 0.71 | 2.06 | | | 2.36 |
| 00-183 | | 27.46 | 0.98 | 2.85 | | | 2.89 |
| 00-188 | | 19.93 | 0.69 | 2.06 | | | 2.47 |

Los Picos

| Analyte Symbol | Lu | Mass | Ga | Pb | Sn | Nb | Rb |
|---|---|---|---|---|---|---|---|
| Unit Symbol | ppm | g | ppm | ppm | ppm | ppm | ppm |
| 98-518 | 0.29 | | | 11 | | | |
| 98-519 | 0.31 | | | 8 | | | |
| 98-520 | 0.4 | | | 19 | | | |
| 98-522 | 0.29 | | | 25 | | | |
| 98-524 | 0.32 | | | 39 | | | |
| 98-525 | 0.39 | | | 18 | | | |
| 98-526 | 0.19 | | | 13 | | | |
| 98-527 | 0.34 | | | 46 | | | |
| 98-540 | 0.37 | | | 13 | | | |
| 98-549 | 0.3 | | | 21 | | | |
| 98-564 | | | | | | | |

**Fortuna Gris**

| Analyte Symbol | Lu | Mass | Ga | Pb | Sn | Nb | Rb |
|---|---|---|---|---|---|---|---|
| Unit Symbol | ppm | g | ppm | ppm | ppm | ppm | ppm |
| 98-532 | 0.21 | | | 10 | | | |
| 98-534 | 0.36 | | | 10 | | | |
| 98-544 | 0.27 | | | 59 | | | |
| 98-548 | 0.3 | | | 36 | | | |
| 98-550 | 0.32 | | | 17 | | | |
| 98-551 | 0.22 | | | 76 | | | |
| 98-552 | 0.22 | | | 9 | | | |
| 98-553 | 0.21 | | | 41 | | | |
| 98-559 | 0.22 | | | 10 | | | |
| 98-561 | 0.25 | | | 17 | | | |
| 98-566 | 0.22 | | | 14 | | | |
| 98-576 | 0.18 | | | 8 | | | |

**Fortuna Clara**

| Analyte Symbol | Lu | Mass | Ga | Pb | Sn | Nb | Rb |
|---|---|---|---|---|---|---|---|
| Unit Symbol | ppm | g | ppm | ppm | ppm | ppm | ppm |
| 98-535 | 0.12 | | | 8 | | | |
| 98-536 | 0.12 | | | 17 | | | |
| 98-538 | | | | | | | |
| 98-541 | 0.11 | | | 12 | | | |
| 98-547 | 0.14 | | | 17 | | | |
| 98-554 | 0.2 | | | 7 | | | |
| 98-556 | | | | | | | |
| 98-567 | 0.1 | | | 14 | | | |
| 98-570 | 0.23 | | | 7 | | | |
| 98-572 | 0.22 | | | 10 | | | |
| 98-575 | 0.14 | | | 7 | | | |
| 98-577 | 0.2 | | | 9 | | | |

## San Lorenzo

| Analyte Symbol | Lu | Mass | Ga | Pb | Sn | Nb | Rb |
|---|---|---|---|---|---|---|---|
| Unit Symbol | ppm | g | ppm | ppm | ppm | ppm | ppm |
| 98-531 | 0.17 | | | 11 | | | |
| 98-542 | 0.11 | | | 11 | | | |
| 98-545 | 0.13 | | | 9 | | | |
| 98-546 | 0.13 | | | 11 | | | |
| 98-560 | 0.14 | | | 15 | | | |
| 98-562 | 0.23 | | | 5 | | | |
| 98-563 | 0.16 | | | 13 | | | |
| 98-568 | 0.13 | | | 62 | | | |
| 98-571 | | | | | | | |
| 98-573 | 0.09 | | | 9 | | | |

## Fortuna Leucocratic Intrusion

| Analyte Symbol | Lu | Mass | Ga | Pb | Sn | Nb | Rb |
|---|---|---|---|---|---|---|---|
| Unit Symbol | ppm | g | ppm | ppm | ppm | ppm | ppm |
| 98-557 | 0.27 | | | 15 | | | |
| 98-558 | 0.29 | | | 14 | | | |
| 98-569 | | | | | | | |

## Pajonal diorite

| Analyte Symbol | Lu | Mass | Ga | Pb | Sn | Nb | Rb |
|---|---|---|---|---|---|---|---|
| Unit Symbol | ppm | g | ppm | ppm | ppm | ppm | ppm |
| 00-194 | 0.46 | | | 14 | | | |
| 00-196 | 0.36 | | | 15 | | | |
| 00-197 | 0.33 | | | 15 | | | |
| 00-199 | 0.36 | | | 16 | | | |
| 00-200 | 0.27 | | | 6 | | | |

## Central Diorite

| Analyte Symbol | Lu | Mass | Ga | Pb | Sn | Nb | Rb |
|---|---|---|---|---|---|---|---|
| Unit Symbol | ppm | g | ppm | ppm | ppm | ppm | ppm |
| 00-128 | 0.28 | | | 12 | | | |
| 00-135 | 0.33 | | | 10 | | | |
| 00-136 | 0.26 | | | 6 | | | |
| 00-178 | 0.26 | | | 8 | | | |
| 00-186 | 0.33 | | | 9 | | | |

## Dark Diorite

| Analyte Symbol | Lu | Mass | Ga | Pb | Sn | Nb | Rb |
|---|---|---|---|---|---|---|---|
| Unit Symbol | ppm | g | ppm | ppm | ppm | ppm | ppm |
| 00-145 | 0.16 | | | 4 | | | |
| 00-160 | 0.24 | | | 4 | | | |
| 00-181 | | | | | | | |
| 00-184 | 0.24 | | | 8 | | | |

## Equis Monzodiorite

| Analyte Symbol | Lu | Mass | Ga | Pb | Sn | Nb | Rb |
|---|---|---|---|---|---|---|---|
| Unit Symbol | ppm | g | ppm | ppm | ppm | ppm | ppm |
| 00-141 | 0.36 | | | 9 | | | |
| 00-146 | 0.25 | | | 11 | | | |
| 00-151 | 0.28 | | | 3 | | | |
| 00-155 | 0.24 | | | 7 | | | |
| 00-173 | 0.38 | | | 13 | | | |

## South Granodiorite

| Analyte Symbol | Lu | Mass | Ga | Pb | Sn | Nb | Rb |
|---|---|---|---|---|---|---|---|
| Unit Symbol | ppm | g | ppm | ppm | ppm | ppm | ppm |
| 00-126 | 0.18 | | | 54 | | | |
| 00-130 | 0.19 | | | 7 | | | |
| 00-156 | 0.13 | | | 11 | | | |
| 00-159 | 0.15 | | | 4 | | | |
| 00-162 | 0.15 | | | 8 | | | |

## El Abra mine porphyry

| Analyte Symbol | Lu | Mass | Ga | Pb | Sn | Nb | Rb |
|---|---|---|---|---|---|---|---|
| Unit Symbol | ppm | g | ppm | ppm | ppm | ppm | ppm |
| 00-138 | 0.09 | | | 9 | | | |
| 00-140 | 0.15 | | | 7 | | | |
| 00-144 | 0.12 | | | 9 | | | |
| 00-168 | 0.23 | | | 6 | | | |
| 00-172 | 0.1 | | | 54 | | | |

## El Abra Apolo leucogranite

| Analyte Symbol | Lu | Mass | Ga | Pb | Sn | Nb | Rb |
|---|---|---|---|---|---|---|---|
| Unit Symbol | ppm | g | ppm | ppm | ppm | ppm | ppm |
| 00-120 | 0.14 | | | 1 | | | |
| 00-125 | 0.26 | | | 19 | | | |
| 00-154 | 0.26 | | | 8 | | | |
| 00-171 | 0.31 | | | 10 | | | |
| 00-187 | 0.18 | | | 6 | | | |

## El Abra Aplite

| Analyte Symbol | Lu | Mass | Ga | Pb | Sn | Nb | Rb |
|---|---|---|---|---|---|---|---|
| Unit Symbol | ppm | g | ppm | ppm | ppm | ppm | ppm |
| 00-124 | 0.27 | | | 10 | | | |
| 00-150 | 0.31 | | | 10 | | | |
| 00-158 | 0.32 | | | 14 | | | |
| 00-169 | 0.36 | | | 12 | | | |
| 00-183 | 0.44 | | | 14 | | | |
| 00-188 | 0.37 | | | 15 | | | |

# Appendix 6 Data from Arnott (2003) Thesis

The following section contains a data table from Arnott (2003). This whole rock geochemical data was used to compare MMH with components of the Chuquicamata Intrusive Complex.

| | SiO2 % | Al2O3 % | Fe2O3(T) % | MnO % | MgO % | CaO % | Na2O % | K2O % | TiO2 % |
|---|---|---|---|---|---|---|---|---|---|
| **Ester** | | | | | | | | | |
| Cu 769 | 70.2 | 16.88 | 2.43 | 0.04 | 0.07 | 3.03 | 4.1 | 1.72 | 0.32 |
| **Banco** | | | | | | | | | |
| Cu-1333 | 68.06 | 17.36 | 1.36 | 0.01 | 0.37 | 1.01 | 3.71 | 4.06 | 0.3 |
| Cu-1333 | 68.02 | 17.88 | 1.13 | 0.01 | 0.47 | 0.94 | 3.58 | 4.15 | 0.29 |
| Cu-93-514 | 69.2 | 16.9 | 2.26 | 0.04 | 0.63 | 1.81 | 5.29 | 3.17 | 0.29 |
| **Oeste** | | | | | | | | | |
| Cu93-516 | 71 | 15.5 | 0.74 | 0.02 | 0.12 | 0.31 | 5.17 | 4.03 | 0.2 |
| **EsteK** | | | | | | | | | |
| Cu-1112 | 70.64 | 15.74 | 0.76 | 0.01 | 0.46 | 0.32 | 5.77 | 4.09 | 0.32 |
| Cu-1115 | 69.94 | 14.95 | 2.02 | 0.04 | 0.76 | 0.21 | 4.1 | 4.79 | 0.24 |
| **EsteSer** | | | | | | | | | |
| Cu-020 | 68.26 | 11.1 | 2.63 | | 0.29 | 3.51 | | 3.43 | 0.26 |
| Cu-070 | 83.6 | 6.42 | 1.17 | 0.01 | 0.49 | 1.92 | | 1.95 | 0.1 |
| Cu-093 | 86.52 | 4.84 | 1.03 | | 0.08 | 1.56 | | 1.46 | 0.07 |
| Cu-102 | 80.87 | 11.74 | 0.89 | | 0.22 | 0.05 | | 3.58 | 0.19 |
| Cu-1144 | 65.56 | 15.53 | 0.53 | 0.23 | 0.28 | 1.69 | 0 | 10.43 | 0.18 |
| **EsteProp** | | | | | | | | | |
| Cu-746 | 69.01 | 16.06 | 1.52 | 0.09 | 0.82 | 1.94 | 4.99 | 2.83 | 0.31 |
| **Ksil** | | | | | | | | | |
| Cu-1334 | 68.96 | 15.19 | 0.5 | 0.01 | 0.49 | 1.42 | 3.92 | 5.79 | 0.23 |
| **Fiesta** | | | | | | | | | |
| Cu-524 | 64.4 | 14.9 | 3.18 | 0.07 | 1.52 | 3.69 | 3.55 | 3.87 | 0.56 |
| Cu-526 | 64.6 | 16.6 | 3.61 | 0.08 | 1.31 | 4.13 | 2.48 | 4.41 | 0.43 |

| | P2O5 % | LOI % | Total % | Au ppb | Ag ppm | As ppm | Ba ppm | Be ppm | Bi ppm |
|---|---|---|---|---|---|---|---|---|---|
| **Ester** | | | | | | | | | |
| Cu 769 | 0.11 | 0.44 | 99.97 | | 0 | | 885 | | |
| **Banco** | | | | | | | | | |
| Cu-1333 | 0.08 | 2.41 | 98.73 | | 2 | | 799 | | |
| Cu-1333 | 0.05 | 2.82 | 99.48 | | | | | | |
| Cu-93-514 | 0.04 | 0.8 | 100.4 | | | | | | |
| **Oeste** | | | | | | | | | |
| Cu93-516 | 0.06 | 1.7 | 98.8 | | | | | | |
| **EsteK** | | | | | | | | | |
| Cu-1112 | 0.06 | 0.42 | 98.59 | | | | 415 | | |
| Cu-1115 | 0.08 | 1.19 | 98.32 | | | | 625 | | |
| **EsteSer** | | | | | | | | | |
| Cu-020 | 0.08 | 8.97 | 98.56 | <1 | | | 129.5 | | |
| Cu-070 | 0.03 | 3.77 | 99.56 | | 1 | | 80 | | |
| Cu-093 | 0.07 | 3.3 | 99.03 | | 11 | | 203 | | |
| Cu-102 | 0.09 | 1.99 | 99.67 | | 6 | | 234 | | |
| Cu-1144 | 0.13 | 4.08 | 98.64 | | | | | | |
| **EsteProp** | | | | | | | | | |
| Cu-746 | 0.15 | 1.09 | 98.81 | | | | | | |
| **Ksil** | | | | | | | | | |
| Cu-1334 | 0.09 | 2.94 | 99.64 | | | | | | |
| **Fiesta** | | | | | | | | | |
| Cu-524 | 0.16 | 0.85 | 96.75 | | | | 649 | | |
| Cu-526 | 0.21 | 1.97 | 99.83 | | | | 704 | | |

| | Br ppm | Cd ppm | Co ppm | Cr ppm | Cs ppm | Cu ppm | Ga ppm | Ge ppm | Hf ppm |
|---|---|---|---|---|---|---|---|---|---|
| **Ester** | | | | | | | | | |
| Cu 769 | | | 3 | | 1.4 | 410 | 20 | | 4 |
| **Banco** | | | | | | | | | |
| Cu-1333 | | | 3 | | 2.4 | 5410 | 22 | | 4 |
| Cu-1333 | | | | | | | | | |
| Cu-93-514 | | | | | | | | | |
| **Oeste** | | | | | | | | | |
| Cu93-516 | | | | | | | | | |
| **EsteK** | | | | | | | | | |
| Cu-1112 | | | | | | | | | |
| Cu-1115 | | | | | | | | | |
| **EsteSer** | | | | | | | | | |
| Cu-020 | | | 4 | | 1.3 | 844 | 23 | | 4 |
| Cu-070 | | | 3.5 | | 0.6 | 347 | 14 | | 1 |
| Cu-093 | | | 3 | | 0.3 | 16600 | 12 | <1 | |
| Cu-102 | | | 1.5 | | 0.8 | 18200 | 26 | | 3 |
| Cu-1144 | | | | | | | | | |
| **EsteProp** | | | | | | | | | |
| Cu-746 | | | | | | | | | |
| **Ksil** | | | | | | | | | |
| Cu-1334 | | | | | | | | | |
| **Fiesta** | | | | | | | | | |
| Cu-524 | | | | | | | | | |
| Cu-526 | | | | | | | | | |

| | Hg ppm | In ppm | Ir ppb | Mo ppm | Nb ppm | Ni ppm | Pb ppm | Rb ppm | S % |
|---|---|---|---|---|---|---|---|---|---|
| **Ester** | | | | | | | | | |
| Cu 769 | | | | | 7 | 0 | | 65 | |
| **Banco** | | | | | | | | | |
| Cu-1333 | | | | | 5 | 20 | | 107 | |
| Cu-1333 | | | | | | | | | |
| Cu-93-514 | | | | | | | | | |
| **Oeste** | | | | | | | | | |
| Cu93-516 | | | | | | | | | |
| **EsteK** | | | | | | | | | |
| Cu-1112 | | | | | 18 | | | 98 | |
| Cu-1115 | | | | | 12 | | | 154 | |
| **EsteSer** | | | | | | | | | |
| Cu-020 | | | | | 7 | 35 | | 90.4 | |
| Cu-070 | | | | | 6 | 110 | | 44.8 | |
| Cu-093 | | | | | 1 | 60 | | 32.6 | |
| Cu-102 | | | | | 6 | 30 | | 91 | |
| Cu-1144 | | | | | | | | | |
| **EsteProp** | | | | | | | | | |
| Cu-746 | | | | | | | | | |
| **Ksil** | | | | | | | | | |
| Cu-1334 | | | | | | | | | |
| **Fiesta** | | | | | | | | | |
| Cu-524 | | | | | | 4 | | 177 | |
| Cu-526 | | | | | | 5 | | 75 | |

| | Sb ppm | Sc ppm | Se ppm | Sn ppm | Sr ppm | Ta ppm | Th ppm | U ppm | V ppm |
|---|---|---|---|---|---|---|---|---|---|
| **Ester** | | | | | | | | | |
| Cu 769 | | | | 0 | 709 | 1 | 2 | 2 | 35 |
| **Banco** | | | | | | | | | |
| Cu-1333 | | | | 7 | 400 | 0 | 3 | 3 | 25 |
| Cu-1333 | | | | | | | | | |
| Cu-93-514 | | | | | | | | | |
| **Oeste** | | | | | | | | | |
| Cu93-516 | | | | | | | | | |
| **EsteK** | | | | | | | | | |
| Cu-1112 | | | | | 158 | | 6 | 2 | |
| Cu-1115 | | | | | 116 | | | | |
| **EsteSer** | | | | | | | | | |
| Cu-020 | | | | 14 | 108 | <0.5 | 4 | 1.5 | 60 |
| Cu-070 | | | | 7 | 94.4 | <0.5 | 1 | <0.5 | 60 |
| Cu-093 | | | | 6 | 212 | <0.5 | 7 | 0.5 | 30 |
| Cu-102 | | | | 13 | 72.9 | <0.5 | 2 | 0.5 | 70 |
| Cu-1144 | | | | | | | | | |
| **EsteProp** | | | | | | | | | |
| Cu-746 | | | | | | | | | |
| **Ksil** | | | | | | | | | |
| Cu-1334 | | | | | | | | | |
| **Fiesta** | | | | | | | | | |
| Cu-524 | | | | | 367 | | | | |
| Cu-526 | | | | | 638 | | | | |

| | W ppm | Y ppm | Zn ppm | Zr ppm | La ppm | Ce ppm | Pr ppm | Nd ppm | Sm ppm |
|---|---|---|---|---|---|---|---|---|---|
| **Ester** | | | | | | | | | |
| Cu 769 | 0 | 7 | 30 | 125 | 24 | 43.5 | 5.1 | 19 | 2.6 |
| **Banco** | | | | | | | | | |
| Cu-1333 | 17 | 9 | 435 | 188 | 12 | 24 | 2.6 | 9 | 1.5 |
| Cu-1333 | | | | | | | | | |
| Cu-93-514 | | | | | | | | | |
| **Oeste** | | | | | | | | | |
| Cu93-516 | | | | | | | | | |
| **EsteK** | | | | | | | | | |
| Cu-1112 | | 12 | | 108 | 15.5 | 30 | 3.5 | 12 | 2.1 |
| Cu-1115 | | 14 | | 102 | | | | | |
| **EsteSer** | | | | | | | | | |
| Cu-020 | 28 | 4 | 145 | 207 | 15.5 | 30.5 | 3.2 | 11 | 1.6 |
| Cu-070 | 12 | 2.5 | 15 | 48 | 4.5 | 8.5 | 1 | 3.5 | 0.6 |
| Cu-093 | 9 | 2.5 | 20 | 46 | 21.5 | 35 | 3 | 9 | 1.2 |
| Cu-102 | 21 | 2 | 15 | 138.5 | 7.5 | 15.5 | 1.6 | 5.5 | 0.9 |
| Cu-1144 | | | | | | | | | |
| **EsteProp** | | | | | | | | | |
| Cu-746 | | | | | | | | | |
| **Ksil** | | | | | | | | | |
| Cu-1334 | | | | | | | | | |
| **Fiesta** | | | | | | | | | |
| Cu-524 | | 27 | | 315 | 28 | 64 | 6.9 | 26 | 4.5 |
| Cu-526 | | 9 | | 156 | 22 | 47 | 4.8 | 16 | 3.2 |

| | Eu ppm | Gd ppm | Tb ppm | Dy ppm | Ho ppm | Er ppm | Tl ppm | Tm ppm | Yb ppm |
|---|---|---|---|---|---|---|---|---|---|
| **Ester** | | | | | | | | | |
| Cu 769 | 0.8 | 2.4 | 0.3 | 1.2 | 0.2 | 0.8 | | 0.1 | 0.8 |
| **Banco** | | | | | | | | | |
| Cu-1333 | 0.4 | 1.7 | 0.2 | 1.3 | 0.3 | 0.9 | | 0.1 | 0.9 |
| Cu-1333 | | | | | | | | | |
| Cu-93-514 | | | | | | | | | |
| **Oeste** | | | | | | | | | |
| Cu93-516 | | | | | | | | | |
| **EsteK** | | | | | | | | | |
| Cu-1112 | 0.4 | 1.4 | 0.4 | 0.7 | <0.1 | 0.3 | <0.1 | | 0.3 |
| Cu-1115 | | | | | | | | | |
| **EsteSer** | | | | | | | | | |
| Cu-020 | 0.4 | 1.1 | 0.1 | 0.7 | 0.1 | 0.4 | <0.1 | | 0.4 |
| Cu-070 | 0.1 | 0.5 | <0.1 | 0.3 | <0.1 | 0.2 | <0.1 | | 0.2 |
| Cu-093 | 0.3 | 0.9 | 0.1 | 0.5 | 0.1 | 0.3 | <0.1 | | 0.2 |
| Cu-102 | 0.1 | 0.6 | <0.1 | 0.3 | <0.1 | 0.2 | <0.1 | | 0.1 |
| Cu-1144 | | | | | | | | | |
| **EsteProp** | | | | | | | | | |
| Cu-746 | | | | | | | | | |
| **Ksil** | | | | | | | | | |
| Cu-1334 | | | | | | | | | |
| **Fiesta** | | | | | | | | | |
| Cu-524 | 1 | 4.3 | 0.6 | 3.4 | 0.8 | 1.7 | | 0.3 | 1.9 |
| Cu-526 | 1.1 | 1.9 | 0.3 | 1.4 | 0.4 | 0.7 | | 0.1 | 0.7 |

| | | Lu | Mass | Ga | Pb | Sn | Nb | Rb |
|---|---|---|---|---|---|---|---|---|
| | | ppm | g | ppm | ppm | ppm | ppm | ppm |
| **Ester** | | | | | | | | |
| Cu 769 | | 0.1 | | | 5 | | | |
| **Banco** | | | | | | | | |
| Cu-1333 | | 0.1 | | | 15 | | | |
| Cu-1333 | | | | | | | | |
| Cu-93-514 | | | | | | | | |
| **Oeste** | | | | | | | | |
| Cu93-516 | | | | | | | | |
| **EsteK** | | | | | | | | |
| Cu-1112 | <0.1 | | | | | | | |
| Cu-1115 | | | | | | | | |
| **EsteSer** | | | | | | | | |
| Cu-020 | <0.1 | | | | 20 | | | |
| Cu-070 | <0.1 | | | | 15 | | | 44.8 |
| Cu-093 | <0.1 | | | | 35 | | | |
| Cu-102 | <0.1 | | | | 20 | | | |
| Cu-1144 | | | | | | | | |
| **EsteProp** | | | | | | | | |
| Cu-746 | | | | | | | | |
| **Ksil** | | | | | | | | |
| Cu-1334 | | | | | | | | |
| **Fiesta** | | | | | | | | |
| Cu-524 | | 0.3 | | | | | | |
| Cu-526 | | 0.1 | | | | | | |